Long-Term Grande Ronde Aquifer Stress Testing to Delineate Aquifer Compartmentalization and Water Level Responses in the Palouse Groundwater Basin

A Thesis
Presented in Partial Fulfillment of the Requirements for the
Degree of Master of Science
with a
Major in Hydrology
in the
College of Graduate Studies
University of Idaho

by
Attila Jonathan Bela Folnagy

June 2012

Major Professor: Dr. James L. Osiensky, Ph.D.

AUTHORIZATION TO SUBMIT THESIS

This thesis of Attila Folnagy, submitted for the degree of Master of Science with a major in Hydrology and titled, "Long-Term Grande Ronde Aquifer Stress Testing to Delineate Compartmentalization and Water Level Responses in the Palouse Basin" has been reviewed in final form. Permission, as indicated by the signatures and dates given below, is now granted to submit final copies to the College of Graduate Studies for approval.

Major Professor James L Osiensky Date June 4, 2012
Dr. James L. Osiensky

Committee Members Kenneth F Sprenke Date May 10, 2012
Dr. Kenneth F Sprenke

C. Kent Keller Date 10 May 2012
Dr. C. Kent Keller

Department Administrator Mickey E. Gunter Date June 4, 2012
Dr. Mickey E. Gunter

Discipline's College Dean Scott A. Wood Date 6/6/12
Dr. Scott A. Wood

Final Approval and Acceptance by the College of Graduate Studies

_____ Date _____
Dr. Jie Chen

ABSTRACT

Accurate aquifer storativity (S) estimates related to aquifer system responses are essential for effective groundwater resource evaluation and management, especially in sole-source systems such as the Palouse Groundwater Basin (PGB) of eastern Washington and northwest Idaho. Uncertainties concerning the hydrogeologic properties, and horizontal and vertical dimensions of the aquifer system complicate evaluation of annual groundwater declines due to municipal pumping. Several lines of evidence such as water level fluctuations, barometric efficiencies, aquifer compressibilities, earthquake responses, and results of short-term and long-term aquifer stress tests, suggest that average aquifer system storativity in the PGB is relatively low.

This investigation examines the details of annual aquifer system responses to specific variations in daily, monthly, and annual pumping stresses. To evaluate the meaning of aquifer system storativity on an annual time frame, a comprehensive year-long, basin-wide, aquifer stress test was completed to calibrate short-term and long-term aquifer system responses to known and anticipated boundary conditions, and estimated hydrogeologic properties. Drawdown data for selected observation wells are analyzed together with all municipal pumping schedules for the cities of Pullman, WA; Moscow, ID; Palouse, WA; and Colfax, WA using the principle of superposition.

Extended analysis of these data over various time scales revealed information about the degree of hydraulic connection within the basin, characteristics of the physical boundary conditions, and reasonable ranges of aquifer system hydrogeologic properties on daily to yearly time frames. The ability to select different “windows” of short and/or long-term pumping/drawdown data from within continuous, annual data sets enhanced the evaluation of aquifer properties through averaging of discrete system responses to spatially and temporally variable pumping stresses. These conditions facilitated interpretation of aquifer system responses by traditional analytical methods of aquifer test analysis.

An alternative method for estimating aquifer storativity (S) also is evaluated by recognizing that seismic stresses induce water level changes in certain PGB wells. Aquifer specific storage (S_s) is estimated for the DOE well based on analysis of these earthquake effects (Appendix C).

The significance of PGB compartmentalization as it relates to potential aquifer storage and recovery (ASR) also is explored (Appendix D).

ACKNOWLEDGEMENTS

There are several people I would like to thank for their support in one form or another during my time (Fall 2008 – Spring 2012) as both an undergraduate and graduate student at the University of Idaho. A large expression of thanks to my Major Professor Dr. Jim Osiensky who provided the early guidance, encouragement, and enthusiasm to study Hydrogeology. Dr. Osiensky always made time to discuss hydrology or entertain me during casual stops by his office. I'm grateful to my advisors Dr Ken Sprenke and Dr. Kent Keller for their support, enthusiasm, and critical reviews of my thesis. Many thanks also to Dr. Jerry Fairley's extensive knowledge and patience in helping me develop my skills in professional communication and as a hydrologist. Other faculty and staff I would like to thank include Mickey Gunter, Debbie Jensen, Simon Kattenhorn, Peter Isacacson and Dennis Geist.

My deepest appreciation goes to the various city and university officials who played such a pivotal role in the Groundwater Monitoring Programs success. Mike Dimmick and Gary Smith (City of Moscow), Terry Schierman and Keith Kirpes (City of Pullman), Don Myott (City of Palouse), Mike Holthaus (UI),Tim Leachmen (WSU), Perry Brown and Bill Bowman (City of Garfield), Kenneth Smith (City of Albion), and Andy Rogers (City of Colfax) who showed tremendous support and cooperation during all of the aquifer tests. Also, I would like to thank the Palouse Basin Aquifer Committee for the funding that supported this project. A special thanks to Steve Robischon for your support and kindness.

Katie Moran was essential to helping me transition smoothly into my thesis investigation with a high level understanding of the PBAC Monitoring Program. Her expertise on how to streamline data processing also was a great asset to my investigation. I'm grateful to Lauren Carey for her support and knowledge of Hydrogeology when discussing hydrology homework. She has the great talent of explaining complicated things so that they make sense. Additional appreciation to the several other students I had the pleasure of associating with during my time at U of I. My sincerest gratitude goes to Heidi for her love and encouragement as we pursue our goals together. A heart filled thanks to my parents and brother for their encouragement and loving support.

TABLE OF CONTENTS

LIST OF TABLES

LIST OF FIGURES

CHAPTER 1

Introduction to Research and Previous Work

1.1 Problem Statement

The Palouse Groundwater Basin (PGB) constitutes the source of groundwater for the greater Moscow-Pullman area, providing 95% of the municipal and university water supplies from the Miocene Columbia River Basalt Group (CRBG). Most of the water derived from the PGB is obtained from the Grande Ronde and Wanapum formations of the CRBG; the majority of the groundwater is obtained from the Grande Ronde formation (PBAC, 2010), and the Grande Ronde aquifer system is the focus of this study.

Due to the importance of the Grande Ronde as a water source it has been the subject of numerous studies that focus on quantifying the storage properties of the basin. Based on stratigraphy, structural geology, and hydrogeology, it has been proposed that the PGB can be subdivided into six geologically distinct Sub-basins, which may or may not be hydraulically connected to one another (Figure 1.1).

The Grande Ronde aquifer is facing increasing demand and declining waters levels, yet little has been reported about the degree of compartmentalization within the groundwater resource system and the nature of hydraulic connections between individual compartments. PGB water managers and scientists do not understand the system well enough to predict whether the system will ever reach equilibrium. With limited recharge, as noted by previous research, municipalities have curtailed pumping.

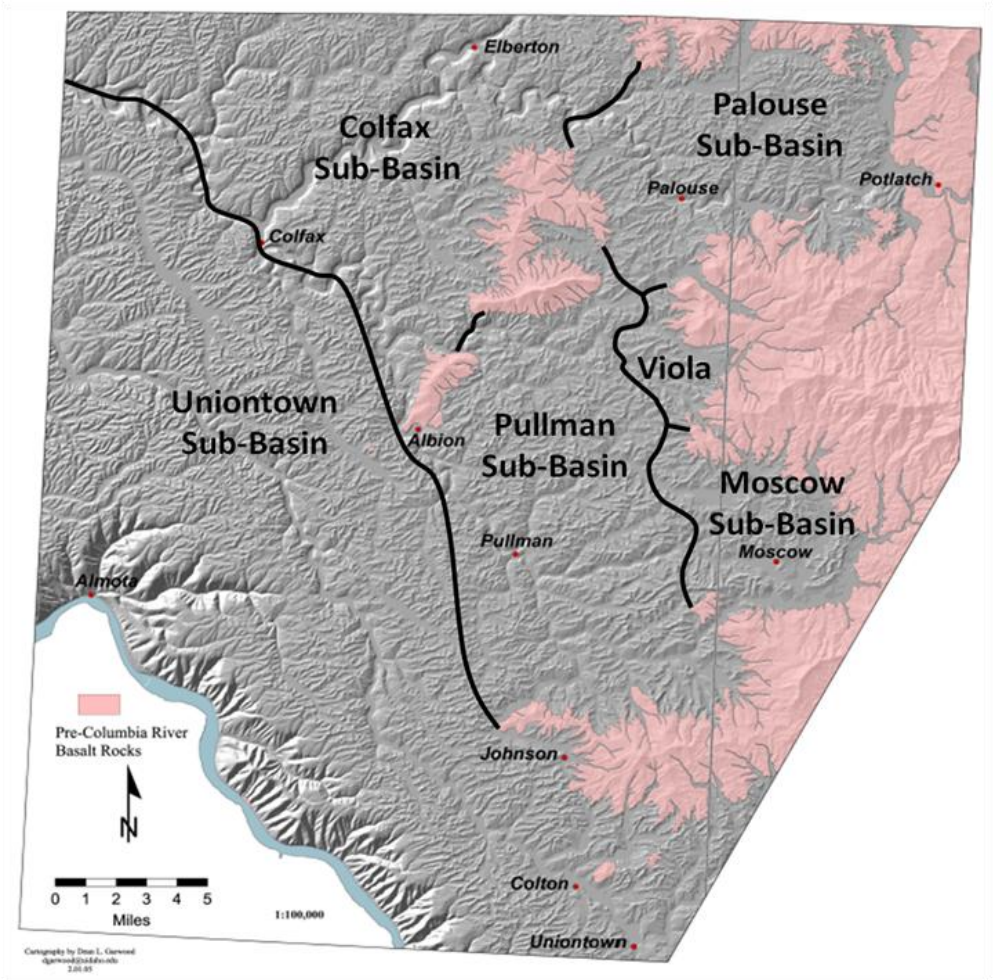

Figure 1.1: Sub-basins of the Palouse Basin (Bush, 2005). Pre-CRBG crystalline rocks (red), Columbia River Basalts (grey), Sub-basin boundaries delineated by black lines and Pre-CRBG rocks.

1.2 Study Area

The study area lies within the agricultural, dry-land farming area known as "the Palouse" of northern Idaho and southeastern Washington. This area encompasses the cities of Pullman, Colfax, Palouse, and Moscow, and multiple smaller communities and rural areas, as well as two large universities, with an estimated total area population of approximately 64,000 (PBAC, 2010). The municipality, university, private, and state agency wells monitored during this investigation are listed in Table 1.1. Specific locations of these groundwater wells are shown in Figure 1.2 for the basin scale and in Figures 1.3 through 1.8 for local scale.

Well ID	2010	2011	2012
Washington State University Well #4 (WSU 4)	ON/OFF	ON/OFF	ON/OFF
Washington State University Well #5 (WSU 5)	WL	WL	WL
Washington State University Well #6 (WSU 6)	ON/OFF	ON/OFF	WL & On/Off
Washington State University Well #7 (WSU 7)	WL & ON/OFF	WL & ON/OFF	WL & ON/OFF
Washington State University Well #8 (WSU 8)	WL & ON/OFF	WL & ON/OFF	WL & ON/OFF
Washington State University Test Well (WSU Test)	WL & BARO	WL & BARO	WL & BARO
Washington State University Dairy Well (WSU Dairy)	---	---	WL
City of Pullman Well #3 (Pull 3)	ON/OFF	ON/OFF	WL
City of Pullman Well #4 (Pull 4)	WL	---	---
City of Pullman Well #5 (Pull 5)	ON/OFF	ON/OFF	ON/OFF
City of Pullman Well #6 (Pull 6)	WL & ON/OFF	ON/OFF	ON/OFF
City of Pullman Well #7 (Pull 7)	ON/OFF	ON/OFF	ON/OFF
City of Pullman Well #8 (Pull 8)	WL & ON/OFF	ON/OFF	ON/OFF
City of Moscow Well #6 (Mos 6)	ON/OFF	ON/OFF	WL & ON/OFF
City of Moscow Well #7 (Mos 7)	WL	---	---
City of Moscow Well #8 (Mos 8)	ON/OFF	ON/OFF	ON/OFF
City of Moscow Well #9 (Mos 9)	ON/OFF	ON/OFF	ON/OFF
City of Colfax Clay Street Well	WL & ON/OFF	WL & ON/OFF	WL & ON/OFF
City of Colfax Fairview Well	ON/OFF	ON/OFF	ON/OFF
City of Colfax Glenwood Well #1	ON/OFF	ON/OFF	ON/OFF
City of Colfax Glenwood Well #2	ON/OFF	ON/OFF	ON/OFF

Table 1.1: Monitoring well type during this investigation: The following are codes used: Water Level Monitoring (WL), HOBO® U9 Pump Motor On/Off Data Logger Monitoring (ON/OFF), and Barometric Pressure Monitoring (BARO).

Well ID	2010	2011	2012
City of Palouse Well #1 (Palouse 1)	WL, ON/OFF, and BARO	WL, ON/OFF, and BARO	ON/OFF and BARO
City of Palouse Well #3 (Palouse 3)	WL and ON/OFF	WL and ON/OFF	WL and ON/OFF
City of Albion Well #2 (Albion 2)	---	ON/OFF	ON/OFF
City of Albion Well #3 (Albion 3)	---	ON/OFF	ON/OFF
City of Garfield Well #3 (Garfield 3)	---	ON/OFF	ON/OFF
City of Garfield Well #4 (Garfield 4)	---	ON/OFF	ON/OFF
Cornelius Well	WL	WL	WL
Washington State Department of Ecology (DOE)	WL and BARO	WL and BARO	WL and BARO
University of Idaho Well #3 (UI 3)	ON/OFF	ON/OFF	ON/OFF
University of Idaho Well #4 (UI 4)	ON/OFF	ON/OFF	ON/OFF
Idaho Department of Water Resources well #1 (IDWR 1)	BARO	BARO	BARO
Idaho Department of Water Resources well #4 (IDWR 4)	WL	WL	WL
Motley-Motley (Premix) Well (M&M)	---	WL	WL

Table 1.1 Cont.: Monitoring well type during this investigation: The following are codes used: Water Level Monitoring (WL), HOBO® U9 Pump Motor On/Off Data Logger Monitoring (ON/OFF), and Barometric Pressure Monitoring (BARO).

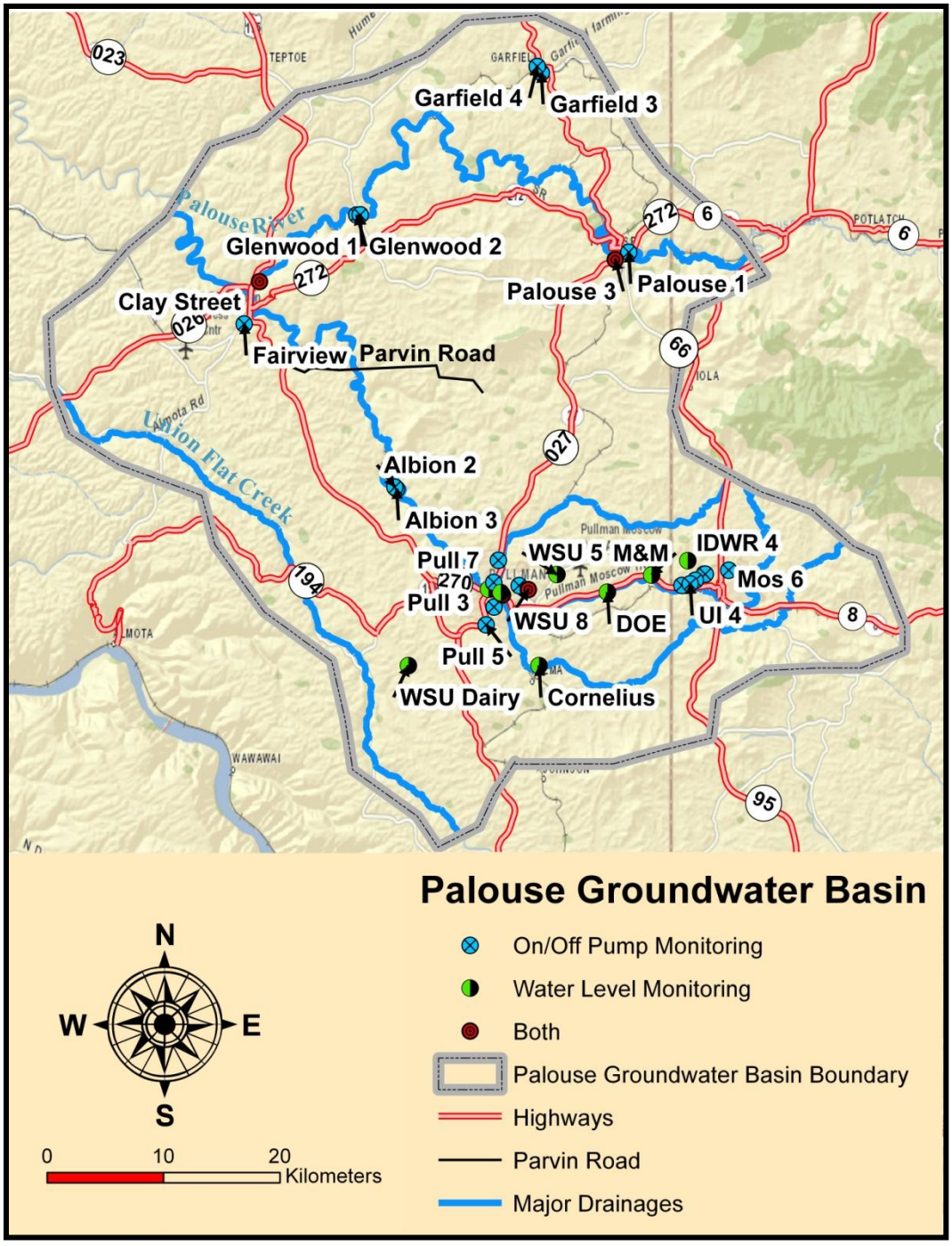

Figure 1.2: Map of the Palouse Groundwater Basin (PGB).

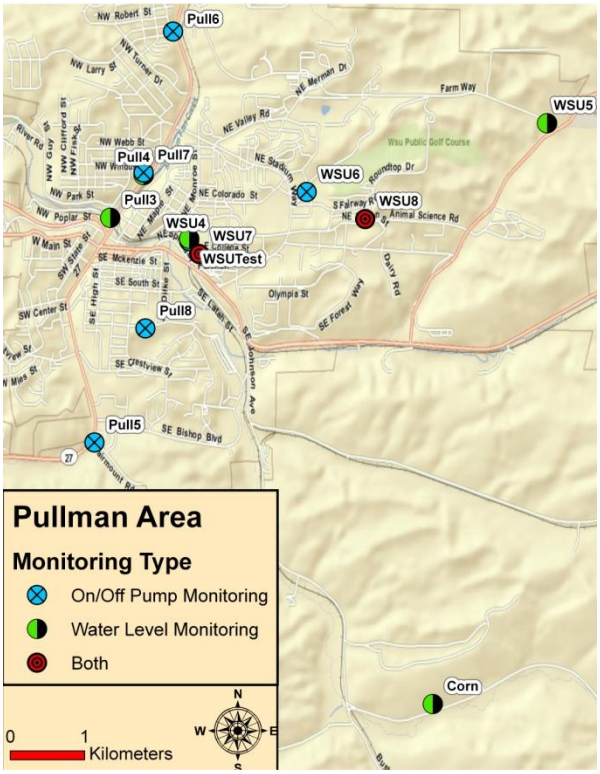

Figure 1.3: Pullman area wells.

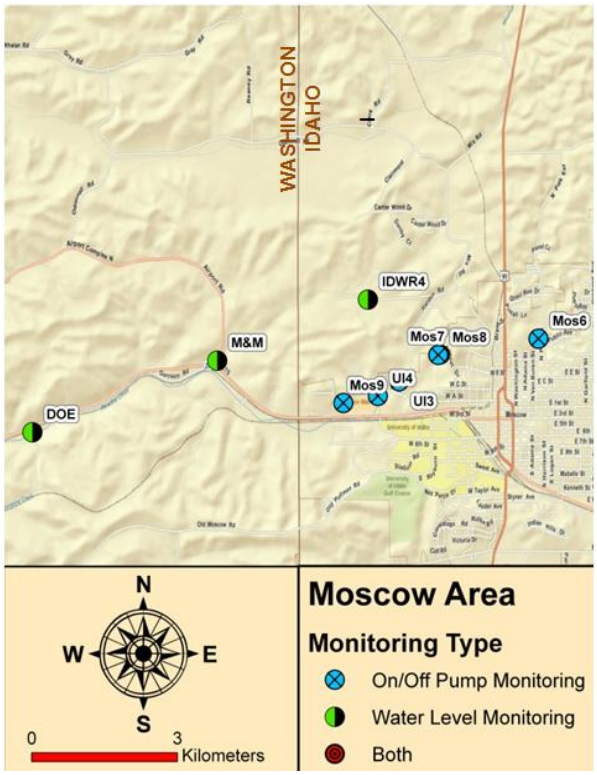

Figure 1.4: Moscow area wells.

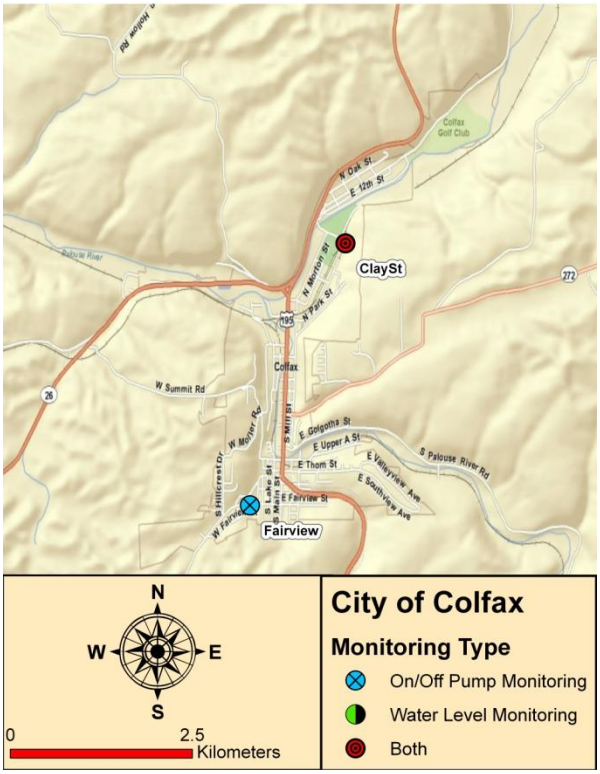

Figure 1.5: City of Colfax wells.

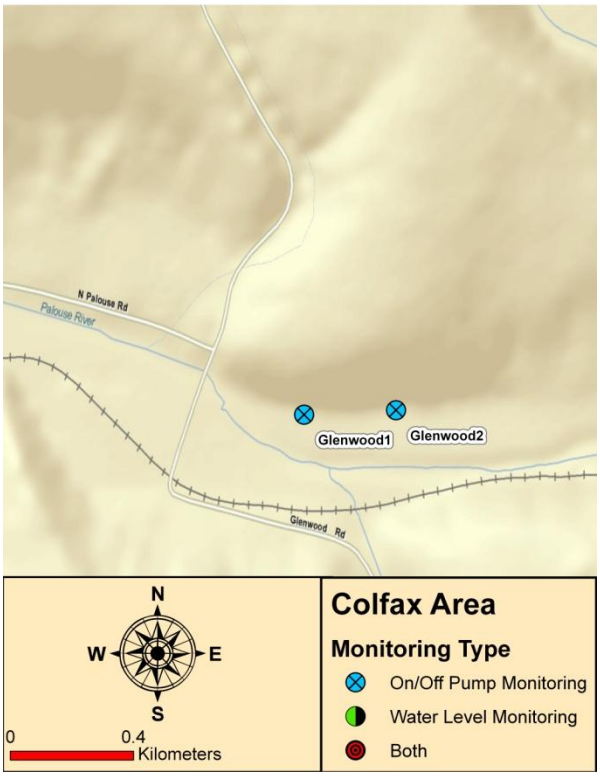

Figure 1.6: Colfax area wells.

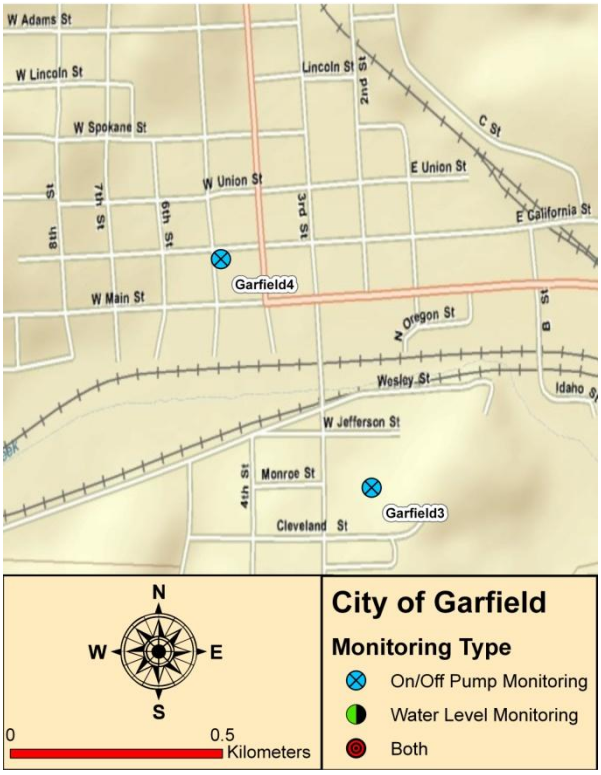

Figure 1.7: City of Garfield wells.

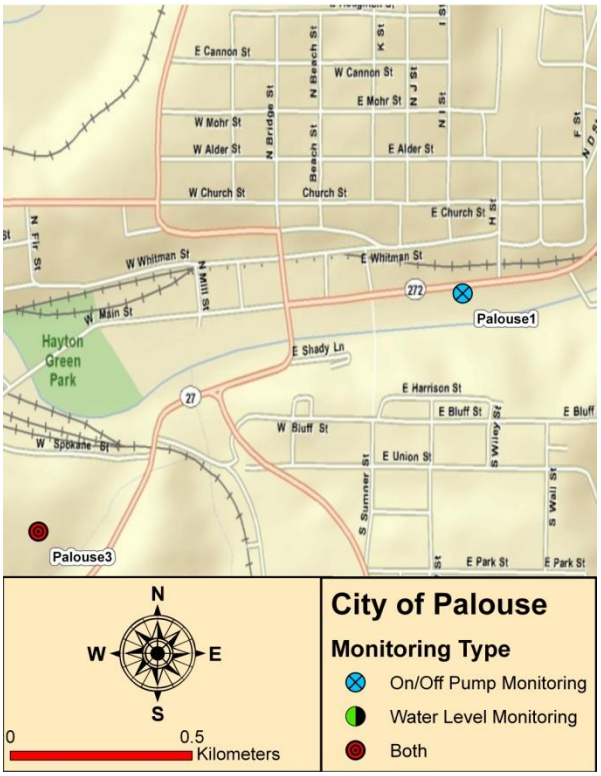

Figure 1.8: City of Palouse wells.

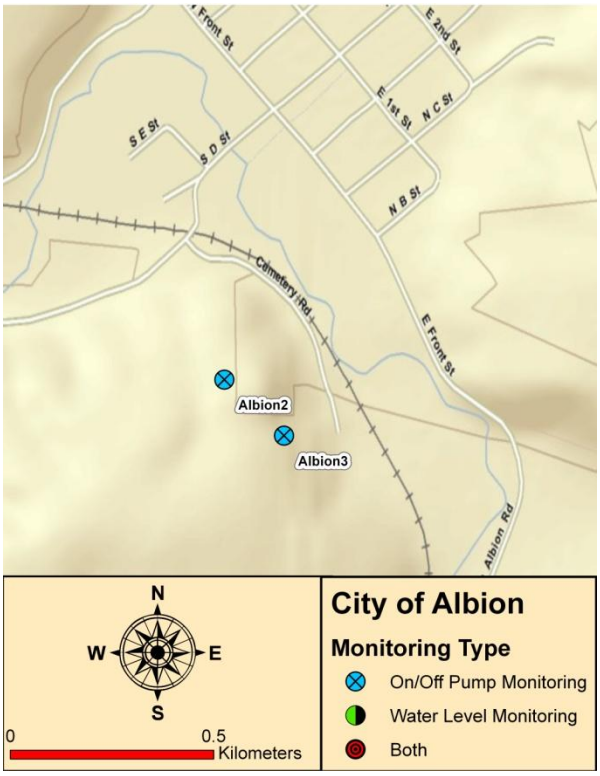

Figure 1.9: City of Albion wells.

1.3 Method of Study

This thesis investigation is designed to help conceptualize aquifer heterogeneities, and compartment boundaries and areas, well hydraulic connections, and aquifer properties. An effort also is made to delineate the causes of water level fluctuations not explained by pumping stresses. Some of these include small magnitude fluctuations that are thought to be related to incomplete removal of the effects of barometric pressure changes. Typically barometric changes cannot be totally removed from all of the data, and when combined with equipment "noise" tend to produce clusters or "clouds of data points on graphs that may mistakenly be attributed to effects of pumping wells if the investigator does not take them into account.

Data collection in the complicated aquifer system provides the opportunity to develop alternative and effective methods for characterizing the system. The Palouse Basin Aquifer Committee (PBAC) has been collecting continuous water level records for approximately a decade for several observation wells in the basin. Several Grande Ronde

investigations funded by PBAC have incorporated short-term aquifer pump tests (e.g., typically 24 hours or less) to study connections between wells across the basin. Short-term aquifer tests provide information about aquifer properties near the wells tested; however, they typically do not provide much information about the rest of the aquifer. Short-term tests previously were designed because area pumpers are not able to remain off-line for more than 12-24 hours because of limited storage capabilities. In order to circumvent this limitation, a multiple-well aquifer testing method was developed using superposition to allow area pumpers to pump as needed, and for aquifer test drawdown data to be collected for an extended period of time for analysis. Some investigators during previous aquifer tests collected drawdown data on one-minute intervals; however, extending the aquifer test for more than one year required increasing the drawdown recording interval to five minutes. A five-minute interval was found to be adequate to capture the shape and details of the observation well drawdown/recovery curves to interpret the hydraulic complexities of the PGB. To address this data need, an extensive groundwater level data collection effort was initiated in November 2009 with a collection interval of five minutes. This study incorporates a two-year long aquifer test data set including all municipal pumping on/off times that have provided the opportunity to confirm and/or refine previous research, and add a wealth of knowledge about the hydrogeologic characteristics of the Grande Ronde aquifer system.

1.4 Purpose and Objectives

The purpose of this investigation is to collect and analyze aquifer test drawdown data for the evaluation of hydraulic continuity across the basin, and to estimate hydrogeologic properties of the Grande Ronde aquifer system. The research was conducted in conjunction with the Moran (2011) investigation, and was extended to 2012 to provide for expanded data analysis. The initial strategy was to reexamine conclusions from previous research and describe how the conclusions from this investigation compare and

contrast with previous investigations. The specific objectives of this investigation include:

- Validate water level trend corrections;
- Develop a data base of calculated drawdown for all observation wells;
- Conduct an analysis of PGB compartmentalization;
- Develop a 10-day moving window" method of analysis for the PGB aquifer test.

This thesis is organized into several chapters. Chapter 2, Hydrogeology of Palouse Basin, describes the local and regional geology while introducing compartmentalization. Chapter 3, Methodology, describes the procedures followed for processing water level data, computation of trend corrections, and estimating specific storage from Rayleigh wave spectral analysis. Delineation of compartments in the Palouse Groundwater Basin is described in Chapter 4. Chapter 5, Data Collection, Compilation and Analysis, outlines the procedure for processing observation well drawdown data to prepare them for analytical modeling input. Chapter 6, Conclusions and Recommendations, summarizes observations from the previous sections and relates the conclusions of this study to the larger context of research on the PGB.

1.5 Previous Research

Previous hydrogeologic investigations in the PGB have made important strides in the understanding of the aquifer properties of the Grande Ronde aquifer system. For a comprehensive review of previous work on the Palouse Basin, the reader is recommended to consult McVay (2007) or the Palouse Groundwater Basin Framework Project (2011). Research presented in this thesis builds on prior research by University of Idaho graduate students using groundwater data loggers and transducers in the PGB. Their research provided important background information about basin aquifer characteristics that were used in the analysis of data collected during this investigation and helped with the completion of this research. A brief review of their conclusions and other research that were crucial to the completion of this investigation is presented below.

1.5.1 Sokol (1966)

This study focused on monitoring water levels in the Moscow and University of Idaho wells. Sokol delineated two hydrologically distinct Grande Ronde aquifers which exist beneath the Moscow area. The aquifers are separated vertically by low permeability layers. The deepest aquifer is located about 328 meters below the land surface (approximate elevation of 460 meters above mean sea level (amsl) and provides water to wells Moscow 6 and Moscow 8. The second aquifer is about 238 meters below the land surface (approximate elevation of 550 meters amsl) and provides water to University of Idaho well #3 (UI 3). This conceptual model of vertical separation has influenced Palouse Basin research ever since. Drilling records for Moscow 6 and Moscow 8 illustrated the irregular and discontinuous nature of the Grande Ronde aquifer system. Moscow 6 did not encounter a basalt unit of the middle Grande Ronde (the production zone for UI 3).

Barometric efficiency (BE) in the PGB was considered for the first time during Sokol's analysis of water levels, which proved to be quite significant. He showed that the sensitivity of Grande Ronde water levels to atmospheric pressure changes was enough to mask seasonal groundwater fluctuations. After removing barometric pressure changes, he was able to describe hydraulic connections in the Moscow Area. He observed a strong connection between Moscow 6 and Moscow 8. Moscow 7 did not show measureable drawdown to any of the area pumping wells. UI 3 did not show a hydraulic connection to either Moscow 6 or Moscow 8.

Sokol was the first researcher in the Palouse Basin to correlate unexplainable water level fluctuations (not related to barometric pressure or pumping) to global seismic events. He observed groundwater fluctuations induced by several distant earthquakes in UI 3 and Moscow 8. From these seismic events, he recorded groundwater fluctuations ranging from 0.01 to 1.5 meters. Contrary to UI 3 and Moscow 8, the Moscow 7 well did not respond to a single seismic event. Sokol concluded this difference is probably due to the fact that UI 3 penetrated one or more zones or horizons below the stratigraphic interval penetrated by Moscow 7. Sokol hypothesized that the granitic rocks penetrated by UI 3 were responsible for transmitting/amplifying the seismic waves. The 1964 Alaskan

Earthquake and aftershocks produced greater hydroseismic magnitudes in PGB wells than in any other well in the three northwestern states (Vorhis, 1967). Vorhis (1967) investigated the geographic distribution of hydrologic effects from the 1964 Alaskan Earthquake in each state, Canadian province, and continent. Sokol believed that these greater hydroseismic magnitudes were due to the PGB plunging westward in the direction of the epicenters. Seismic responses observed during this investigation will be discussed in Chapter 3 and Appendix C.

1.5.2 Owsley (2003)

Owsley (2003) conducted several aquifer tests to evaluate the hydraulic connectivity between wells completed into the Grande Ronde basalts in Moscow, Pullman, and Palouse. Conclusions included:

- The DOE monitoring well (approximately halfway between Moscow and Pullman) responded to Moscow pumping, but no response to Pullman pumping.
- A geological barrier separates the Pullman pumping producing zones from the DOE completion zone.
- The Grande Ronde system is compartmentalized into hydraulically separated units on short time scales (aquifer tests).
- Three hydraulically separate Grande Ronde aquifers were delineated from cross-sections and aquifer tests.
- Hydraulic connections between the city of Palouse and Moscow/Pullman were believed to have been observed during aquifer tests.
- Pre-test water level trend corrections were used to identify specific antecedent trends and derive calculated drawdown responses.

1.5.3 McVay (2007)

McVay (2007) conducted aquifer tests utilizing existing municipal, university, and domestic wells completed in the Grande Ronde aquifer system. PGB hydraulic connectivity and boundary conditions were interpreted from the aquifer test data. The following conclusions were made:

- Grande Ronde aquifer system is comprised of multiple producing zones that are connected on a regional scale, but isolated to some degree on local scale.
- Hydraulic connections between Moscow, Pullman and possibly the city of Palouse were observed during aquifer tests.
- A shifting hydraulic boundary develops between the pumping centers of Moscow and Pullman because of seasonal variations in groundwater withdrawals.
- Aquifer testing suggests that aquifer transmissivity in the Pullman area is approximately one order of magnitude higher than in the Moscow area.

1.5.4 Fiedler (2009)

Fiedler (2009) modeled aquifer test data using analytical methods with the goal of delineating the PGB hydraulic connectivity. Aquifer characterizations were based on the Hantush-Jacob (1955) method for a leaky or multiple aquifer system. Conclusions included:

- The Grande Ronde aquifer system in the Moscow-Pullman area consists of an interconnected, multiple aquifer/aquitard system.
- Cornelius and Pullman 6 respond to Pullman 8 and WSU 7 pumping.
- The IDWR 4 well is very responsive to pumping of the Moscow 9, UI3, and UI 4 wells.
- No apparent connection exists between the WSU 7 well and the Palouse 1 well for pumping periods of less than 10 hours.
- Evidence was found that some variety of multiple leaky aquifers exists in the Grande Ronde aquifer system.

1.5.5 Snyder and Haynes (2010)

Snyder and Haynes (2010) is a regional investigation that mapped declining groundwater levels and groundwater compartments beyond the boundaries of the PGB. The investigation evaluated groundwater elevations in the Grande Ronde formation in the Columbia Plateau Regional Aquifer System (CPGAS). Because the CPRAS includes several distinctive structural regions with markedly different densities of folds and faults

that may be impediments to groundwater flow, their analysis was designed to evaluate whether the spatial correlation between groundwater levels differed within these structural units for the Grande Ronde formation. This process included variography, which provides statistical measures of the degree of correlation between a groundwater measurement and other groundwater measurements based on the distance and direction that separates them. Typically, wells that are closer together in the same aquifer have similar water levels and respond similarly to stresses. As distance between wells increases, however, the similarity of measured values generally decreases (Snyder and Haynes, 2010). They divided the CPRAS by geographic or structural regions on the basis of significantly different variography to improve the estimates of groundwater elevation developed using a kriging analysis. The regional trend and the kriged residuals, representing the configuration of the groundwater surface without the regional influence, were subsequently added together to produce the generalized groundwater-elevation maps.

1.5.6 Carey (2011)

Carey (2011) conducted an investigation of the PGB groundwater age using isotopic methods. Groundwater samples were collected for age dating using Carbon 14 and Oxygen18/Deuterium. Data collection schemes focused on the data gaps in the PGB. Numerous samples were analyzed for Tritium concentrations which indicate the existence of modern aged water. Her conclusions suggested:

- Modern recharge reaches the upper aquifer (Wanapum) and substantial modern recharge occurs near certain wells in the lower aquifer (Grande Ronde).
- Groundwater in the area is distinctly stratified, and the apparent age of the water increases with depth.

1.5.7 Moran (2011)

Moran (2011) attempted to resolve some of the data consistency problems noted by earlier studies by using standardized data collection equipment and a coordinated approach throughout the basin. Moran monitored water levels and municipal pumping cycles throughout the PGB. Her conclusions included:

- Results from analytical modeling suggest that vertical leakage has a significant effect on water levels in the Grande Ronde aquifer system.
- Direct hydraulic connection exists between wells in Pullman, Moscow, and Palouse.
- The Hantush-Jacob (1955) leaky-confined aquifer solution is appropriate for approximating observed water level drawdown on daily, weekly, and annual time scales.
- The average storativity of the Grande Ronde aquifer system is estimated to be within the range of 3×10^{-5} to 3×10^{-4}.
- Water levels measured in the Colfax Clay Street well exhibit significantly smaller annual declines and long-term declines than water levels measured in Pullman, Moscow, and Palouse.

CHAPTER 2

Hydrogeology of Palouse Groundwater Basin

2.1 Geography and Demographics

The PGB is located on the eastern margin of the Columbia Plateau, in Whitman County, Washington and Latah County, Idaho. The PGB boundaries are formed by the granite and metasediments of Bald Butte and Paradise Ridge to the south, Tomer Butte to the southeast, and the Palouse range to the east and northeast. Kamiak Butte and Smoot Hill, comprised of metasediments and granite, respectively, form part a discontinuous boundary at the land surface along the north and northwest sides of the basin; depth to crystalline rocks in the gaps is not known, but both Grande Ronde and Wanapum basalts are known to exist in the Four Mile creek gap. The western extent of the groundwater basin is yet to be defined.

PGB boundaries, as estimated by Bush (2005), encompass an area of approximately 1300 square kilometers (518 square miles) as depicted in Figure 1.2. The boundary is only an estimate, and is based on political and water-use demarcations as much as hydrogeologic research (Bush, 2005). It includes the surface water drainage basins of the upper Palouse River and its tributaries, as well as, parts of the Union Flat Creek drainage. The primary reason for a lack of definitive basin boundaries is a paucity of deep monitoring wells outside of the municipal centers (Moran, 2011).

This area is considered semi-arid with average annual precipitation in the area ranging from 50 centimeters per year in Colfax, Washington to 60 centimeters per year in Moscow, Idaho based on approximately 100 years of record (Hopster, 2003). Higher elevations east of Moscow receive more than 100 centimeters per year (Lum et al., 1990).

According to PBAC (2011), 90 % of the PGB population gets its water from the municipal infrastructure. The PGB annual water use was 9.528 and 9.842 million cubic meters (2.517 and 2.600 billion gallons) per year for 2010 and 2011, respectively, resulting in an average per capita usage of approximately 120 gallons/day. Whitman County, Washington encompasses 1170 square kilometers (87%) of the basin and

according to the 2010 U.S. Census, 37,585 of its residents are dependent on the groundwater resource system. Latah County, Idaho has 26,250 water users accounting for 41% of the basin's population. From 2000 to 2010, the PGB population increased by 7,383 people (1.2%).

2.2 Regional Hydrogeology

The Columbia Plateau regional aquifer system (CPRAS) covers approximately 44,000 mi^2 of Idaho, Oregon, and Washington (Burns et al., 2011). The CPRAS can be divided into four structural regions (Reidel, 2002), with two of these, the Yakima Fold Belt and the Palouse Slope, contained within the Columbia River basin proper. The Yakima Fold Belt is included in the western and central parts of the Columbia Plateau and consists of a series of anticlinal ridges and synclinal valleys. The Palouse Slope in the northern and eastern parts of the plateau is much less deformed and dips gently westward (Burns et al., 2011).

The primary aquifers of the CPRAS are basaltic lava flows of the Columbia River Basalt Group (CRBG) and overlying basin-fill sediments. The CRBG has been divided into six geologic formations by Swanson et al. (1979): Imnaha Basalt, Picture Gorge Basalt, Prineville Basalt, Grande Ronde Basalt, Wanapum Basalt, and Saddle Mountains Basalt. The CRBG erupted intermittently over an 11 million-year period during the Miocene to Early Pliocene (17 to 6 million years ago).

The basalt is very dense, and gray to black in color when unweathered. Fractures are common throughout the basalt in three main forms: columnar hexagonal joints, vertical blocky joints, and horizontal platy fractures. These fractures present possible conduits for water flow and may represent areas where vertical recharge can occur (Figure 2.1). Folding and faulting of the basalts have occurred during periods after emplacement.

Typically, lava erupted quickly and advanced away from the fissure or vent as a single, uniform sheet of lava; however, towards the margin of the CPRAS, depositional style

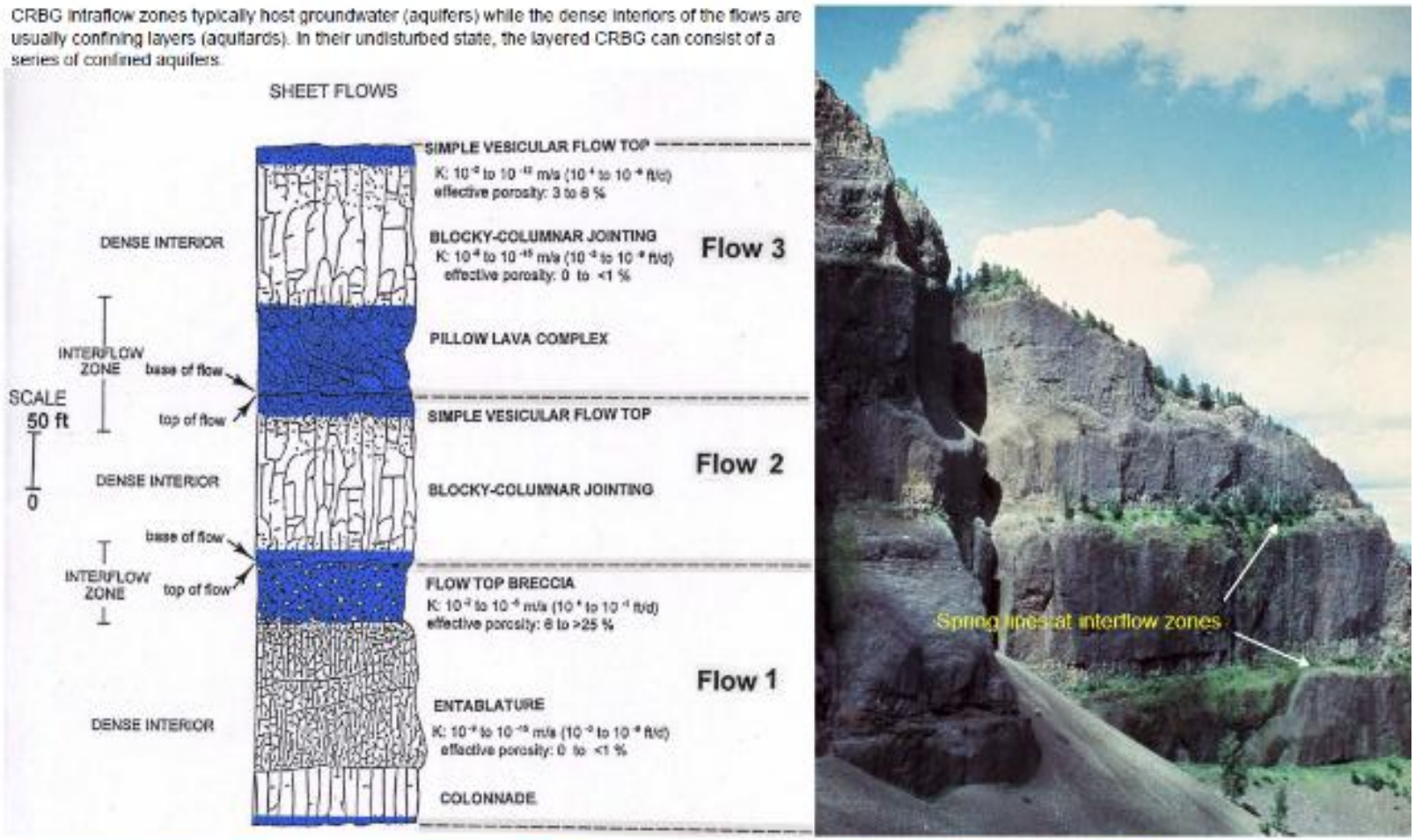

Figure 2.1: CRBG intraflow structures and their relationship to groundwater occurrence (from Porcello et aL, 2011) Note: the interflow zones depicted are rubble zones between indiv idualbasalt flows.

commonly changed from sheet-flow to intra-canyon flows as the volume of lava decreased and the terrain became rugged enough to funnel subsequent flows into valleys and canyons (Burns et al., 2011). Distribution and thickness of younger basalt flows were dominated by the presence structurally controlled valleys. When the hiatus between flows was sufficiently long, soils developed or fluvial and lacustrine sediments were deposited on the surface of a flow. If these deposits were preserved, then a sedimentary interbed or paleosol typically was encased between flows.

According to the Porcello et al. (2011), the following stratigraphic features control groundwater flow in the Grande Ronde:

- Lithology of the basalt flows and interflow zones.
- The lateral pinching out of individual basalt flows and interflow zones.
- The types of rocks lying beneath basalt flows, and significant water bodies or adjoining aquifers that are either potential sources of groundwater recharge or potential receiving areas for groundwater discharge.

2.3 Local Hydrogeology

The basement rocks of the PGB are composed of crystalline pre-Cambrian and Cambrian metasediments, and Cretaceous granite. These rocks are overlain by the flood basalts of the Miocene Columbia River Basalt Group (CRBG), and sedimentary deposits and interbeds of the Latah formation, that comprise the aquifer systems of PGB (Figure 2.2).

The total thickness of the Grande Ronde Basalt (GRB) varies spatially, but the thickest areas of the basin are over 400 meters (Figure 2.3). The Grande Ronde formation is separated from the overlying Wanapum formation by the sedimentary interbeds of the Vantage (Equivalent) member which are part of the Miocene Latah formation. The upper aquifer stratigraphy is shown in Figure 2.4 and includes the Sediments of Bovill (Latah formation), Loess of the Pleistocene Palouse formation, and Holocene alluvium which all overlie the Wanapum formation. The Sediments of Bovill (Latah formation) are located mostly east of the Idaho/Washington state line in the Moscow area that had experienced pre-deposition subsidence. The Saddle Mountains formation is a sequence of minor basalt

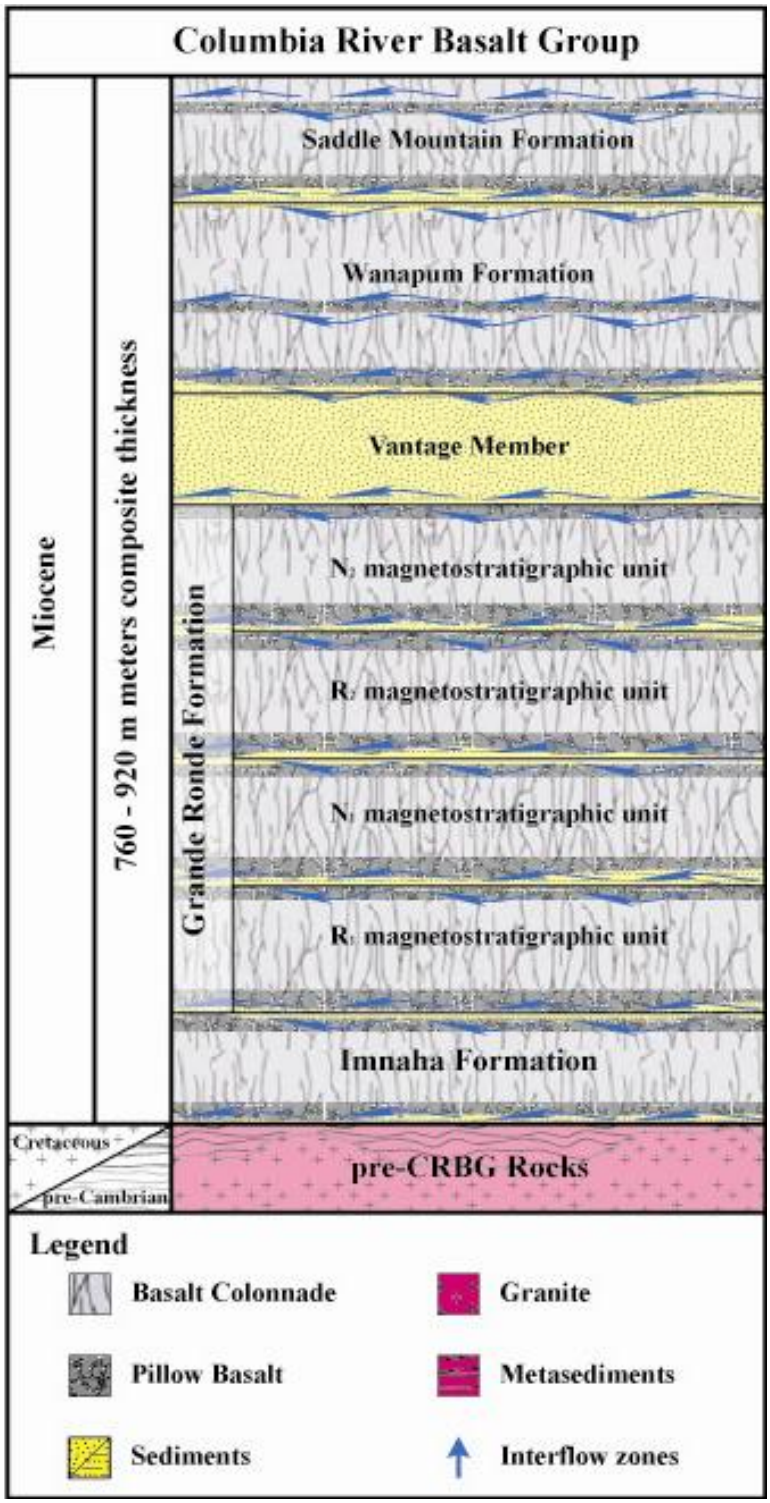

Figure 2.2: Palouse Basin stratigraphy Modified from Bush (2006).

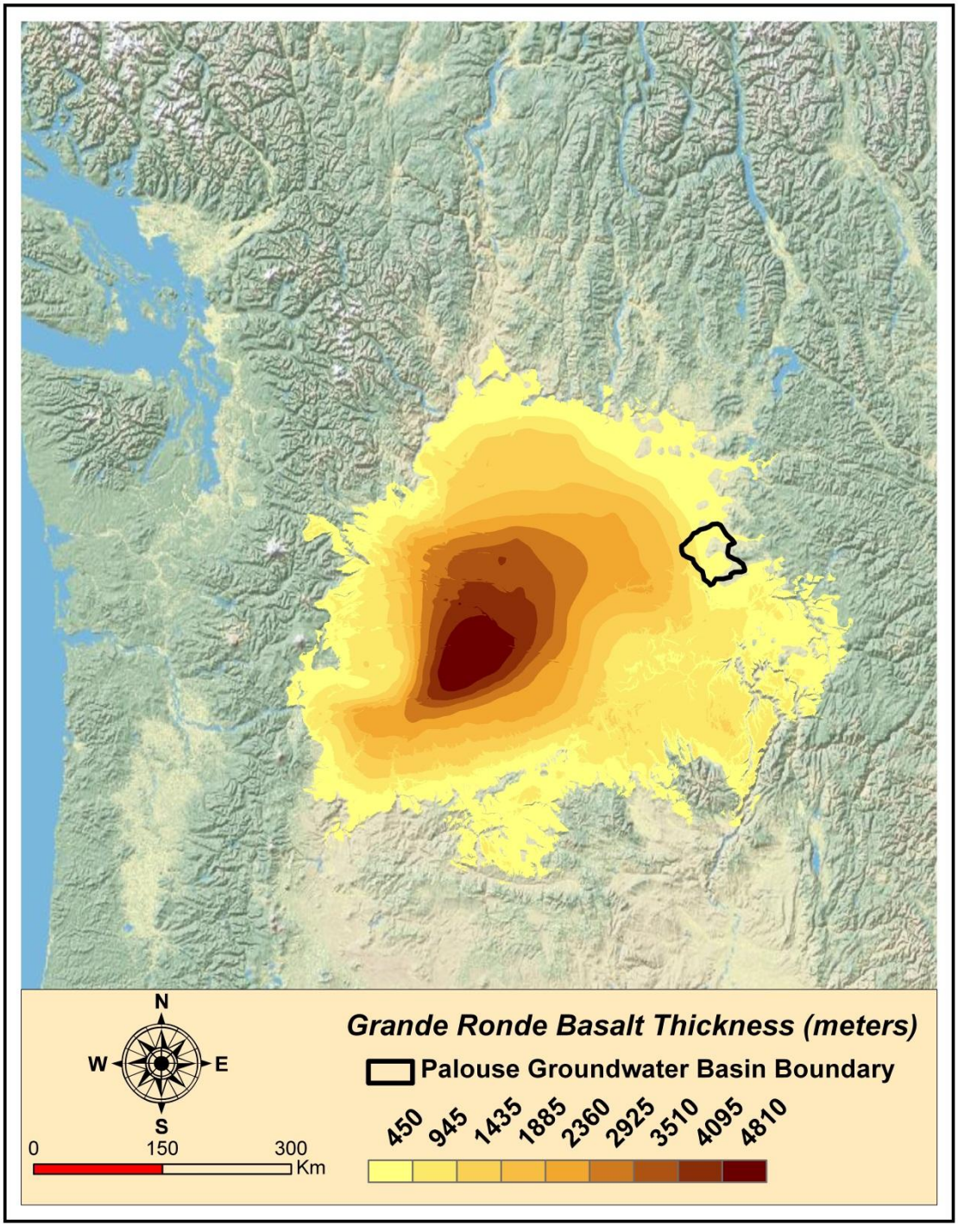

Figure 2.3: Areal extent of the Grande Ronde formation and thickness (Burns et. al., 2011) with PGB boundary in black.

flows that filled paleo-channels. Saddle Mountains basalt has been identified several miles west of Pullman (along Union Flat Creek) (Swanson et al, 1979), and locally under McClure Hall at the University of Idaho (Provant, 1995; Owsley, 2003). In addition, ten feet of the Lewiston Orchards flow of the Weissenfels Ridge Member was identified within the Sediments of Bovill in the IDWR 1 well in northwest Moscow (Bush, 2006).

Four formations of the CRBGs have been identified in the PGB: from bottom to top they are the Imnaha, Grande Ronde, Wanapum, and Saddle Mountains. The Imnaha is stratigraphically below the Grande Ronde and has only been encountered by one well borehole (WSU 7) at approximately 574 meters below the ground surface (Ralston 1987). The Wanapum and Saddle Mountains both exist above the Grande Ronde; the Saddle Mountains is above the Wanapum, but the Wanapum is much more wide spread in the PGB. Basalt flows in the PGB dip slightly to the east between Moscow and Pullman (Bush, 2006). The Grande Ronde comprises about 90% of the total CRBG by volume (Reidel and Hooper, 1989), and consists of fine to very fine grained Miocene aphyric basalt flows that are interbedded with layers of Latah formation sediments (Wright et al., 1973; Swanson et al., 1979). Up to 17 different flows are believed to exist in the western part of the PGB; however, geochemical, stratigraphic, and paleomagnetic analyses are required to distinguish them from each other (Reidel and Hooper, 1989; Provant, 1995; Teasdale, 2002).

Water in the Grande Ronde is stored in the interflow zones and flow tops that have been exposed to weathering between basalt flow events. These interflow zones are made up of complex internal structures such as pillow lava complexes and flow top breccias that provide highly permeable pathways for productive aquifers. The exchange of groundwater between these interflow zones occurs through a series of cracks, joints and fractures. Both horizontal sheet joints and vertical joints serve as conduits for water transport. The flow interiors are very dense and consequently have low permeability, but quench fractures protrude through entire flows (Sawlan, 2011). Quench fractures are hypothesized to provide conduits for the leakage that support long-term system wide hydraulic connections between upper and lower aquifers in the Grande Ronde aquifer system.

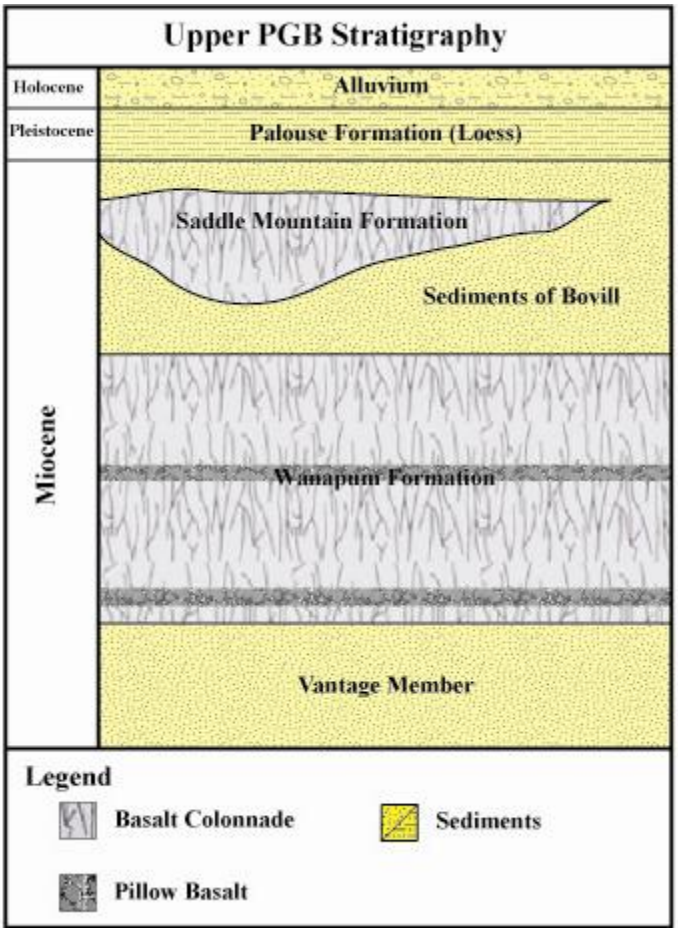

Figure 2.4: Upper PGB stratigraphy Modified from Bush (2006).

The CRBG interflow zones are commonly confined systems that occur in thin, highly compartmentalized interflow zones overlain by dense, low permeability flow interiors. Many such water-bearing interflow zones exist in the PGB, but their compartmentalized nature results in little direct connection between compartments. Compartmentalization in the PGB will be discussed further in Chapter 4.

CHAPTER 3

Methodology

3.1 Introduction

Much of the data analyzed in this thesis is derived from Moran (2011); however, one important difference exists in their interpretation. Moran (2011) was able to show localized pumping connections in monitoring wells in the vicinity of the individual pumping centers. From the data, no apparent connection was found to exist on the order of days or weeks between the cities of Moscow and Pullman cones of depression. This lack of hydraulic connections as described by Moran (2011) was the most important factor that led to the current conceptual hydrogeologic model that subdivides the aquifer system into separate compartments for the delineation of water level responses, and subsequent analytical modeling of aquifer test drawdown data.

Groundwater levels and municipal pumping schedules were recorded for all major wells within the PGB from November 2009 through May 2012. Compilation of both datasets was completed during the test with the objective of comparing measured drawdown to model theoretical drawdown. The aquifer test (372-day test) used for this analysis started on November 24, 2009 at 21:50 with the resumption of pumping in WSU 4 (t=0) after a 24-hour period during which all major Grande Ronde pumping wells including WSU 4 were shutdown (pre-test no pumping period). Elapsed time for the aquifer test is expressed from this t=0 unless specified otherwise. The raw water levels required some preprocessing. The absolute pressures recorded by the Leveloggers® were first converted to gage pressures by subtracting the barometric pressures from the absolute pressures for each time increment. Water levels were converted to depths-to-water using a reference point on the well casing, and then converted to groundwater elevations using surveyed top-of-casing elevation data (Appendix A, Table A02). A good review of the methods used in this project to preprocess water level data can be found in Moran (2011). The process of barometric correction will be discussed in the following section.

3.2 Barometric Correction of Water Levels

Barometric pressure fluctuations have a significant impact on PGB water levels. These barometric effects, if not accounted for, can lead to erroneous interpretations of hydraulic head and hydrogeologic characteristics. The methods for barometric correction of water levels used herein follow the same procedures applied by Moran (2011). In a confined aquifer system, well water levels (WL) theoretically respond instantly to changes in atmospheric pressure (ΔB). This instantaneous ratio of change in water level (due to barometric effects) to barometric change is constant for any given well, and designated as its barometric efficiency (BE).

$$BE = \frac{\Delta WL}{\Delta B} \qquad \text{Eq. 3.1}$$

In order to calculate BE from well data, the dataset must include water levels and barometric measurements collected simultaneously (or within a justifiably short time span). Barometric efficiency can vary between zero and one. BE=1 typically describes confined aquifers with incompressible skeletons, and BE=0 represents shallow unconfined aquifers with direct connection between the water table and the atmosphere through pore spaces in the vadose zone. The individual well barometric efficiency values presented in Table A01 in Appendix A are used to analyze water level data for this investigation. This section describes the use of the barometric correction procedures.

Static water levels in PGB wells typically show an inverse relationship to the barometric pressure changes as illustrated in Figure 3.1; M&M water levels not corrected for BE mirror the barometric pressure changes over time. These fluctuations related to barometric pressure variations potentially conceal water level changes caused by pumping, recharge, and long-term trends. "Barometric correction" of water levels can be performed with Eq. 3.2, where $WL_{correct}$ is the corrected water level, WL is the original (gage) water level, BE is the barometric efficiency, B is the barometric pressure , and B_1 is the initial barometric pressure for the series being corrected.

$$WL_{correct} = WL + [BE \times B] - [BE \times B_1] \qquad \text{Eq. 3.2}$$

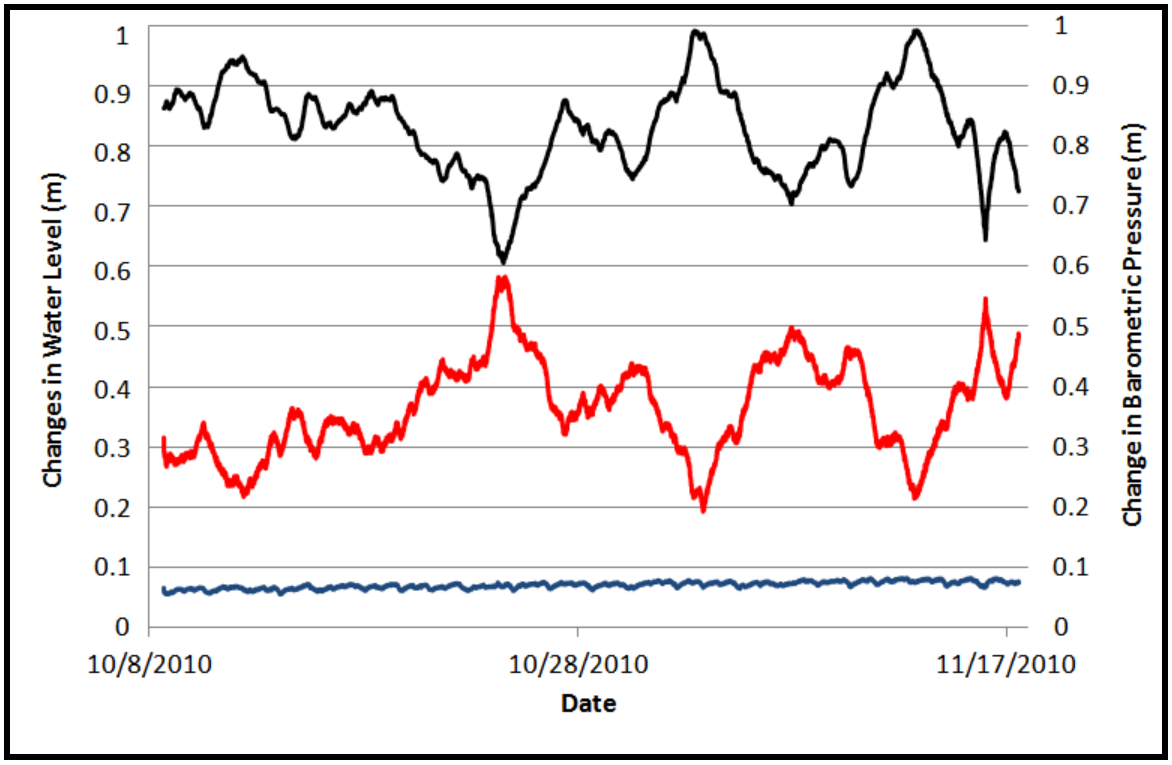

Figure 3.1 Plotted Motley-Motley (M&M) uncorrected water levels (red) versus time compared to water levels corrected for a BE = 0.99 (blue). Barometric pressure is recorded continuously by a Solinst Barologger® in the IDWR 1 well. Barometric pressure changes versus time are shown in black for reference.

A trial-and-error (graphical) method was used to estimate the BE value for the M&M, Pullman 3, WSU 6, and Moscow 6 wells. This method was selected because water levels in these wells vary widely due to effects of Moscow or Pullman area pumping. The most effective way to apply the trial-and-error method is to eliminate unlikely BE values from consideration by plotting water levels that were corrected for a range of BE values (Figure 3.2 A.). The best time periods to compare different calculated BE values is during periods of less basin pumping. During these periods one can easily remove water level fluctuations related to barometric pressure variations. Estimated BE values that are too low will result in a plot of water levels versus time that mirror the barometric pressure record while plots for BE values that are too high will mimic the barometric pressure record. Using visual judgment, the best BE is the one that generates the smoothest water level plot without exhibiting the aforementioned characteristics. Figure 3.2 A. shows that barometrically corrected water levels using BE values equal to 0.70 and 0.80 mirror the

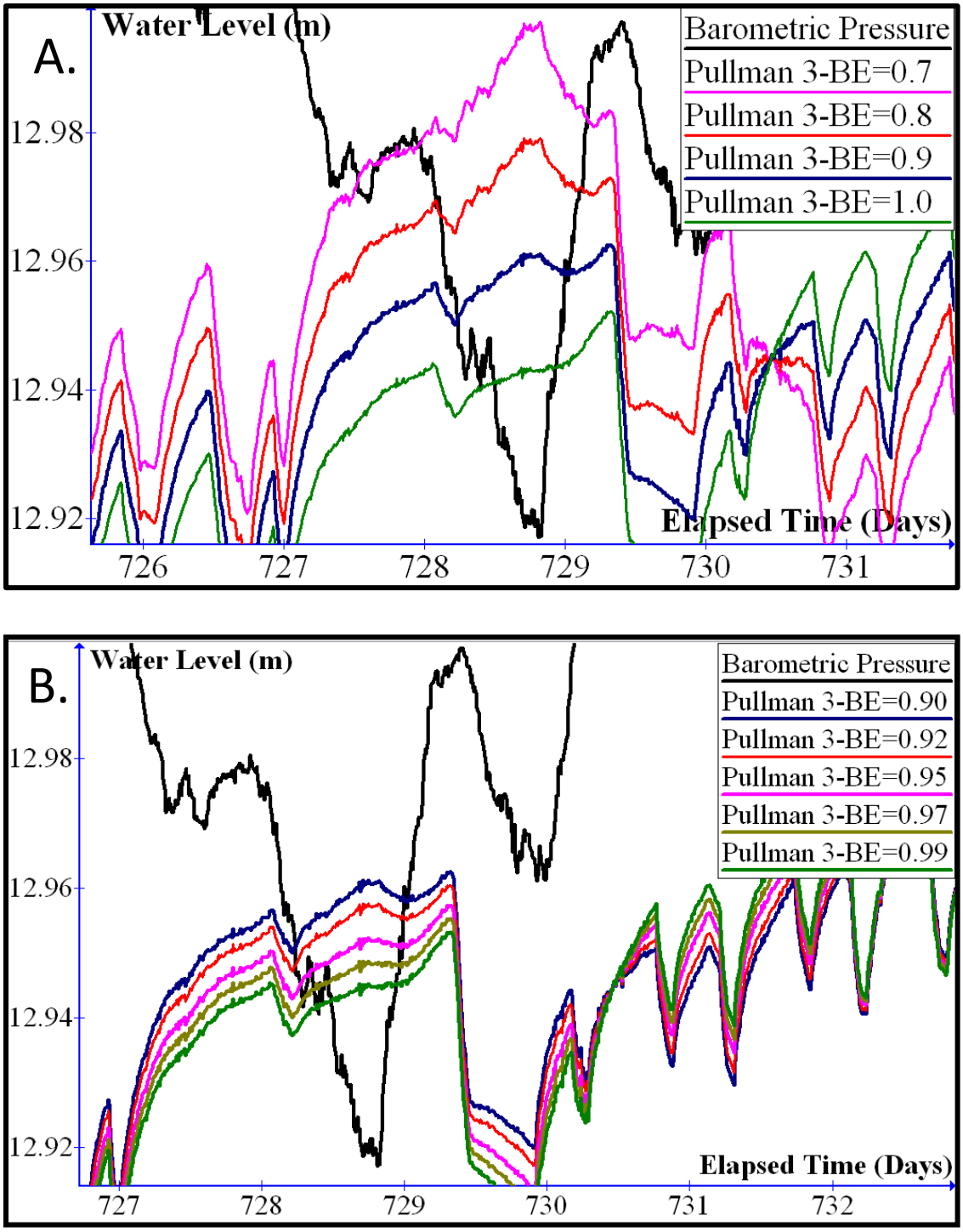

Figure 3.2: A. Plotted Pullman 3 barometrically corrected water levels using a range of BE values (0.70, 0.80, and 0.90). B. Plotted Pullman 3 barometric corrected water levels using a range of BE values (0.90, 0.93, 0.95, 0.97 and 0.99).

barometric pressure record. BE values greater than 0.90 generate the smoothest water level plots while the plot for BE=1.0 mirrors the barometric record. Figure 3.2 B compares five different BE values and the BE=0.92 generates the smoothest water level plot.

3.3 Barometric, Solar, Lunar and Levelogger® "Noise"

Accurate barometric corrections are considered vital to the analysis of the meaning of changes in water levels. Barometric effects will always cause some degree of uncertainty when small magnitude water level fluctuations are observed in hydrographs. For example, the "remnants of basin pumping" interpreted by Moran (2011) throughout the basin during the periods of reduced pumping are now interpreted to correspond to dramatic changes in atmospheric pressure. The barometric efficiencies generated by Moran for Palouse 1, IDWR4, and DOE are too high causing the "barometrically corrected" water levels in the three wells to mimic the barometric pressure rather than indicate an artifact of previous basin pumping as Moran (2011) suggested (Figure 3.3). Since these changes in water level are diurnal, they also may partially be related to earth tide influences. These characteristic changes in water level are only visible when pumping in a compartment hasn't occurred for greater than 48 hours.

A Solinst® Gold Barologger® and a Solinst 10 m. Gold Levelogger® were placed in the IDWR1 well (IDWR 4 vicinity) at the same elevation above the water level (i.e., both loggers recorded barometric pressure at the same time) for the collection of barometric data to understand how individual loggers affect the process of barometric corrections. The results showed that as much as 0.01 meters of discrepancy occurred between the Barologger® and the Levelogger® records (Figure 3.4) when they both recorded identical conditions(i.e., atmospheric pressure). The Solinst 10 m. Gold Levelogger® manual gives the sensitivity ratings for the Gold Barologger® as 0.001 meters and Gold Levelogger® as 0.005 meters. The barometric data recorded by the Solinst® Gold Barologger® were removed (subtracted) from the Solinst 10 m. Levelogger® to evaluate how much potential noise is generated by the differing sensitivities of the two types of loggers.

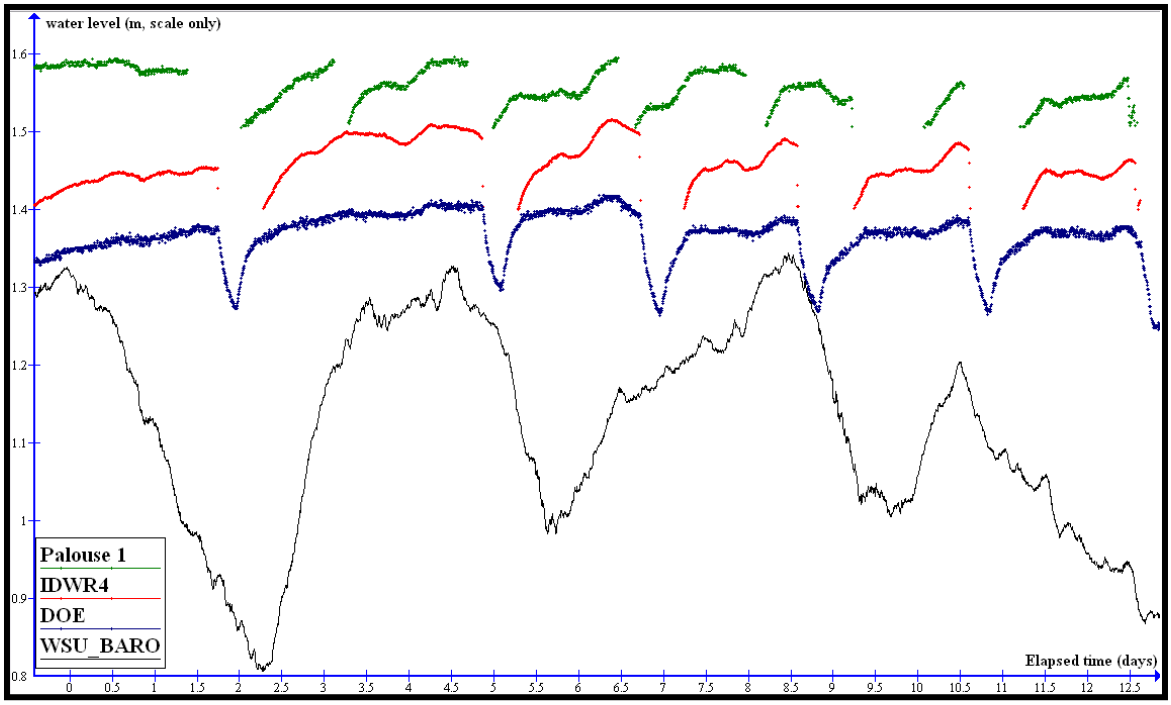

Figure 3.3: Illustration of "low-magnitude features" in well water levels relative to the barometric pressure record (from Moran, 2011). Note: the WSU_BARO in the legend refers to the gold Barologger® record for the WSU Test well location.

"Noise" can also be attributed to the model of Solinst® groundwater Levelogger® used. For data analysis purposes, older Levelogger® models such as the Solinst® silver give lower quality water level results. This is illustrated in Figure 3.5, when comparing the water levels from two different Levelogger® models in the WSU Test well for identical times and water levels (note: scales are offset to show spiky nature of the data). As illustrated, a lot of "noise" (i.e., spiky data) is contributed by the older Levelogger® that could potentially mask other small pumping influences in the area or mistakenly be interpreted as pumping effects during aquifer tests. Updating to a newer gold Levelogger® in the Cornelius observation well revealed water level changes related to solar and/or lunar tidal stresses that were not discernible before.

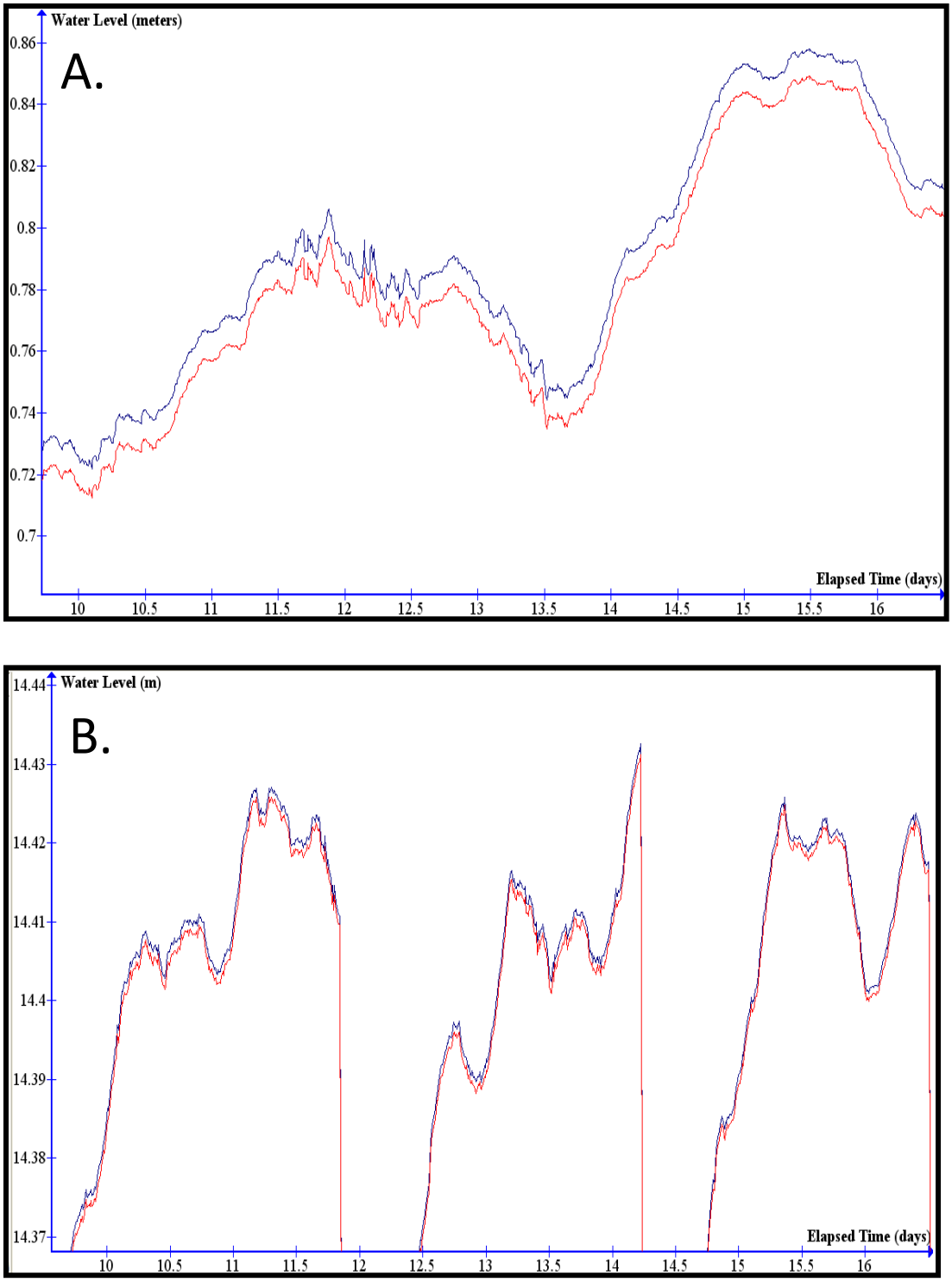

Figure 3.4: A. Examination of raw barometric data from the actual deployed Barologger® (blue) and the test Levelogger® (red). B. IDWR 4 water level barometrically corrected by the actual deployed Barologger® (blue) relative to the test Levelogger® barometric correction (red). Vertical axis is for scale comparisons only and does not indicate relative elevations.

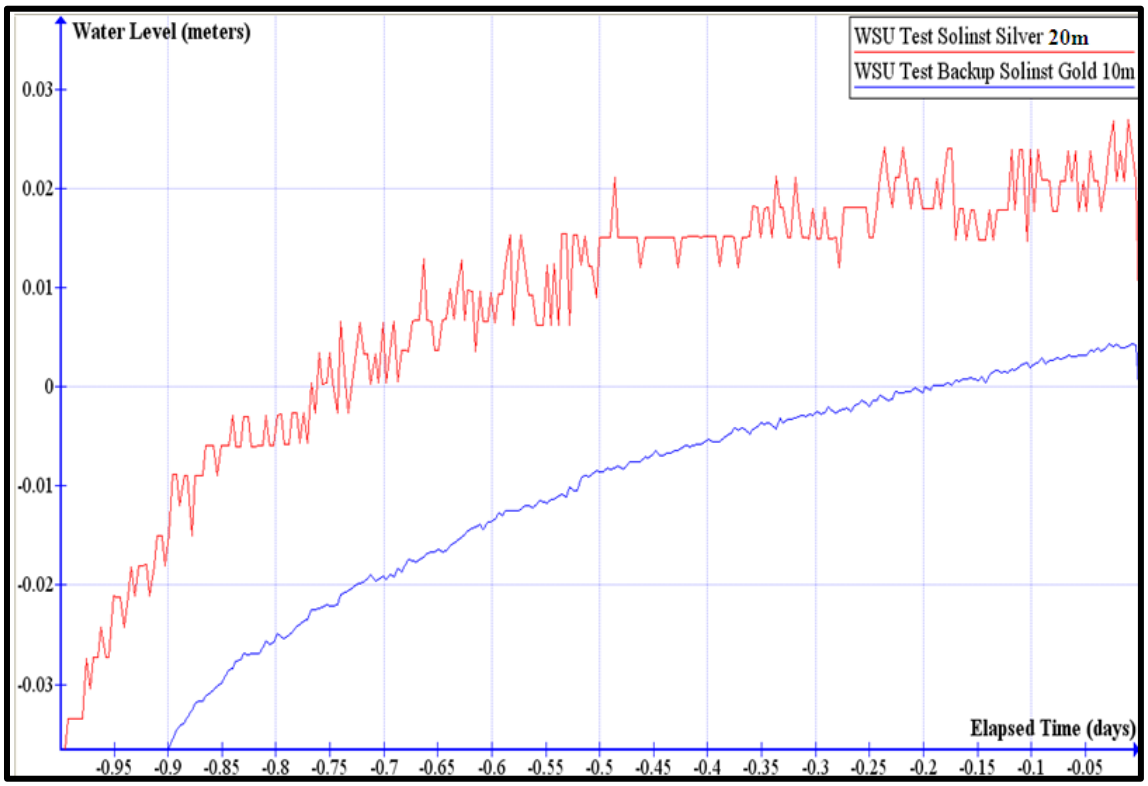

Figure 3.5: Comparison of barometrically corrected water levels recorded by a Solinst LT 2005 20 meters (red) versus a Solinst Mini LT Gold 10 meters (blue). Vertical axis is for scale comparisons only and does not indicate relative elevations.

The gravitational influences of the sun and moon cause sea level to rise slightly at some locations on the surface of the earth and to fall at other locations, depending on the geometric relation of each location with the astronomic bodies and the mass of the earth (Merritt, 2004). These sea-level oscillations vary periodically with the changing positions of the sun and moon at a given location and are referred to as ocean tides. Small fluctuations have been observed in numerous PGB wells after the pumping has ceased. The pumping in an individual compartment must be off for a time period varying between 12 hours to over 48 hours depending on the wells recovery response in order to detect these small fluctuations. This section will examine three wells that exhibit these gently sloping "rolling hills" shaped features in plots of the water level data.

Two of these wells, WSU 5 and Cornelius showed limited to no hydraulic connection to municipal pumping wells in their compartment. Cornelius water levels are influenced by Mr. Cornelius private pumping activity in the well and this creates noise that decreases

the accuracy of the earth tide analysis. However, Palouse 3 has a strong hydraulic connection to Palouse 1 and because the city pumps small volumes of water compared to the other municipalities, these wells provide relatively clean water level data for an earth tide analysis. The rolling hills in the Palouse water levels are examined; however, no filter exists to remove pumping effects for earth tide analyses, and pumping drawdown masks earth tide influences.

Using Matlab® software code, solar and lunar earth tides are examined by spectral analysis of groundwater in the PGB. The code is presented in Appendix E. The code requires a text file of water levels starting at the beginning of the day (time equal to 0:00) for a minimum of 150 days of data. For the most accurate analysis the data collection interval should be at 5 or 10 minutes.

Gravitational theory predicts that the lunar diurnal tide will result in harmonic subsurface dilatations within a few hundred meters of the earth's surface. At latitude θ (N 46.75), the resulting water level deflection in an open water well in a confined aquifer is given by

$$A_{O1} = - 1.56 \times 10^{-8} \sin(\theta) \cos(\theta) / S_s \qquad \text{Eq. 3.3}$$

where: A_{O1} is the amplitude of the lunar diurnal fluctuation at time periods of 0.517 and 1.0758 days and S_s is the aquifer specific storage (Bredehoeft, 1967; Merritt, 2004). Figure 3.6 A through Figure 3.6 C shows the amplitude spectrum of the water level fluctuations for the Cornelius, WSU 5, and Palouse 3 wells. The WSU 5 spectrum shows both solar and lunar tidal effects; however, the lunar tide amplitudes are hidden in the noise of the pumping for Cornelius and Palouse 3. The two solar tides spectral peaks cannot be used because all solar tidal effects are contaminated by daily atmospheric pressure changes (Merritt, 2004).

Using the Matlab® code, the amplitude value at the time periods 0.517 and 1.0758 days and the resulting S_s were generated from Eq. 3.3. Cornelius had an A_{O1} obtained from either Figure 3.6 A or Matlab® equal to 0.0011 m. Eq. 3.3 yields a S_s value equal to

2×10^{-5} 1/m. A_{O1} generated from Figure 3.6 B or Matlab® equals 7.1×10^{-5} m for WSU 5, resulting in a S_s value of 1.2×10^{-4} 1/m. Data for Palouse 3 yielded an A_{O1} from Figure 3.6 C or Matlab® equal to 0.0039 m, resulting in a S_s value of 1.8×10^{-6} 1/m.

Examination of Cornelius shows that it is strongly influenced by solar tides at 0.5 and 1.0 days. The local pumping in the well creates spectral noise so that the lunar tides can't be delineated visually. The Matlab® code analyzes the expected time of the lunar influence, but the accuracy of the aforementioned results can't be confirmed. The code calculates a percent error of 15.6% for Palouse 3 and 65.3% for Cornelius which are high due to the noisy datasets. This solar response is large enough that the Cornelius water levels need to be corrected for solar tides before examination of hydraulic connections can be made. The WSU 5 spectrum is significantly influenced by both solar and lunar tides. The absence of pumping influences in WSU 5 makes the well data appropriate for lunar tidal spectrum analysis. Palouse 3 shows no visual earth tide influence because the amplitude noise is too large due to large drawdown in the well. A complete analysis of the Palouse 3 spectrum is limited by the drawdown in the well. The rolls in the data plot can't for certain be attributed to earth tides, because non-pumping periods of sufficient length do not exist for Palouse 3.

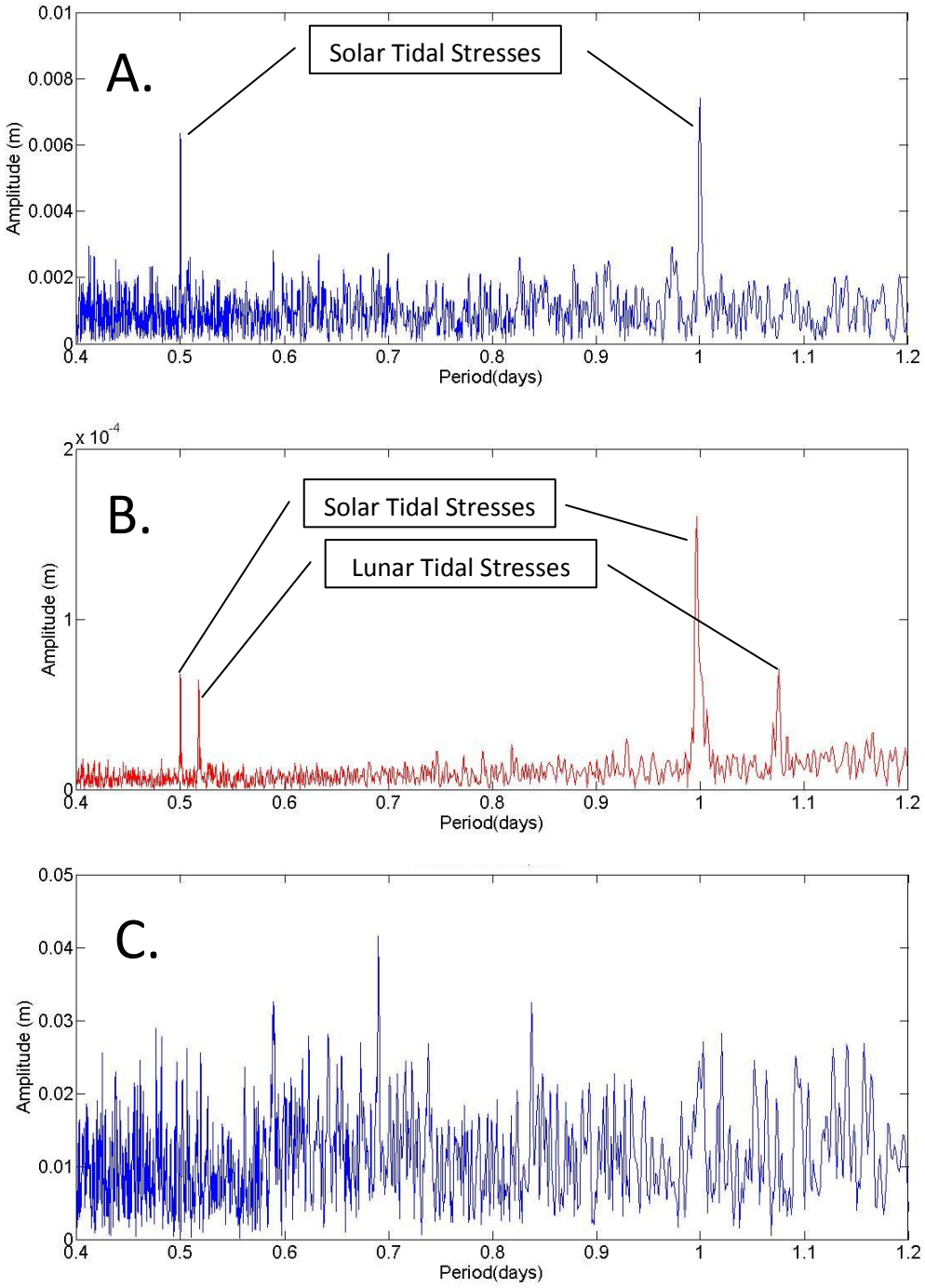

Figure 3.6: A. Cornelius Earth Tide Spectrum. B. WSU 5 Earth Tide Spectrum. C. Palouse 3 Earth Tide Spectrum (372-day dataset).

3.4 Grande Ronde Aquifer System Trend Corrections

This basaltic aquifer system experiences typical aquifer drawdown and recovery plus apparent recharge during the fall/spring seasons of the year. During the summer, irrigation pumping stresses far in excess of non-irrigation season, municipal pumping result in substantial system drawdown. Fiedler (2009) observed frequent short-term and long-term trends in DOE, IDWR4, and WSU Test wells and recognized similarities in magnitude between water level fluctuations in the WSU Test and DOE observation wells.

This information posed the question: how many, if any trend corrections would be needed for the generation of trend corrected drawdown (termed "calculated drawdown" in this thesis). Moran (2011) evaluated the first 372 days of the data set with the application of a unique trend correction for each well developed from the water level recovery recorded in each well during the 2009 pre-test, shutdown period (i.e., 24 hours). For this investigation, several different trend correction methods were evaluated; the following section explains the process of selecting the most consistent procedure. The trend correction method that was selected for the data analysis is based on the regionally composited water level dataset for the entire 2009-2010 groundwater recovery period.

3.5 Groundwater Level Correlations

Groundwater level correlations are apparent over the long-term when observed visually, but further quantitative support is needed. Microsoft Excel® correlations are performed to provide additional evidence; however, this process is biased by the individual spikes and troughs in the data. If these drawdown spikes could be ignored and only the non-pumping "static" water levels correlated, the R^2 values would be greater.

Several steps needed to be taken to determine which observation wells exhibited similar recovery and seasonal groundwater trend changes. This was achieved by performing a Pearson Correlation of the water levels from the same time (t=0) in Microsoft Excel®. This method measures a linear relationship between two variables and a positive correlation means that when one variable increases, the other tends to increase. This process was achieved by organizing all the continuous observation well water levels from

t=0 into the same Excel spreadsheet. A Data Analysis® Package had to be added to an Excel workbook through Excel options. This package includes many different statistical analysis tools, thus the correlation analysis tool must be selected (Figure 3.7).

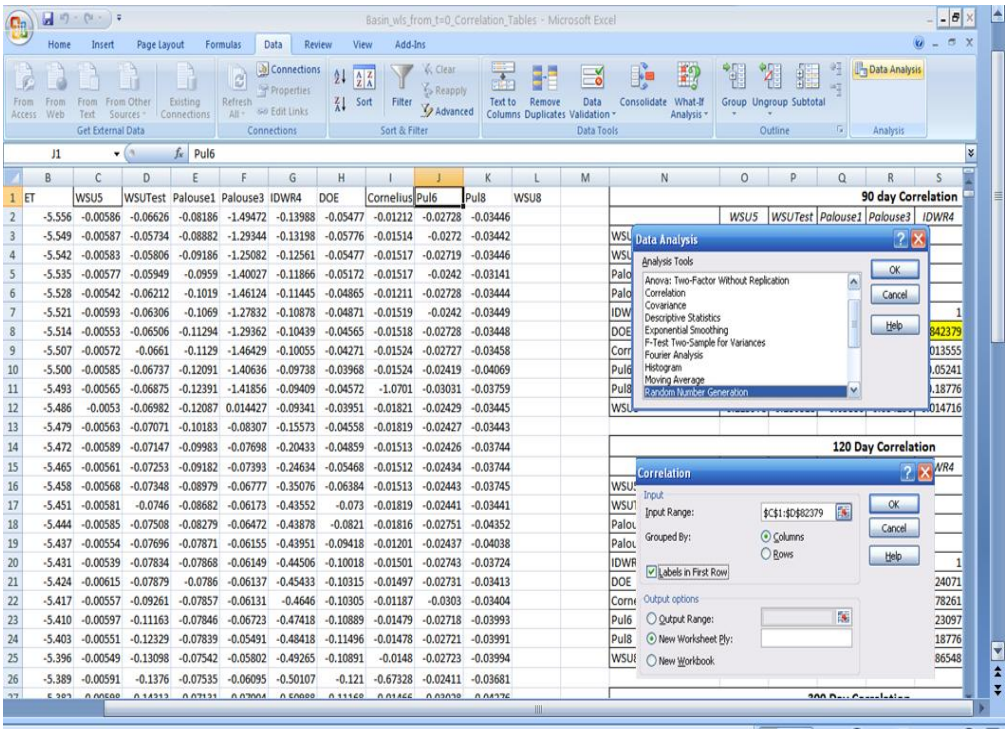

Figure 3.7: Example of the Excel Data Analysis® Package with Correlation Tool window.

To run a correlation on a dataset for a specific time period the correct input data range must be placed into the correlation analysis tool input parameters section. After the correlation is complete, a table will be generated similar to Table 3.1 with the Pearson Correlation Coefficient (ρ). These values demonstrate how well the values are correlated (the closer ρ is to +/- 1 illustrates a better correlation).

Early time data correlations are poor for most wells because each one has a different magnitude of drawdown from a certain pumping well. Also, each well is a different distance from pumping wells so well interference effects can't be accounted for unless all the data are normalized. The magnitude of the influences from well interference can be greatly reduced when larger data sets are correlated.

As the time period for the correlation dataset gets larger, a regional trend and a good correlation (R^2> 90%) between the Moscow-Pullman wells develop. WSU 5, WSU Test, Cornelius, DOE and IDWR 4 with their good water level correlation are used in a regional composite of water levels to develop a regional trend for the Moscow-Pullman area. This composite was generated by combining together all 372 days of data for these five wells and plotted in aggregate. Because the Palouse 3 water levels do not correlate well with the Moscow-Pullman water levels, a separate trend was developed for the Palouse observation wells. Water level correlation between WSU 8 and other wells is very poor due to active pumping in WSU 8. WSU 7 would fall into the same category if a complete dataset was available. The Cornelius correlations are performed on noisy data collected with an older silver Levelogger®; the "noise" played a role in the correlation results. The Cornelius results still show relatively good correlations with the rest of the Moscow-Pullman wells. Both Cornelius and WSU 5 (distinct drawdown spikes and recovery troughs are absent) correlate well with WSU Test (responsive well), this highlights the importance of the wells having similar long-term trends (Figure 3.8).

Pre-Test Trend and 500-Day Correlation							
	WSU5	*WSUTest*	*Palouse3*	*DOE*	*IDWR4*	*Corn*	*WSU8*
WSU 5	1						
WSU Test	0.95	1					
Palouse 3	0.33	0.35	1				
DOE	0.89	0.93	0.37	1			
IDWR 4	0.53	0.61	0.26	0.81	1		
Cornelius	0.86	0.80	0.37	0.74	0.43	1	
WSU 8	0.11	0.21	0.11	0.25	0.25	0.08	1

Table 3.1: Pearson Correlation of groundwater normalized to time t=0 (start of aquifer test) for a 500-day dataset.

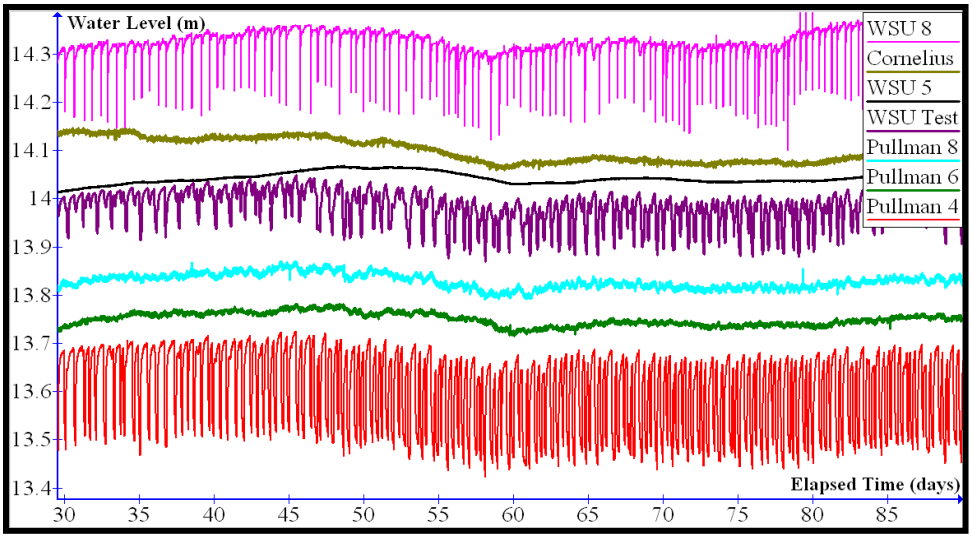

Figure 3.8: Arithmetic plot of water levels for Pullman 4, Pullman 6, Pullman 8, WSU 5, WSU 8, WSU Test, and Cornelius well in LC 3 for the time period of 12/17/2009 to 2/23/2010. Individual plots have been offset vertically in order to compare water level changes (pumping spikes in WSU 8 have been truncated vertically to fit the vertical scale of the plot).

3.6 Regional Trend Development

Water level data for observation wells with complete datasets were used in the development of a single regional trend correction for the Moscow-Pullman portion of the PGB. This trend was developed for the aquifer test period up to the time when continual summertime drawdown started, which occurred at approximately t=200 days for the 372-day test. The trend correction was applied to the data before the summertime drawdown began because the best pre-test trendline proved to be a continuously rising natural log (ln) function as shown in Figure 3.9. After the start of summertime drawdown, a straight line function was applied to calculate drawdown until end of the 372- day test because the rising trend due to system recovery effectively ceased at this time. This straight line function had the following equation: $DD_{calc}=WL_{calc}-WL$ where: DD_{calc} is calculated drawdown, WL_{calc} is the last trend predicted water level before the start of summertime drawdown, and the WL is any measured water level value after summertime drawdown until the end of the 372-day test. Complete water level data sets for four non-pumping observation wells (DOE, IDWR 4, WSU Test, WSU 5) and one pumping domestic well (Cornelius) were plotted together, and a best fit natural log curve was generated

(Figure 3.9). They were all plotted in order from the first well to respond to system recovery (DOE) and that time was considered to be zero. This was done so that all the elapsed time values were positive for the fitting of natural log (ln) function. As shown in Table 3.2, the DOE recovery trend started first, all five water level records from the same t=0 (November 24, 2009 21:50) were compiled together with the start of their respective trends correlated to the start of the DOE recovery trend at 21:00 on 9/15/2009 or 372-day Aquifer Test ET of -70.03.

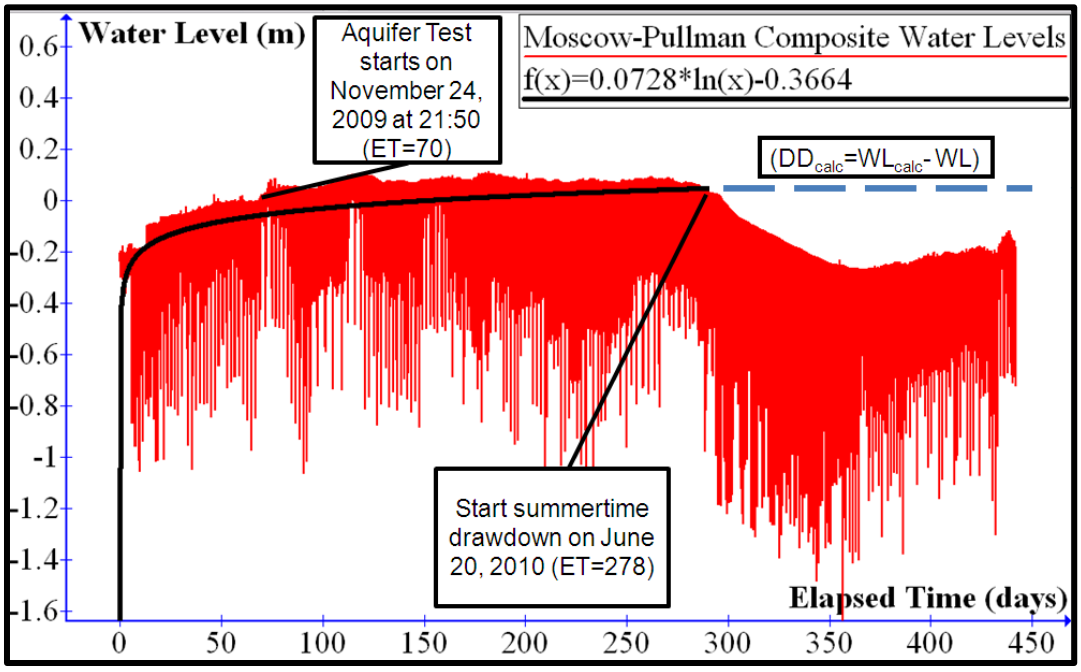

Figure 3.9: Moscow-Pullman area regional trend composite with rising trendline (black line) presented until start of summertime drawdown. A straight line function ($DD_{calc}=WL_{calc}-WL$) was applied after summertime drawdown until end of 372-day test (blue dashed line). The x-axis is elapsed time from start of the DOE recovery period (first Moscow-Pullman well to show seasonal recovery at 21:00 on 9/15/2009 or a 372-day Aquifer Test ET of -70.03 and start DOE trend ET of 70) and the y-axis is change in water levels relative to the water level at the start (zero meters) of the aquifer test (21:50 on November 24, 2009).

Well	ET (days before start of aquifer test)	Estimated start of the 2009 recovery trend after summertime drawdown
DOE	-70.03	9/15/2009 21:00
IDWR4	-64.03	9/21/2009 21:00
WSUTest	-59.91	9/26/2009 0:00
WSU5	-49.83	10/6/2009 2:00
Pullman8	-66.49	9/19/2009 10:00
Cornelius	-56.78	9/29/2009 3:00
Palouse1	-97.03	8/19/2009 21:00
Palouse3	-97.03	8/19/2009 21:00

Table 3.2: Estimated start of 2009 water level recovery from summertime drawdown for selected PGB wells.

The shapes of the trend plots for the other wells (WSU 7, WSU 8, Pullman 4, Pullman 6, and Pullman 8) visually are very similar; however, water level data for these wells were not used to develop the trend because short-term data are skewed more by pumping and recovery spikes than long-term data (Figure 3.9).

Palouse 1 and Palouse 3 water levels correlate poorly with other PGB wells. The differences basically are that water levels were declining continuously in Palouse, where water levels recovered continuously in the Moscow-Pullman area until summertime pumping began. In addition, system recovery from summertime pumping in the Palouse area was distinctly different than for the rest of the PGB and followed a different trend (Figure 3.10). Trend corrections for Palouse were accomplished using the same methods described above. The water levels plotted in Figure 3.10 appear to be more spiky than those plotted in Figure 3.9. This is because far fewer data points are plotted in this graph leaving more space between data points (i.e., less overlapping of data points). However, a distinct difference in water level trends is obvious beginning at about t=200 days for Palouse wells compared to the rest of the PGB wells when Figure 3.10 is compared with Figure 3.9.

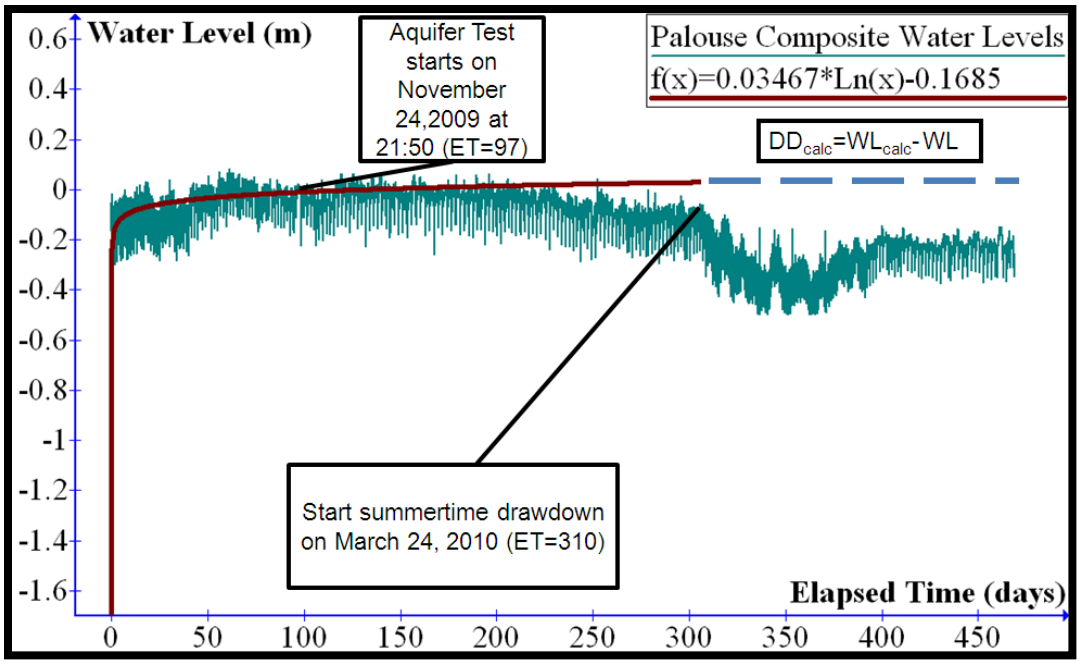

Figure 3.10: Palouse sub-regional trend composite with rising trendline (black line) presented until start of summertime drawdown. A straight line function ($DD_{calc}=WL_{calc}$-WL) was applied after summertime drawdown until end of 372-day test (blue dashed line). The x-axis is elapsed time from start of the Palouse trend (21:00 on 8/19/2009 or a 372-day Aquifer Test ET of -97.03 and start Palouse 3 trend ET of 97.03) and the y-axis change in water levels relative to the water level at the start (zero meters) of the aquifer test (21:50 on November 24, 2009).

The regional trend corrections can be applied to all observation wells that have comparable full-system recovery responses. For the DOE example above, water levels in the entire system (except for Palouse and Colfax area wells) continued to rise in the same manner as before the November 24, 2009 aquifer test, because the aquifer test was designed to restore the same general pumping cycles that existed before the 24-hour pre-test non-pumping period. Short-term aquifer system recovery during the Thanksgiving and university breaks is observed in the Moscow-Pullman area of PGB; however, those effects are considered to be part of the general regional trend. These short-term recovery periods are just "bumps in the road" that get eliminated as soon as the normal pumping is resumed. The separate general sub-regional trend developed for the observation wells in the Palouse area is applicable only for Palouse 1, Palouse 3, Garfield 3, and Garfield 4. Not enough high quality data are available to evaluate whether the general regional trend or a separate sub-regional trend existed for the Colfax area.

3.7 Computation of Calculated Drawdown

The aquifer test started on November 24, 2009 at 21:50 with the resumption of pumping in WSU 4. This is considered to be time t=0 for the computation of drawdown. A general regional or sub-regional rising trend was underway in all wells at the start of the test. Arithmetic plots of water levels versus time were evaluated visually to identify the first consistent (i.e., several measurements) downward deviation ($\geq$0.003 m.) in the general rising trend for each observation well. These deviations occurred at different times in each observation well due to variable distances from the nearest pumping well(s), and are considered to reflect the initiation of drawdown (to the nearest 5 minutes based on 5-minute measurements) due to the resumption of basin-wide pumping. An identical trend correction for the general regional trend was applied for wells DOE, IDWR 4, WSU Test, WSU 5, Cornelius, Pullman 6, and Pullman 8 at the time of the first 0.003 m. of measurable drawdown to "correct" the data for the rising trend, and to allow the "calculated drawdown" to be computed. A different trend correction for a sub-regional trend was applied for wells Palouse 1 and Palouse 3. The calculated drawdown for each observation well was derived from the numerical difference between the measured water levels and water levels predicted for the regional or sub-regional trend (trend predicted water level) for all times $\geq$ the initiation of measurable drawdown. The procedure is illustrated in Figure 3.11 for a graphical definition of drawdown. Figure 3.12A shows the first measurable drawdown (deviation due to pumping) in the WSU Test well and the estimated regional trend. Figure 3.12 B shows the calculated drawdown derived from the regional trend application. This figure is just an example showing the first 100 days of the test, in actuality the trend was extrapolated to the time that summertime system drawdown began in each well. From that time forward until the end

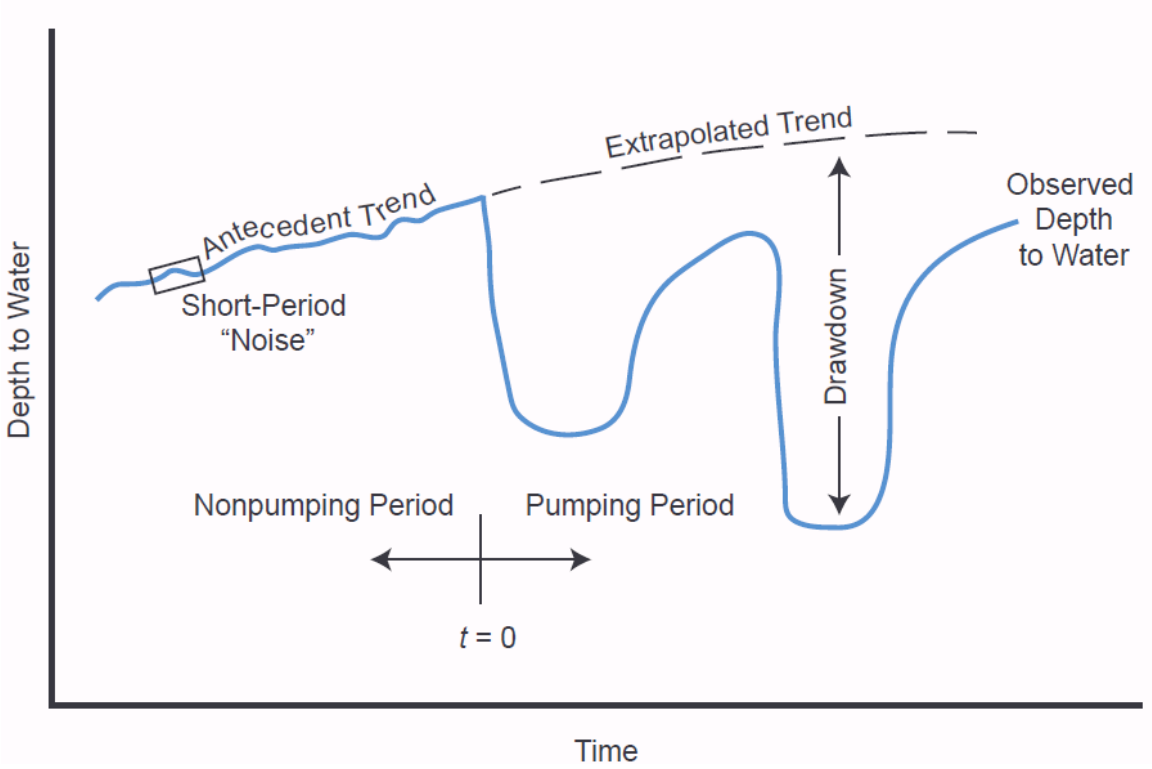

Figure 3.11: Hydrograph for hypothetical observation well showing definition of drawdown (modified from Stallman, 1971).

of the 372-day test, calculated drawdown was derived by subtracting the measured water level in each well from the last trend predicted water level immediately before the onset of summertime system drawdown. The logic behind the change in the trend correction procedure is that at the beginning of summertime irrigation pumping all rising water level trends in the PGB effectively ceased in all observation wells. This cycle of rising and falling water levels occurs each year throughout the PGB at very close to the same times each year. Calculated drawdown for each observation well was derived as described above for the entire 372-days of the aquifer test.

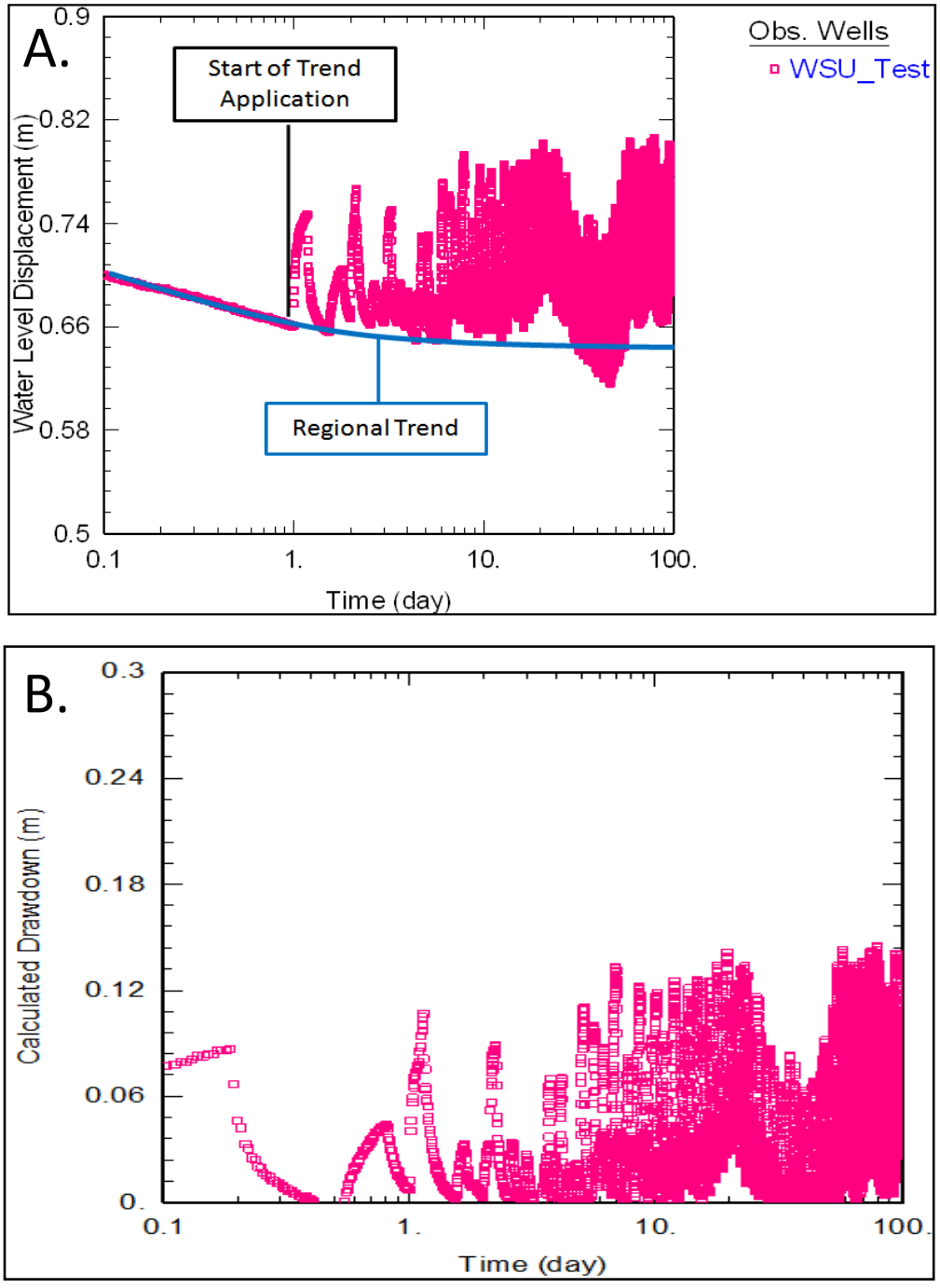

Figure 3.12: A. Semi-log plot illustrating the start of trend application for the WSU Test well. B. Semi-log plot of calculated drawdown derived from the application of the regional trend to the first 100 days of the 372 day aquifer test.

3.8 Storativity Calculation Approach for Water Level Deflections due to Earthquakes

Ordinarily the analysis of earthquake effects on water levels would not be incorporated into aquifer test analyses. However, during the detailed analysis of the water level data and drawdown data collected during this investigation, distinct fluctuations due to notable, "opportunistic", earthquakes that occurred during the aquifer test were delineated. These fluctuations potentially provide an independent means to derive aquifer specific storage for direct comparison with estimates of aquifer storativity based on the same water level data. Based on this comparison, the effective aquifer thickness of the basalt aquifers in the PGB potentially can be derived. Therefore, a method of analysis for the estimation of aquifer specific storage from earthquake effects is introduced herein.

In confined aquifers, observation wells can be sensitive to large global earthquakes and commonly produce hydroseismograms with centimeter scale water level fluctuations. Networks of high quality broadband seismographs cover much of the world while most conventional water well recorders, though digital, sample several orders of magnitude too slowly for comprehensive comparison with seismic shaking. Nonetheless, it is possible to extract a reasonable assessment of aquifer properties even from well records sampled on the order of minutes during the passage of the seismic Rayleigh wave. This section will discuss the foundation of the method based on work done by Shih (2009) followed by an example application of the method to the PGB.

This analysis requires a discussion of the terms used in this method. Groundwater fluctuations from earthquakes are caused by the seismic waves that radiate outward from the earthquake's epicenter. The surface-wave amplitude is usually measured from 20 second (s) period Rayleigh waves, which are very well transmitted along Earth's surface and thus usually well observed. The Rayleigh wave is responsible for the larger magnitude groundwater fluctuations. A Rayleigh wave is a surface wave and includes both longitudinal and traverse motions that decrease exponentially in amplitude. The

wave number (k_x) is the property of a wave that represents its periodicity in space and is calculated from Eq. 3.4 with λ representing the wavelength.

$$k_x = \frac{2\pi}{\lambda} \qquad \text{Eq. 3.4}$$

Eq. 3.5 provides a solution for the aquifer specific storage (S_s) in the proximity of a well by relating the expected amplitude (w) of 20s Rayleigh waves, the wave number (k_x) for the 20s period wave, and the water level deflection (Δh) (i.e., water level change due to the earthquake) with respect to the Rayleigh wave.

$$S_s = \frac{0.918 k_x w}{\Delta h} \qquad \text{Eq. 3.5}$$

Phase arrival times and the expected 20s period surface wave amplitude (w) can be obtained for each individual earthquake from the USGS travel time calculator (http://neic.usgs.gov/neis/travel_times/). Table 3.3 gives the respective 20s period surface wave amplitude (w) and the associated wave number (k_x) used for the PGB specific storage investigation.

Earthquake	20s period surface wave amplitude (w) 1/meters	20s period surface wave number (k_x) 1/meters
M9.0 Japan	8.77E-03	1.12E-04
M8.8 Chile	3.51E-03	1.12E-04
M7.0 Haiti	1.73E-04	1.12E-04
M7.8 Sumatra	2.16E-04	1.12E-04

Table 3.3 USGS referenced amplitudes (w) and calculated wave numbers (k_x).

For each individual well that records a change in water level generated by the arrival of the Rayleigh waves, a specific storage value can be calculated. This provides a method (known here as the Shih method) to estimate specific storage of the aquifer from an event based stress that is applied uniformly over the entire areal extent of the basin. However, the Shih method must be modified because it requires sampling of water levels on a time scale of less than seconds rather than the more typical time scale of minutes or hours

employed in most well recorders. Also, Shih didn't account for borehole response which is included in this investigation.

The Shih method and equation are the theoretical basis for the method discussed below. The method presented herein was applied to PGB water level changes that resulted from the passing seismic waves of four large earthquakes (M8.8 Chile, M9.0 Japan, M7.0 Haiti, and M7.8 Sumatra). Rayleigh wave arrival times and epicenter distances are presented in Table 3.4.

EARTHQUAKE	LR START (PST)	LR END (PST)	Distance (Km)
Chile M8.8 2010 02 27	23:17:09	00:25:25	10198.0
Japan M9.0 2011 03 11	22:19:02	23:27:18	7714.4
Haiti M7.0 2010 01 12	14:14:48	15:23:04	5124.9
Sumatra M7.8 2010 04 06	15:13:34	16:21:50	13617.3

Table 3.4: Rayleigh (LR) waveform time span for the PGB, and distance to the earthquake epicenters.

The analysis will use the M9.0 Japan earthquake as the example. Two quantities that are important parameters in the method will be discussed in further detail. The mean squared water level fluctuations ($E\{h^2\}$) are derived from the squared summation of the change in water level from a static water level that is disturbed by the Rayleigh wave. To compute the spectral density (W_k) of the Rayleigh wave displacement for the M9.0 Japan Earthquake and mean spectral density ($E\{H_k\}$) of the predicted water level fluctuation for a trial value of S_s, an adjustment for the wavelength and the borehole response is applied in the frequency domain that acts partly like a high-pass filter, reducing the influence of the longer wavelength (and typically higher amplitude) Rayleigh waves on the process and partly as a band-pass filter enhancing components near the resonant frequency of the borehole.

In Eq. 3.6, one finds that the mean squared water level deflection ($E\{h^2\}$) can be predicted from the mean value of the Rayleigh wave displacement (W_k) spectral density after adjustment for wavelength and borehole effects. That is,

$$E\{h^2\} = E\{(1/S_s^2)(33.3\,R_k^2/\lambda_k^2)\,W_k\} = E\{H_k\} \qquad \text{Eq. 3.6}$$

where: the borehole storage adjustment ($33.3\,R_k^2/\lambda_k^2$) coefficients include R_k which is the borehole amplification factor and λ_k is the wavelength. Note that λ and R are dependent on frequency as indicated by the subscript k. A more complete explanation for the derivation for the methods equations is presented in Appendix Section C 1.0.

This method takes the mean squared water level fluctuations ($E\{h^2\}$) as measured in the time domain in each well and compares them to the mean spectral density $E\{H_k\}$ of the predicted water level fluctuation for a trial value of S_s (after adjusting to the wavelengths). Figure 3.13 highlights the process of generating these key parameters in graphical form. Figure 3.13A shows the mean square of the water level deflection ($E\{h^2\}$) (orange line) with respect to the Rayleigh wave. Figure 3.13 B shows frequency versus predicted and observed expected values of head with the predicted values being derived from trial and error estimation of S_s. Using Figure 3.13 B, the S_s calculated in this analysis is the value obtained when the standard error is less than one percent as denoted when the two horizontal lines meet resulting in the mean spectral density $E\{H_k\}$ of the predicted water level fluctuation. Additional details about earthquake effects on water levels in the PGB are presented in Appendix Section C 2.0.

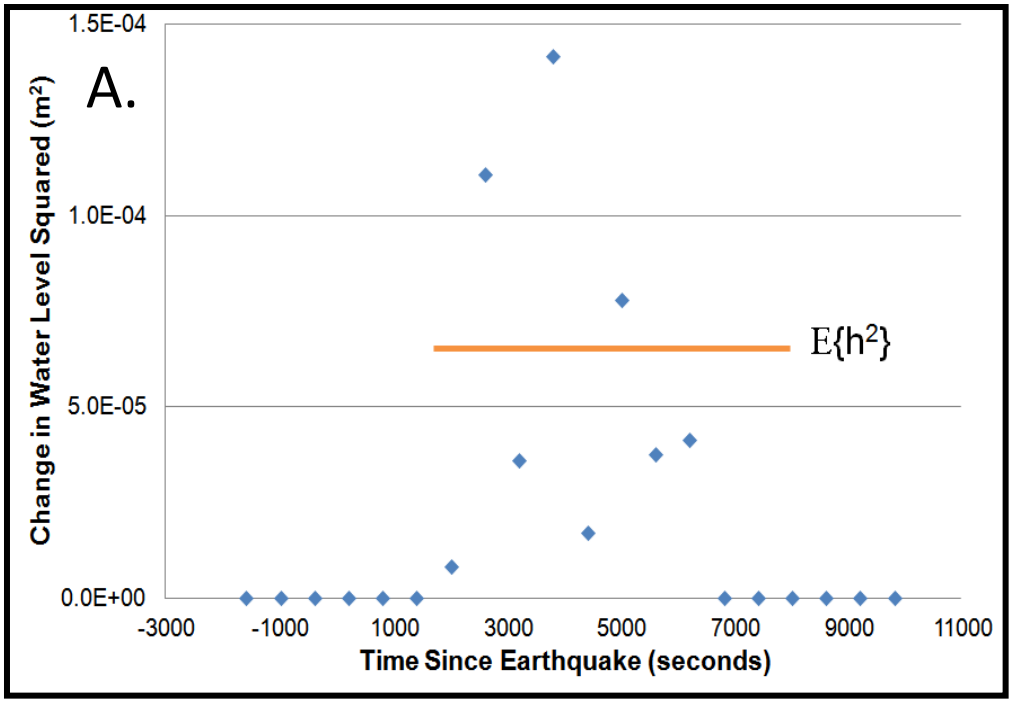

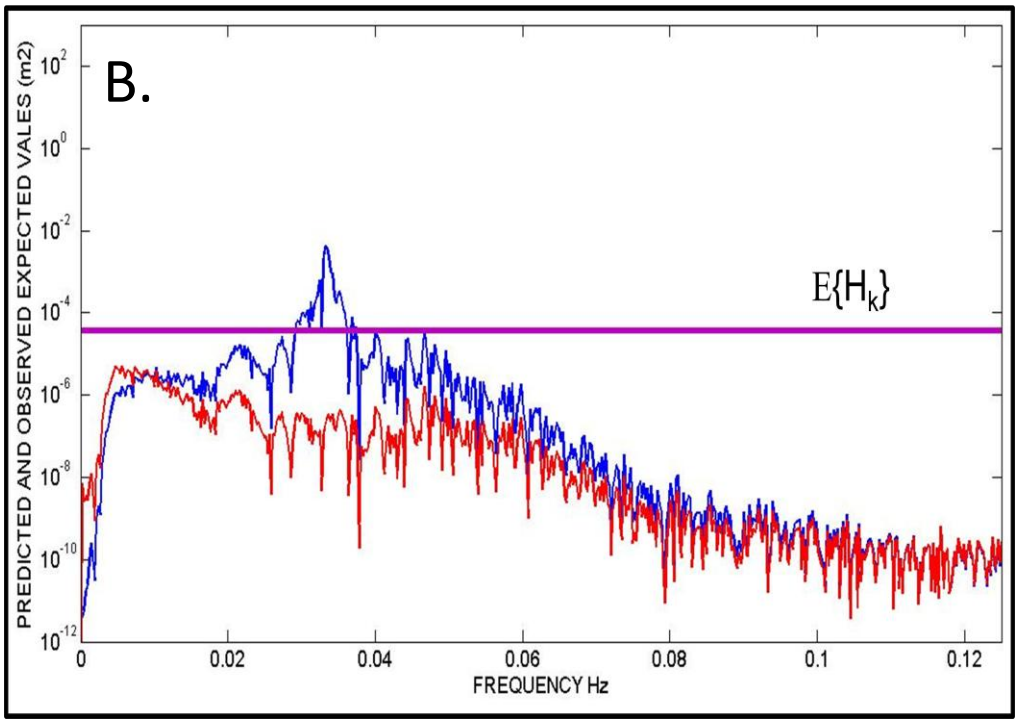

Figure 3.13: A. DOE Mean Squared water level deflection *E* {h^2} (Orange horizontal line) B. Magnitude 9.0 Japan Earthquake Spectral density (W_k)of the Rayleigh wave displacement for the Chile earthquake (red curve) and spectral density (H_k) of the predicted water level fluctuation for a trial value of S_s (blue curve). The purple horizontal line is *E* {H_k}, the mean value of H_k used for comparison with time domain measurements of *E* {h^2}.

Chapter 4

Aquifer Compartmentalization in the PGB

4.1 Introduction

Ever since the first investigators started evaluating well hydraulic connections among Grande Ronde wells, they realized that variable degrees of hydraulic continuity exist spatially within the PGB. Wells were found to respond differently to short-term (days to weeks) hydraulic stresses on a spatial basis, but similarly to long-term (annual) hydraulic stresses. Annual water level declines throughout much of the PGB were found generally to mimic the long-term records for the WSU Test well. Questions often were raised relative to the actual size PGB because of these somewhat misleading, temporal aquifer responses especially after C-14 age dates for the groundwater became available (Douglas et al., 2006).

This investigation is focused on the analysis of aquifer test drawdown data for Grande Ronde wells completed throughout the PGB during an 800-day aquifer test designed specifically to compare short-term and long-term responses to basin-wide pumping stresses. Analysis of the data to evaluate both short-term and long-term responses simultaneously provides a means to evaluate the conditions of groundwater flow within the PGB that were heretofore unavailable to investigating hydrogeologists.

Analysis of water level data and drawdown data for the PGB clearly indicate that the groundwater resource system known locally as the Grande Ronde aquifer is compartmentalized on both short-term and long-term time frames. Aquifer compartmentalization has been identified within the PGB during this investigation (Lateral Compartmentalization). Lateral Compartmentalization is defined in this thesis as the division of the Grande Ronde formation into irregularly shaped blocks (i.e., compartments) that are hydraulically separated laterally by sub-vertical, low hydraulic conductivity zones. Wells within an individual lateral compartment (LC) respond predictably to short-term pumping stresses. Well responses between adjacent compartments lag as the pressure transients due to pumping pass through the low

hydraulic conductivity zones that separate individual compartments. Aquifers are defined in this thesis by the division of the Grande Ronde formation into multiple, sub-horizontally oriented, producing zones that are hydraulically separated vertically by low hydraulic conductivity aquitards. Well responses between adjacent producing zones lag as the pressure transients due to pumping pass through the low hydraulic conductivity aquitards that separate the producing zones. This is the classic leaky Neuman-Witherspoon (1969) aquifer model. Estimated PGB aquifer compartments are shown in Figure 4.1, and the delineation methods used in this investigation will be discussed in the following sections.

Both lateral compartments and at least one upper aquifer (s) within the Grande Ronde formation are hydraulically connected via leakage through the low hydraulic conductivity materials. Analytical models exist to simulate the conditions of vertical leakage between upper and lower Grande Ronde aquifers. However, analytical models currently do not exist to simulate hydraulic communication between individual lateral compartments.

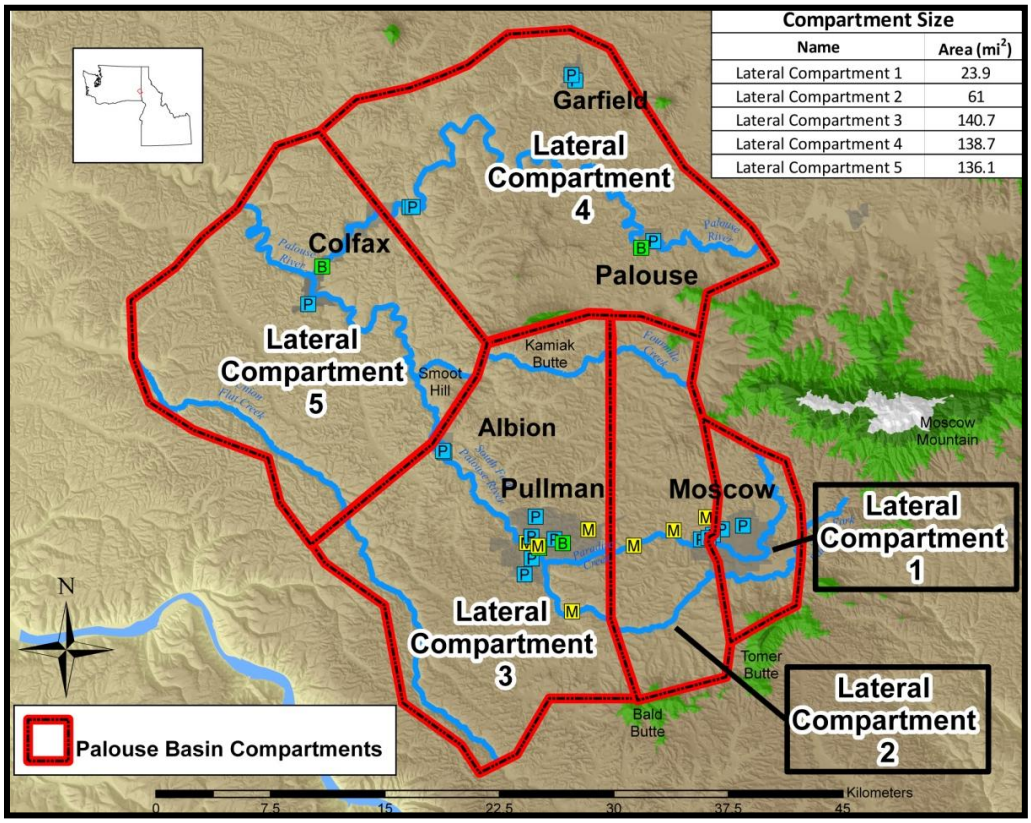

Figure 4.1: Palouse Groundwater Basin Compartments.

4.2 Potential Compartment Forming Features

Many combinations of several conditions potentially exist spatially that could cause compartmentalization. These features include the following, but are not limited to: fine grained interbeds, saprolite layers and buried soil horizons, folds, faults, dikes, and discontinuous fractures.

Hydrostructures may exist sub-regionally and locally that consist of geologic folds and fault/fracture zones that play a role in defining the limits of groundwater compartments inside the PGB. These features can be either barriers to, or pathways for, groundwater flow; however, only those that form partial or nearly complete barriers to flow are considered to be important compartment forming features.

Faults that are barriers have the type of displacement that grinds up rock and creates very low permeability fault gouge along the fault plane, isolating the aquifers on each side. Additionally, faults with significant vertical displacements may offset the interflow zones that host the aquifers on each side of the fault (Figure 4.2). However, significant water level differences as depicted in Figure 4.2 have not been identified in the PGB with the possible exception of the zone between Albion and Colfax. Faults that transect Columbia River Basalt Group (CRBG) flows often create linear zones of low permeability that affect the lateral continuity of groundwater flow in aquifers hosted by CRBG interflow zones. Faulting has been shown to disrupt the principal directions of anisotropy in the CRBG by offsetting tabular, permeable interflow zones and creating linear features of low horizontal and high vertical permeability (Burt et al., 2009).

Folds often occur near or on fault planes. Folds and their associated faults can create barriers to groundwater flow and define the limit of a groundwater compartment. Figure 4.3 illustrates folds in the Grande Ronde basalts that can reduce hydraulic conductivity. The Grande Ronde basalts within the Palouse Basin exhibit evidence of complex folds that trend northwest (Bush, 2006).

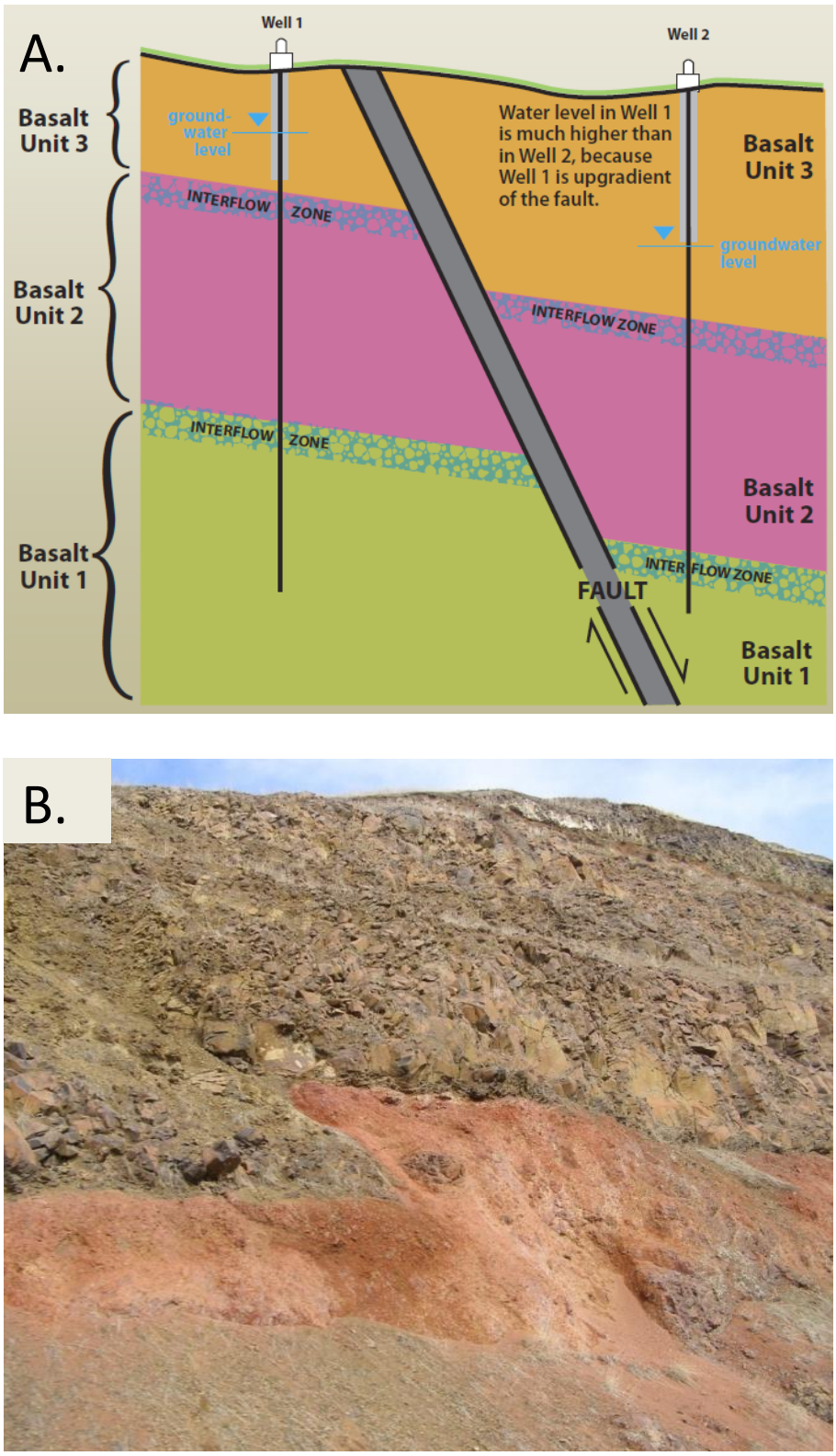

Figure 4.2: A. Example of a fault displacing interflow zones in the basalt in graphical form- not to scale (from Porcello et al., 2011). B. Field scale example of a fault within Grande Ronde basalts on the Lewiston grade, Idaho.

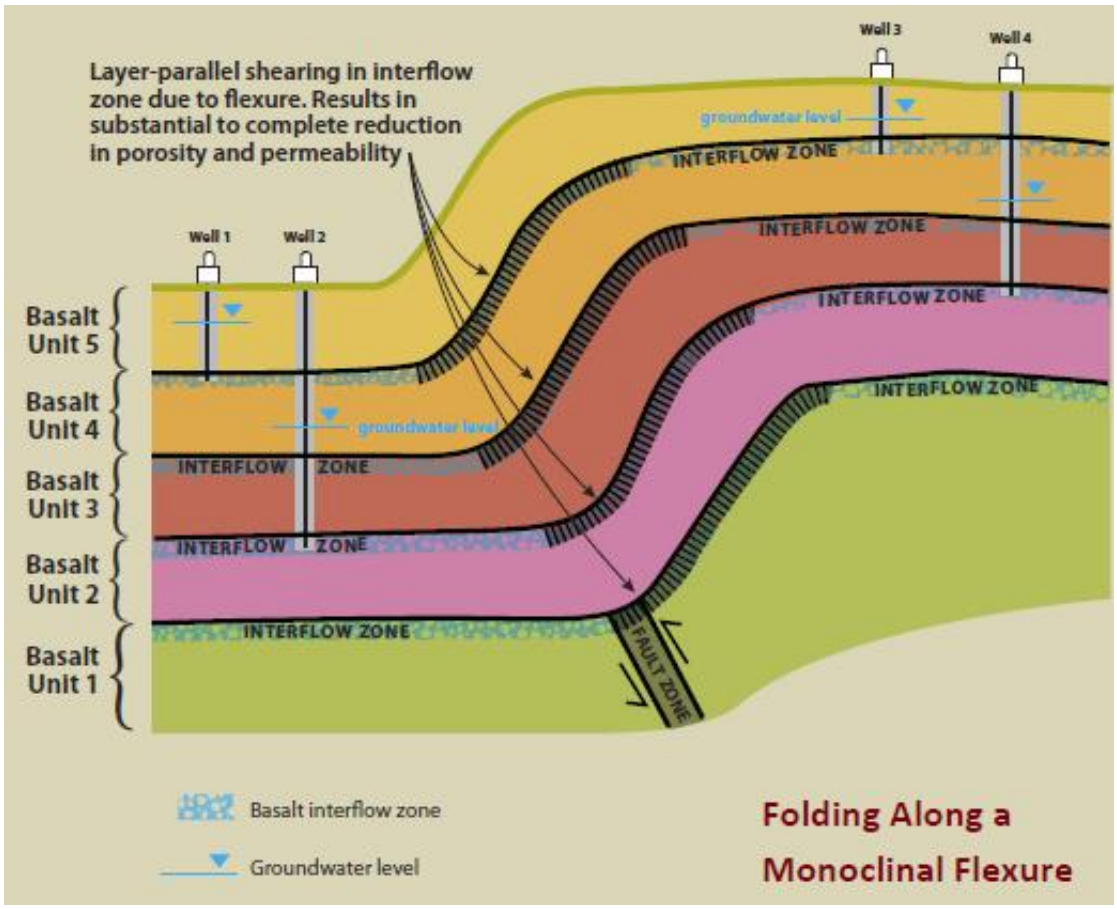

Figure 4.3: Example of a compartment geological structural boundary (from Porcello et al., 2011).

Vertical dikes contain solidified basalt that originated from the deep magma chambers that fed the lava flows. Each dike has very high density and low permeability and cuts through the rocks that pre-date the intrusion of the dike (Figure 4.4). Hence, many of these dikes are buried and form barriers to groundwater flow in deep basalt aquifers. Because the dikes commonly occur as a swarm (grouping) of dikes over a larger area, groundwater flow through a dike swarm is thought potentially to be limited. In the Columbia Plateau, geologic mapping and significant contrasts in well yields and water levels are common indicators of the presence of a buried dike swarm (Porcello et al., 2011).

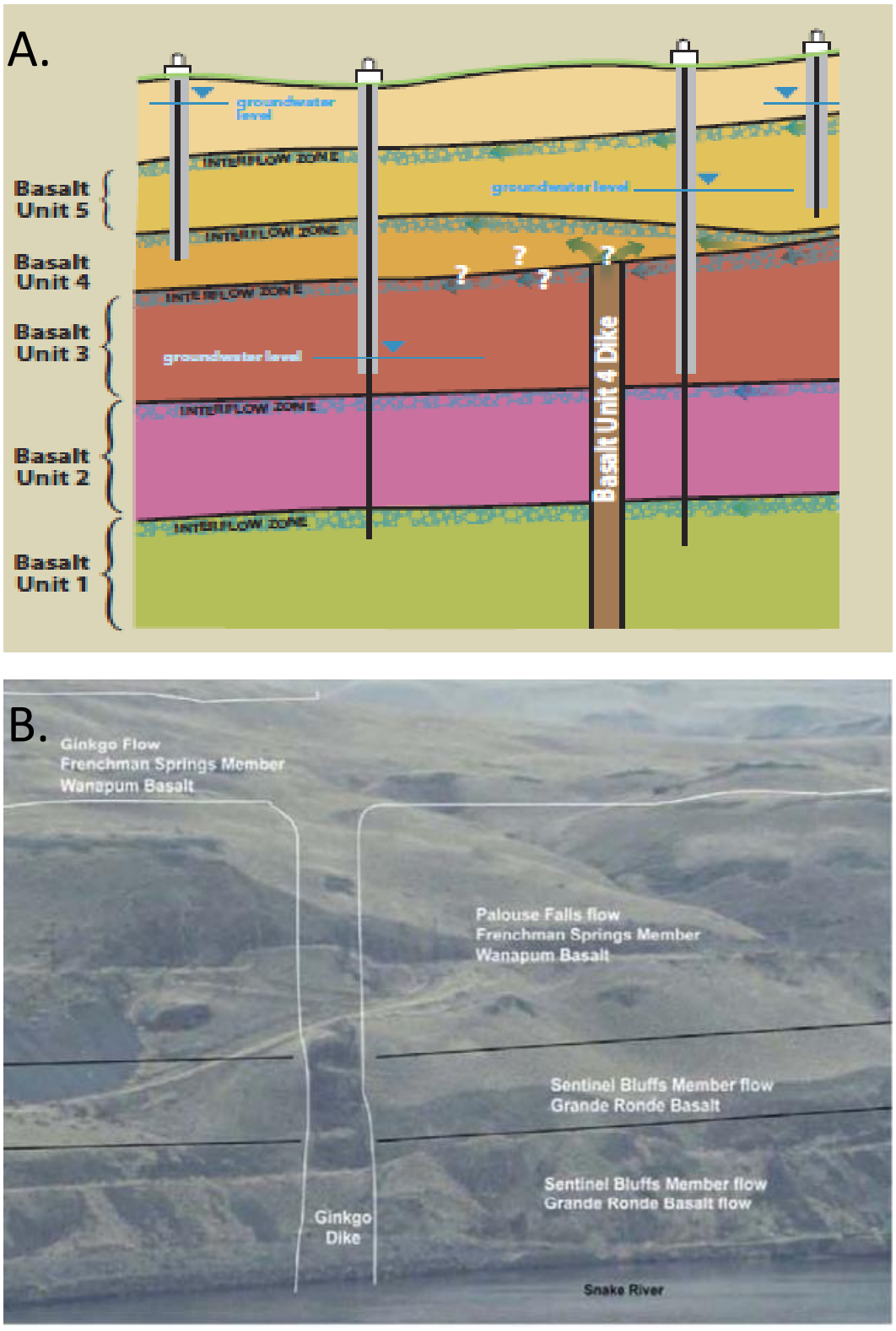

Figure 4.4: A. Example of a dike in the Grande Ronde basalts- not to scale. B. Field scale example of a dike along the Snake River (location not known) (from Porcello et al., 2011).

4.3 Potential Compartment Connecting Features

Where a given basalt flow is present, groundwater on top of the flow is often separated hydraulically from groundwater at the bottom of the flow. This occurs because the center of each flow generally is very dense and devoid of open fractures, creating highly compartmentalized aquifers in a vertical sense. At the edge of the flow, where it pinches out laterally (Figure 4.5), groundwater zones above and below the basalt layer can be hydraulically connected, allowing for mixing.

If fractures exist, the fracture type that is postulated to support groundwater exchange between interflow zones are quench fractures. Quench fractures are expressed as a 3D network of gently curviplanar surfaces, spaced ~0.5 to 2 m apart, extending from near or at the flow base to the upper flow crust (Sawlan, 2011).Observations to date suggest two processes occur in rapid succession and iteratively: upward incremental propagation of fractures, and rapid cooling outward from such fractures. Cooling is attributed to filling of fractures by steam, generated by conductive heating of groundwater residing in the vesicular flow top and fractures of the underlying lava flow (Sawlan, 2011). The generation of these fractures in the Grande Ronde from steam emanating from a shallow sediment water table would fit the conceptual models of the thick sedimentary interbeds in the Moscow area. These features do not act as instant aquifer stress propagation pathways through the dense flow interiors, but instead as conduits for small volumes of interchange between interflow zones.

4.4 Apparent Compartmentalization

Apparent compartmentalization is the similar response or lack thereof between wells caused by variable well completion depths. The apparent minor hydraulic communication between certain wells undoubtedly is due to cross bed water flow through aquitards. This type is typical multiple aquifer/aquitard conditions (Neuman-Witherspoon, 1969) and is different from lateral leakage through vertical compartment boundaries. For example, the M&M and Champion Electric wells see a delayed response to area pumping, but that time-lagged response is due to passage of the pressure transient upward from the primary producing zone to an overlying producing zone.

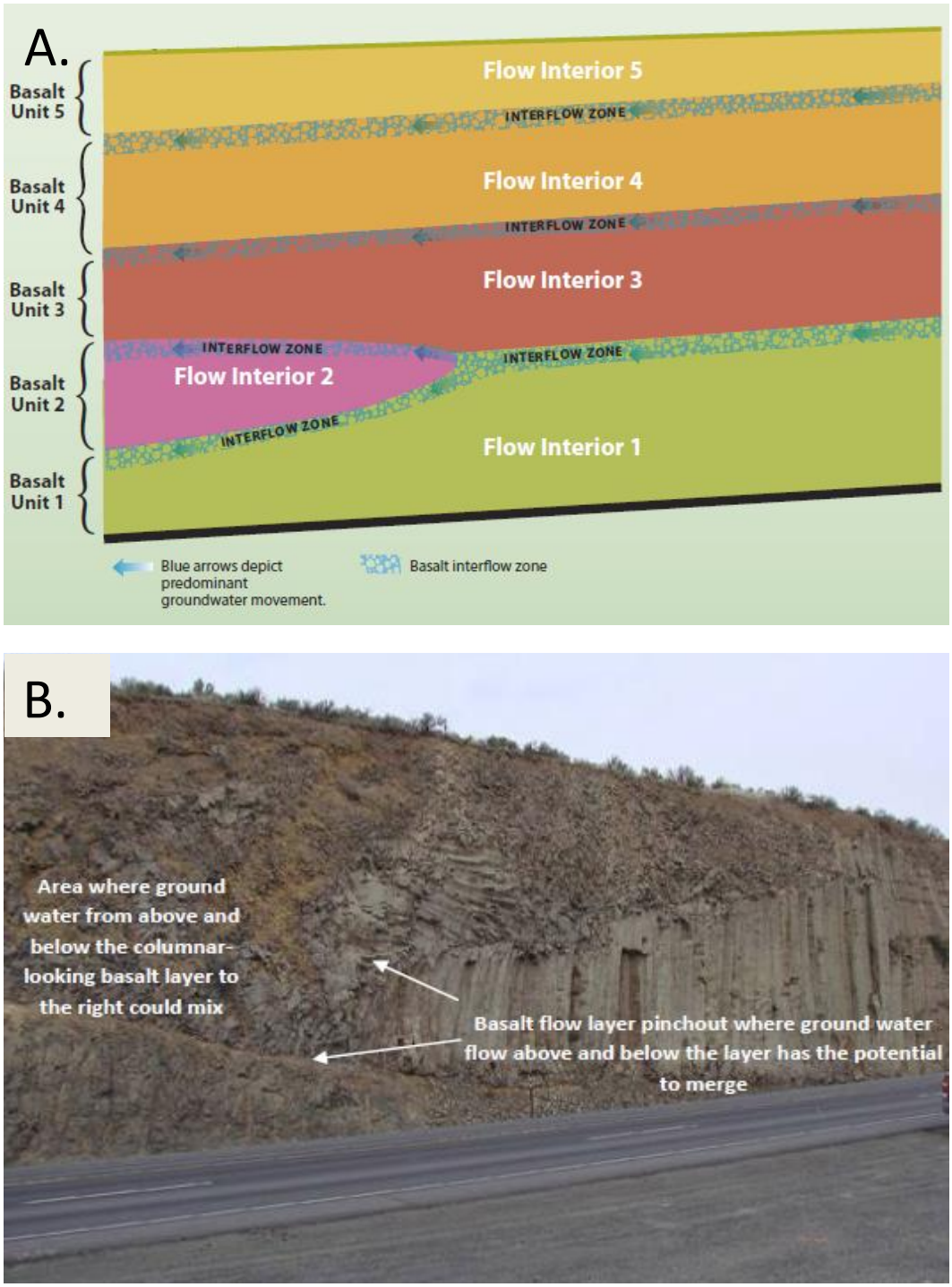

Figure 4.5: Example of basalt flow pinch outs in graphical form (not to scale). B. Field scale example of a flow pinch out (location not known) (from Porcello et al., 2011).

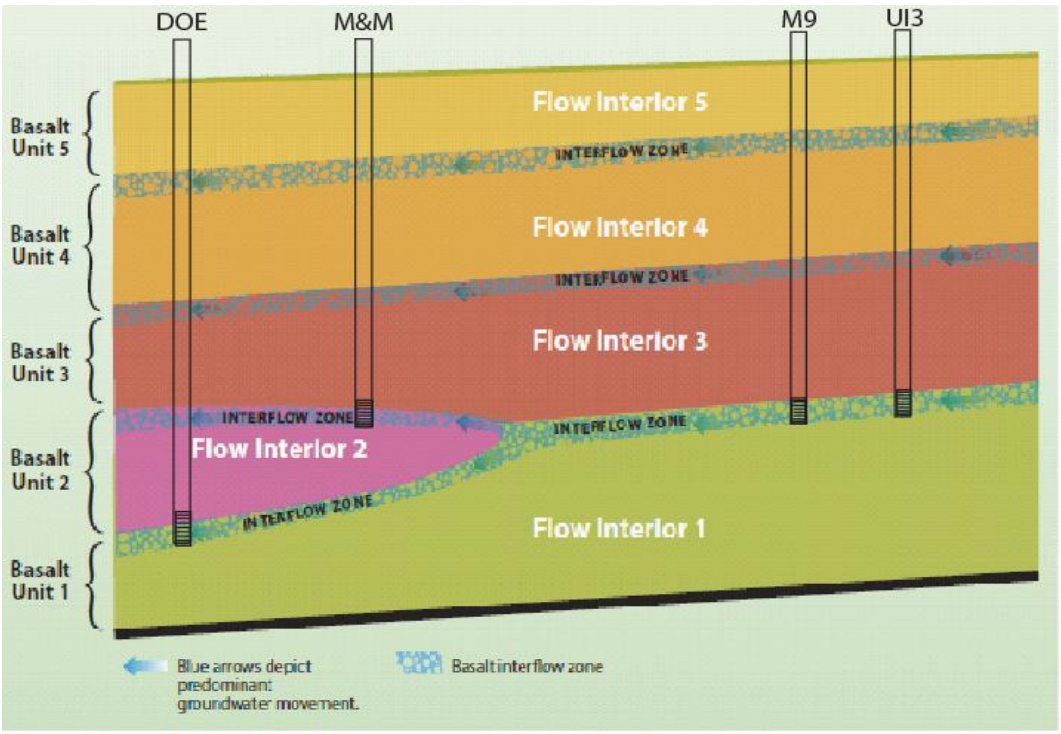

Figure 4.6: Example of a basalt flow pinch out in graphical form (not to scale) (modified from Porcello et al., 2011).

Strictly speaking, this is not compartmentalization as defined herein, but instead is related to horizontally oriented geologic heterogeneity damping the drawdown magnitudes.

The East Moscow compartment (LC 1 in Figure 4.1) is located on the eastern margin of the basin where lateral pitchouts of basalt flows exist. These basalt flow pinch outs are hypothesized to be responsible for the well connections between the upper and lower Grande Ronde aquifer producing zones by forming discontinuities in the aquitard (s) that separates producing zones. An example of this phenomenon occurs in LC 2; both the M&M well completed in the upper producing zone and the DOE well (lower producing zone) exhibit changes in water level when Moscow 9, UI 3, and UI 4 pump (Figure 4.6). However, the DOE well responds sooner than the M&M well even though it is approximately four kilometers farther from these pumping wells. Bush (2006) interpreted the topographical high in the vicinity of the DOE well to be the result of basalt flows pinching out as they advanced from the southwest. The existence and hydrogeological significance of basalt flow pinch outs in the LC 2 are discussed in Section 4.5.3.

Tritium was observed in the Champion Electric well which is in the vicinity and the same producing zone as the M&M well (Carey, 2011). This implies that there may be surface water leakage into the upper Grande Ronde basalts in this area as suggested by Crosby and Chatters (1965) and Douglas (2004).

Carbon 14 (^{14}C) percent modern carbon concentrations (pmc) from Douglas (2004) and Carey (2011) are presented in Table A04 in Appendix A, and support potential water leakage into the upper Grande Ronde. Grande Ronde ^{14}C pmc exhibit a general trend of increasing age (lower ^{14}C pmc) with depth (Figure 4.7). Specifically, ^{14}C age dates indicate a stratified body of water with two distinct groups of groundwater ages with ages ranging between 12,993 and 26,406 years before present for the lower Grande Ronde, and from 4,420 to 11,832 years before present for the upper Grande Ronde (Douglas, 2004). This leakage may be due to the existence of quench fractures in the upper Grande Ronde aquifer. These leakage pathways could exist in areas within the PGB that have thin overburden thickness as shown in Figure 4.8 A. Douglas (2004) showed that the thin overburden thickness between Moscow and Pullman correlated with the young upper Grande Ronde ^{14}C age dates.

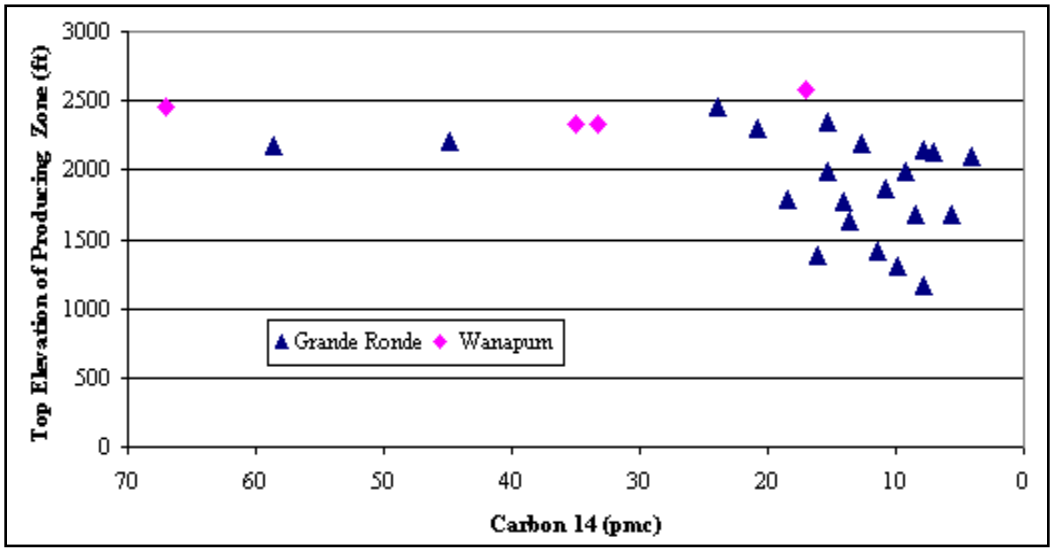

Figure 4.7: Arithmetic plot of ^{14}C percent modern carbon (pmc) concentrations versus elevation of the producing zone for groundwater samples collected in PGB (from Douglas. 2004).

Douglas (2004) found the oldest ^{14}C age dates in the PGB to be located near Palouse and Moscow, and the youngest water near Pullman and Colfax (Figure 4.8 B). These results suggest that Holocene age recharge has percolated to an elevation of about 670 meters (2198 feet) above mean sea level, which includes all of the Wanapum and upper portions of the Grande Ronde. The ages do not reflect identifiable horizontal flow paths, so are therefore taken to represent the vertical travel times. Douglas (2004) concluded that the stratification of groundwater ages is consistent with areally distributed recharge and hypothesized that younger water would be found near a groundwater divide between Moscow and Pullman. Thus more evaluation must be conducted in the Grande Ronde aquifer to understand the vertical effects of stratification on the groundwater flow systems in the PGB.

Another process that potentially could create apparent compartmentalization is mineral precipitation and/or clay deposition restricting groundwater flow through the pore spaces and fractures. Due to the Grande Ronde aquifer having high concentrations of manganese and iron oxides, geochemical reactions could be partially responsible for the lack of well hydraulic connections between wells such as WSU 5, Moscow 7, and other wells in the PGB. The plugging of the well screens with mineral deposits in these wells may restrict free water flow between the well and the aquifer as was documented in a high-definition video for log well UI 2 (plugged and sealed in 2010) produced during the thesis investigation by Opatz (2007).

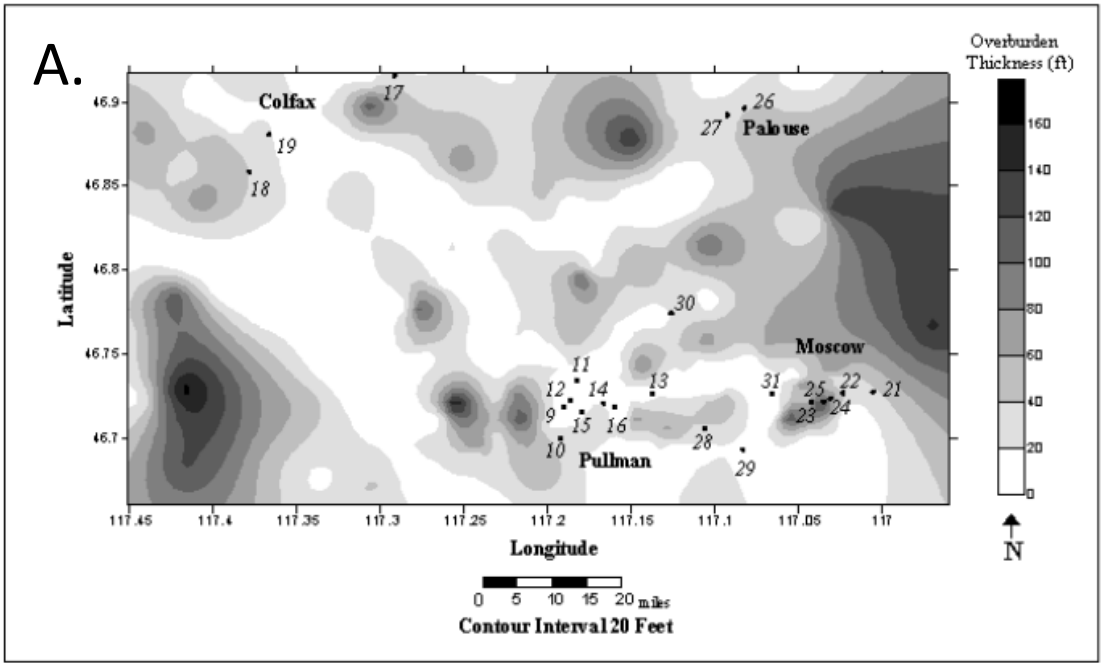

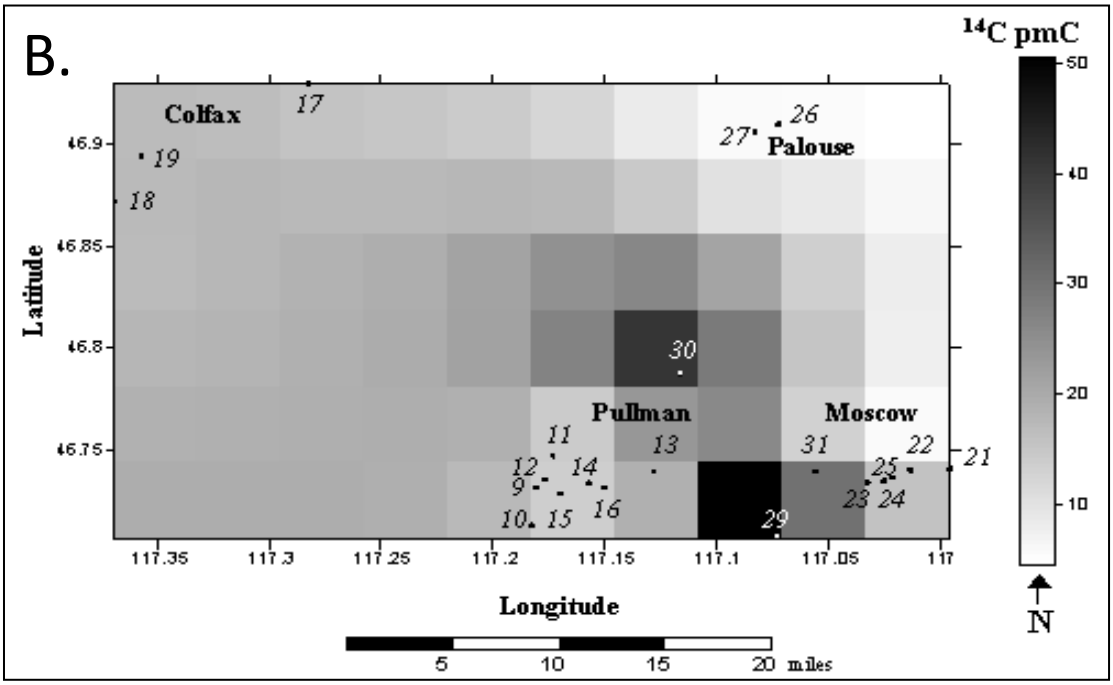

Figure 4.8: A. Isopach map of overburden thickness in the PGB. Darker areas represent greater overburden thickness for Grande Ronde aquifer wells. B. Shaded cell map of groundwater ^{14}C pmc concentrations in the Grande Ronde aquifer system. Darker cells represent areas of younger age. These two areas suggest potential recharge areas for the Grande Ronde system. Wells sampled are identified through sample numbers given in Table A04 in Appendix A (from Douglas, 2004).

4.5 Hydraulic Evidence for Compartments

Well hydraulic connections identified in previous investigations (Sokol, 1966; Owsley, 2003; McVay, 2007; Fiedler, 2009; and Moran, 2011) and during this present investigation were used for designating compartment sizes within the PGB. Each hydraulic connection identified by previous investigators was evaluated during this investigation when data were available.

The technique used in this investigation for determining well hydraulic connections will be discussed using the WSU Test well as an example. Water levels measured in observation wells are preprocessed and corrected for barometric pressure fluctuations so pumping drawdown is delineated (Section 3.2). The barometrically corrected water levels, and the Hobo® pumping motor on/off records are plotted with the freeware program Graph© 4.3. Hydraulic connections are determined by matching pumping intervals of vicinity wells to the observation well water levels. As shown in Figure 4.9 B and Figure 4.9 D, the WSU Test well shows a strong connection to WSU 4, WSU7, and Pullman 7. It shows a damped response to Pullman 8 and WSU 8 (Figure 4.9 C). The WSU Test well shows minimal to no hydraulic response to WSU 6, Pullman 5, and Pullman 6 (Figure 4.9 E). Further hydraulic connection evidence in the basin will be discussed compartment by compartment in section 4.5 in their respective compartment section that follows.

This investigation considers responses in observation wells that are damped (i.e., a non-theoretically predicted response for a homogeneous and isotropic, infinite aquifer) to be due to the pressure transient having to travel through the compartment walls. Observation wells that show drawdown spikes as predicted by aquifer test type curve responses are assumed to have no compartment walls between them. The heterogeneity of each compartment can cause short-term differences in hydraulic behavior (McVay, 2007). Many studies, including those by Foxworthy and Washburn (1963), Crosby and Chatters (1965), Lin (1967), Barker (1979), Teasdale (2002), Owsley (2003) and Bush (2005), have proposed the existence of a hydraulic barrier between Moscow and Pullman

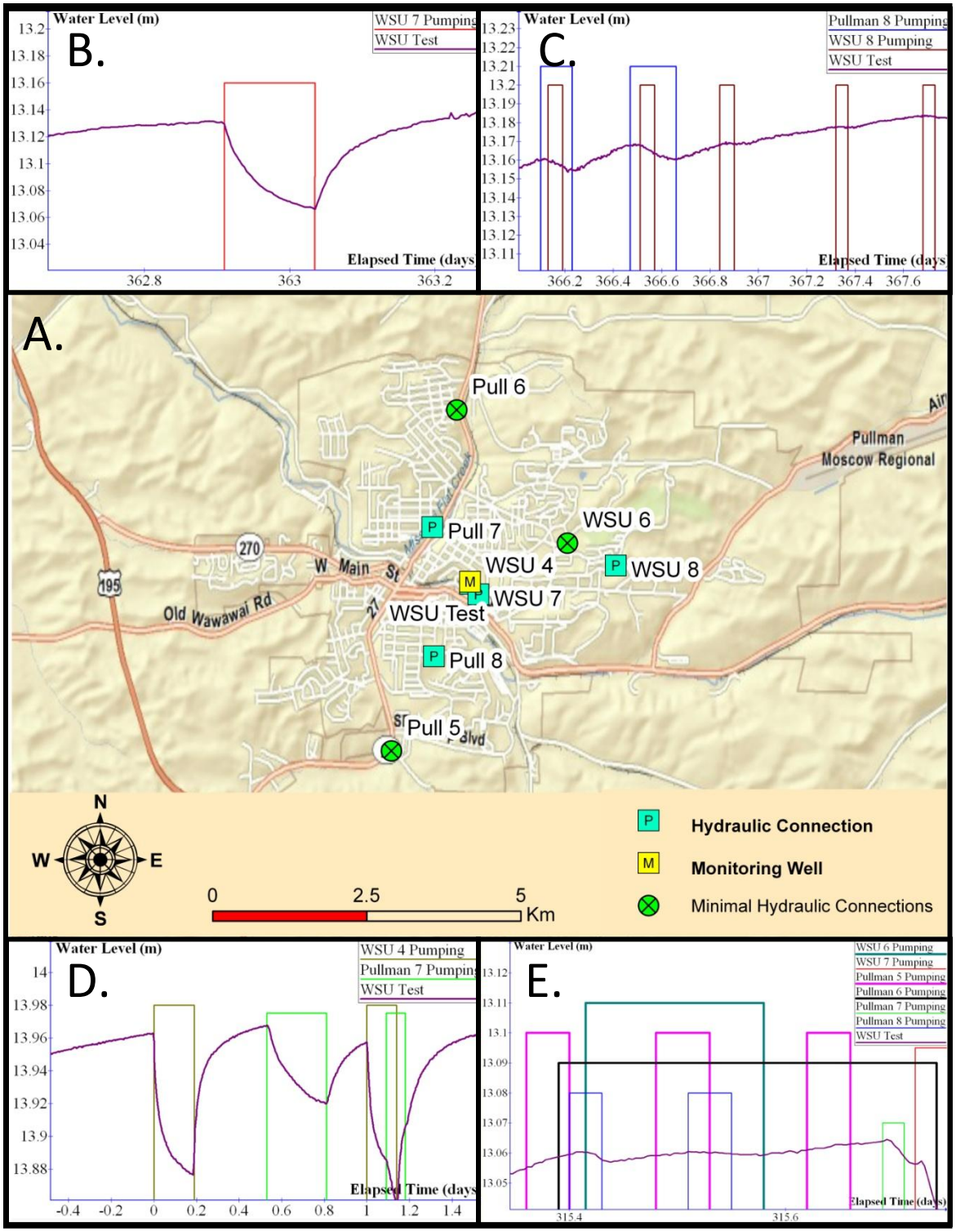

Figure 4.9: A. Well location map. B. through E. WSU Test well hydraulic connections in graphical form. Periods of active pumping are designated by the vertical rectangles identifying individual pumping wells. Relative water levels are shown in meters above an arbitrary datum.

based on different seasonal water level fluctuations, lack of measured hydraulic connection during aquifer tests, or water chemistry differences between the two cities. McVay (2007) and Moran (2011), however, came to the conclusion that Moscow and Pullman share a connected Grande Ronde aquifer over the time frame of days/weeks.

Cross compartmental leakage constitutes the best hydrogeologic conceptual model to fit the aforementioned scenarios. Evidence for long-term inter-compartmental leakage includes the similar system recovery trends observed in wells in different compartments and similar magnitudes of annual drawdowns. In Section 4.6, additional evidence for delineating compartments will be discussed through mapping the water levels, comparing groundwater temperatures, and correlation of relative age dates in PGB Grande Ronde wells. Correlation of water level trends over time for the same time period can also be used as a tool to help delineate compartments (Table 3.1).

4.6 Compartment Delineation

Lateral Compartmentalization (LC) is defined in this thesis as the division of the Grande Ronde formation into irregularly shaped blocks (i.e., compartments) that are hydraulically separated laterally by sub-vertical, low hydraulic conductivity zones. Wells within an individual compartment respond predictably to short-term pumping stresses. The compartments are numbered from east to west in the Moscow-Pullman area followed by the Palouse and Colfax compartments.

With the evidence for compartmentalization discussed above, five individual compartments in the PGB are hypothesized. The following discussion includes well connections observed during this investigation and previous investigations combined with geological evidence to support the hydraulic evidence. The compartments are delineated by lateral compartment number for all lower Grande Ronde Aquifer wells and individual upper Grande Ronde wells that exhibit drawdown spikes from lower Grande Ronde pumping. Observation wells in the upper Grande Ronde that do not exhibit such drawdown spikes will be discussed individually.

4.6.1 Lateral Compartment 1 (Eastern Moscow Compartment)

Lateral Compartment 1 (LC 1) is located along the eastern margin of the PGB and is bounded by the granite and metasediments of Tomer Butte and Paradise Ridge to the south, the Palouse Range to the east and north, and Farm and Horton Road in the city of Moscow to the west (Figure 4.1). Strong well connections between Moscow 6 and 8 have been observed in this investigation and previous work, but not between these wells and other wells (Sokol, 1966; Owsley, 2003; McVay, 2007; and Fiedler, 2009). The UI 3 well did not produce drawdown in Moscow 6 or 8 (Sokol 1966). No evidence of Moscow 6 and Moscow 8 pumping signatures exist for other PGB monitoring wells (Owsley, 2003; McVay, 2007; Fiedler, 2009; and Moran, 2011).

On February 26, 2012 through March 2, 2012, a coordinated Moscow/UI pumping shutdown and pumping restart was completed in the attempt to observe drawdown from other Moscow/UI wells in Moscow 6. According to the results in Figure 4.10 B, Moscow 6 has a strong hydraulic connection to Moscow 8 (1.5 to 4 meters of drawdown), but drawdown related to Moscow 9, UI 3, or UI 4 was not observed (Figure 4.10 C). The troughs observed in the plots of Moscow 6 water levels in Figure 4.10 C are attributed to lunar/ tidal influences that are observed in all basin wells when pumping has ceased in the well compartment for more than 48 hours. The wells Moscow 6 and Moscow 8 produce from a separate lateral compartment than that monitored by IDWR 4; the two lateral compartments are separated from each other by a thick section (~ 80 meters) of the Latah formation (Fiedler 2009). Figure 4.11 shows the geologic variability as interpreted from well logs.

The geologic variability does not clearly demonstrate the reason for the lack of connection between the LC 1 and LC 2. The absence of evidence for faulting in the well log geology implies something else such as clay beds is responsible for creating the compartmentalization.

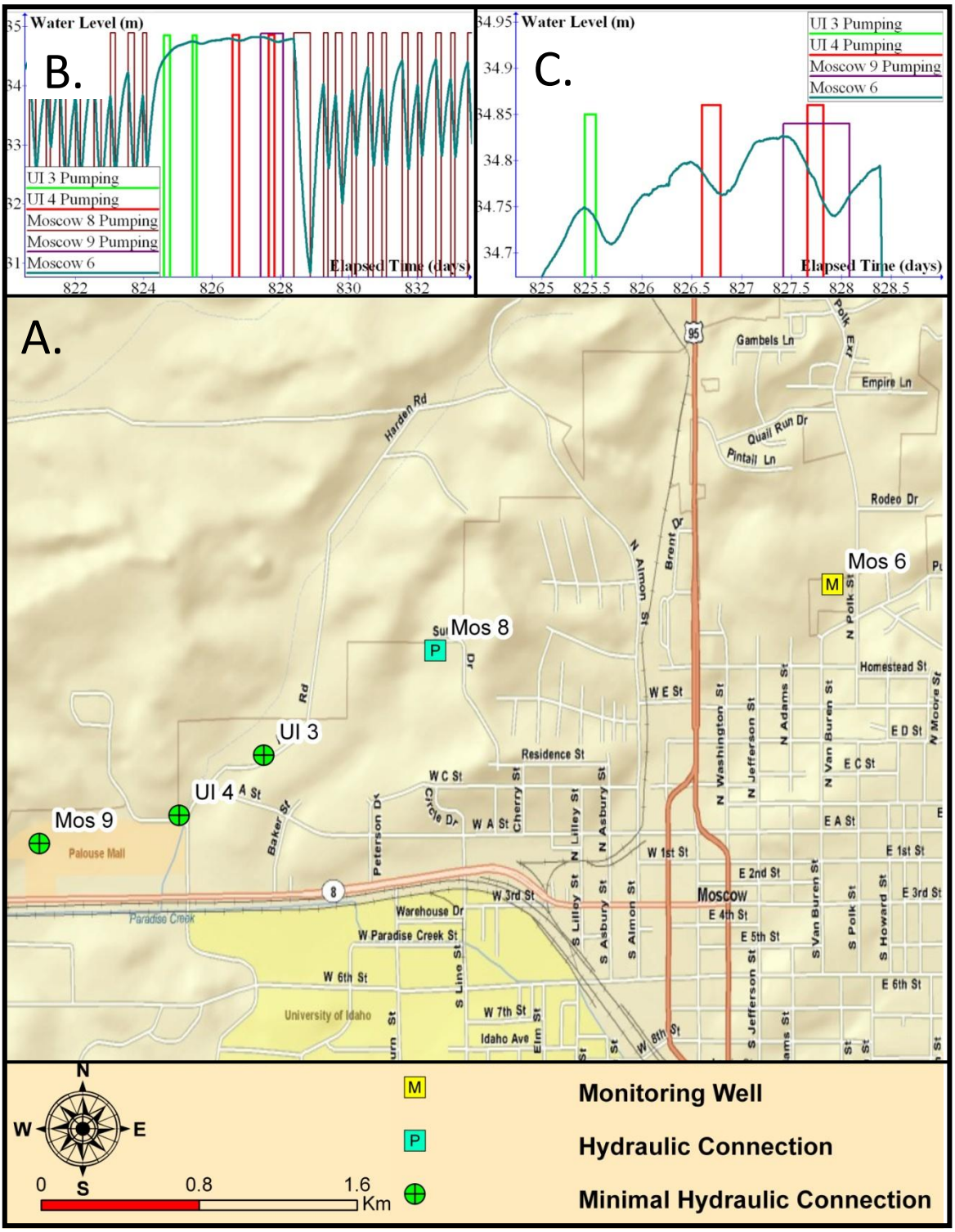

Figure 4.10: A. Well location map. B. and C. Moscow 6 well hydraulic connections in graphical form. Periods of active pumping are designated by the vertical rectangles identifying individual pumping wells. Relative water levels are shown in meters above an arbitrary datum.

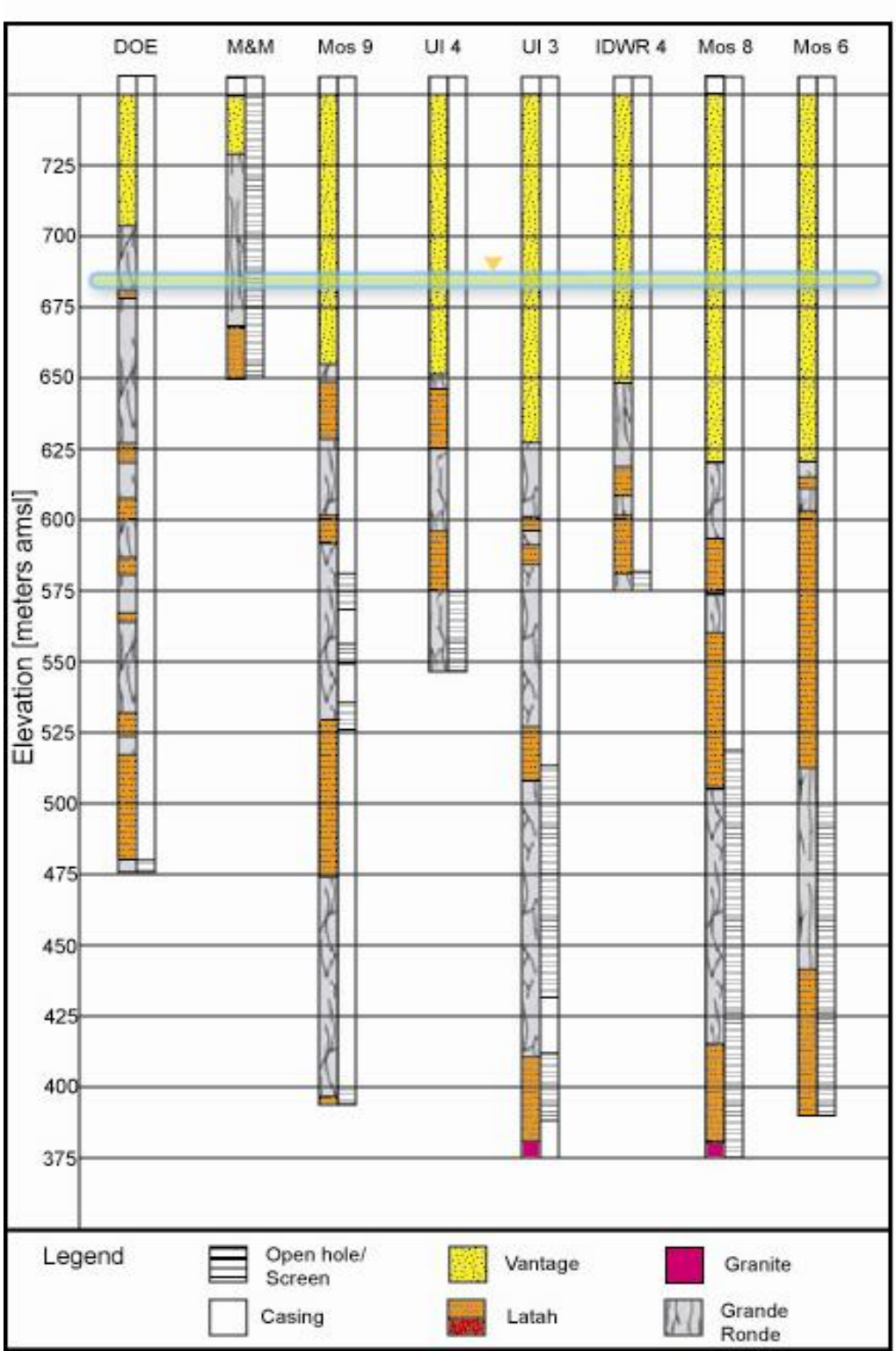

Figure 4.11: Lateral Compartment 1 and Lateral Compartment 2 (west (left) to east (right)) geology. Includes the cased (white) and open (screened design) sections displayed next to lower aquifer geology with 2011 water level of ~684 meter amsl.

4.6.1.1 LC 1 Upper Producing Zone #1 (Moscow 7)

Moscow 7, WSU 5, and Cornelius are completed in the upper Grande Ronde and do not exhibit drawdown spikes from local municipal pumping. Therefore these wells were determined to be in their own upper aquifer producing zones. These producing zones are influenced by their local lateral compartment, because their hydrographs show intercompartmental influences (i.e., similar long-term trends).

Moscow 7 is located near the northern Moscow city limits at the end of Sunset Drive, approximately 30 meters west of Moscow 8 (Figure 4.12). This well was never in production, but was used as an injection well for the water discharged from the Moscow 8 pump control valve. Moscow 7 no longer can handle the water and hasn't been used as an injection well since 2010. Moscow 7 water levels were recorded for 175 days as part of this investigation, but no identifiable drawdown spikes from any nearby production wells including Moscow 8 are visible in water level plots. Sokol (1966) also did not measure any direct pumping effects in Moscow 7 during his investigation. However, minor influences, apparently from some unidentified local area pumping, are detected in the Moscow 7 water level data as shown in Figures 4.12 B through D. These fluctuations are significantly smaller than the Theis (1935) equation would predict for an infinite homogeneous and isotropic aquifer; therefore, Moscow 7 appears to be separated vertically from the other LC 1 and LC 2 Grande Ronde wells by very low hydraulic conductivity aquitards.

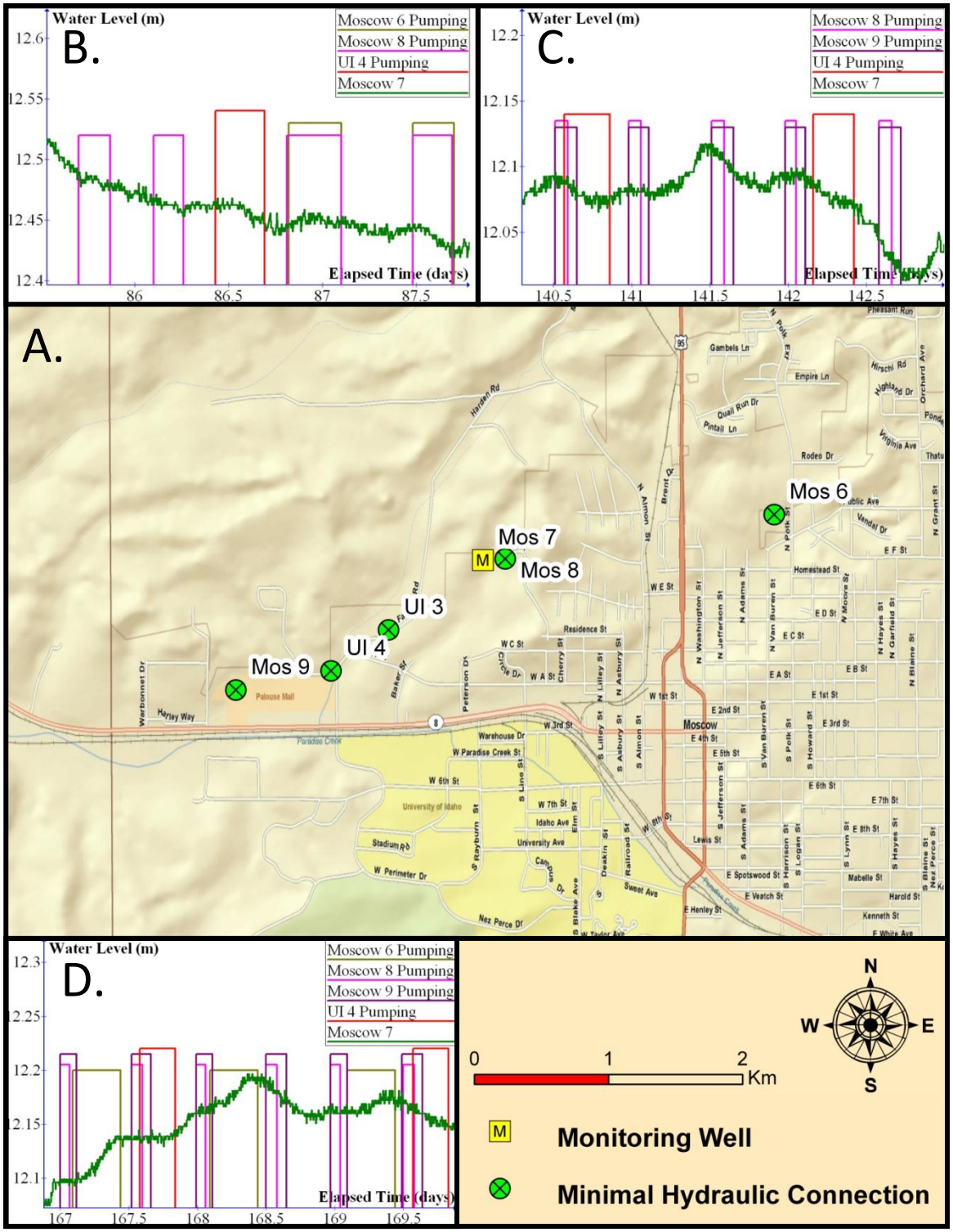

Figure 4.12: A. Well location map. B. through D. Moscow 7 well hydraulic connections in graphical form.

4.6.2 Lateral Compartment 2 (Western Moscow Compartment)

Lateral Compartment 2 (LC 2) is located on the eastern side of the PGB and is bounded by the granite and metasediments of Paradise Ridge to the south, the Palouse Range to the north, Farm and Horton Road in the city of Moscow to the east, and Sunshine Road to the west (Figure 4.1). The DOE, M&M, and IDWR 4 monitoring wells in this compartment respond to pumping of UI 3, UI 4, and Moscow 9. Evidence from the water level correlation shows that the only well with a good correlation (R^2>85%) with IDWR4 is the DOE well (M&M data are unavailable for correlation).

For comparison purposes, calculated drawdown plots were generated using the methods described in Section 3.7. Calculated drawdown is more advantageous to use here, because it normalizes the data to a time t=0 and removes regional trends from the data. So rather than plotting water levels, plotting calculated drawdown versus time shows changes in water level that occurred since the beginning of the test for each observation well. Wells that show similarities in long-term trend slopes and drawdown patterns are considered to be in the same lateral compartment. A visual correlation can be made by observing LC 2 calculated drawdowns versus time in Figure 4.13.

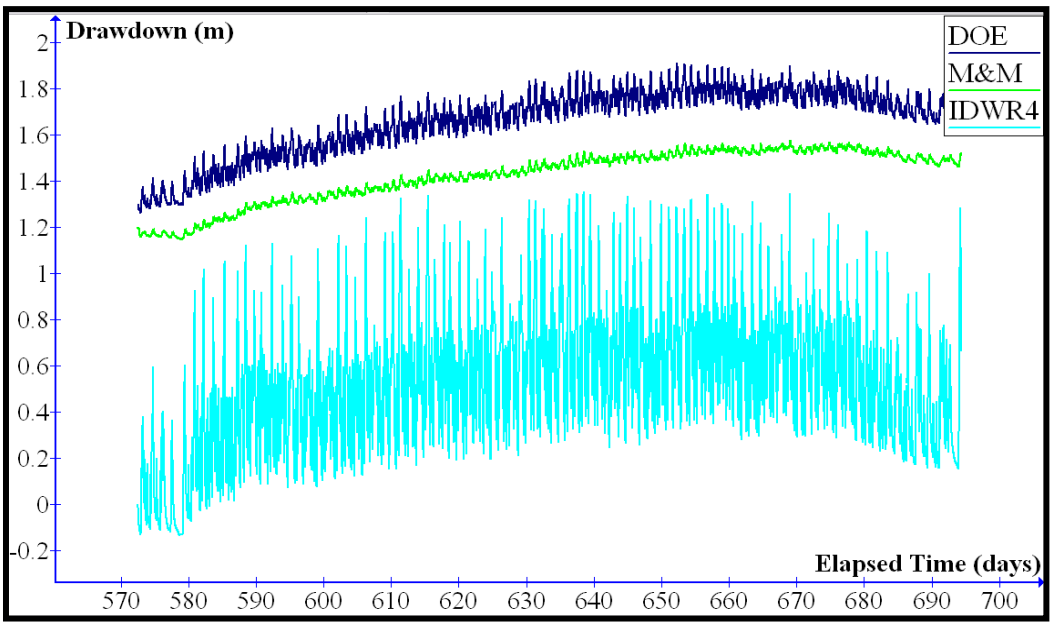

Figure 4.13: Arithmetic plot of calculated drawdown versus time for selected wells in LC 2. Individual plots have been offset vertically in order to compare drawdown magnitudes.

Figure 4.14 B through Figure 4.14 D show that well IDWR 4 with a distance of 1.2 kilometers (km) from UI 3 exhibits the strongest connection to the Moscow 9 and UI pumping wells. The DOE well is the furthest away (5.2 km) and draws down more than the closer M&M well (1.2 km) in response to pumping of UI 3, UI 4, or Moscow 9 (Figure 4.15 B through Figure 4.15 D). The M&M well is located in an upper Grande Ronde aquifer that is separated vertically from the lower (primary) producing aquifer by a sub-horizontal aquitard; M&M responds as would be predicted by the Neuman-Witherspoon (1969) method for a well completed in the unpumped aquifer (Figure 4.16 B through Figure 4.16 D). All monitoring wells in this compartment are influenced by intercompartmental leakage to/from LC 1, but do not show a theoretically predicted connection (Figure 4.14D, Figure 4.15 D, and Figure 4.16 D). Plots of water level versus time in most of these wells show only a flattening of the rate of water level recovery or a slight slope reversal (Figure 4.15 D) rather than a major slope reversal from rising to declining water levels (Figure 4.15 B) as would occur with direct hydraulic connection within the same compartment.

Figure 4.11 illustrates the geologic variability that exists between wells in the Moscow area as interpreted from well logs. The geological information presented in the well logs shows that the uppermost Grande Ronde basalt flow pinches out between the M&M well and Moscow 9. This may help explain the reason for vertical communication between the wells.

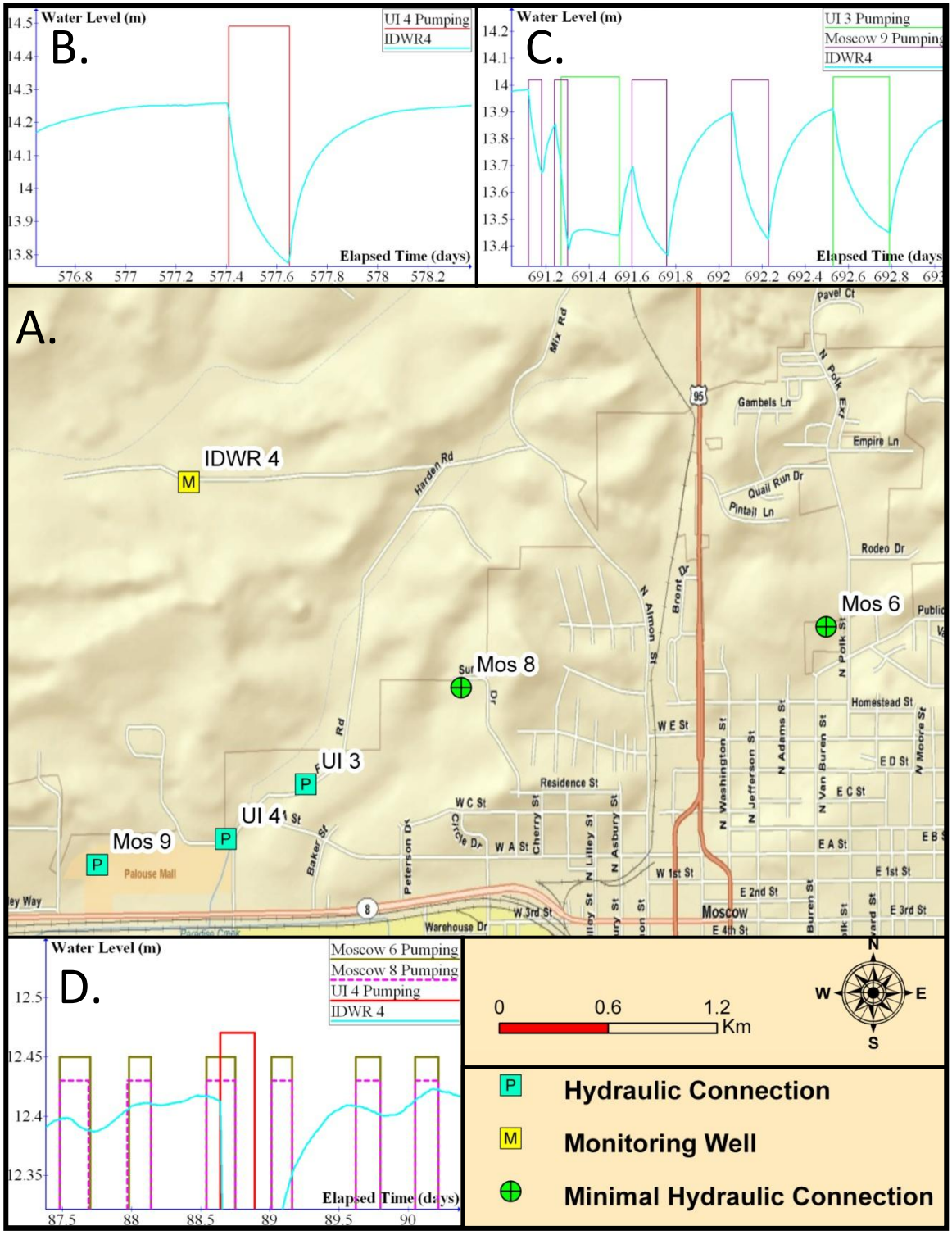

Figure 4.14: A. Well location map. B. through D. IDWR 4 hydraulic connections in graphical form.

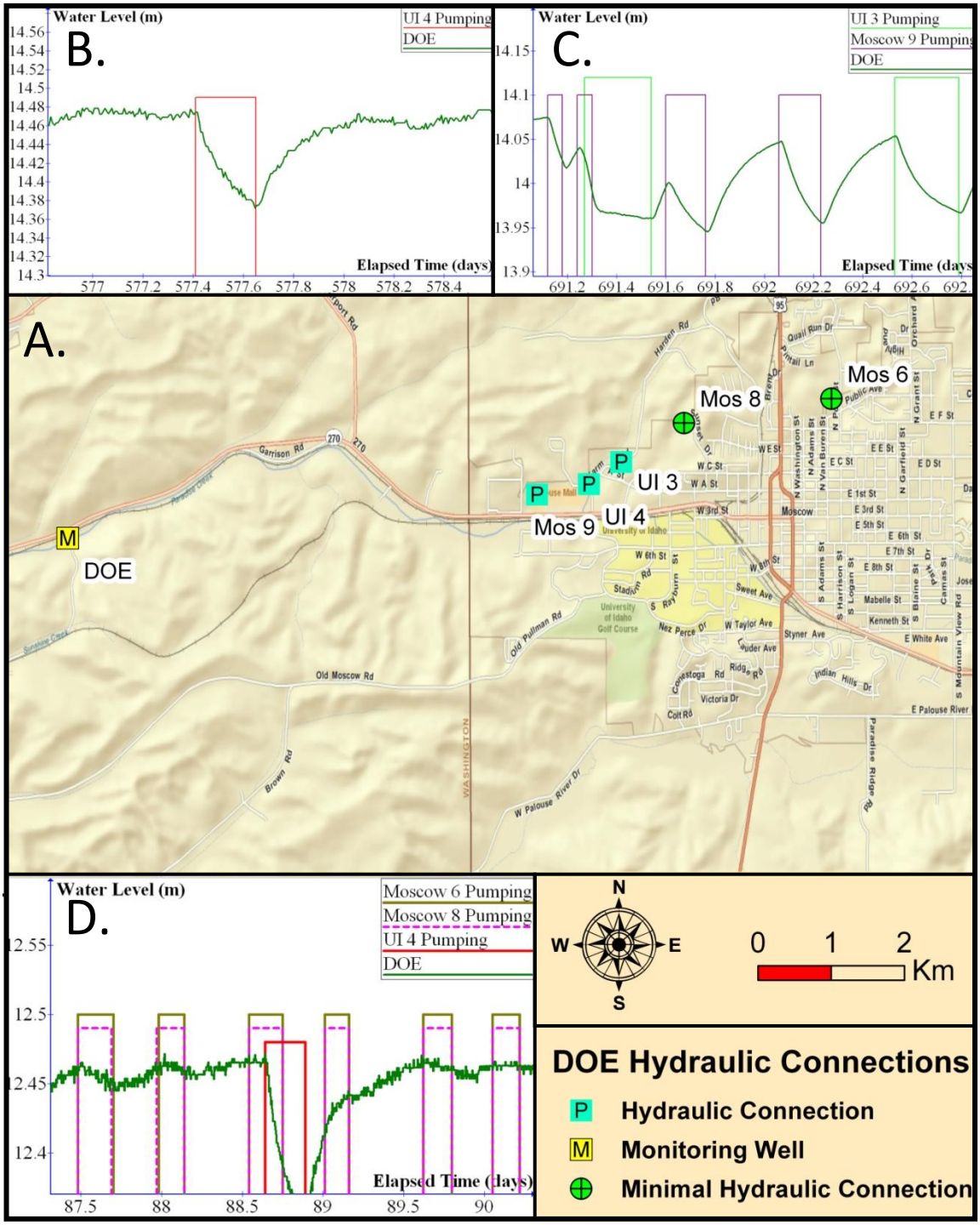

Figure 4.15: A. Well location map. B. through D. DOE hydraulic connections in graphical form.

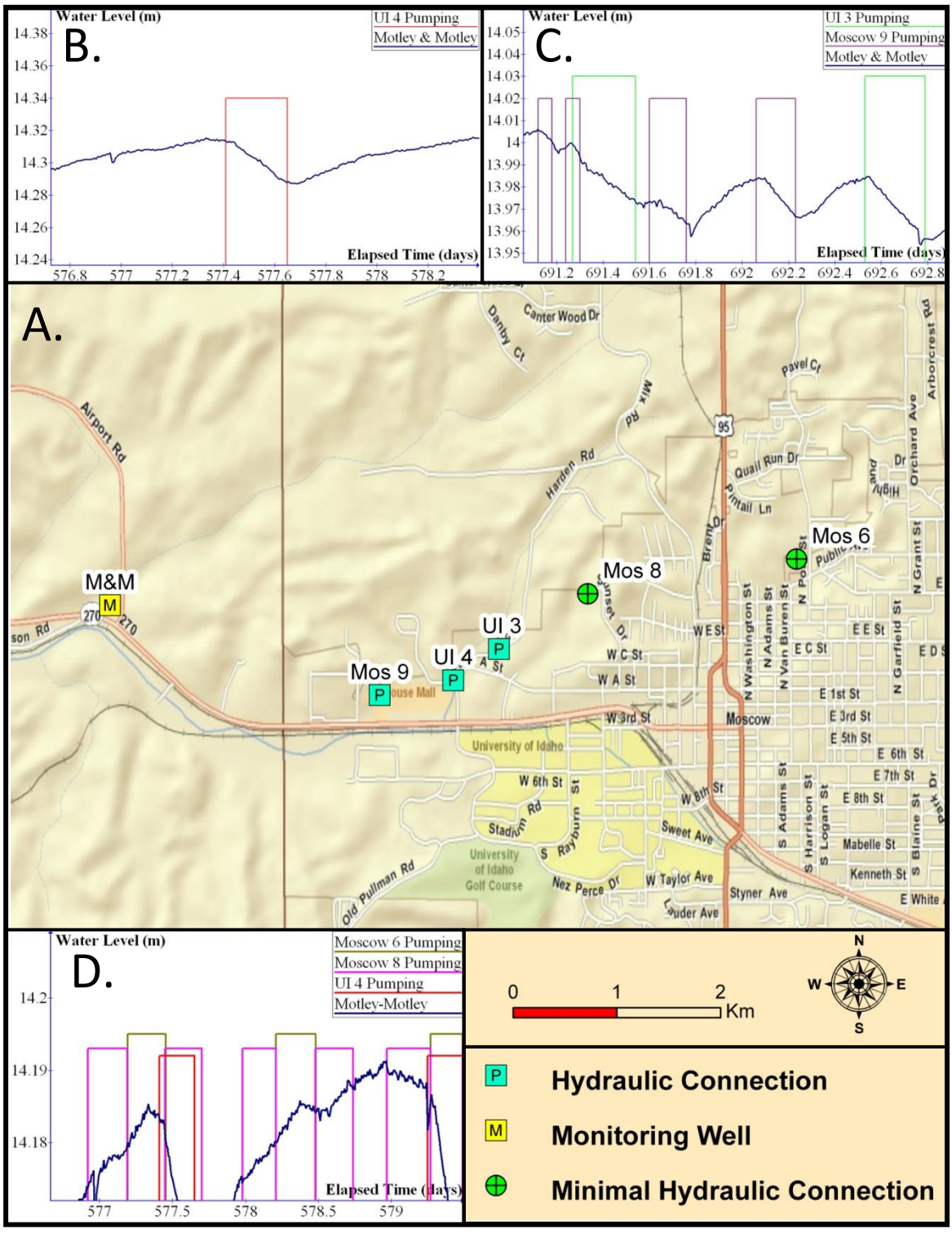

Figure 4.16: A. Well location map. B. through D. Motley & Motley hydraulic connections in graphical form.

4.6.3 Lateral Compartment 3 (Pullman Compartment)

Lateral Compartment 3 (LC 3) includes part of the city of Pullman and is bounded by Bald Butte to the south, Union Flat Creek to the southwest, Kamiak Butte and Smoot hill to the north, and the compartment's eastern boundary is west of the Sunshine Road (Figure 4.1). The western boundary is unclear due to the unknown hydrogeologic characteristics of that area of the PGB; however the boundary is hypothesized to be near Albion. Unlike LC 1 and LC 2, the hydraulic connections vary for each well within LC 3 (Figures 4.17 through 4.24). This is due to hydrostructures that have not been delineated. Bush (2006) concluded that the differences in well connections are due to a combination of rapid changes in thicknesses, nature of flow features, and the location of Pullman in a deformation zone. X-ray fluorescence (XRF) analysis of drill chips from nine wells in the basin suggest that a fault (South Fork Fault) exists between WSU 6 and WSU 7 (Conrey and Wolff, 2010). Well connection data suggest that if this fault does exist, it forms a pathway for flow to some of the producing zones (interbeds/flowtops) and a partial barrier to flow for others. While no distinctive WSU 6 pumping signature is discernible in the WSU Test well or WSU 7 water level records, both observation wells do show a damped response to WSU 8 pumping. WSU 6 water levels show WSU 7 and WSU 8 spikes clearly, but the data are too noisy to discern other hydraulic connections. This difference in WSU 6 and WSU 7 water level responses to each others pumping must be due to their different pumping rates (1050 gpm and 2700 gallons per minute (gpm), respectively). The Principle of Reciprocity suggests that the same response should be seen in each well when both wells pump at the same rate. The South Fork Fault may also impede growth of the cone of depression from the Pullman wells toward WSU 8, and growth of the Pullman 6 cone of depression toward other Pullman and WSU wells. Pullman 6 water levels show damped responses to both WSU 7 and Pullman 7. No further hydraulic connections can be determined because of the paucity of quality data. These well connections or lack thereof may be evidence of the fault being discontinuous (relay zone) to the east, but a partial barrier to the north and south.

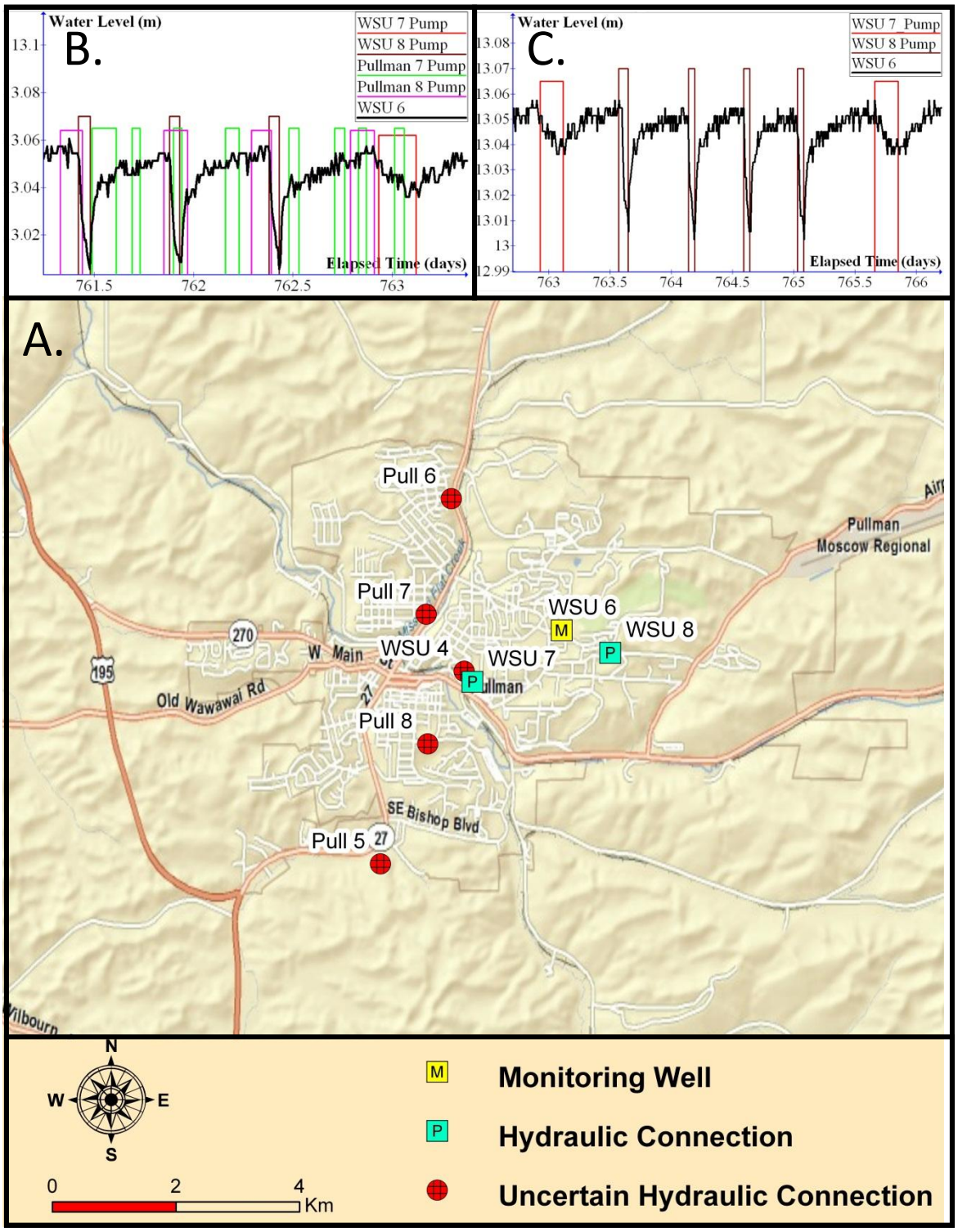

Figure 4.17: A. Well location map. B. and C. WSU 6 hydraulic connections in graphical form. Note: the spiky nature of the WSU 6 water levels in 4.17 B and Figure 4.17 C is believed to be due to data logger noise as described in section 3.3.

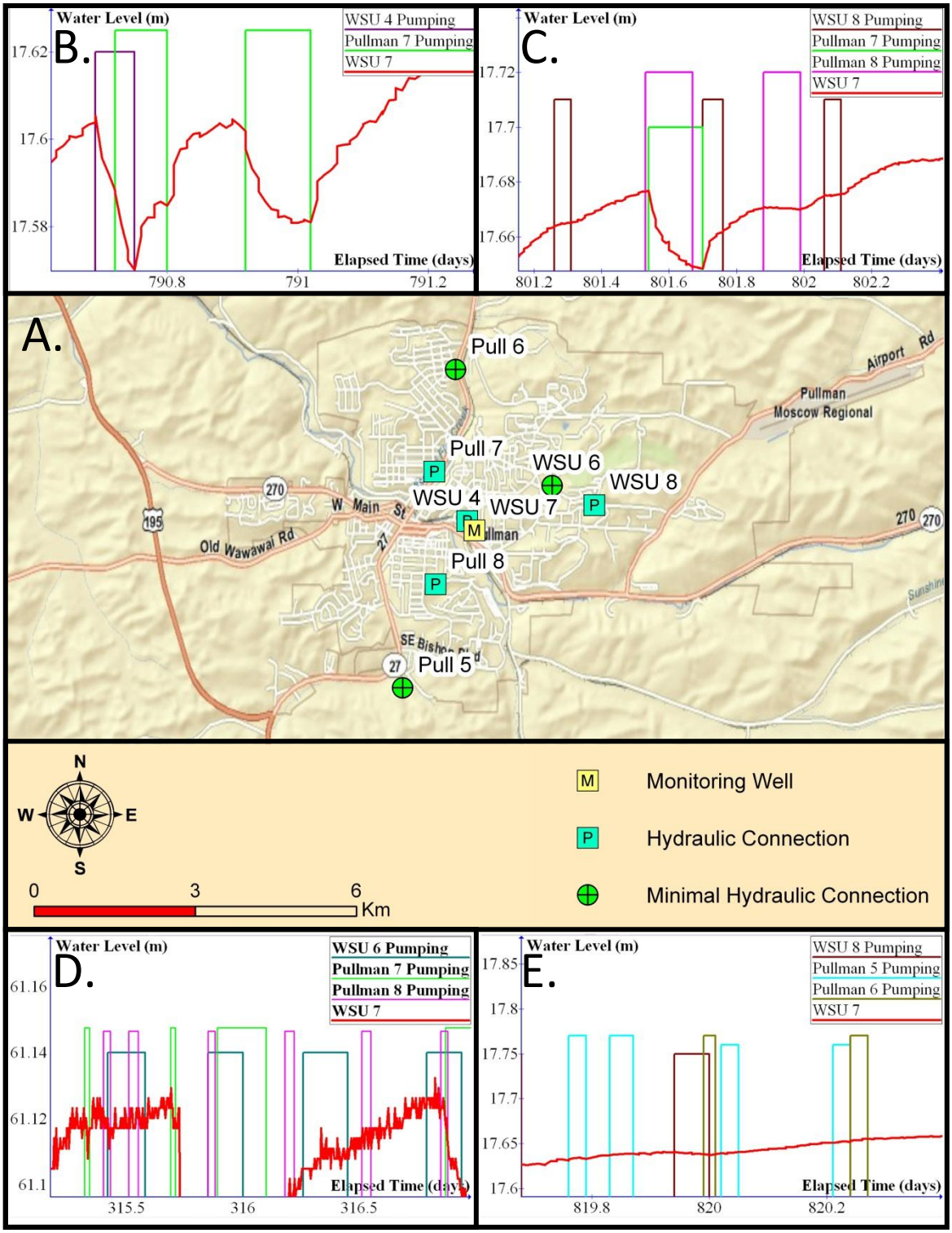

Figure 4.18: A. Well location map. B. through E. WSU 7 hydraulic connections in graphical form. Note: the spiky nature of the WSU 7 water levels in Figure 4.18 D (the only time period monitored with the old silver levelogger®) is believed to be due to older data logger noise as described in section 3.3.

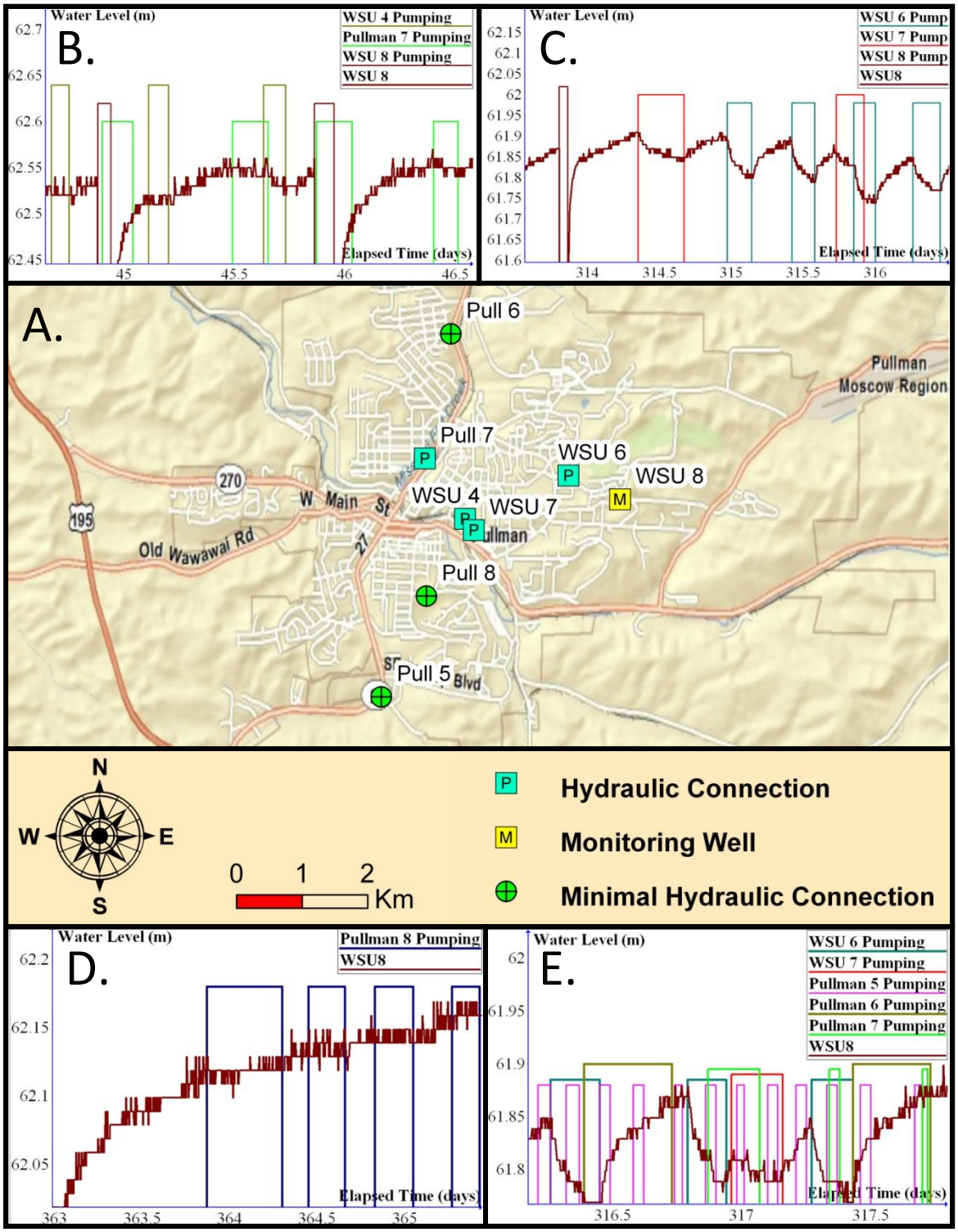

Figure 4.19: A. Well location map. B. through E. WSU 8 hydraulic connections in graphical form. Note: the spiky nature of the WSU 8 water levels in Figures 4.19 B through E is believed to be due to data logger noise as described in section 3.3.

Well connections in LC 3 are evaluated by comparing the on/off pumping periods designated by rectangles in the plots with the water level fluctuations that occurred in observation wells. If the water levels demonstrate an expected drawdown curve, the connection is deemed to be direct through the aquifer. If the well experiences a damped connection, the connection is deemed to be through an aquitard. The following well connections are delineated from drawdown spikes in the water level records when correlated with detailed pumping records (starting in 2009).

The WSU Test monitoring well experiences a strong, direct hydraulic response to the pumping of WSU 4, WSU 7, and Pullman 7 (Figure 4.9 B and Figure 4.9 D). The test well shows a damped hydraulic connection to WSU 8 and Pullman 8 represented by changes in slope of the water level plots when these pumps turned on (Figure 4.9 C). The WSU Test well shows minimal to no response to the pumping of WSU 6, Pullman 5 and Pullman 6 (Figure 4.9 E).

The WSU 6 monitoring well shows a strong, direct hydraulic connection to WSU 7 and WSU 8 (Figure 4.17 B and Figure 4.17 C). Poor data resolution (e.g., noise) and a short data collection period precluded the identification of other potential hydraulic connections.

The WSU 7 well responds to pumping of WSU 4 and Pullman 7 with distinct drawdown spikes (Figure 4.18 B). However, WSU 8 and Pullman 8 pumping only causes slope changes in the water level plots for WSU 7 (Figure 4.18 C) of similar magnitude to the slope changes seen in the WSU Test well data from pumping of these two wells (Figure 4.18 C). WSU 7 showed minimal to no hydraulic connection to WSU 6, Pullman 5 and Pullman 6 (Figure 4.18 D and Figure 4.18 E).

The WSU 8 well in LC 3 shows a hydraulic connection to pumping of WSU 6 and WSU 7 (Figure 4.19 C); Pumping of WSU 4 and Pullman 7 causes slope changes in the water level plots that correspond to the pumping on/off times (Figure 4.19 B). It was concluded that WSU 8 shows minimal to no hydraulic connection to Pullman 5, Pullman 6 and Pullman 8 (Figure 4.19 D and Figure 4.19 E).

The Pullman 3 water levels show a strong hydraulic connection to WSU 7, Pullman 7, and Pullman 8 (Figure 4.20 B). It was concluded that Pullman 3 shows minimal to no hydraulic connection to Pullman 5, Pullman 6, and WSU 8 (Figure 4.20 C through Figure 4.20 E). No water level data were collected during the time periods that WSU 4 and WSU 6 were pumped.

The Pullman 4 monitoring well shows a strong connection to Pullman 7 pumping and also responds to pumping of WSU 4 and WSU 7 (Figure 4.21 B and 4.21 C). The Pullman 4 well shows minimal to no response to the pumping of WSU 6, WSU 8, and Pullman 5 (Figures 4.21 D and 4.21 E). No water level data were collected during the time periods that Pullman 6 and Pullman 8 pumped.

The Pullman 6 monitoring well shows a damped response to pumping of WSU 7 and Pullman 7 (Figure 4.22 B). These damped responses are explained by the fact that the producing zone for Pullman 6 is separated from the producing zone for WSU 7 vertically by an aquitard similar to the geologic conditions near Pullman 8. The Pullman 6 well shows minimal to no response to the pumping of WSU 6, WSU 8, and Pullman 5 (Figures 4.22 C and 4.22 D). No water level data were collected for Pullman 6 during the time periods that Pullman 8 was pumped.

The Pullman 7 monitoring well shows a strong connection to Pullman 4 pumping, and also responds to pumping of WSU 7 and Pullman 8 (Figures 4.23 B and 4.23 C). A short data collection period precluded the identification of other potential hydraulic connections.

Water level data were collected for Pullman 8 for a short period of time between when the well was drilled and when the pump was installed. Pullman 8 was found to respond to the pumping of WSU 4, WSU 7 and Pullman 7 (Figure 4.24 B and Figure 4.24 C). However, because water level plots for Pullman 8 do not show predicted drawdown spikes, Pullman 8 is interpreted to be separated from WSU 4, WSU 7 and Pullman 7 by an aquitard (s). The Pullman 8 well shows minimal to no response to WSU 6, WSU 8, and Pullman 5 (Figure 4.24D). No record exists for Pullman 8 during the time periods that Pullman 6 was pumped.

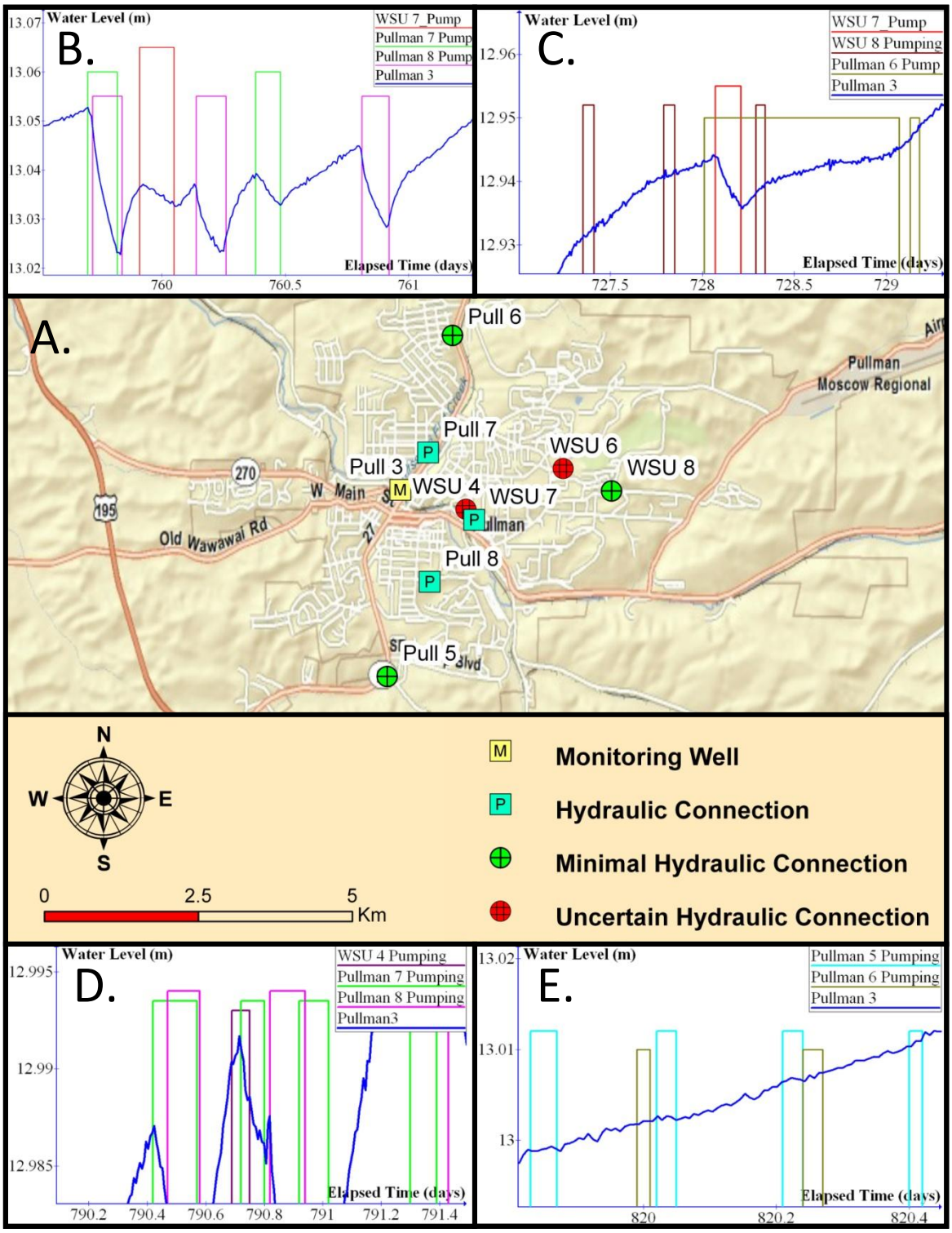

Figure 4.20: A. Well location map. B. through E. Pullman 3 well hydraulic connections in graphical form. Periods of active pumping are designated by the vertical rectangles identifying individual pumping wells. Relative water levels are shown in meters above an arbitrary datum.

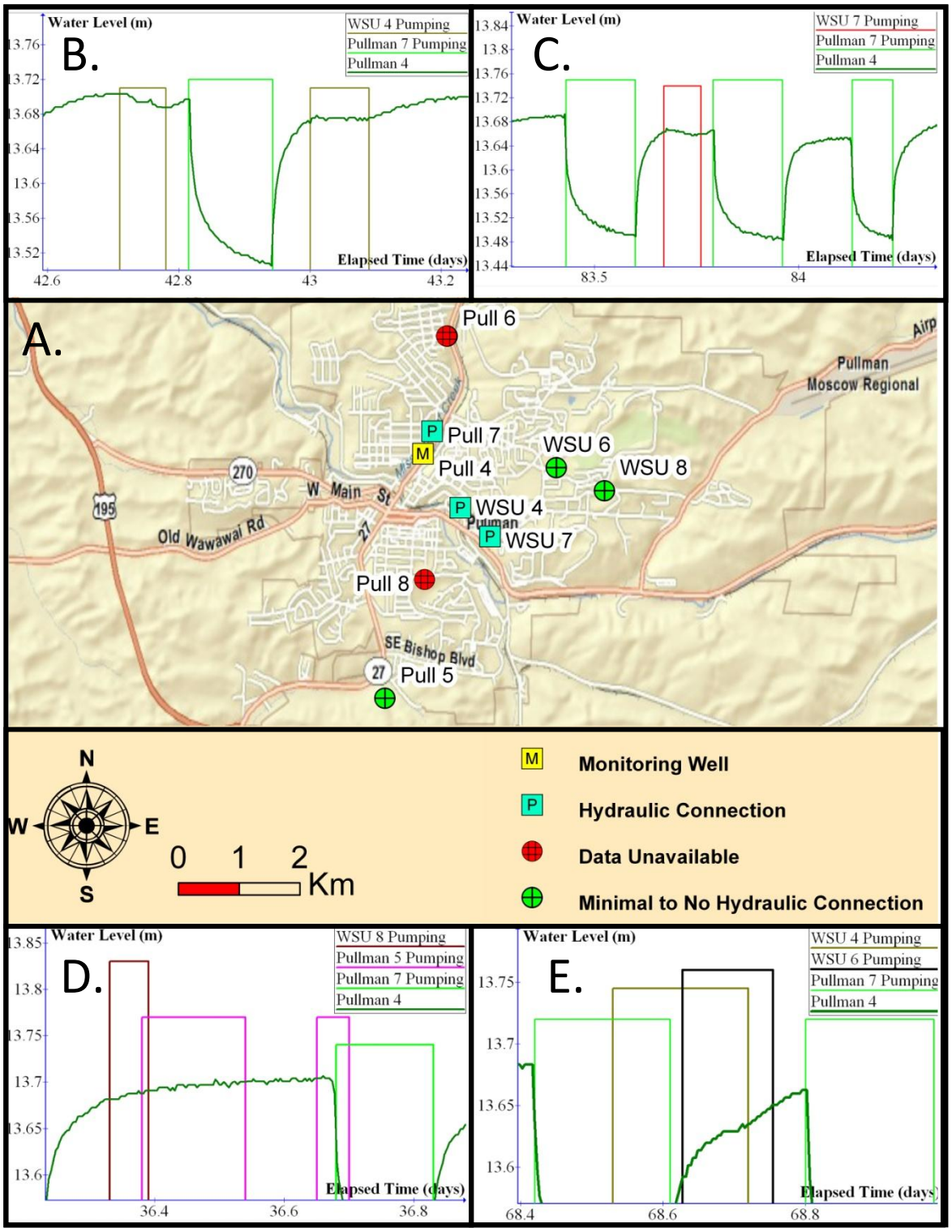

Figure 4.21: A. Well location map. B. through E. Pullman 4 well hydraulic connections in graphical form.

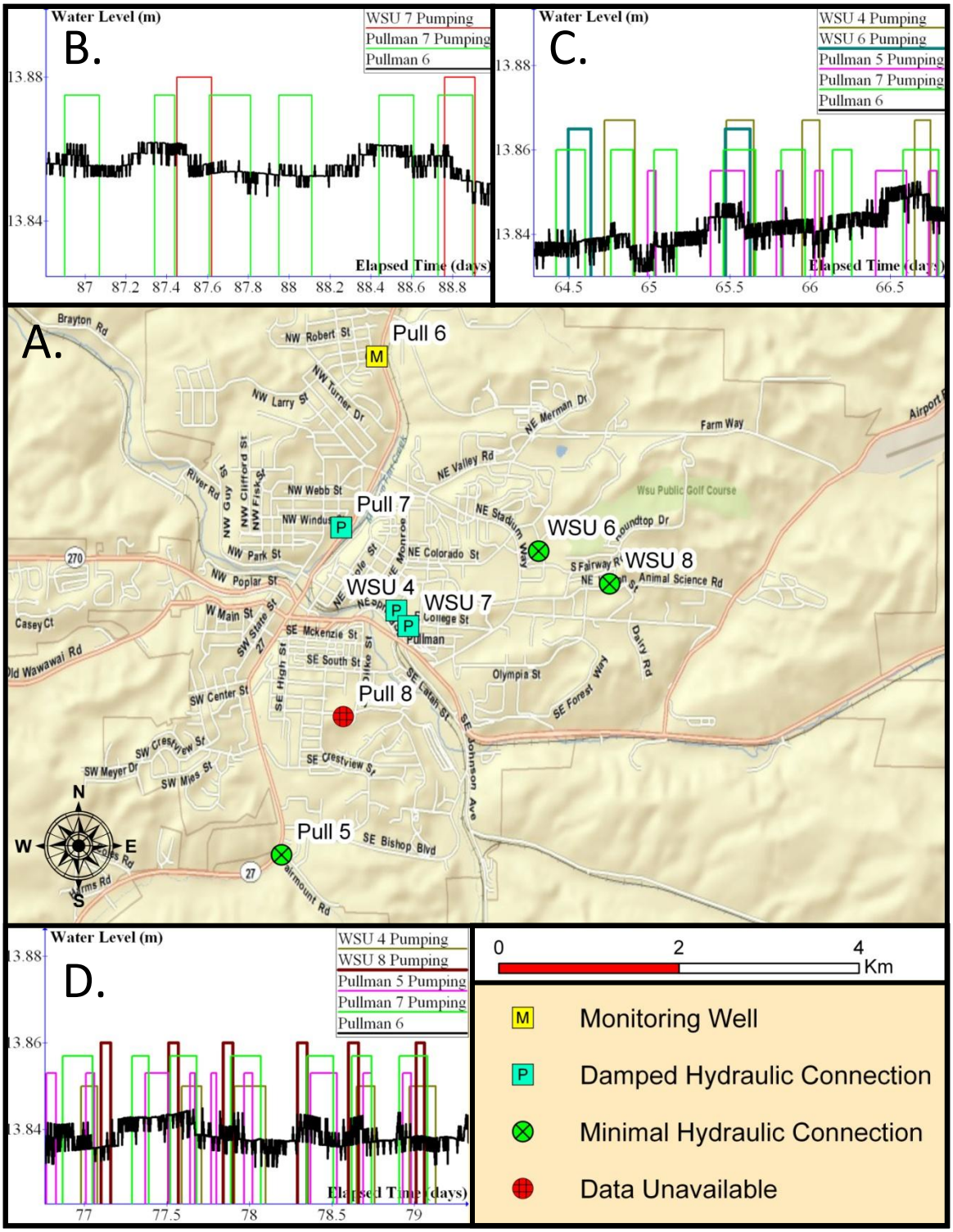

Figure 4.22: A. Well location map. B. through D. Pullman 6 well hydraulic connections in graphical form. Note: the spiky nature of the Pullman 6 water levels in Figures 4.22 B. through D is believed to be due to data logger noise as described in section 3.3.

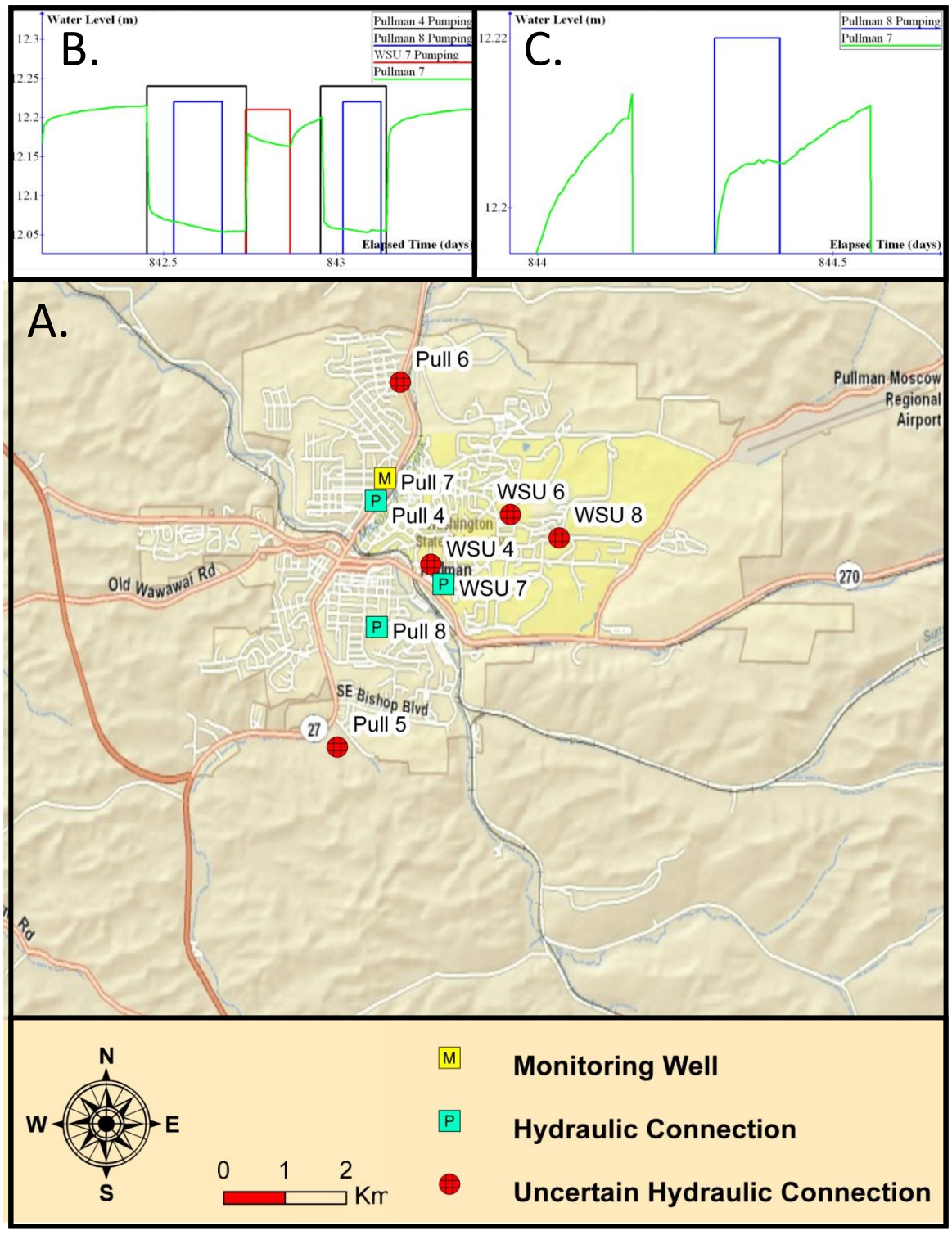

Figure 4.23: A. Well location map. B. through C. Pullman 7 well hydraulic connections in graphical form.

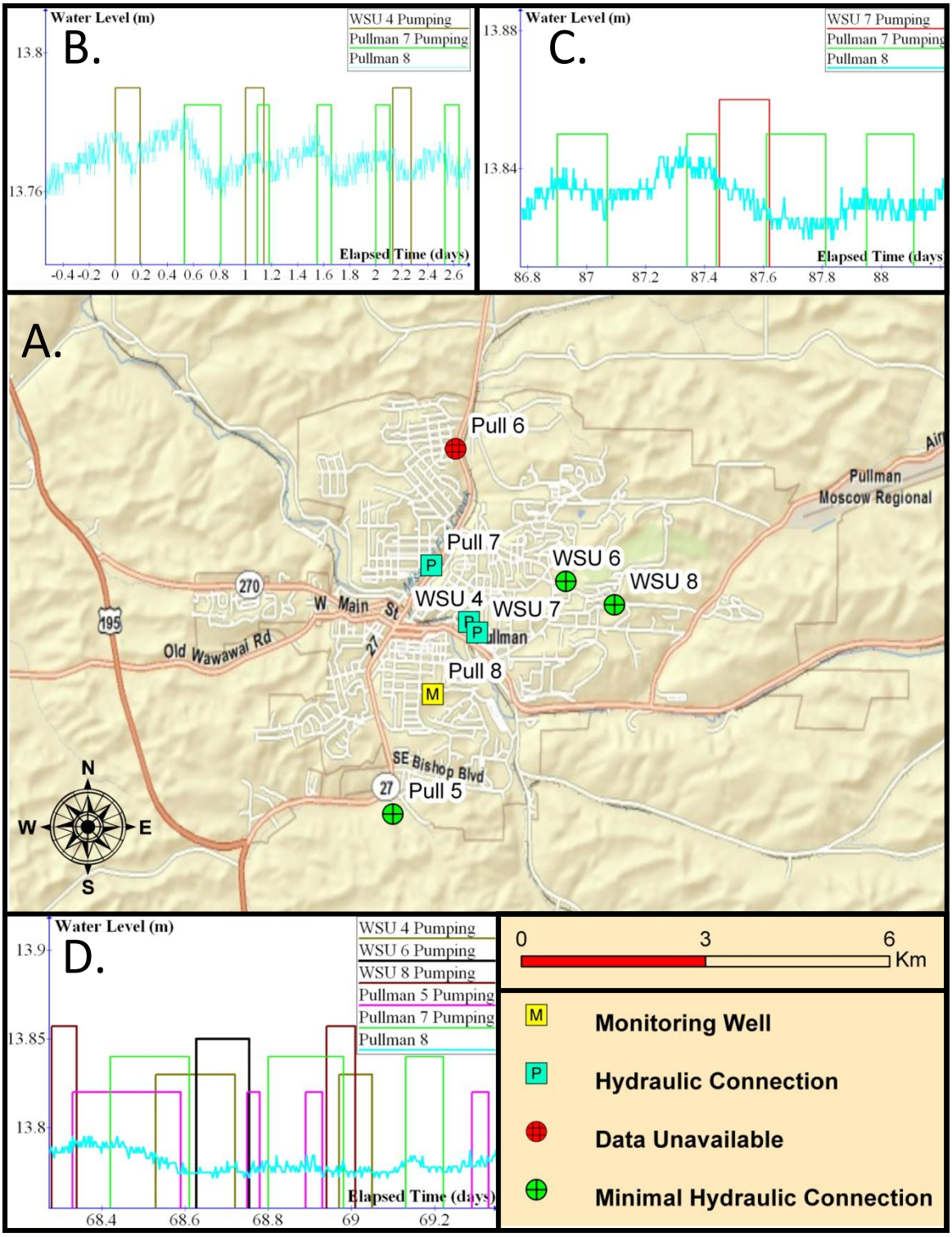

Figure 4.24: A. Well location map. B. through D. Pullman 8 hydraulic connections in graphical form. Note: the spiky nature of the Pullman 8 water levels in Figure 4.22 B. through D is believed to be due to data logger noise as described in section 3.3.

Calculated drawdown in all wells completed in LC 3 exhibit similar seasonal and annual water level trends as shown in Figure 4.25 and Figure 4.26. Pullman 5 pumps more than 1600 gpm and Pullman 6 pumps more than 650 gpm; the two wells both are approximately 2 km south and north, respectively from the WSU Test well (Figure 4.9 A). During this investigation, no evidence of hydraulic connection between Pullman 5 or Pullman 6 with any other basin wells was identified based on short-term or annual data. The lack of response in basin wells from these pumpers suggests that some type of hydraulic discontinuity exists (Owsley, 2003).

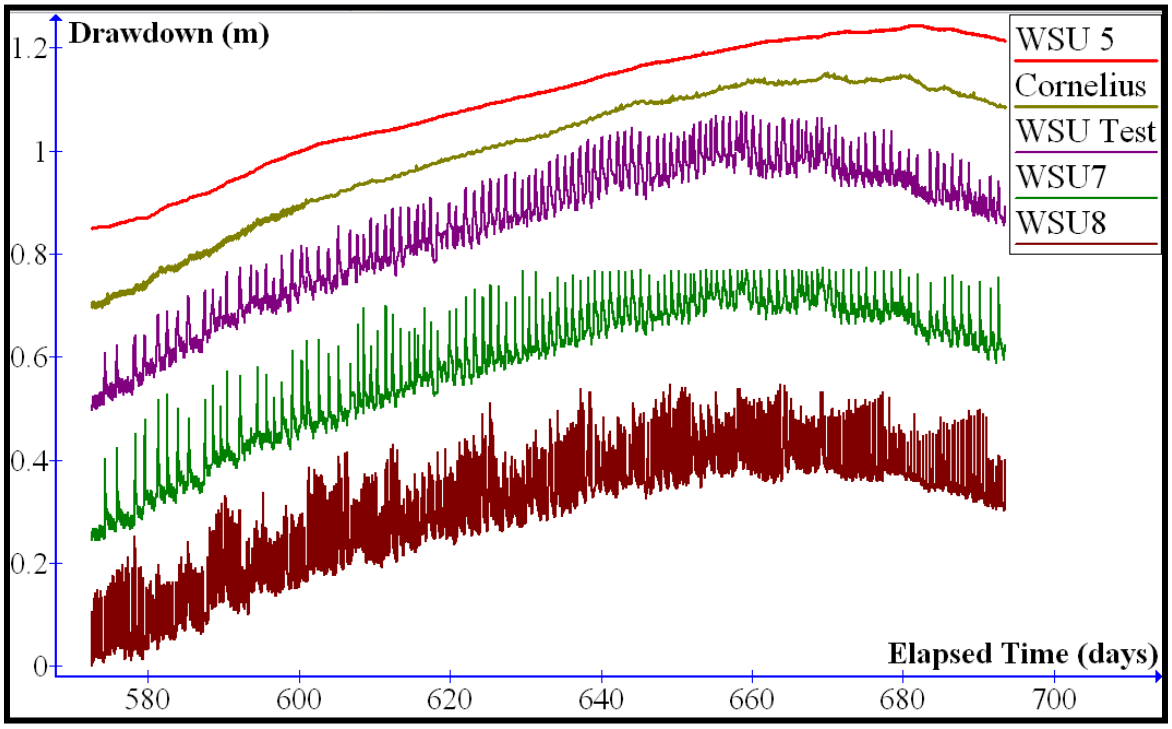

Figure 4.25: Arithmetic plot of calculated drawdown versus time for selected wells in LC 3 (pumping spikes in WSU 7 and WSU 8 have been truncated vertically to fit the vertical scale of the plot for visual purposes). Individual plots have been offset vertically in order to compare drawdown magnitudes.

No water level data were collected for the Pullman 5 well during the test. Future researchers who collect water level data for Pullman 5 will probably find other area pumping well signatures in plots of the water level data. Therefore, the conceptual model described herein places Pullman 5 in a different producing zone or lateral compartment from other Pullman area wells, but more data are needed to allow delineation of the aquifer conditions for this well.

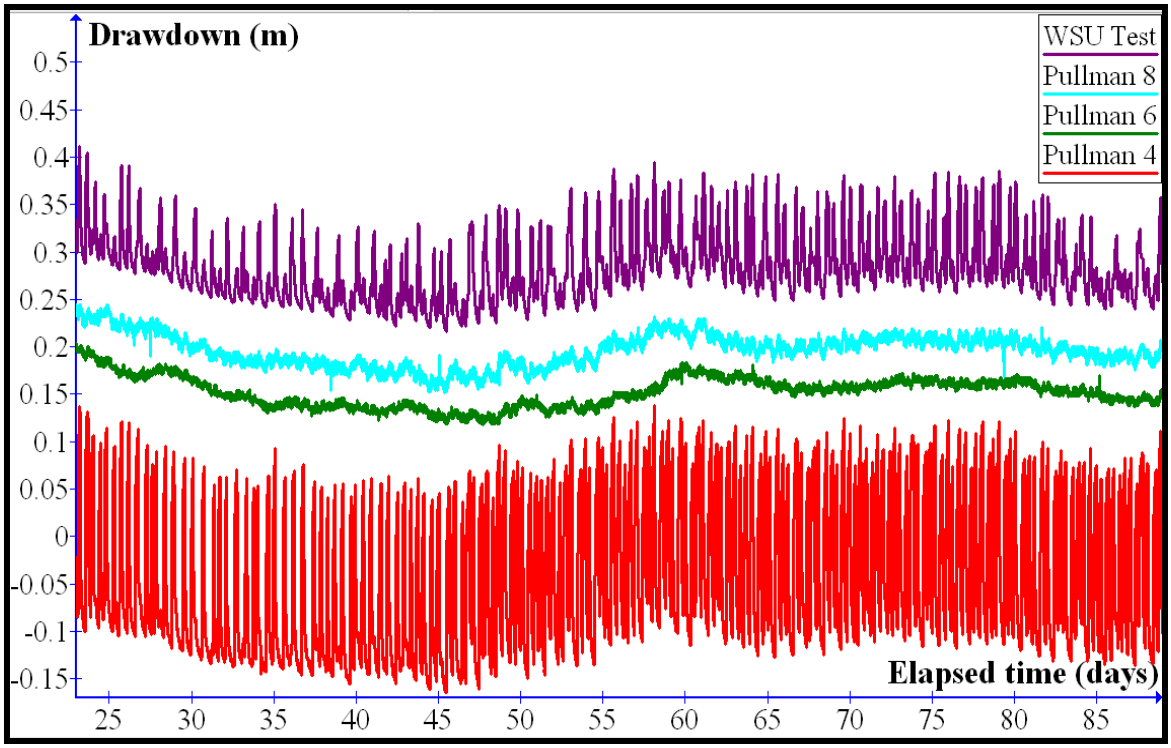

Figure 4.26: Arithmetic plot of calculated drawdown for Pullman 4, Pullman 6, Pullman 8, and the WSU Test well in LC 3 for the time period of 12/17/2009 to 2/23/2010. Individual plots have been offset vertically in order to compare drawdown magnitudes.

Figure 4.27 illustrates the geological variability within LC 3. The Latah formation interbeds are not as prevalent or thick in LC 3 compared to LC 1 and LC 2. Where these interbeds are present in LC 3, they have a similar damping effect on the migration of cones of depression similar to what is seen in LC 1 and LC 2 observation wells when Moscow 6 and Moscow 8 pump. In LC 3, the bottom of WSU 6, WSU 8, and Pullman 8 are completed in the Latah sediments which dampens the cone of depression from each well resulting in only small slope changes in plots of WSU 7 and WSU Test well water levels.

The evaluation of hydraulic connection may be incomplete for some of the wells discussed due to the absence of data for the time periods that certain wells were pumped. The WSU Test well and Pullman 3, both instrumented with more accurate Solinst® Gold Leveloggers®, do not respond to pumping of Pullman 5 or Pullman 6, but do respond to other pumping wells; therefore, the water level records for the WSU Test well and Pullman 3 best illustrate the varying degrees of heterogeneity in the Pullman area.

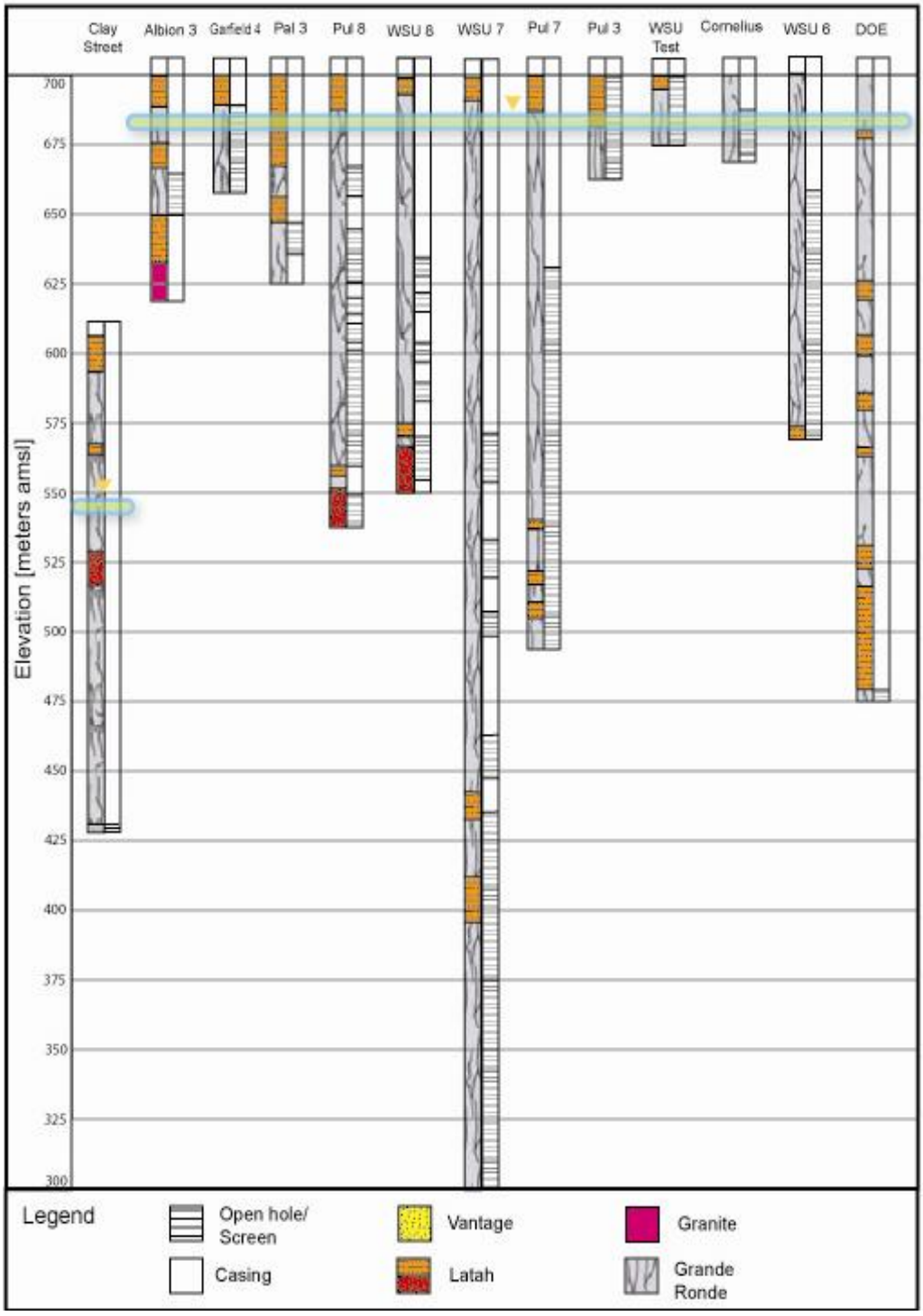

Figure 4.27: LC 5 water level (~541.6) and open hole or screened zones geology compared with current LC 2, LC 3, and LC 4 compartment water level of ~684 meter amsl. The bottom portion of the WSU 7 well log is not shown in order to fit the scale of the figure, and the DOE well log is shown for comparison. No horizontal scale. Note: the gravel unit in WSU 8, Pullman 8, and the Colfax Clay Street well are evidence for an ancestral fluvial system (s) that drained surface water from the eastern side to the western side of the basin.

Accurate description of hydraulic connections was difficult for the following wells: Pullman 4, Pullman 6, Pullman 8, WSU 6, WSU 7, and WSU 8. This was potentially due to data logger noise masking the evidence of small magnitude drawdown and recovery spikes from other wells in LC 3.

4.6.3.1 LC 3 Upper Producing Zone #1 (WSU 5 and Cornelius)

WSU 5 and Cornelius are upper Grande Ronde aquifer wells that are monitored within LC 3. WSU 5 is a decommissioned production well located northeast of Pullman in the vicinity of the Pullman Regional Airport (Figure 4.28 A). The Cornelius well is a domestic pumping well that is located southwest of Pullman in the vicinity of the Sand Road (Figure 4.29 A). The WSU 5 and Cornelius calculated drawdowns clearly mimic the non-pumping (e.g., "semi-static") drawdowns in the WSU Test, WSU 7 and WSU 8 wells (i.e., bottom surface of each plot); however, distinct drawdown spikes and recovery troughs are absent in the WSU 5 and Cornelius records compared to the other wells when plotted at the same scale (Figure 4.25). Spikes and troughs clearly are masked or buffered by one or more low hydraulic conductivity aquitards that cause separation from the main producing zone (s) in LC 3.

WSU 5 and Cornelius appear to be completed in a shallow, overlying aquifer that is unpumped by the major production wells in LC 3. Figure 4.30 illustrates the similar pattern of drawdown in the overlying aquifer in LC 3. WSU 5 and Cornelius show a different pattern beginning about 660 days in the arithmetic plot. Recovery from summertime drawdown in both wells lags behind the other LC 3 wells with WSU 5 having the gentlest recovery water level slope.

According to Fiedler (2009), the Cornelius well appears visually to be affected by Pullman 8 and WSU 7 pumping. WSU 7, WSU 8, Pullman 7, and Pullman 8 are all frequently-pumped, high volume production wells (between 1700 and 2400 gpm). This investigation found that the Cornelius water levels are extremely sensitive to solar and

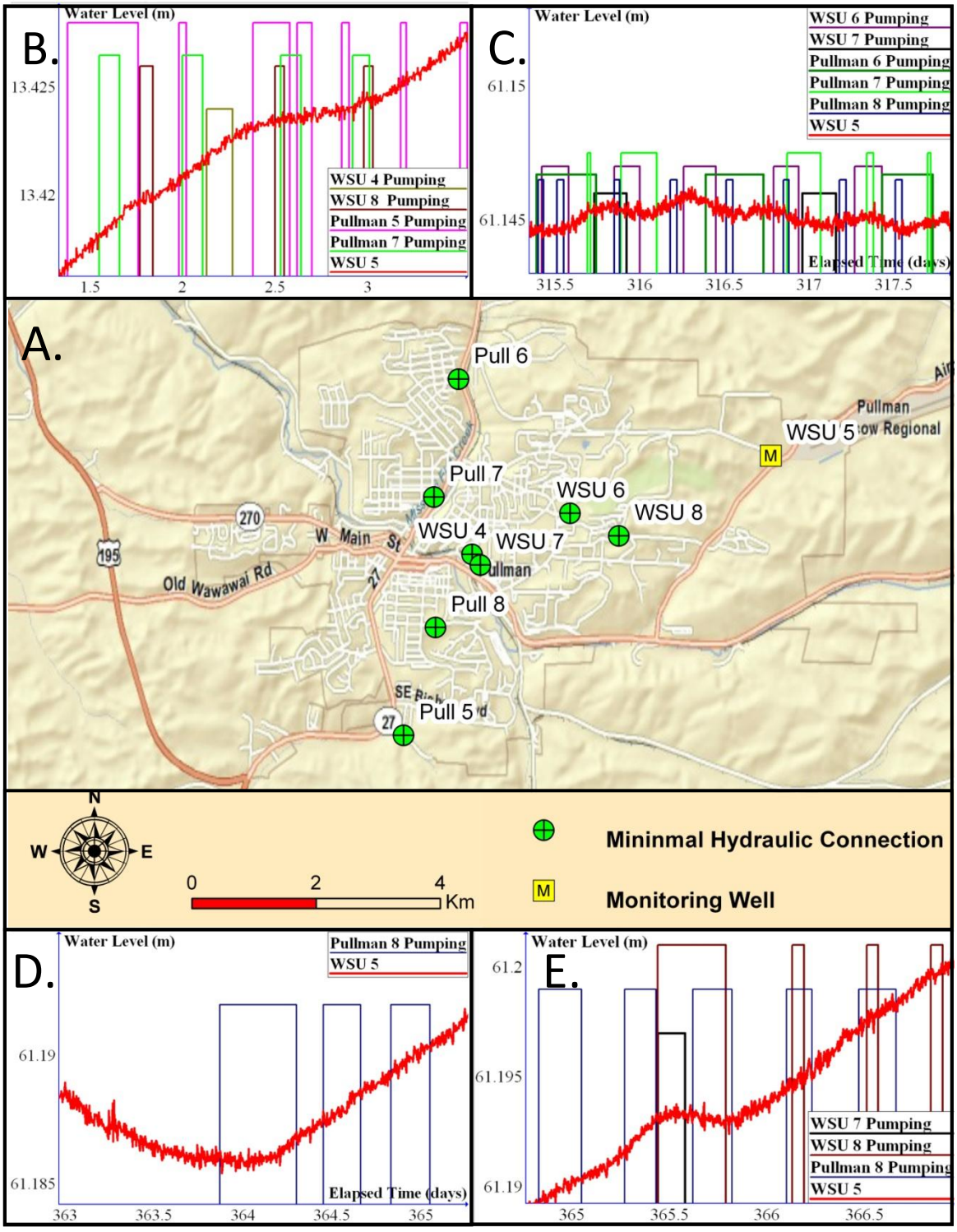

Figure 4.28: A. Well location map. B. through E. Relative water level plots for WSU 5 showing the lack of hydraulic connections to area pumping. Note: the spiky nature of the WSU 5 water levels in Figure 4.28B. through 4.28E is believed to be due to data logger noise as described in section 3.3.

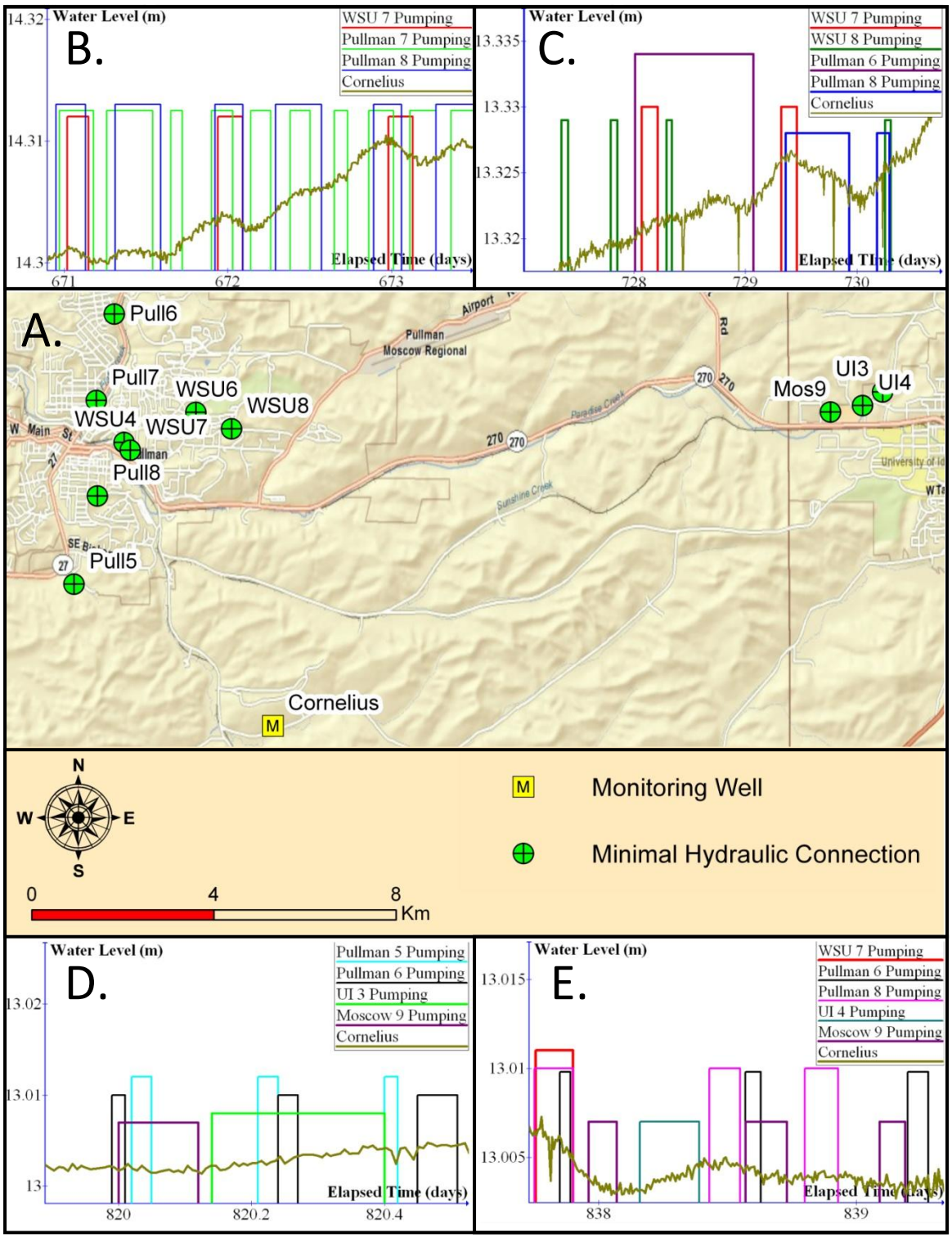

Figure 4.29: A. Well location map. B. through E. Relative water level plots for Cornelius showing the lack of hydraulic connections to area pumping. Note: the spiky nature of the Cornelius water levels in Figure 4.28 B. through 4.28 E is believed to be due to data logger noise as described in section 3.3.

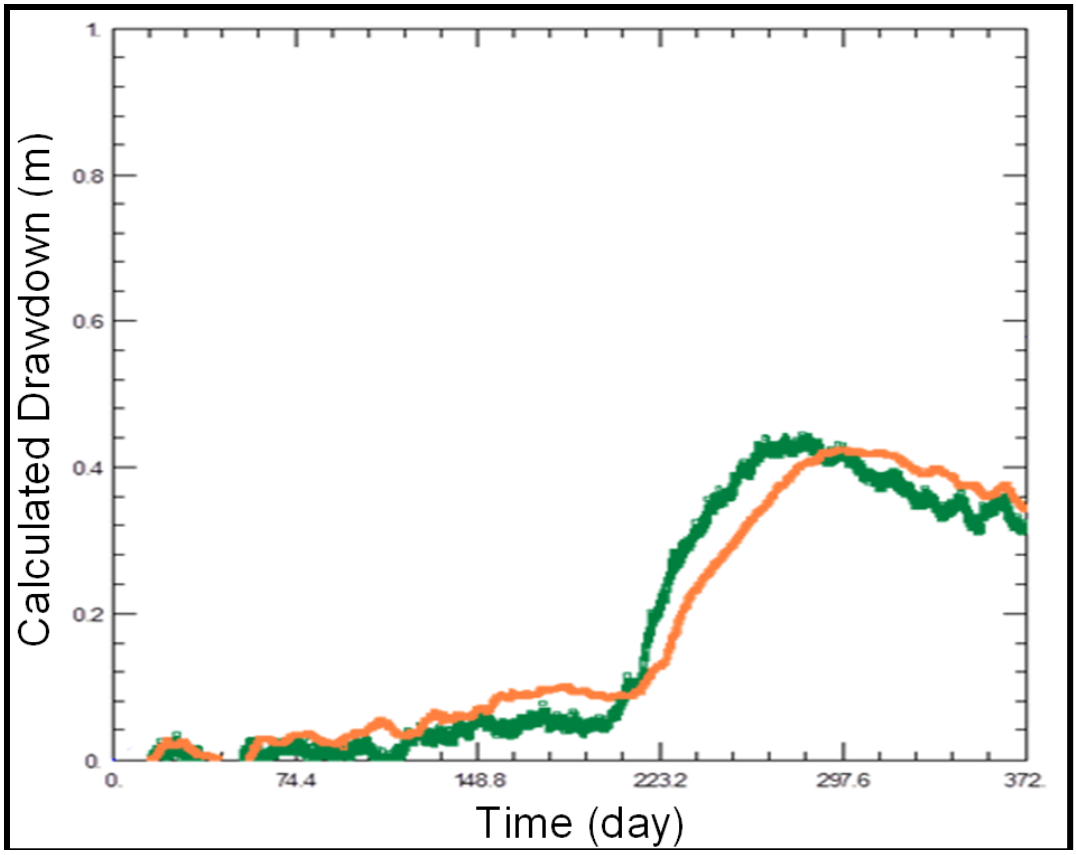

Figure 4.30: Corrected drawdown for WSU 5 (Orange) and Cornelius (Green).

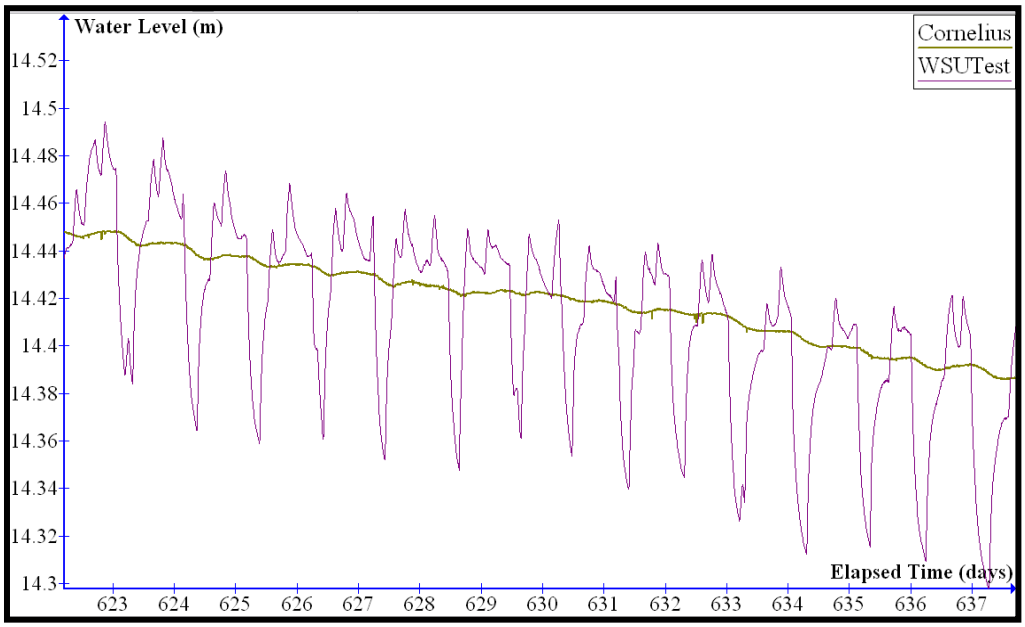

Figure 4.31: Observed WSU 7 drawdown effects in the WSU Test well compared to the Cornelius well from WSU 7 pumping combined with other smaller compartmental pumping influences.

lunar tides, which were originally confused with drawdown from the pumping of WSU 7. Figure 4.31 demonstrates a strong connection between WSU 7 and the WSU Test well (0.2 km) and a possible damped connection between WSU 7 and the Cornelius well (4.7 km). However, based on a preliminary examination of the amplitude of water level fluctuations related to solar tides in the Cornelius well, hydraulic connection between WSU 7 and Cornelius cannot be confirmed until a solar tide correction is developed.

4.6.4 Lateral Compartment 4 (Garfield-Palouse (Gar-Pal) Compartment)

Lateral Compartment 4 (LC 4) is located north of the Kamiak Gap and includes the cities of Palouse and Garfield (Figure 4.1). Correlation of Palouse 1 and Palouse 3 water level data with Garfield 3 and Garfield 4 pumping records show that no direct connection between the wells is obvious (Figure 4.32 B and Figure 4.32 C). However, not enough data exist to place Garfield in a separate compartment. The Palouse hydrographs in Figure 4.32 B through Figure 4.32 E also show changes in water level that probably represent the effects of lunar cycles; the lunar effects appear as small magnitude rolling hills and valleys in water level plots rather than steep spikes or troughs. Long-term calculated drawdown in LC 4 correlates poorly with all the other wells in the PGB. This poor correlation is illustrated between Palouse 3, DOE, and the WSU Test well in Figure 4.33. Palouse 3 calculated drawdown includes numerous short-term trends that do not appear in other PGB calculated drawdown records during the summertime drawdown and system recovery periods. The primary difference between Palouse trends and the rest of the PGB are discussed in Section 5.2. The timing of these summertime pumping caused trends in Palouse during this investigation is a phenomenon that has only been identified in the Palouse area. This compartment includes Glenwood 1 and Glenwood 2 due to them being flowing wells (groundwater discharge areas by definition). Due to Clay Street and Fairview wells having lower water level elevations, the groundwater flow to the Glenwood wells appears to come from Palouse or Garfield. Further analysis is needed to understand the extent that Garfield, Palouse, and Glenwood pumping might have on water levels in each location within LC 4.

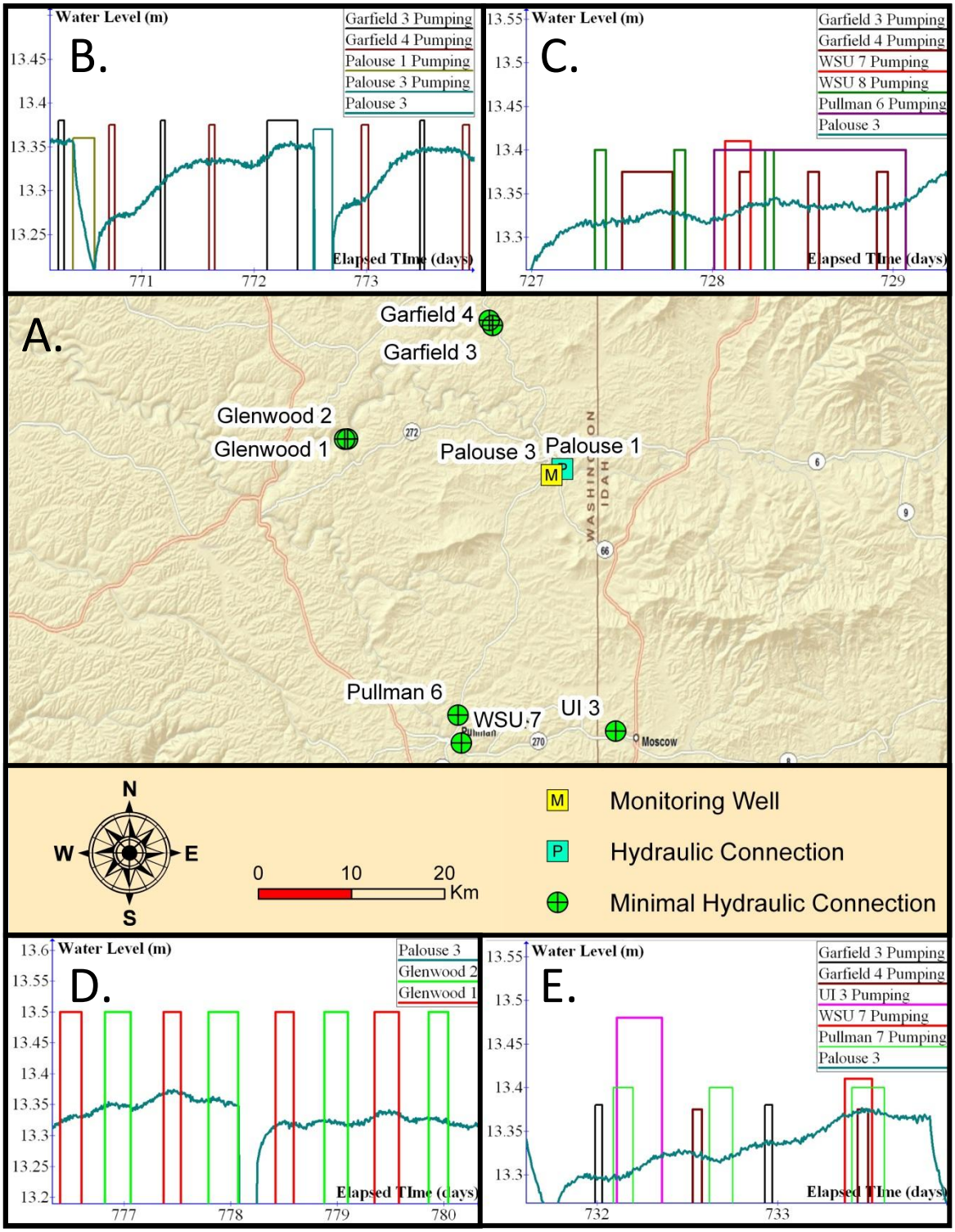

Figure 4.32: A. Well location map. B. through E. Palouse 3 hydraulic connections in graphical form.

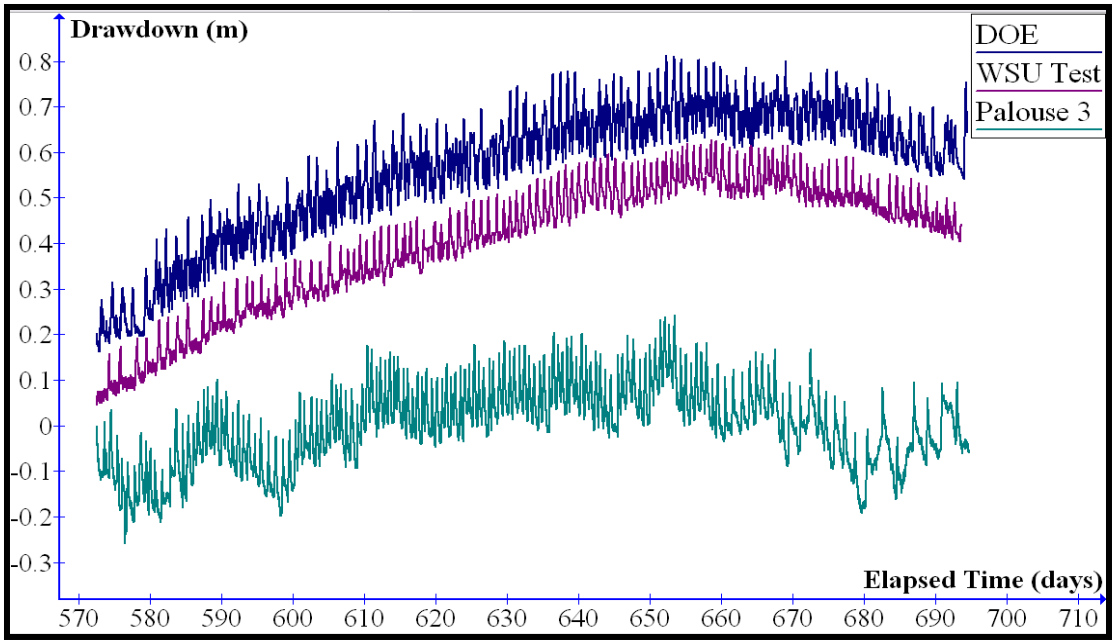

Figure 4.33: Arithmetic plot of calculated drawdown versus time for Palouse 3, DOE, and WSU Test well. Relative calculated drawdown values are in meters above an arbitrary datum. Individual plots have been offset vertically in order to compare drawdown magnitudes.

As part of this investigation, 2003 groundwater records for Garfield 4, Palouse 1 and the DOE well from the PBAC database were examined. Comparing of Palouse 1and Garfield 4 water levels showed a poor visual correlation (Figure 4.34 A). Garfield 4 water levels showed typical PGB summertime drawdown and system recovery; the water levels in Garfield 4 and DOE were measured with first generation Solinst® Leveloggers which were not as sensitive or accurate as the third generation Solinst® Gold Leveloggers. Palouse 1 water level data showed sporadic, larger fluctuations during the summertime drawdown and recovery periods that are similar to those observed during this investigation; however, unfortunately the water level data for Palouse 1 were recorded with an old Druck® transducer of somewhat questionable sensitivity and accuracy. Garfield and Palouse wells show comparable summertime slopes and timing which provides evidence that they are both located within LC 4 (Figure 4.35).

When Garfield 4 water levels are visually compared to DOE water levels a good visual correlation exists (Figure 4.34 B). Both summertime drawdown and system recovery occur at similar time periods for these two wells. However, Garfield 4 and DOE water

levels exhibit different summertime drawdown slopes and magnitudes which suggest that these two wells are in different compartments. According to Figure 4.35, the summertime drawdown slope is the smallest for Garfield followed by Palouse suggesting that the slope decreases the farther north from the large pumping centers of Moscow and Pullman the observation well is located. All three wells exhibit similarly shaped, smaller groundwater trends from seasonal pumping variations that occur at ET=110 and ET=150.

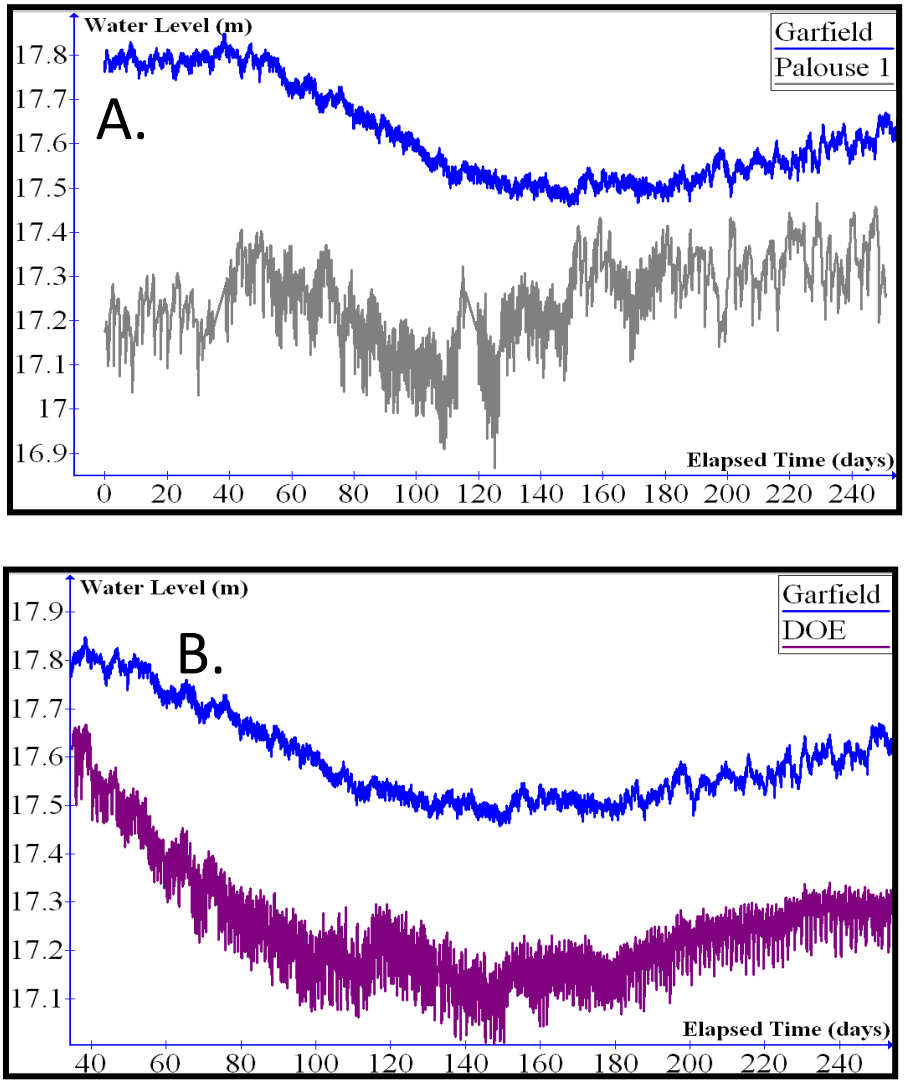

Figure 4.34: A. Arithmetic plots of relative water levels measured in Garfield 4 and Palouse 1 in 2003 (ET=0 days is 04/10/2003 at 16:00 and ET=240 is 12/6/2003 at 16:00). B. Arithmetic plots of relative water levels measured in Garfield 4 and DOE in 2003 (ET=40 days is 05/20/2003 at 16:00 and ET=240 is 12/6/2003 at 16:00). Relative water levels in meters above an arbitrary datum.

Because poor investigator notes were kept on how the data were collected and/or modified, it is not possible to evaluate the quality of the data used to develop Figures 4.34 and 4.35. Also, no water level data exist for the Glenwood wells to evaluate whether these wells exhibit similar slopes and timing compared to LC 4 or LC 5.

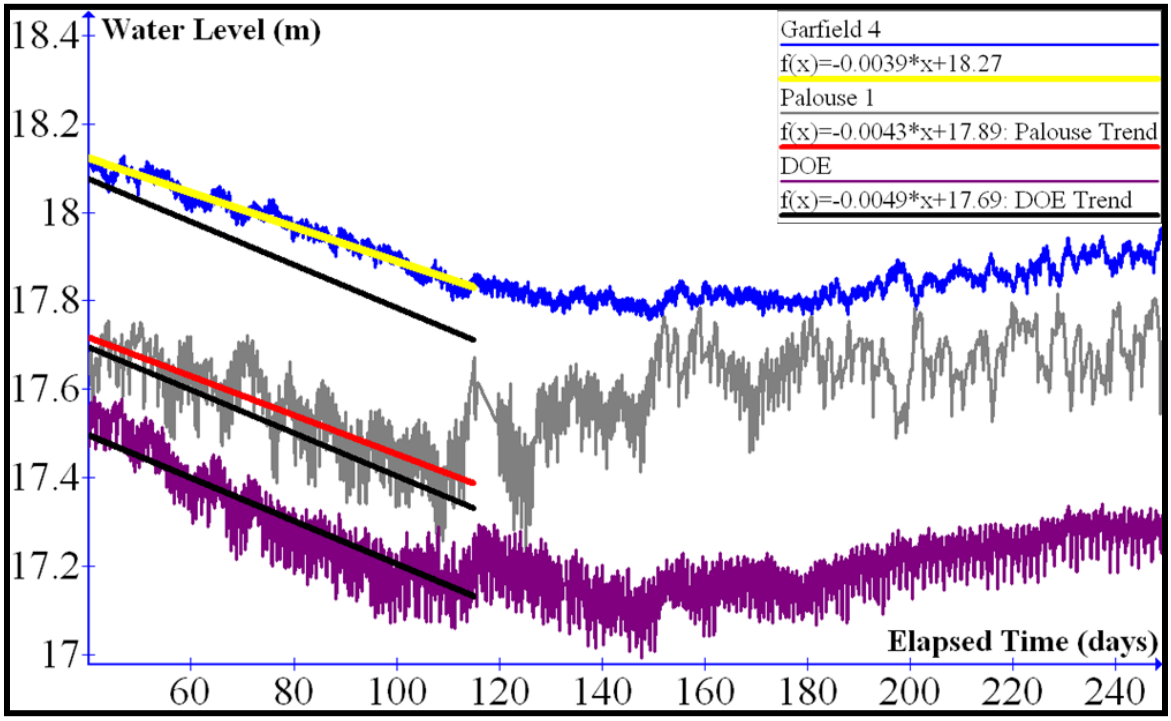

Figure 4.35: Arithmetic plots of relative 2003 summertime water level slopes for the Garfield 4, Palouse 1, and DOE wells (ET=40 days is 05/20/2003 at 16:00 and ET=240 is 12/6/2003 at 16:00). Black lines showing the DOE water level slope for 117 days are superposed on to the Garfield 4 and Palouse 1 plots for comparison purposes. Individual plots have been offset vertically in order to compare drawdown magnitudes.

4.6.5 Lateral Compartment 5 (Colfax Compartment)

Lateral Compartment 5 (LC 5) includes the city of Colfax and is bounded by Union Flat Creek to the southwest, Steptoe Butte to the north, Kamiak Butte and Smoot Hill to the southeast (Figure 4.1). For this investigation, the northeastern boundary is considered to be located just west of the Glenwood wells. The east boundary is considered to be located just west of Albion because according to the Framework Project (TerraGraphics, Inc., 2011), Albion water levels apparently are consistent with LC 3 water levels. This compartment includes pumping wells Clay Street and Fairview.

Clay Street water levels have been monitored periodically during the past three years (2009-2012), and the most dependable data from the Schlumberger Micro-Diver® are used in this analysis. However, the Micro-Diver® water levels are noisy when compared to the newest generation levelogger®. No hydraulic connections have been identified between Clay Street and any other wells in LC 5 (Figure 4.36 B and Figure 4.36 C). The Fairview well was not pumped during the recent water level data collection period; therefore, it is not known if the Clay Street and Fairview wells are hydraulically connected. Additional aquifer tests are needed to further characterize LC 5. Water level trends were used as the strongest evidence for demonstrating that Colfax is in its own compartment. As shown in Figure 4.37, Colfax water levels do not show any of the short-term trends that are observed in LC 2, LC 3, and LC 4.

An accurate water level measurement was taken in the Clay Street well when the old Druck® transducer was replaced with a Schlumberger Micro-Diver® direct read data logger on December 1, 2011 at 12:10 pm. At that time, the water level elevation above mean sea level (amsl) was 541.6 meters (not corrected for barometric). Groundwater elevation data indicate that a large drop (approximately 142 m) in the potentiometric surface of the Grande Ronde exists between Albion and Colfax (straight-line distance of 14.42 kilometers obtained from Table A03 in Appendix A), corresponding to a horizontal gradient of 0.0098 m/m between the Albion 2 well and the Clay Street well. This relatively large gradient between Colfax and the rest of the PGB suggests that the long-term westward groundwater flow out of the PGB is slow. The small leakage rate from LC 3 to LC 5 suggests a very different type of boundary exists at this location compared to other compartments walls in the PGB. Leakage from LC 3 to LC 5 is hypothesized to occur through features such as relatively small, gravel filled, buried stream channels or a narrow, basalt and sediment filled, scour feature with a small cross-sectional area.

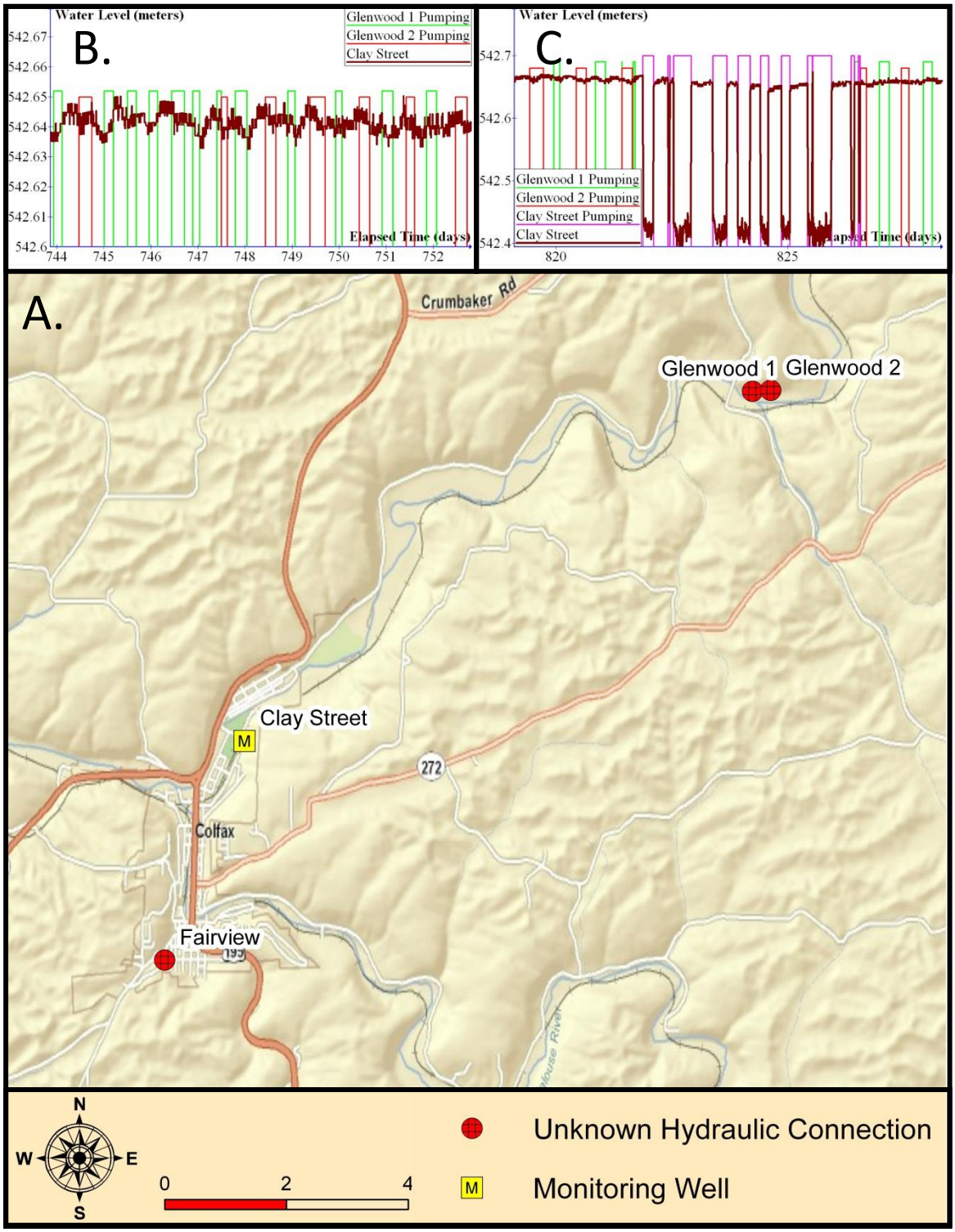

Figure 4.36: A. Well location map. B. and C. Clay Street hydraulic connections in graphical form. Note: the spiky nature of the Clay Street water levels in Figure 4.36 B is believed to be due to data logger noise as described in Section 3.3.

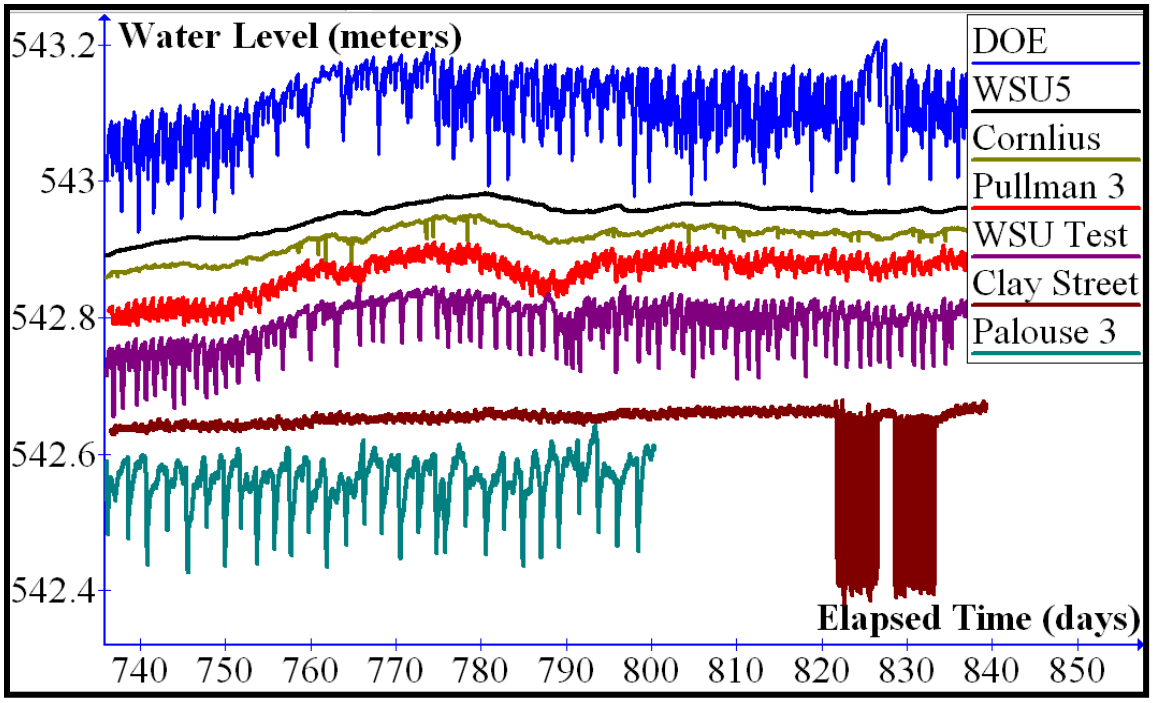

Figure 4.37: Relative water levels for the Colfax Clay Street well (LC 5) versus water levels for wells in LC 2, LC 3, and LC 4 from December 1, 2011 to March 10, 2012. Clay Street started pumping at approximately ET=820 days. Individual plots have been offset vertically in order to compare magnitudes of water level changes.

As shown in Figure 4.27, the Pullman 8 and WSU 8 well logs record gravel units at different elevations suggesting that streams deposited gravel beds on the top of some basalt flows during the hiatus between extrusions of individual flows. The well log for the Clay Street well indicates a similar gravel bed exists in Colfax, but at a significantly deeper stratigraphic location. These gravel beds in the Colfax and Pullman areas are hypothesized to be part of the ancestral fluvial system (s) that drained surface water from the eastern side to the western side of the basin over several millions of years during extrusion, and subsequent weathering and erosion of the Grande Ronde basalts. These buried paleo-drainage system (s) are believed to provide present-day conduits for groundwater underflow from LC 3 to LC 5. Further evidence for a small outflow exists in the area of Parvin Road (located between Colfax and Albion in Figure 4.1); Grande Ronde wells drilled in this area are poor water producers, and many wells have had to be deepened to increase yields. This area has the reputation as being a low productivity,

"dead zone" for Grande Ronde well yields in the PGB. This zone is an area of relatively low hydraulic conductivity which is consistent with limited underflow from LC 3 to LC 5.

4.7 Compartment Delineation Techniques

Snyder and Haynes (2010) created generalized groundwater-elevation maps for the CPRAS Grande Ronde aquifer system using a three-stage geostatistical process. Unlike, Snyder and Haynes (2010), geostatistical methods may not be useful for the PGB because they generally mask discontinuities by assuming a correlation exists between water levels which is contrary to the compartmentalization conceptual model. For this investigation PGB compartment evaluations were conducted by mapping of groundwater temperature and groundwater age dates in relation to measured or non-measured hydraulic responses in wells from known hydraulic stresses. An GIS Arc Map®10.0 developed by the inverse distance weighting method with nearest neighbor estimation was used herein to present the data in map form to help estimate compartment boundaries. These smoothed maps provide rough estimates of variations in these parameters, but better definition requires larger sample sizes in the PGB.

4.7.1 Grande Ronde Groundwater Temperature Mapping

Mapping of the groundwater temperature at the same instant in time in the PGB provides additional evidence to help identify individual compartments. Table 4.1 displays the range of temperatures measured in the basin wells during the data collection period of this investigation.

Range in Temperatures ^{o}C				
Well	**Max**	**Min**	**Difference**	**Data Collection Period**
Clay Street	19.71	17.62	2.09	12/1/2011 to 3/13/2012
DOE	13.89	13.69	0.20	11/24/2009 to 3/15/2012
IDWR 4	13.18	12.99	0.18	11/24/2009 to 3/15/2012
WSU 8	15.58	14.44	1.14	11/24/2009 to 3/13/2012
WSU 7	16.42	14.57	1.85	3/1/2010 to 3/13/2012
WSU 6	14.53	13.80	0.73	12/12/12 to 1/24/2012
WSU 5	12.07	10.85	1.22	11/24/2009 to 3/13/2012
WSUTest	14.60	13.12	1.48	11/24/2009 to 3/13/2012
Corn	14.13	13.12	1.01	11/24/2009 to 3/13/2012
Pal1	15.73	11.14	4.59	11/24/2009 to 9/21/2010
Pal3	15.75	7.43	8.32	11/24/2009 to 2/3/2012
Pullman 3	13.91	13.40	0.51	11/10/2011 to 3/13//2012
Pullman 4	14.84	14.54	0.30	12/17/2009 to 2/23/2010
Pullman 6	13.79	13.02	0.77	11/24/2009 to 3/26/2010
Pullman 8	11.83	11.42	0.41	11/24/2009 to 2/23/2010
Moscow 6	16.53	16.19	0.34	2/23/2012 to 3/7/2012
Moscow 7	13.98	13.84	0.14	11/24/2009 to 12/18/2010
Motley-Motley	11.37	10.92	0.45	10/8/2010 to 3/13/2012

Table 4.1: Groundwater temperatures measured in PGB wells for the data collection period.

Figure 4.38 illustrates the areal distribution (2-D) of relative groundwater temperature data as interpolated between measurement points (wells). Temperature data for March 1, 2012 were normalized by the average, well producing zone (screened intervals) depth below land surface, for each well (i.e., temperature/well depth) to test whether groundwater temperature patterns are consistent with compartments that have been identified in the PGB.As shown in Table 4.1 groundwater temperatures in the Grande Ronde vary by as much as 12 ^{o}C seasonally across the PGB. The temperature regime is highly variable throughout the basin owing to the complexity of the recharge, hydrogeology, and hydraulic isolation. Groundwater temperature in a specific well typically is dependent on the length of time since pumping stopped. Therefore, the temperature measurements recorded during periods with no pumping were used in the interpolation.

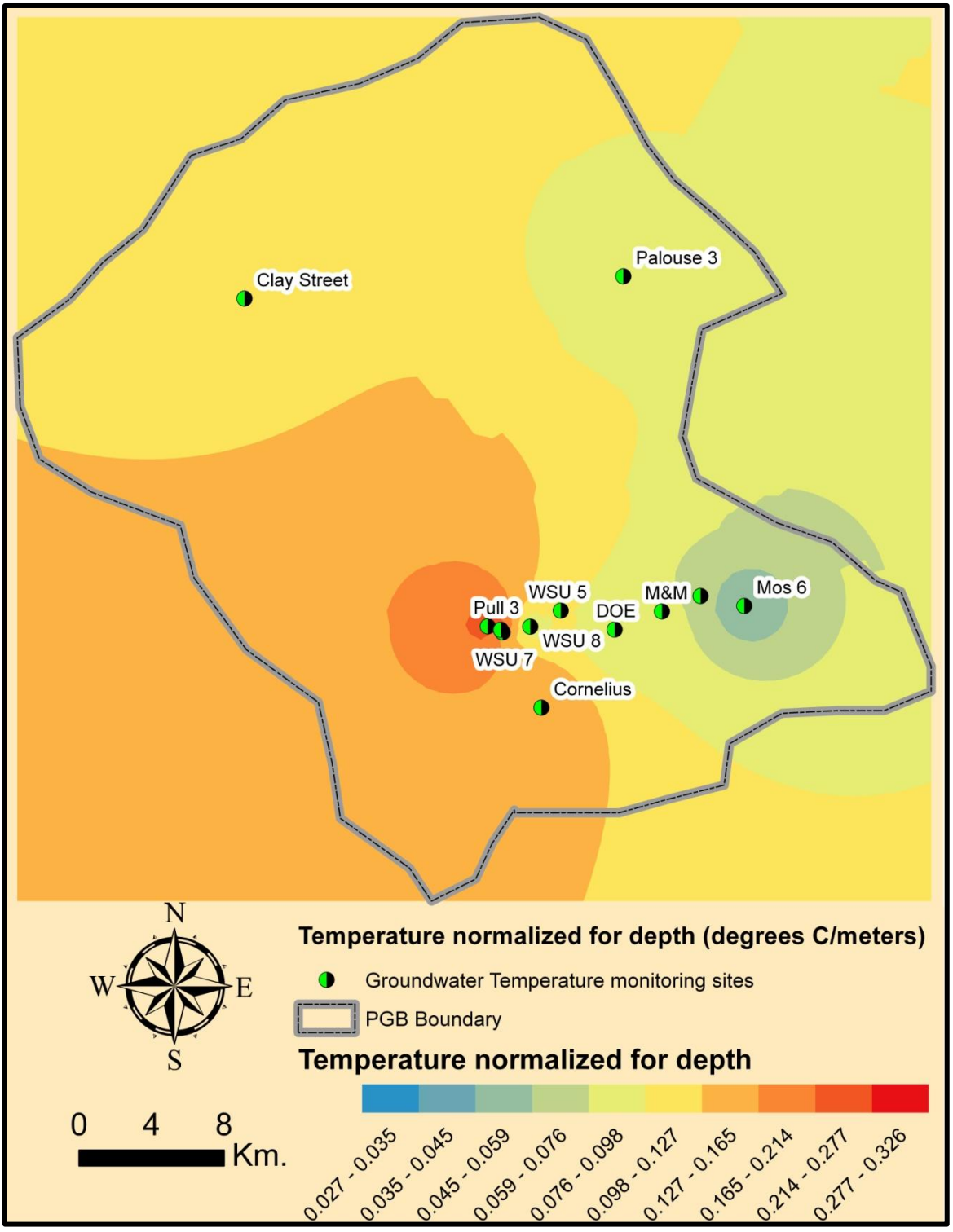

Figure 4.38: Two-dimensional map of interpolated PGB Grande Ronde groundwater temperatures recorded on March 1, 2012 0:00 and normalized for depth. Cool colors (blue) reflect relatively cool temperatures, and warm colors (orange) reflect warm temperatures.

4.7.2 Grande Ronde Groundwater Age Date Mapping

Maps of water level data reflect primarily incomplete, transient effects of pumping centers, where maps of groundwater temperature and groundwater carbon 14 (^{14}C) concentrations better define the long-term conditions at specific locations in the PGB. Table A04 in Appendix A presents age dates collected by Douglas (2004) and Carey (2011) for selected Grande Ronde wells in the PGB. Geochemical modeling by Douglas (2004) showed that the age dates reflect groundwater residence times (e.g., approximate travel times) related to the vertical movement of recharge from the land surface to depths of the sample locations, and not horizontal flow across the basin (Figure 4.8B). Groundwater ^{14}C samples were shown to be segregated into an upper Grande Ronde group and a lower Grande Ronde group based on depth of the well producing zone (s) below land surface consistent with Figure 4.7. Groundwater ^{14}C samples were normalized by depth for mapping purposes due to ^{14}C ages generally increasing with well depth. Wells screened in the Grande Ronde lower producing zone are considered to only exist in the Moscow and Pullman pumping blocks. As shown in Figure 4.39, LC 1 and LC 2 approximate boundaries are generated except that Moscow 9, UI 3, and UI 4 should be located in LC 2 based on other information. Due to complexities in the compartments of the Pullman area, the boundaries need more investigations especially in the Albion area.

The Palouse wells have the oldest ^{14}C age date of the groundwater in the basin (26,400 years before present). The reason for this anomaly is unknown, and the old age is the largest outlier not agreeing with groundwater stratification in the basin. The neighboring small city of Garfield has a younger groundwater age (9,230 years before present) similar to other shallower Grande Ronde wells in the PGB. This would suggest a separate compartment between Palouse and Garfield, but there are numerous examples across the basin were wells of two opposite ends of the spectrum age dates show hydraulic connection (e.g., Motley and Motley connection to UI and Moscow wells). The ^{14}C age of the groundwater requires further investigation in the Albion to Colfax area and Garfield/Palouse/Glenwood area.

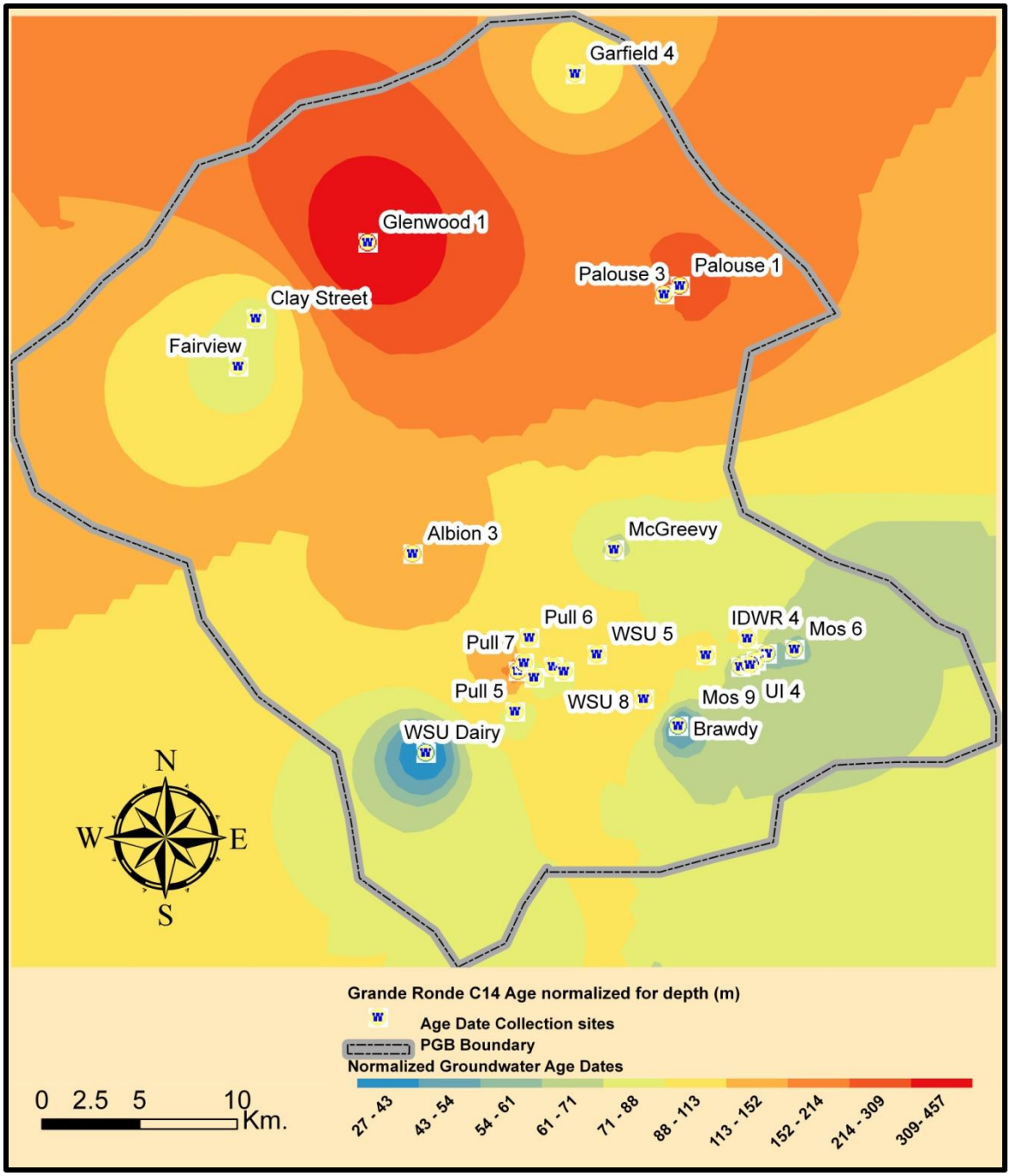

Figure 4.39: Two-dimensional map of relative, interpolated PGB Grande Ronde aquifer system C-14 age dates normalized by well depth. Cooler colors (blue) reflect relatively younger (faster flow) groundwater. Warmer colors (orange) reflect relatively older groundwater (slower flow).

4.7.3 Discussion of Mapping Techniques

The normalized PGB aquifer age dates provide the best compartment delineation when compared to the other methods. Mapping normalized groundwater temperature is more accurate than groundwater elevation due to the unknown accuracy of the top of casing elevations. Comparing the two methods, each showed different boundaries that contradict each other. It appears that when normalized ages are plotted, they show relative travel times rather than age. Figure 4.39 also suggests that the groundwater flow is to the NW from Moscow. Normalized groundwater temperatures show a warming trend as one moves east in the PGB. The temperatures do a decent job defining approximate boundaries of all the compartments.

Each dataset was smaller than what was needed for an accurate delineation. The areas of contradiction are areas that need more investigation in future. Each of the maps provides useful information about the variability throughout the basin. This variability shows the important differences between compartments. Each of these differences influences the maps generated, but water columns with similar well elevations as seen in the PGB have temperature and age characteristics that are useful for comparison. Even though it does not delineate the exact boundaries, it provides visual evidence of differences in the PGB that are used in support of hydraulic connections. The variation in temperatures and groundwater ^{14}C age dates suggest little cross compartment flow which is consistent with the aquifer test data discussed in Chapter 5.

Chapter 5

Data Collection, Compilation, and Analysis

5.1 Basin Groundwater Trends

Water level data and drawdown data for the PGB can be evaluated at many different time scales to help delineate the effects of aquifer compartmentalization and well hydraulic connections. This section is intended to explore the reasons different trends are observed, and to quantitatively analyze their significance.

5.1.1 Basin Recovery Trend

Plots of PGB water levels exhibit numerous changes in slope during the seasonal recovery period. In addition, several other minor changes in slope can be recognized throughout the year. One example of a minor slope change due to changes in basin pumping frequency occurs when the university students leave the area, and then return from the fall-spring semester break. When the students leave, plots of water levels exhibit a steeper recovery (rising) slope compared to the average seasonal recovery trend. This is followed by a steeper, short-term drawdown (declining) trend when the students return followed by reestablishment of the normal seasonal recovery trend. Other examples occurred when three, separate, organized basin (all lateral compartments together) pumping shutdowns were implemented during the Thanksgiving week breaks of 2009, 2010, and 2011. Each pre-shutdown period resulted in noticeable flattening of the normal, seasonal recovery trend for a short period of time; these flattened trends coincided with the increased pumping required for the municipalities to fill their storage tanks in preparation for the shutdown. After all tanks were filled, a steeper, short-term recovery trend formed in response to the cessation of pumping until normal pumping resumed. At that time, the usual seasonal recovery trend also resumed.

Controlled, orderly shutdowns of basin pumping were organized in order to help delineate well hydraulic connections. Water level data were collected in four wells over a 24-hour pre-aquifer test period during the first shutdown in 2009. The data were used

by Moran (2011) to determine the slopes of the short-term recovery trends for four wells, and to extrapolate those trends over a period of 372 days to calculate observation well drawdowns during the first 372 days of the aquifer test.

For this investigation, the first well to resume normal pumping after the Thanksgiving week shutdown period in 2009 established the start (time t=0) for a two-year, multiple well aquifer test. This two-year period includes the first 372 days of the aquifer test analyzed previously by Moran (2011). However, a different method was used in this investigation to calculate drawdown for the observation wells. The method used in this investigation is derived from a robust recovery trend analysis. The following assumptions, based on observations, were made to derive a robust recovery trend fit to water levels normalized from t=0:

- The same general regional trend exists in all Moscow-Pullman observation wells and pumping wells (e.g., IDWR 4, DOE, WSU 5, WSU Test, Cornelius).
- The same distinct regional trend exists in Palouse 1 and Palouse 3. However, this trend is different from the regional trend for the Moscow-Pullman wells.
- Every minor trend is 1) proportional to the change in basin pumping frequencies, 2) each minor trend (e.g., individual well drawdown and/or recovery) is superposed on the regional trend, and 3) the effects of each minor trend can be separated by computation to derive calculated drawdown for each observation well.

5.1.2 Short-term Groundwater Trends

Short-term trends can be evaluated on an hourly, daily, weekly, and/or monthly time scale. Short-term trends can be identified in observation well water levels and drawdown curves for wells located within the same compartment. A comparison of their magnitudes provides evidence for the strength of the well connection, and character of compartment boundaries (cone of depression areal extent).

Trends that develop over a monthly time scale include the fall-spring semester university breaks when the students leave the area. Water level recovery as students leave the area,

and the subsequent decline in water levels when they return, are observed in the data. These occurrences may help answer questions related to the degree of hydraulic connection that exists within the PGB.

Differences in observed water level fluctuations in LC 4 suggest that the Garfield and Palouse city wells are located in a compartment that is hydraulically separated from other compartments in the PGB. The Palouse wells do not respond to the same regional recovery observed in the Moscow-Pullman area during semester breaks (Figure 5.1).

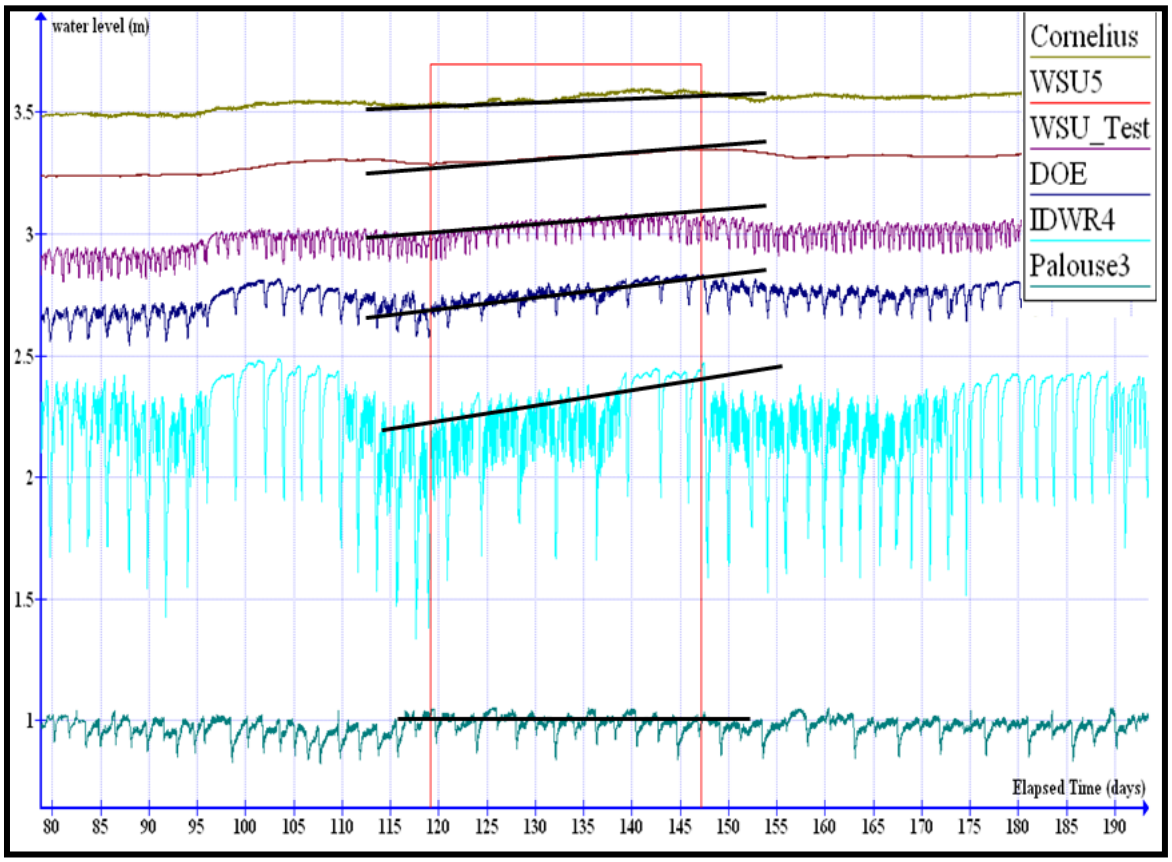

Figure 5.1: Observed fall-spring semester break 2009 recovery period (red box) in Moscow-Pullman area observation wells (five uppermost records), and continuing water level decline in Palouse 3 (teal color: bottom record). Elapsed time is from start of Palouse 3 recovery trend following the 2009 summertime drawdown period (21:00 on 8/19/2009 or 97.03 days before the start of the 372-day aquifer test)(Figure 3.10). Individual plots have been offset vertically in order to compare magnitudes of water level changes.

The distinct difference in water level slopes for Palouse 3 compared to other wells within the PGB clearly shows that the Palouse area does not respond to variations in pumping stresses that occur south of the Kamiak Gap on a time frame of a few weeks.

5.1.3 Long-Term Groundwater Trends

Interpretation of long-term trends continues to support the conceptual hydrogeologic model that suggests the Palouse area Grande Ronde wells are located hydraulically in a different compartment than other municipal or university wells in the PGB. The Palouse wells show a continuous declining water level trend for a period greater than two years which suggests that these wells are located in a distinctly isolated compartment. Further evidence is presented in Figure 5.2 which shows observation well water levels for LC 2, LC 3, and LC 4 with their respective linear trend lines representing the slopes of the changes in water level over time.

In addition to the fact that all the wells show basically the same long-term downward trend in water levels, several additional similarities exist between the Palouse 3 water levels and the water levels for other PGB wells. For example, Palouse water levels do show approximately the same summertime dips (elapsed time equal to the time period between 300-400 days and 675-775 days in Figure 5.2). This is due to the heaviest summer irrigation occurring at the same times in both locations, and the general summer irrigation seasons are the same lengths in both locations. However, the Palouse 3 water levels do not show the same magnitude of summertime drawdown or seasonal recovery as the other PGB wells.

The continuously declining water levels in Palouse 3 were distinctly different from those in the Moscow-Pullman wells; the Palouse 3 water levels were declining continuously from about 50 days to 300 days and from 400 days to 670 days while during the same periods water levels were rising in the other PGB wells. The Palouse 3 declining trends were both followed by short (50-day) rising trends that occurred after summertime drawdown (about ET=350 and ET=725, respectively). By comparison, Moscow-Pullman area water levels did not begin declining until 300 days and 670 days (about June 12, 2010 and June 20, 2011, respectively); however, they all showed a long-term (350-day) recovery trend until the onset of the next summertime pumping period. These PGB summertime drawdown periods are identified in Figure 5.2 as the blue rectangles.

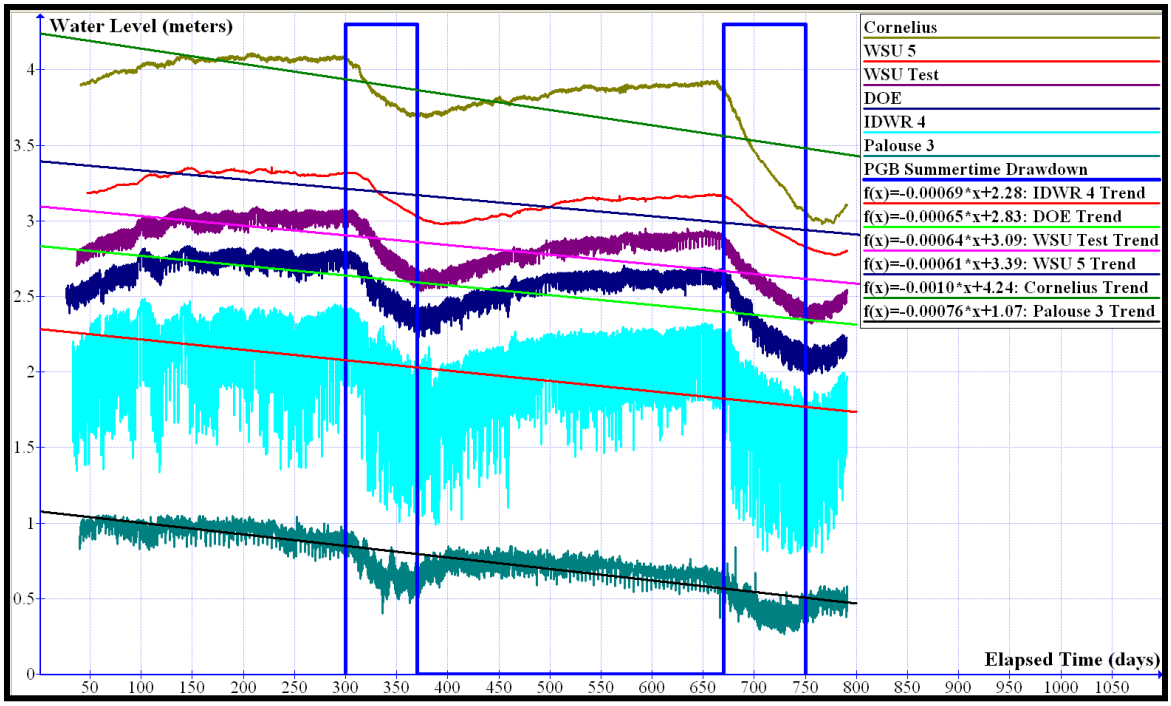

Figure 5.2: Arithmetic plots of observed two-year barometrically corrected water level records for selected wells in the PGB with fitted linear trend lines compared to the Palouse trend line. The plot shows the approximate time intervals of summertime drawdown for the PGB (blue rectangles). Elapsed time is from start of Palouse 3 recovery trend following the 2009 summertime drawdown (21:00 on 8/19/2009) 97.03 days prior to the beginning of the 372-day aquifer test. Individual plots have been offset vertically in order to compare magnitudes of water level changes. (Pumping spikes in Palouse 3 have been truncated vertically to fit the vertical scale of the plot for visual purposes).

5.1.4 Aquifer Test Drawdown Corrected for Trends

Logarithmic trend lines were generated from regional water level composites (i.e., water level data for several wells combined) to account for the effects of pre-test pumping and post summertime water level recovery for the period of the aquifer test. Results in Section 3.5 showed that good correlations exist between Moscow-Pullman water levels, but poor correlations exist between Moscow-Pullman water levels and Palouse water levels. Therefore, two separate water level composites were generated, one for the Moscow-Pullman area and one for the Palouse area, as described in Section 3.6. With the appropriate "best fit" trendline matching equations, calculated drawdown was derived for each well. The logarithmic function fit to the Moscow-Pullman wells regional recovery trend data, and used for water level adjustments is f(t)=0.0728*ln(t)-0.3664, for units of meters and days (t) (Figure 3.9). The logarithmic function fit to the Palouse area wells

regional recovery trend data, and used for water level adjustments is f(t)=0.0347*ln(t)-0.1685, for units of meters and days (t) (Figure 3.10). When applying the trend equations, the time parameter was normalized to the start of the seasonal recovery for each particular well. Calculated drawdown values were derived by subtracting the measured water levels from the water levels predicted by the logarithmic function. These calculated drawdown values were generated beginning at the time that the first measurable drawdown (i.e., 0.003 meters or 0.01 feet) was detected in each observation well after the start of the aquifer test (t=0, November 24, 2009 at 21:50). The aforementioned equations were applied to all observation well water level data collected prior to the beginning of summertime drawdown (Table 5.1). After the start of summertime drawdown in each well, a straight line function was applied to calculate drawdown until the end of the 372-day test (Figure 3.9 and Figure 3.10). Calculated drawdown data for the observation wells are presented in Appendix B.

Well	Elapsed Time (days since the beginning of the aquifer test)	Estimated start of summertime drawdown
WSU 5	210.9	6/23/2010 18:35
WSU Test	209.3	6/22/2010 4:25
DOE	208.3	6/21/2010 5:00
IDWR 4	208.3	6/21/2010 5:00
Cornelius	202.8	6/15/2010 17:10
Palouse 3	208.5	6/21/2010 9:50

Table 5.1: Start of summertime drawdown for selected PGB wells during 372-day aquifer test.

5.2 Aquifer Test Analysis

One of the primary methods for the analysis of leaky confined aquifers is demonstrated here to best simulate aquifer test drawdown in the PGB. Aquifer test drawdown curves for PGB Grande Ronde wells indicate that significant vertical leakage exists in the finite, bounded, multiple aquifer-aquitard system known locally as the Grande Ronde aquifer. Modeling aquifer test drawdown in the Grande Ronde formation in the PGB as a leaky confined system provides an important tool to characterize present, and predict future, water level decline in this complex multiple aquifer system. Drawdown for three wells in

the PGB using data for the first 372 days of the basinwide aquifer test are analyzed using a new "moving windows" technique developed specifically for this aquifer test. The pumping rates used in the model are estimates provided by the municipal pumping managers (Table 5.2) based on flowmeter averages.

The data are analyzed for this investigation by the Neuman-Witherspoon (1969) method for confined two-aquifer systems with a leaky aquitard between them. The lower Grande Ronde aquifer is the primary pumped aquifer in the PGB and is modeled as the pumped aquifer while the upper Grande Ronde is modeled as the overlying unpumped aquifer. The three observation wells (DOE, WSU Test, and Palouse 3) and all pumping wells were modeled as fully penetrating, with an aquifer thickness of 400 meters. Because each observation well is modeled in a specific compartment, only the pumping rate data for wells located in that compartment are used to generate the AQTESOLV® (HydroSOLVE, Inc., 2007) predicted drawdown that is matched to the observation well calculated drawdown data.

Neuman-Witherspoon (1969) derived a solution for unsteady flow to a fully penetrating well in a confined two-aquifer system. The solution assumes a line source for the pumped well, and therefore neglects wellbore storage. The Neuman-Witherspoon solution can simulate variable-rate tests including recovery through the application of the principle of superposition in time. This solution is used for analyzing both pumping and recovery data for multiple, pumping wells with variable rates, plus aquifer boundaries. The method is capable of analyzing drawdown data for wells completed in the pumped aquifer, the unpumped aquifer or in the aquitard. Wells in the aquifers are assumed to be fully penetrating; wells in the aquitard may be partially penetrating (HydroSOLVE, Inc., 2007). Analyses for this investigation were completed with the Neuman-Witherspoon solution for wells screened in the pumped aquifer.

City	Well	Estimated rate (gpm)
Moscow	2	750
	3	1100
	6	1015
	8	950
	9	2100
WSU	4	1400
	6	1050
	7	2700
	8	2400
Pullman	5	1600
	6	600
	7	1750
	8	1921
UI	3	2000
	4	2000
Palouse	1	725
	3	800
Colfax	Fairview	625
	Clay Steet	500
	Glenwood #1	555
	Glenwood #2	555
Albion	2	225
	3	225
Garfield	3	500
	4	350

Table 5.2: PGB Pumping Rate Estimates in gallons per minute (gpm).

5.2.1 Curve matching Techniques

Analyzing a large aquifer test dataset allowed for the trial and error testing of many different techniques. Development of the most consistent method for utilizing AQTESOLV® curve matching techniques will be discussed below. AQTESOLV® is analytical modeling software that uses image well theory and the principle of superposition to account for boundary effects, and relies on superposition to accurately simulate the variable-rate pattern of pumping in the PGB over the 372-day aquifer test. AQTESOLV® uses all of the pumping rates prior to the end of the time window being analyzed to compute the drawdowns. For example, if the time window on the computer screen ends at 103.4 days, the pumping rate changes after 103.4 days do not factor into

the calculations, but all pumping information up to and including 103.4 days will be used to generate the AQTESOLV® predicted drawdown for the window.

Evidence for compartmentalization discussed in Chapter 4 was used to determine which wells would be used for each individual model. Approximate compartment boundary locations were estimated from that analysis and are shown in Figure 5.3. Because AQTESOLV® is limited to linear, no-flow boundaries with perpendicular intersections; variable shaped boundaries were approximated as rectangles to accommodate this limitation. Note: in AQTESOLV®, no-flow boundaries that do not intersect another boundary extend to infinity by default. Two of three compartments analyzed herein (LC 2 and LC 3) were simulated with three intersecting no-flow boundaries instead of four (i.e., the north boundary was absent) to approximate the conditions of a partially closed system with intercompartmental leakage. LC 4 was modeled as a semi-infinite system with two intersecting boundaries (east and south) to simulate the presence of Moscow Mountain granite and zero flow through the Kamiak Gap, respectively. LC 4 was modeled as open to the north and west to accommodate potential hydraulic connections between the Palouse wells, Garfield wells and Glenwood wells.

Matching the AQTESOLV® predicted drawdown to 372 days of calculated drawdown data requires a computer with more processing capabilities than the average desktop. Therefore, the 372-day dataset was divided into ten, 10-day windows for analysis. The 372 days of drawdown data were divided into 10 moving windows spaced approximately on a log scale (time period multiplier of 1.2). This produced ten approximately evenly spaced 10-day windows over the entire 372 days of the aquifer test (Figure 5.4). Each 10-day window was plotted on arithmetic scales rather than the customary log-log scales for analysis. This method of analysis allows the selection of different "windows" of short and long-term pumping/drawdown data from within the continuous, 372-day dataset. Dividing the 372 days into 10-day windows provided a computer efficient way to analyze the large amount of data, and provided an enhanced procedure to evaluate aquifer storativity through averaging of discrete system responses to spatially and temporally variable pumping stresses. This new method of analysis provides a distinct advantage over the typical log-log curve matching procedure for the evaluation of large datasets,

and yields realistic average "annual" and short-term T and S values. The following sections illustrate the 10-day window method of aquifer test analysis for the 372-day aquifer test.

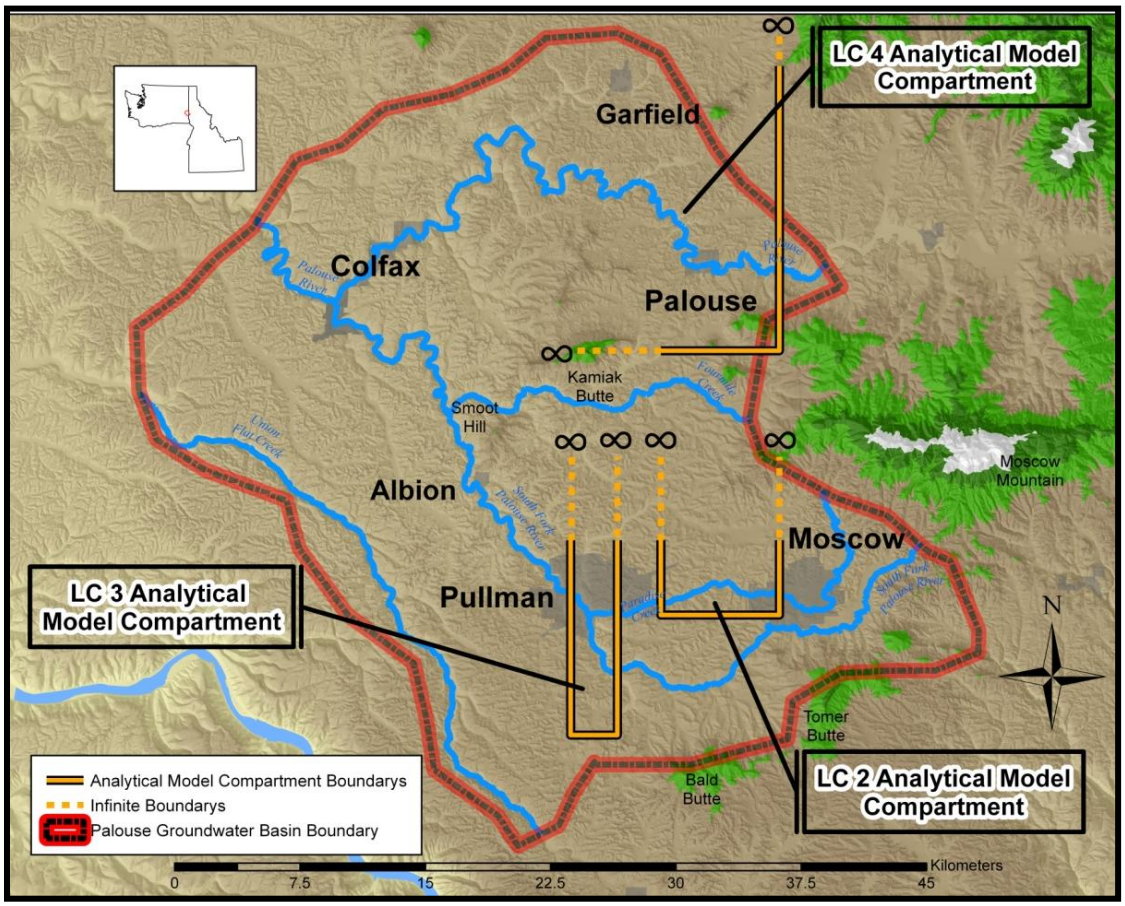

Figure 5.3: Approximate compartment boundaries as modeled in AQTESOLV® for LC 2, LC 3 and LC 4. Note: boundaries extend to infinity unless intersected by a perpendicular boundary.

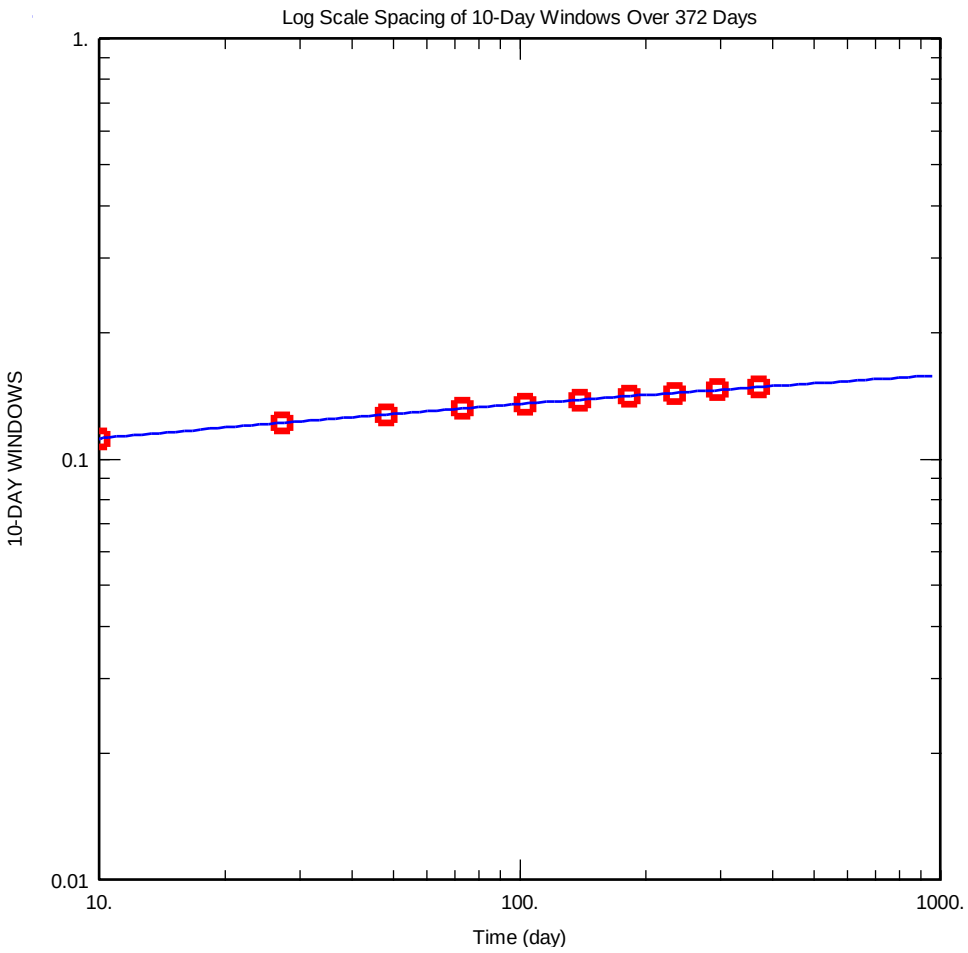

Figure 5.4: 10-day log scale windows for the 372-day test. The blue line is a Theis (1935) type curve for illustration purposes only.

5.3 Moving Windows Analytical Modeling Results

The ability of investigators to analyze large datasets is crucial to understanding the complexities of any groundwater system. The 10-day window curve matching technique on an arithmetic scale as described herein allows for complete evaluation of the PGB aquifer systems that experience dynamic changes in water levels related to seasonal fluctuations in pumping. The aquifer system parameters including transmissivity (T) and storativity (S), and aquitard leakage parameters (r/B and β), were adjusted by trial and error in AQTESOLV® to derive a best-fit visual match between the calculated drawdown data and the theoretical AQTESOLV® predicted drawdown generated by the Neuman-Witherspoon (1969) equation for each 10-day window. **IT IS IMPORTANT TO NOTE** that the curve matching process was completed on an arithmetic scale for

each 10-day window because it is not feasible to complete the curve matching process on a log scale. Because the axis scales are compressed on a log scale, AQTESOLV® is not capable of producing the computer screen resolution necessary for curve matching with very large datasets as illustrated herein. The smallest single window that can be analyzed on a log scale is one log cycle (e.g., 1 to 10 days, 10 to 100 days, 100 to 1000 days, etc.).

The arithmetic mean for each aquifer system parameter was derived based on the mean of all ten, 10-day windows combined to yield the best average type curve match for each 372-day observation well drawdown curve. This method was applied to observation wells in three separate compartments (LC 2, LC 3, and LC 4) to estimate the aquifer properties within each compartment. AQTESOLV® uses image wells to simulate boundary conditions; therefore, leaky boundaries or partial boundaries cannot be simulated accurately. The effects of pumping wells located in different compartments (i.e., beyond the compartment boundaries of the specific compartment being analyzed) must be analyzed separately as isolated compartments.

5.3.1 LC 2 Aquifer Test Analysis

The DOE well is located in LC 2; no flow boundaries were approximated as shown in Figure 5.3 to account for the lack of hydraulic connections between the DOE well and wells in LC 1 and LC 3. Data analysis shows that only three pumping wells (UI 3, UI 4 and Moscow 9) within the PGB cause measurable drawdown in the DOE well directly. Only UI 4 and Moscow 9 were pumped during the aquifer test. The effects of intercompartmental leakage between compartments were simulated with AQTESOLV® using three no-flow boundaries to define LC 2, so the condition of groundwater communication with the rest of the PGB was approximated (i.e., one no-flow boundary was absent). This approximate condition was needed because summertime pumping causes long-term system-wide drawdown and leakage through compartment boundaries.

Visual curve matching for each 10-day window was completed to evaluate the average aquifer properties in LC 2. These properties were derived from matching the theoretical AQTESOLV® predicted drawdown to the dynamic changes in water level related to seasonal fluctuations in pumping. The 10-day moving windows show both good and

poor quality curve fits (Figures 5.5 A through 5.5 J). The 0 to 10-day window is an example of a good fit while the 287 to 297-day window is not as good of a fit. Moran (2011) observed similar discrepancies around 290 days where the Neuman-Witherspoon equation under predicts drawdown in the DOE well. This discrepancy most likely is an artifact of the model not being able to simulate outward intercompartmental leakage through compartment boundaries comprised of leaky aquitards. Moscow 6 and 8 in LC 1 continued pumping during the 294.5 to 297.2 time period and their stress on the aquifer system is believed to have caused the drawdown (lateral leakage out of LC 2 and into LC 1) for which the model under predicts in Figure 5.5I. Other discrepancies in the AQTESOLV® predicted drawdown matches may be artifacts of errors made in recording the pumping on/off periods for the pumping wells.

The average aquifer coefficients that yield the best matches include transmissivity T= 134,100 m^2/day and aquifer storativity S= 1.6 x 10^{-4}. The aquifer leakage parameter r/B ranges from 0.06 to 0.20, and β values range from 0.047 to 0.100 as shown in Table 5.3. Figure 5.6 shows the "best" average log-log, AQTESOLV® predicted drawdown match for the complete 372 days of drawdown data as derived from the arithmetic mean of all ten, 10-day window AQTESOLV® predicted drawdown matches shown in Figure 5.5. However, the overall match is poor due to poor resolution of the large dataset on a log-log scale. Figure 5.6 clearly shows that matching 372 days of drawdown data on a log-log scale has serious resolution problems compared to the arithmetic, 10-day moving windows method of analysis.

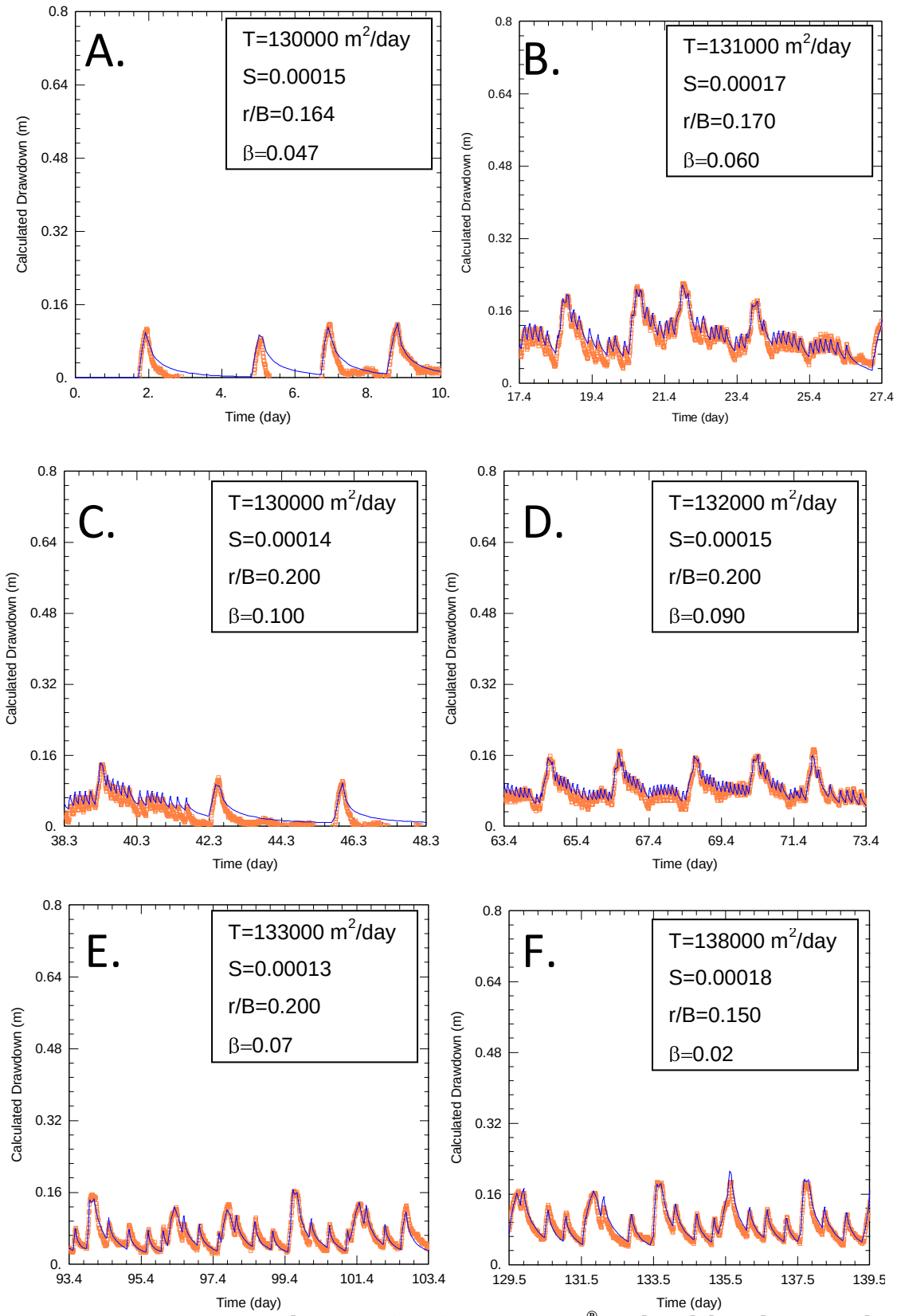

Figure 5.5 A-F: Neuman-Witherspoon (1969) AQTESOLV® predicted drawdown matches for the 10-day moving windows for the DOE well.

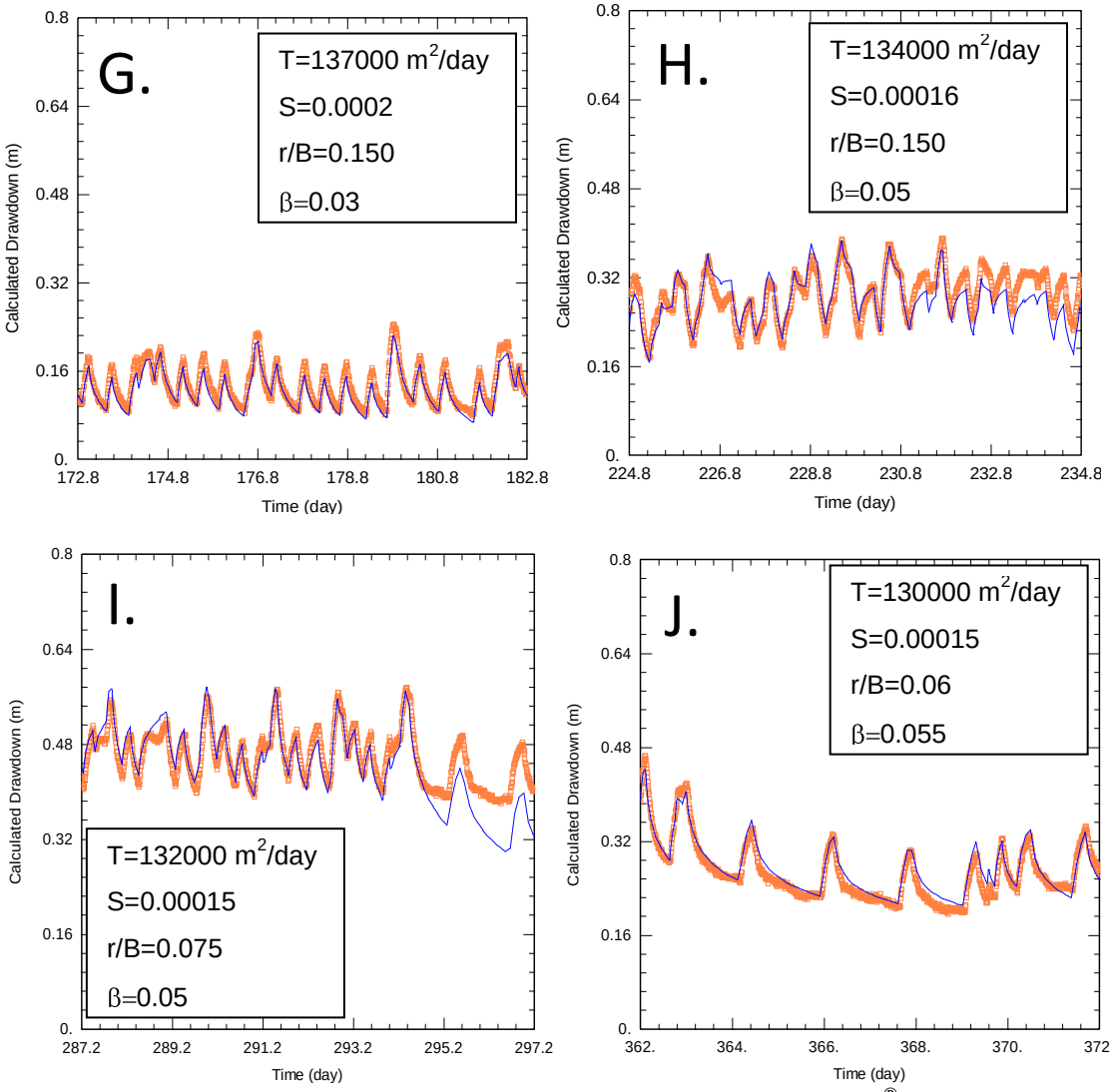

Figure 5.5 continued: G-J: Neuman-Witherspoon (1969) AQTESOLV® predicted drawdown matches for the 10-day windows for the DOE well.

Log scale Windows	DOE			
Method	Neuman-Witherspoon (1969)			
Aquifer Coefficients	T (m2/day)	S	r/B	β
Window A	130000	0.00015	0.164	0.047
Window B	131000	0.00017	0.170	0.060
Window C	130000	0.00014	0.200	0.100
Window D	132000	0.00015	0.200	0.090
Window E	133000	0.00013	0.200	0.070
Window F	138000	0.00018	0.150	0.020
Window G	137000	0.00020	0.150	0.030
Window H	134000	0.00016	0.150	0.050
Window I	132000	0.00015	0.075	0.050
Window J	130000	0.00015	0.060	0.055
Average	134000	0.00016	0.152	0.057

Table 5.3: Neuman-Witherspoon (1969) aquifer property results for the moving 10-day window analysis for the DOE well in LC 2. Lower Grande Ronde aquifer average aquifer properties are T= 134,000 m^2/day, S= 1.6 x 10^{-4}, r/B= 0.152, and β= 0.057. The upper Grande Ronde aquifer transmissivity and storativity were kept constant at 30,000 m^2/day and 0.06, respectively.

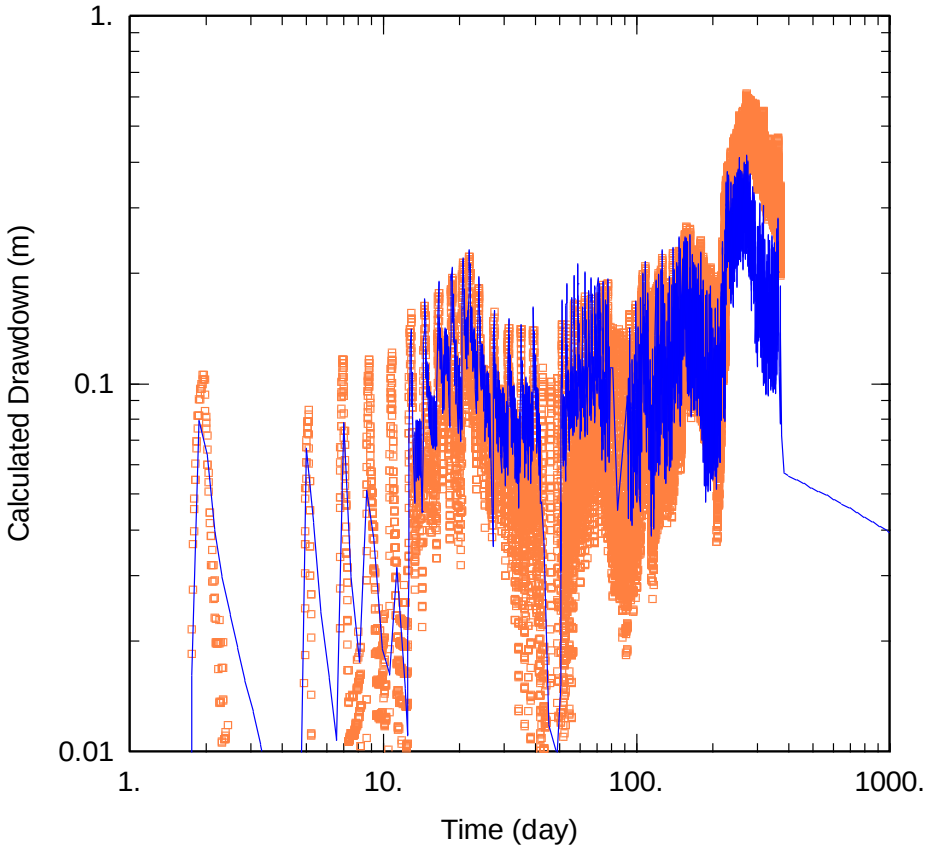

Figure 5.6: Log-log plot of calculated drawdown versus time for 372 days for the DOE well in LC 2. The blue line represents the AQTESOLV® predicted drawdown based on the Neuman and Witherspoon (1969) equation for average T= 134,000 m^2/day, average S= 1.62 x 10^{-4}, average r/B= 0.152, and an average β= 0.057. The upper Grande Ronde aquifer T= 30,000 m^2/day and S=0.06 were kept constant because of model insensitivity.

5.3.2 LC 3 Aquifer Test Analysis

The WSU Test well is located in LC 3; no flow boundaries were approximated as shown in Figure 5.3 to account for the lack of hydraulic connections between the WSU Test well and the pumping wells in LC 2, LC 4, and LC 5 compartments. Data analysis shows that only four pumping wells (WSU 4, WSU 7, Pullman 7, and Pullman 8) within the PGB cause measurable drawdown in the WSU Test well directly. The effects of intercompartmental leakage between compartments was simulated in AQTESOLV® using three no-flow boundaries to define LC 3, so the conditions of groundwater communication with the rest of the PGB were approximated (i.e., one no-flow boundary was absent).

The AQTESOLV® predicted drawdown match for each ten-day window has a different degree of variability for the WSU Test well. Figures 5.7 A through 5.7 J show calculated drawdown versus elapsed time for the ten, 10-day windows with the best visual AQTESOLV® predicted drawdown matches. The WSU Test well is influenced by each well in LC 3 directly; however, substantial intercompartmental effects also appear to influence drawdown. Good matches exist for window A and window B (Figures 5.7 A and 5.7 B, respectively), and for window I and window J (Figures 5.7 I and 5.7 J, respectively). Relatively poor matches for windows C through H may be due to pumping discrepancies during the Thanksgiving week breaks for 2009 and 2010 that occurred at the beginning and end of the 372-day aquifer test, respectively. During these two, week long periods, only wells that showed a direct connection to the WSU Test well were pumped. These atypical basin pumping stresses may have allowed water levels to equilibrate to intracompartment conditions in LC 3 that are more closely approximated by the theoretical Neuman-Witherspoon (1969) equation yielding better AQTESOLV® predicted drawdown matches.

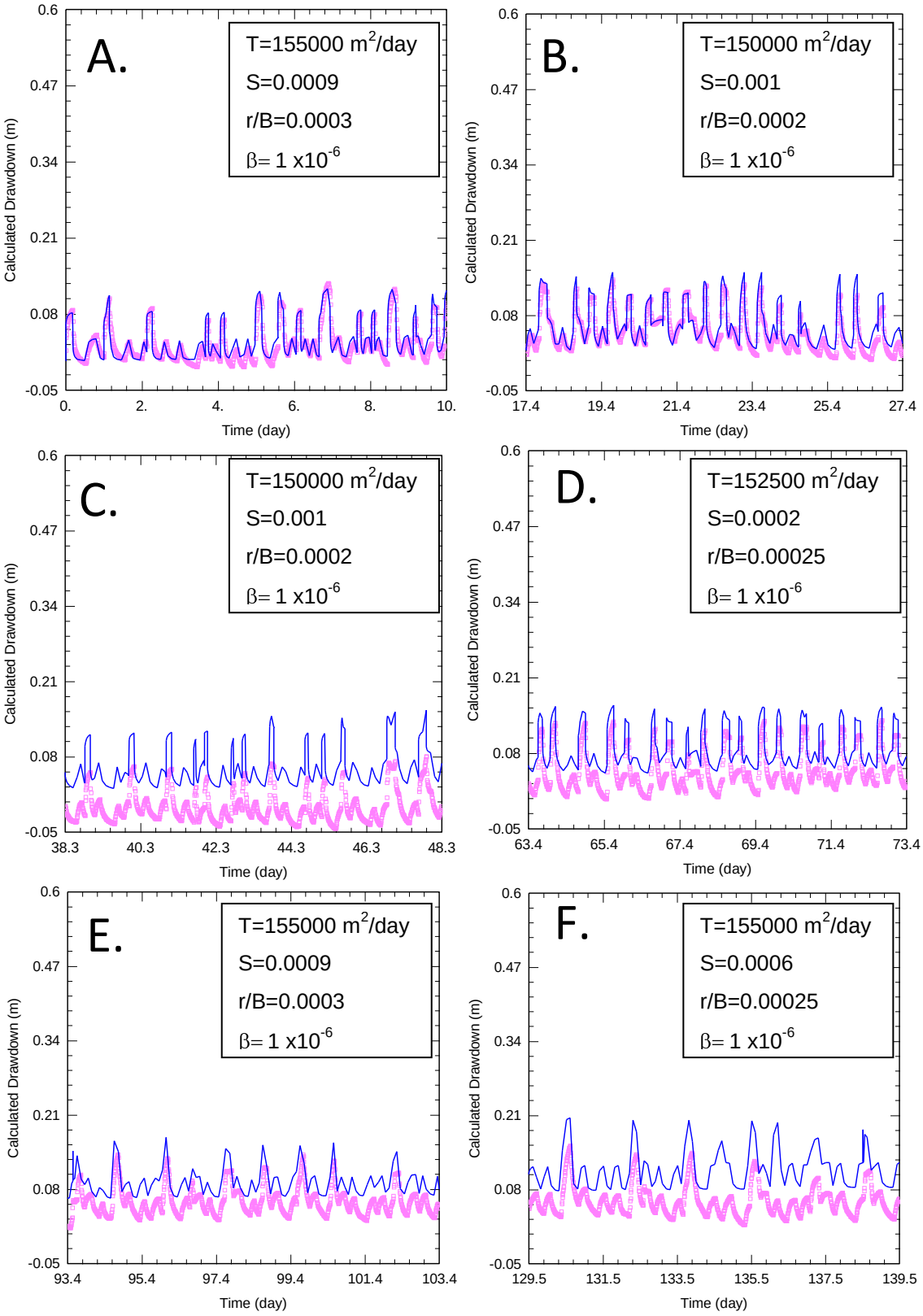

Figure 5.7 A-F: Neuman-Witherspoon (1969) AQTESOLV® predicted drawdown matches for the 10-day moving windows for WSU Test well.

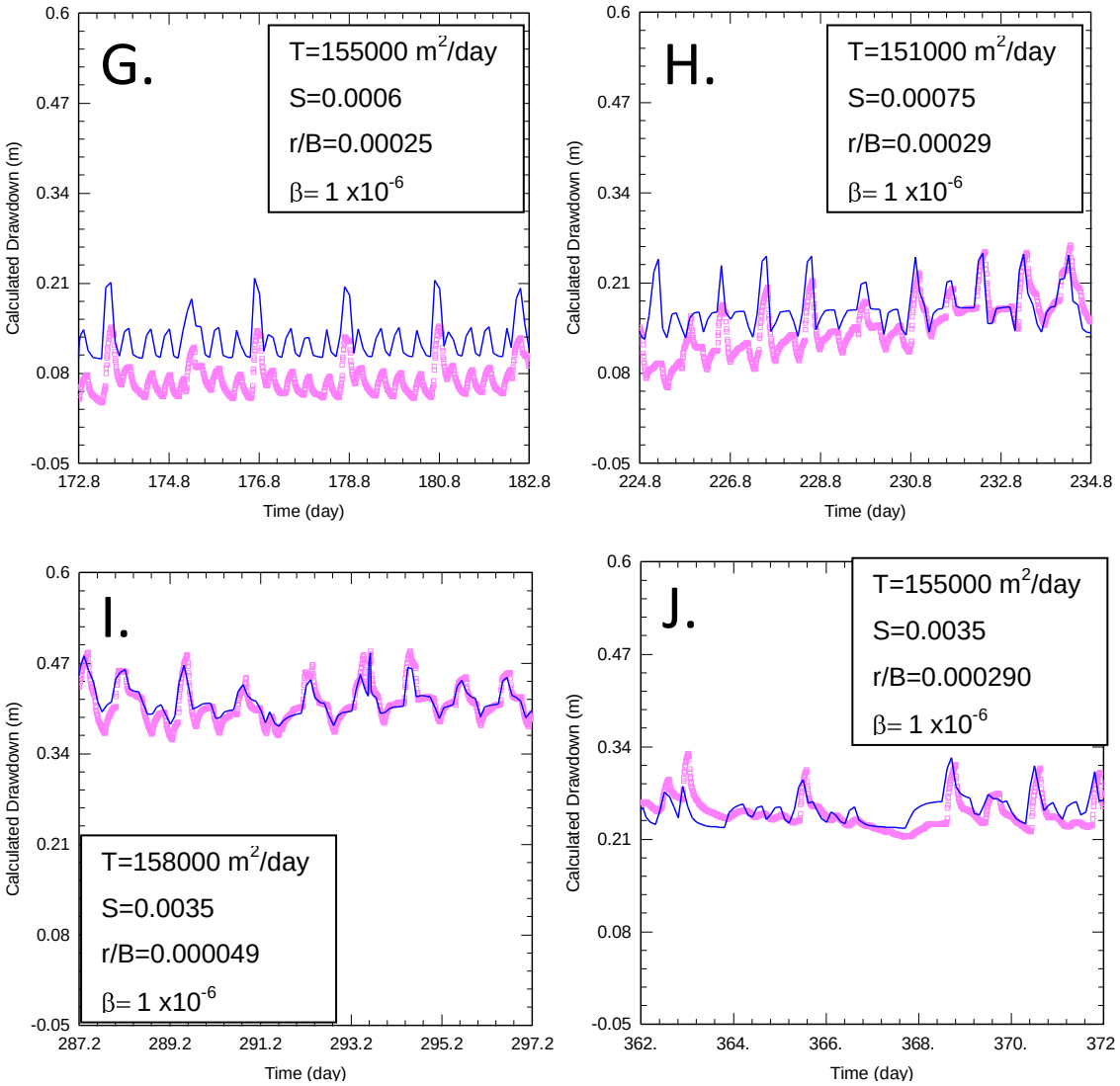

Figure 5.7 G-J continued: Neuman-Witherspoon (1969) AQTESOLV® predicted drawdown matches for the 10-day moving windows for WSU Test well.

The average aquifer system property values that yield the best visual AQTESOLV® predicted drawdown matches include T= 153,500 m^2/day, S= 1.30 x 10^{-3}, and r/B values range between 4.9 x 10^{-5} and 3.0 x 10^{-4}. The value for β= 1.0 x 10^{-6} was kept constant for the best matches (Table 5.4). Figure 5.8 shows "best" average log-log, AQTESOLV® predicted drawdown match for the complete 372-day dataset. A relatively good fit occurs until ET=103 days when WSU 7 was substituted for WSU 4 as the main pumping well for the WSU campus. Due to this unexplained discrepancy in the AQTESOLV® predicted drawdown match, the LC 2, 372-day average fit visually is relatively poor

Log scale Windows	WSU Test			
Method	Neuman-Witherspoon (1969)			
Aquifer Coefficients	T (m^2/day)	S	r/B	β
Window A	155000	0.00090	0.000300	0.0000001
Window B	150000	0.00100	0.000200	0.0000001
Window C	150000	0.00100	0.000200	0.0000001
Window D	152500	0.00020	0.000250	0.0000001
Window E	155000	0.00090	0.000300	0.0000001
Window F	155000	0.00060	0.000250	0.0000001
Window G	155000	0.00060	0.000250	0.0000001
Window H	151000	0.00075	0.000290	0.0000001
Window I	158000	0.00350	0.000049	0.0000001
Window J	155000	0.00350	0.000290	0.0000001
Average	153500	0.00130	0.000238	0.0000001

Table 5.4: Neuman-Witherspoon (1969) aquifer property results for the moving 10-day window analysis for the WSU Test well in LC 3. Lower Grande Ronde average aquifer properties are T= 1.535 x 10^5 m^2/day, S= 1.30 x 10^{-3}, r/B= 2.38 x 10^{-4}, and β= 1.0 x 10^{-6}. The upper Grande Ronde aquifer T=30 m^2/day and S= 0.15 were kept constant.

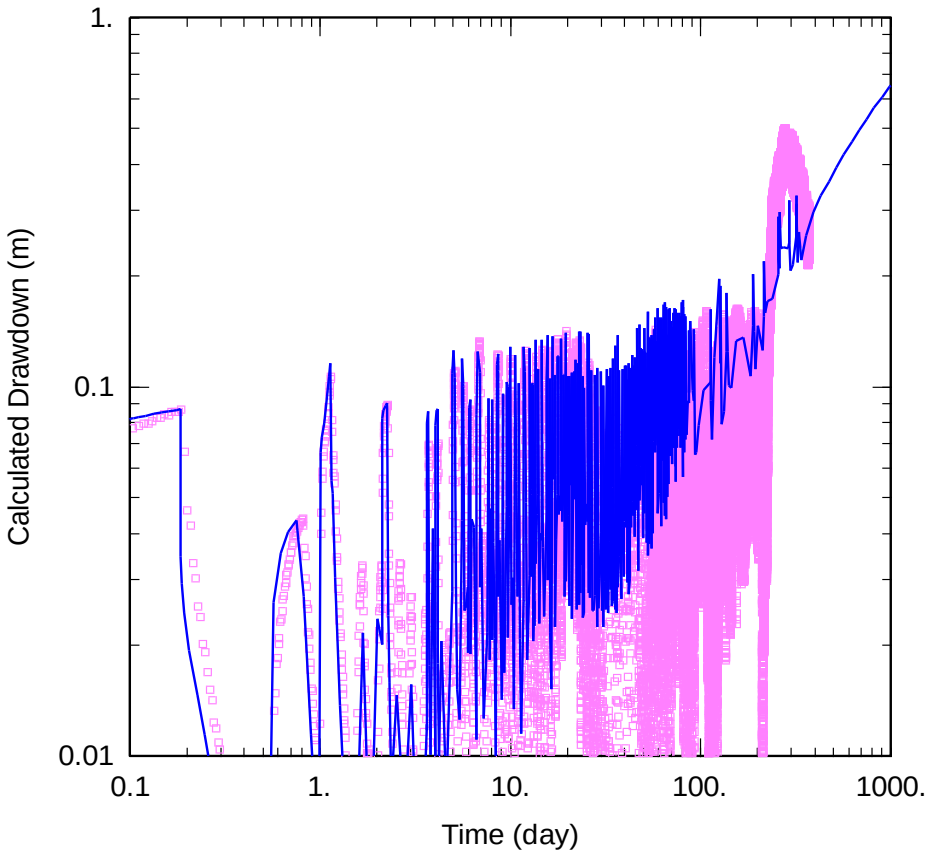

Figure 5.8: Log-log plot of calculated drawdown versus time for 372 days for the WSU Test well in LC 3. The blue line represents the AQTESOLV® predicted drawdown based on the Neuman and Witherspoon (1969) equation for average T= 1.535 x 10^5 m^2/day, average S= 1.30 x 10^{-3}, average r/B= 2.38 x 10^{-4}, average β= 1.0 x 10^{-6}. The upper Grande Ronde aquifer T= 30 m^2/day and S= 0.15 were kept constant because of model insensitivity.

compared to the DOE AQTESOLV® predicted drawdown match. Another potential explanation for the poor AQTESOLV® predicted drawdown match is that the WSU Test well is very sensitive to intercompartmental leakage that is not accounted for accurately by the AQTESOLV® boundary conditions. However, the overall match is poor due to poor computer screen resolution of the large dataset on a log-log scale compared to an arithmetic scale.

5.3.3 LC 4 Aquifer Test Analyses

The Palouse 3 well is located in LC 4; no flow boundaries were approximated as shown in Figure 5.3 to account for the lack of hydraulic connections between LC 4 and compartments LC 1, LC 2 and LC 3. Data analysis shows that only two pumping wells (Palouse 1 and Palouse 3) within the PGB cause measurable drawdown in the Palouse 3 well directly. The effects of intercompartmental leakage between compartments was simulated with AQTESOLV® using two no-flow boundaries to define LC 4, so groundwater communication to the west and north extends to infinity (i.e., two no-flow boundaries were absent). This boundary configuration is different from LC 2 and LC 3 because the Palouse 3 hydrograph suggests that the Glenwood wells may influence Palouse 3 water levels (Figure 4.32 D).

Visual curve matching for each 10-day window was completed to evaluate the average aquifer properties for LC 4. These properties were derived by matching the theoretical AQTESOLV® predicted drawdown to the dynamic changes in water level related to seasonal fluctuations in compartmental pumping. The 10-day moving windows show both good and poor quality curve fits (Figures 5.9 A through 5.9 J). All of the 10-day windows are examples of a good fit except window 4 (Figure 5.9 D), where a few extraneous data points (at $t \approx 65.5$ days) are not predicted by the AQTESOLV® predicted drawdown. These data points are due to the pump turning on for 17 minutes and the water being evacuated from the borehole rather than creating actual drawdown in the aquifer which is what AQTESOLV® predicted. As observed in all the windows, the large drawdown spikes related to active pumping of the Palouse 3 well itself are predicted by

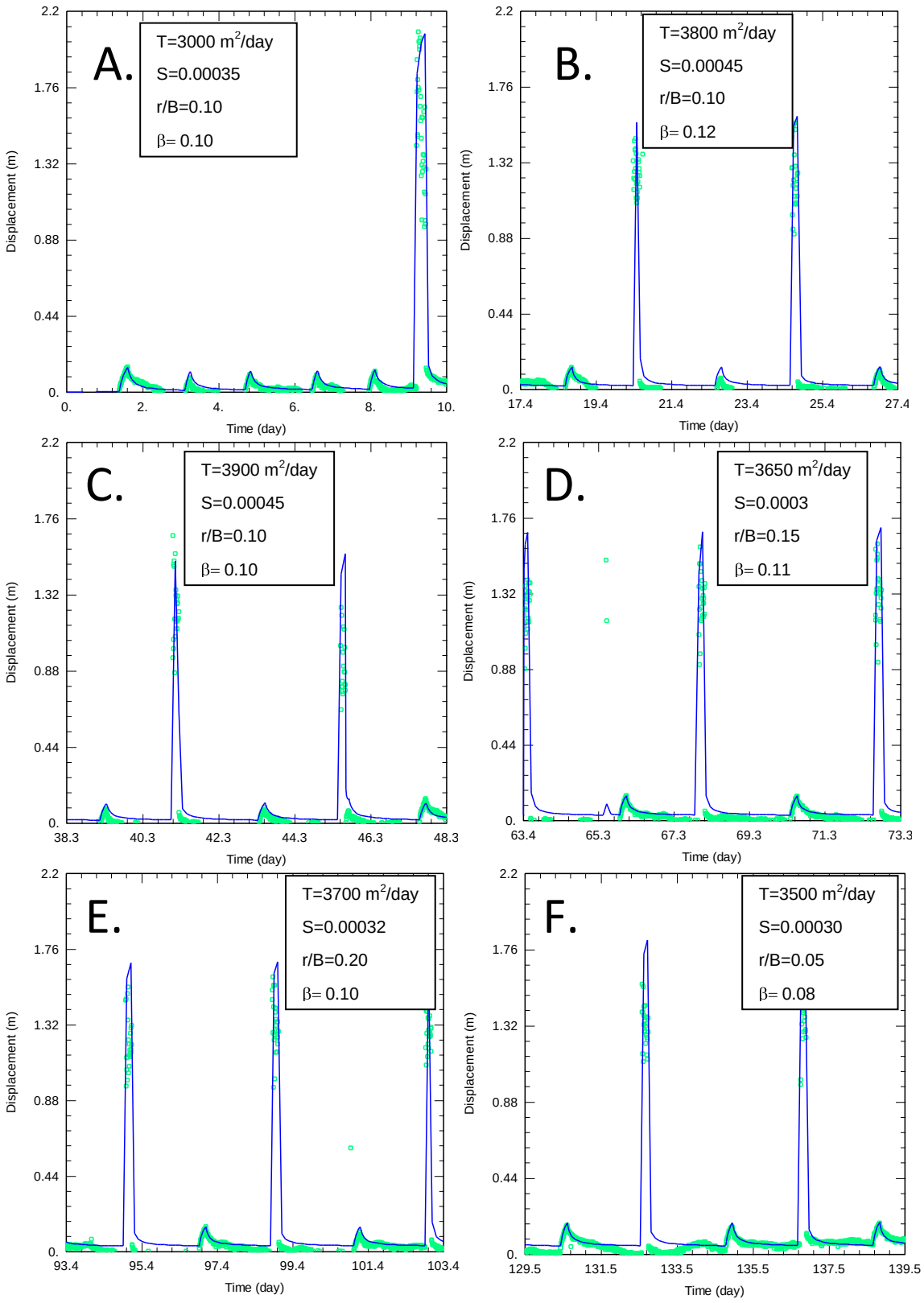

Figure 5.9 A-F: Neuman-Witherspoon (1969) AQTESOLV® predicted drawdown matches for the 10-day moving windows for Palouse 3.

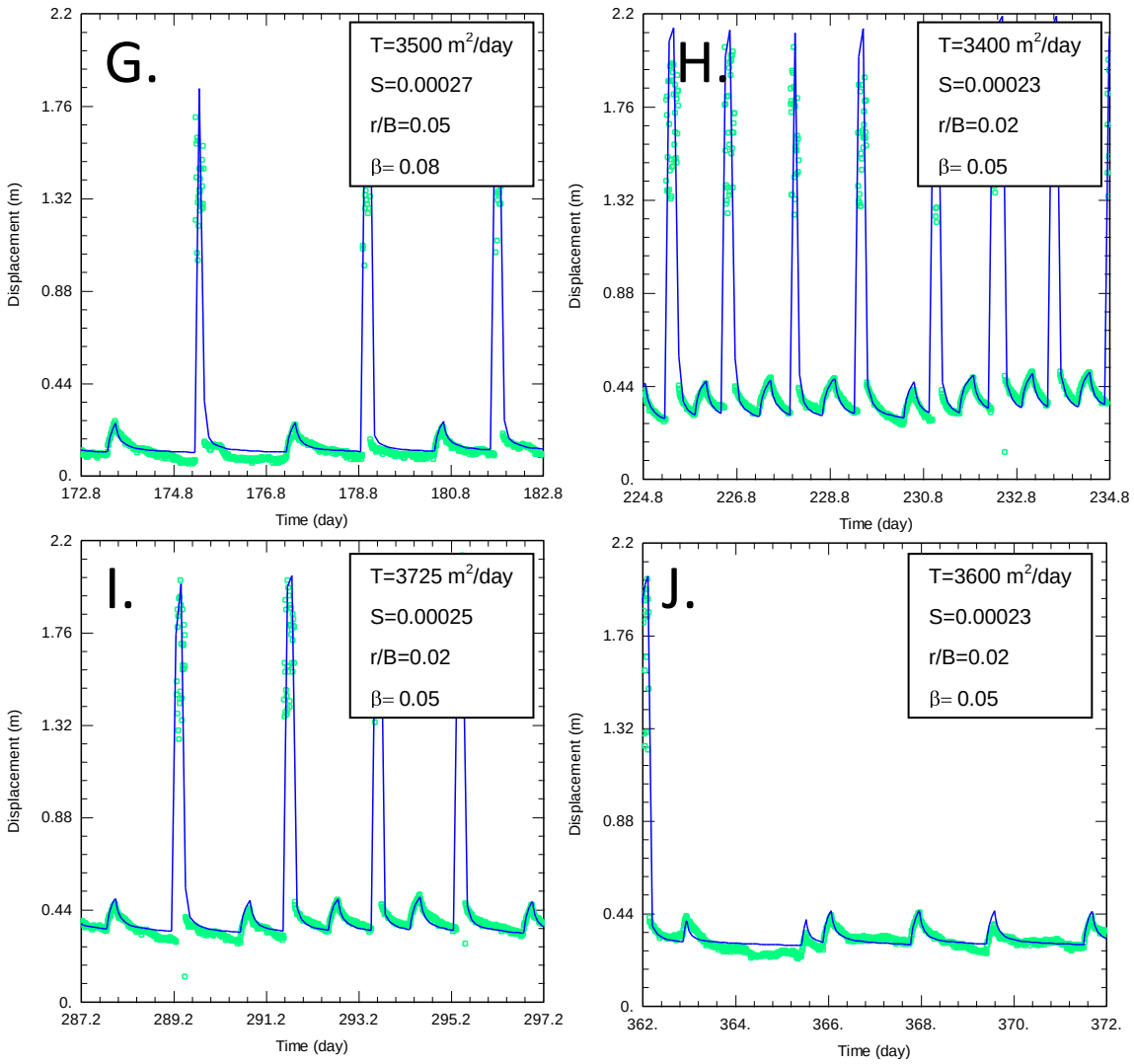

Figure 5.9 G-J continued: Neuman-Witherspoon (1969) AQTESOLV® predicted drawdown matches for the 10-day windows for Palouse 3.

the AQTESOLV® predicted drawdown. This implies that the Palouse 3 well is essentially a 100% efficient well with virtually no well loss.

The average aquifer system property values that yield the best visual AQTESOLV® predicted drawdown matches include T= 3577 m^2/day and S=3.2 x 10^{-4}, r/B values range between 0.070 and 0.25, and β values range between 0.02 and 0.10 (Table 5.5). Figure 5.10 shows "best" average log-log, AQTESOLV® predicted drawdown match for the complete 372-day dataset. A relatively good match exists between the AQTESOLV® predicted drawdown and the continuous negative slope of the Palouse water levels.

Log scale Windows	Palouse 3			
Method	Neuman-Witherspoon (1969)			
Aquifer Coefficients	T (m^2/day)	S	r/B	β
Window A	3000	0.00035	0.1	0.1
Window B	3800	0.00045	0.1	0.12
Window C	3900	0.00045	0.25	0.1
Window D	3650	0.00030	0.15	0.11
Window E	3700	0.00032	0.2	0.1
Window F	3500	0.00030	0.15	0.07
Window G	3500	0.00027	0.05	0.08
Window H	3400	0.00023	0.02	0.05
Window I	3725	0.00025	0.02	0.05
Window J	3600	0.00023	0.02	0.05
Average	3578	0.00032	0.11	0.08

Table 5.5: Neuman-Witherspoon (1969) aquifer property results for the moving 10-day window analysis for the Palouse 3 well in LC 4. Lower Grande Ronde average aquifer properties are T= 3578 m^2/day, S= 0.00032, r/B= 0.11, and β= 0.08. The upper Grande Ronde aquifer T= 1 m^2/day and S= 0.01 were kept constant.

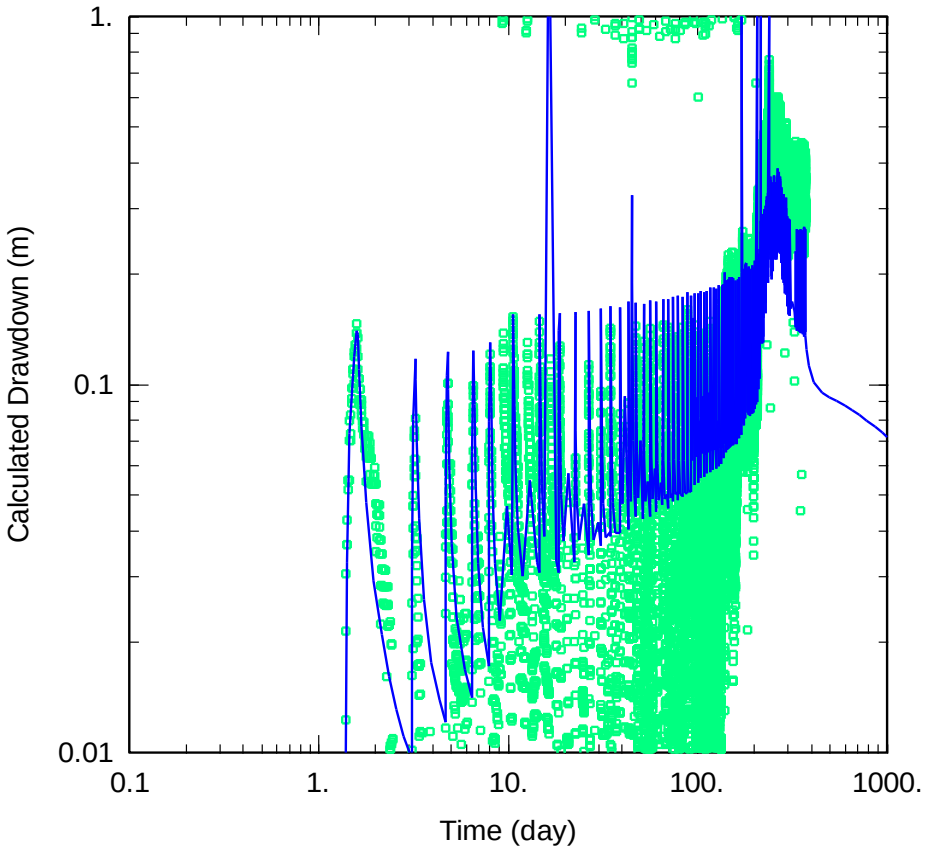

Figure 5.10: Log-log plot of calculated drawdown versus time for 372 days for the Palouse 3 well in LC 4. The blue line represents the AQTESOLV® predicted drawdown based on the Neuman and Witherspoon (1969) equation for average T= 3,577 m^2/day, average S= 3.15 x 10^{-4}, average r/B= 0.11, and average β= 0.08. The upper Grande Ronde aquifer T=1 m^2/day and S= 0.01 were kept constant because of model insensitivity.

However, the overall match is poor due to poor computer screen resolution of the large dataset on a log-log scale compared to an arithmetic scale.

Modeling Palouse 3 in a semi-infinite, two boundary system generated relatively good matches for all ten, 10-day windows. The Palouse 3 water levels also exhibit gently sloping, rolling hills that cannot be attributed to any individual pumping well through comparison with the Hobo data. These rolling hills occur on a diurnal cycle and appear to be related to earth-tide influences that are not predicted by the model. Implications and ideas related to aquifer properties, aquifer compartmentalization and potential aquifer storage and recovery in the PGB are presented in Appendix D.

CHAPTER 6

Conclusions and Recommendations

6.1 Introduction

Due to the heterogeneity of the Grande Ronde basalts, it is helpful to accurately describe the physical character of various basalt flows and to identify the probable positions of groundwater zones within each type of basalt to aid in groundwater exploration. The additional data collected during this study provide important information about the regional groundwater trends and the relevance of earthquake signatures in the Palouse Basin Aquifer. In general, the data illustrated the complex nature of cross compartment and upper Grande Ronde aquifer leakage that occurs throughout the basin. The 372-day aquifer test demonstrated the following:

6.2 General Conclusions

1. Water level noise that appeared as rolling hills on diurnal cycles is related to lunar and solar stresses.

2. Estimation of specific storage can be obtained for each observed seismic event by comparing time domain measurements of water level fluctuations to spectral measurements of the LR displacement.

3. Aquifers within the PGB Grande Ronde basalts are distinctly compartmentalized in the horizontal dimension on daily, monthly and yearly time scales.

4. Upper Grande Ronde aquifer wells (WSU 5 and Cornelius) show similar short and long-term trends, but no direct hydraulic connection to lower aquifer pumping.

5. Vertical groundwater leakage occurs from the upper Grande Ronde aquifer to the lower Grande Ronde aquifer.

6. Garfield pumping affects the trends seen in the Palouse wells, but no direct hydraulic connection can be seen because of the low pumping rates relative to the great distance between the wells.

7. Garfield and Palouse wells are located in a different compartment than Moscow-Pullman wells based on the fact that 1) water levels do not respond to system wide recovery, 2) they are declining continuously, and 3) they do not respond to Moscow-Pullman area pumping.

8. The effects of intercompartmental groundwater pumping stresses are described accurately by the Neuman and Witherspoon (1969) model for a bounded, leaky, two-aquifer system composed of a confined pumped aquifer overlain by an unconfined unpumped aquifer.

9. Aquifer test data show that transmissivity and storativity values vary spatially from compartment to compartment, but are constant with time (i.e., values do not change on daily, monthly or yearly time scales).

10. Based on this research, the main portion of the PGB is contained within the ring of crystalline rock outcrops that include Smoot Hill, Kamiak Butte, Angel Butte, Moscow Mountain, Tomer Butte, Paradise Ridge and Bald Butte. Lateral leakage out of the main portion of the PGB westward toward Colfax is suggested by a relatively steep hydraulic gradient in that direction.

11. Hydraulic connection between the main portion of the PGB and the Palouse sub-basin (LC 4) is questionable based on the distinctly different seasonal water level trends in LC 4, combined with the lack of drawdown responses in LC 4 to Moscow-Pullman area pumping over the 372-day aquifer test.

6.3 Recommendations for future research

A better understanding is needed of the geometry of joints, variation in thickness of individual lava flows and interflow units, and the nature of flow contacts, all of which are significant in understanding the hydraulics of the GRBs.

The modeling conclusions and data provided herein are intended to be a guide for future modeling and basin characterization. Further numerical and analytical modeling is

needed; it is recommended that it be contracted to a hydrologic consulting firm or the USGS because of the complexity of the PGB.

Research should continue to analyze water level responses to earth tides and lunar diurnal cycles. This is critical to understanding the rolls and gentle sloping hills occurring in the Palouse water levels. These affects occurred numerous times during this test and where considered limitations when analyzing PGB water levels during times of less pumping in compartments. These phenomena should be examined further and corrected for in future water level examinations.

To satisfy public requests of PBAC, the monitoring network should continue to expand with observation wells located in uncharacterized areas. These areas include west of Pullman, Albion, Kamiak Gap, and Garfield/Palouse. To develop a better understanding of the gradient between Colfax and the rest of the basin, private wells between the two areas should have access tubes and dataloggers installed in them to collect valuable data to understand the significance of this gradient. The Pullman 5 and Pullman 6 connections to other Pullman area compartment wells should also be evaluated in more detail by upgrading to more accurate leveloggers® in Pullman 5 and 6. ASR research should be implemented in areas that are made up of small compartments to maximize containment of injected water and increase recovery efficiency.

REFERENCES

Banner, Aaron, **"**Questions abound concerning Palouse's main water source," September 30, 2009, University of Idaho Argonaut Newspaper.

Barker, R. A., 1979. Computer simulation and geohydrology of a basalt aquifer system in the Pullman-Moscow Basin, Washington and Idaho. Washington Department of Ecology Water-Supply Bulletin 48, Pullman, Washington.

Bear, J., 1972. Dynamics of Fluids in Porous Media. Dover Publications. ISBN 0-486-65675-6.

Blanchard F.B. and Byerly P., 1935. A study of a well gauge as a seismograph. Bulletin of the Seismological Society of America 25: 313–321.

Bredehoeft, J.D., 1967. Response of well-aquifer systems to earth tides: Journal of Geophysical Research v. 72, no. 12, p. 3,075-3,087.

Brodsky, E. E., E. A. Roeloffs, D. Woodcock, and I. Gall, 2003. A mechanism for sustained groundwater pressure changes induced by distance earthquakes, J. Geophys. Res., 108, 2390, doi:1029/2002JB002321.

Burns, E.R., Morgan, D.S., Peavler, R.S., and Kahle, S.C., 2011. Three-dimensional model of the geologic framework for the Columbia Plateau Regional Aquifer System, Idaho, Oregon, and Washington: U.S. Geological Survey Scientific Investigations Report 2010-5246, p. 44, also available at http://pubs.usgs.gov/sir/2010/5246.

Burt, W., Wells, R.E., Conlon, T.D. Tolan T.L., Porcello J.J., 2009. Effects of Faults and Stratigraphic variability on Groundwater flow in Columbia River Basalt Group Aquifers, Geological Society of America Abstracts with Programs, Vol. 41, No. 7, p. 354.

Bush, J.H., 2005. The Columbia River Basalt Group of the Palouse Basin with hydrological interpretations, western Latah County, Idaho, and easternWashington Whitman County, Washington, Palouse Basin Aquifer Committee.

Bush, J.H., 2006. Geologic Report on Moscow Monitoring Wells.

Carey, L., 2011. Evaluation of Oxygen and Hydrogen Isotopes in Groundwater of the Palouse Basin of Moscow Sub-Basin. MS Thesis, University of Idaho: Moscow, ID.

Clark, W. E., 1967. Computing the barometric efficiency of a well. Journal of the Hydraulics Division ASCE, 93(HY4): 93-98.

Conrey, R.M. and Wolff J.A., 2010. Basalt Lava Stratigraphy Beneath Pullman and Moscow: implications for the flow of groundwater.

Cooper, H. H., Jr., J. D. Bredehoeft, I. S. Papadopulos, and R. R. Bennett, 1965.The response of well-aquifer systems to seismic waves, J. Geophys. Res., 70, 3915–3926.

Crosby, J. W. III, and Chatters, R. M., 1965. Water Dating Techniques as Applied to the Pullman-Moscow Ground-water Basin. Bulletin No. 296, Research Division, Washington State University, Pullman, Washington.

Douglas, A.A., 2004. Radiocarbon Dating as a Tool for Hydrogeological Investigations in the Palouse Basin. M.S. Thesis, University of Idaho, Moscow, Idaho.

Earthquake Travel Time Information and Calculator, Earthquake Hazards Program, 2012. Department of Interior, United States Geological Survey, March 20, 2011, http://neic.usgs.gov/neis/travel_times/.

Elkhoury J.E., Brodsky E.E., and Agnew D.C., 2006. Seismic waves increase permeability. Nature 441: 1135–1138.

Fiedler, A.2009. Well interference effects in the Grande Ronde aquifer system in the Moscow-Pullman area of Idaho and Washington. MS Thesis, University of Idaho: Moscow, ID.

Foxworthy, B.L. and Washburn, R.L., 1963. Ground water in the Pullman area Whitman County, Washington. U. S. Geological Survey.

Graph for Windows, 2007. Version 4.3. written by Ivan Johansen.

Hantush, M.S., and C.E. Jacob. 1955. Non-steady radial flow in an infinite leaky aquifer. Transactions American Geophysical Union, 46: 95-100.

Hantush, M.S., 1960. Modification of the theory of leaky aquifers, Jour. of Geophys. Res., vol. 65, no. 11, pp. 3713-3725.

Hopster, Diane, 2003. A Recession Analysis of Springs and Streams in the Moscow-Pullman Basin. M.S. Thesis, Department of GeologicalSciences, University of Idaho, Moscow, Idaho.

HydroSOLVE, Inc. 2007. AQTESOLV for Windows, v.4.5. written by G.M. Duffield.

Jacob, C.E., 1940. On the flow of water in an elastic artesian aquifer. American Geophysical Union, Transactions, 14: 446-460.

Kitagawa Y., Koizumi N., Takahashi M., Matsumoto N., and Sato T., 2006. Changes in groundwater levels or pressures associated with the 2004 earthquake off the west coast of northern Sumatra (M9.0). Earth, Planets and Space 58: 173–179.

Lin, C.L., 1967. Factors affecting ground-water recharge in the Moscow Basin, Latah County, Idaho. MS thesis, Washington State University, Pullman, WA.

Linde A.T., Sacks I.S., Johnston M.J.S., Hill D.P., and Bilham R.G., 1994.Increased pressure from rising bubbles as a mechanism for remotely triggered seismicity. Nature 371: 408–410.

Liu LB, Roeloffs E, and Zheng XY, 1989. Seismically induced water level oscillations in the Wali well, Beijing, China.

Lum, W.E., Smoot, J.L., and Ralston, D.R., 1990. Geohydrology and numerical analysis of ground-water flow in the Pullman-Moscow Area, Washington and Idaho. U.S. Geological Survey Water-Resources Investigations report 89-4103, 73 p.

Matlab® Student Version, 2011. MathWorks®, Version 7.12.0.635, 32-bit (Win32).

McVay, M. 2007. Grande Ronde aquifer characterization in the Palouse Basin. MS Hydrology Thesis, University of Idaho: Moscow, ID.

Merritt, M. L., 2004. Estimating Hydraulic Properties of the Floridan Aquifer System by Analysis of Earth-Tide, Ocean-Tide, and Barometric Effects, Collier and Hendry Counties, Florida U.S. Geological Survey Water-Resources Investigations Report 03–4267.

Microsoft® Office Excel® 2007. Microsoft Office Enterprise.

Moran, K., 2011. Interpretation of Long-Term Grande Ronde Aquifer Testing in the Palouse Basin . MS Thesis, University of Idaho: Moscow, ID.

Neuman, S. P. and P. A. Witherspoon, 1969. Theory of Flow in a Confined Two Aquifer System, *Water Resour. Res.*, 5(4), 803–816, doi:10.1029/WR005i004p00803.

Opatz, C., 2007. Evaluation of Cleaning and Rehabilitation of University of Idaho Well #2 on the Local Groundwater Systems, in the Moscow, Idaho Area. MS Thesis, University of Idaho: Moscow, ID.

Owsley, D., 2003. Characterization of Grande Ronde Aquifers in the Palouse Basin Using Large Scale Aquifer Tests. M.S. Thesis, University of Idaho, Moscow, Idaho.

Palouse Basin Aquifer Committee. 2010. 2010 Palouse ground water basin water use report.

Palouse Basin Aquifer Committee. 2011. 2011 Palouse ground water basin water use report.

Porcello, J., Lindsey, K., Tonkin, M.J., Karanovic, M., 2011. Groundwater Flow Model of the Columbia Basin Groundwater Management Area Development, Calibration, and Application to Evaluate groundwater supplies in four sub-regions, The Columbia Basin Groundwater Management Area of Adams, Franklin, Grant, and Lincoln Counties http://cbgwma.org/groundwater%20modeling/Groundwater%20Flow%20Model%20Development%20Report.pdf.

Provant, A.P., 1995. Geology and Hydrogeology of the Viola and Moscow West Quandrangles, Latah County, Idaho and Whitman County, Washington. M.S. Thesis, Department of Geology, University of Idaho, Moscow, Idaho.

Pyne, R. David G., 1995. Groundwater Recharge and Wells, A Guide to Aquifer Storage Recovery, Lewis Publishers by CRC Press, Inc.

Ralston, D.R. 1987. Construction Report for the WSU No. 7 Production/Test Well. Washington State University, Pullman, WA.

Ralston, D.R. 2000. Report of construction and testing of a new well for the city of Palouse, Washington. Ralston Hydrologic Services.

Reidel, S. P., and P. R. Hooper, 1989. Volcanism and tectonism in the Columbia River flood-basalt province, Spec. Pap. Geol. Soc. Am., 239, 386 pp.

Reidel, S. P., V. G. Johnson, and F. A. Spane, 2002. Natural Gas Storage in Basalt Aquifers of the Columbia Basin, Pacific Northwest USA: A Guide to Site Characterization. PNL-13962, Pacific Northwest Laboratory, Richland, Washington, also available at http://www.pnl.gov/main/publications/external/technical_reports/PNNL-13962.pdf.

Rexin, E. E., Oliver, J., and Prentiss D., 1962. Seismically induced fluctuations of the water level in the Nunn-Bush well in Milwaukee, Bull. Seismol.Soc. Am., 52, No. 1, 17–25.

Roeloffs, E., 1998. Persistent water level changes in a well near Parkfield, California, due to local and distant earthquakes, Journal Geophysics Research., 103 (B1), 869-889.

Sawlan, M.G., 2011. A Chilling Observation: Sub vertical quench fractures are widespread in lavas of the Columbia River Basalt Group, GSA Rocky Mountain Meeting.

Shih Ching-Fang David, 2009. Storage in confined aquifer: Spectral analysis of groundwater responses to seismic Rayleigh waves. Journal of Hydrology 374 ,p 83-91.

Snyder, D.T., and Haynes, J.V., 2010. Groundwater conditions during 2009 and changes in groundwater levels from 1984 to 2009, Columbia Plateau Regional Aquifer System, Washington, Oregon, and Idaho: U.S. Geological Survey Scientific Investigations Report 2010–5040, 12 p., at **http://pubs.usgs.gov/sir/2010/5040/.**

Sokol, D., 1966. Interpretation of Short Term Water Level Fluctuations in the Moscow Basin Latah County, Idaho. Pamphlet No. 137, Idaho Bureau of Mines and Geology, State of Idaho, Moscow, Idaho.

Solinst Levelogger Series Model 3001 Data Sheet, 2009. http://www.solinst.com/.

Stallman, R.W., 1971. Aquifer-test design, observation and data analysis.Techniques of Water-Resources Investigations, United States Geological Survey, Chap. B1, Book 3. 26p.

Stein, S., Wysession, M., 2003. An Introduction to Seismology, Earthquakes, and Earth Structure. Blackwell Publishing.

Swanson, D.A., Wright, T.L., Hopper, P.R., and Bentley, R.D., 1979. Revisions in Stratigraphic Nomenclature of the Columbia River Basalt Group. U.S. Geological Survey Bulletin 1457-G, p.59.

Teasdale, E. W., 2002. Hydrogeologic Sub-Basins in the Palouse area of Idaho and Washington. M.S. thesis, Department of Geology, University of Idaho, Moscow, Idaho.

TerraGraphics, Inc. 2011. Palouse Ground Water Basin Framework Project Final Report. Palouse Basin Aquifer Committee, Moscow, ID.

Theis, C.V., 1935. The relation between the lowering of the piezometric surface and the rate and duration of discharge of a well using groundwater storage, Am. Geophys. Union Trans., vol. 16, pp. 519-524.

Vorhis, R. C., 1965. Earthquake Magnitudes from Hydroseismic Data. Ground Water, 3: 12–20. doi: 10.1111/j.1745-6584.1965.tb01196.

Vorhis, R.C.,1967. Hydrologic Effects of the Earthquakes of March 27, 1964 outside Alaska, Geologic Survey Professional Paper 544-C.

Wright, T.L., Grolier, M.J., and Swanson, D.A., 1973. Chemical Variation Related to the Stratigraphy of the Columbia River Basalt, Geological Society of America Bulletin, Vol. 84, No. 2, p. 371-385.

Woodcock, D. and E. A. Roeloffs, 1996. Seismically induced water-level oscillation in a fractured-rock aquifer well near Grants Pass, Oregon, Oregon. Geology, 58, 27–33.

Yang, Y., and D. W. Forsyth, 2006. Rayleigh wave phase velocities, small-scale convection, and azimuthal anisotropy beneath southern California, *J. Geophys. Res.*, *111*, B07306, doi:10.1029/2005JB004180.

APPENDIX A

Processing of Water Level Attributes

Well ID	BE	Method
WSU 5	0.98	Clark (1967)
WSU 6	0.98	TE
WSU 7	1.0	TE
WSU 8	0.98	TE
WSU Test	0.95	TE
WSU Dairy	0.95	TE
Cornelius	0.97	TE
Pullman 3	0.92	TE
Pullman 4	0.97	TE
Pullman 6	0.91	Clark (1967)
Pullman 7	0.98	TE
Pullman 8	0.95	Clark (1967)
Palouse1	0.95	TE
Palouse3	0.95	TE
DOE	0.94	Clark (1967)
Motley-Motley	0.99	TE
IDWR4	1.0	TE
Moscow 6	0.99	TE
Moscow 8	0.90	TE (Sokol, 1966)
UI 3	0.90	TE (Sokol, 1966)

Table A01: Palouse Basin Barometric Efficiencies (Modified from Moran 2011).

Well Name	Latitude	Longitude	Elev. (m)	Elev. (ft)	Source
IDWR 4	46.7472214	-117.0267538	799.95	2623.85	Hernandez 2006
Moscow 6	46.7410170	-116.9954297	788.41	2586.00	McVay 2007
Moscow 7	46.7403473	-117.0134573	797.18	2614.76	McVay 2007
Moscow 8	46.7403865	-117.0132146	798.17	2618.00	McVay 2007
Moscow 9	46.7346033	-117.0323448	779.57	2557.00	McVay 2007
Palouse 1	46.9098801	-117.0723113	741.31	2431.51	McVay 2007
Palouse 3	46.9058673	-117.0828005	763.84	2505.41	McVay 2007
Cornelius	46.6917660	-117.1415600	744.39	2441.60	Marshall 2011
Motley (Premix)	46.7394050	-117.0057290	768.73	2521.42	McVay 2007
Pullman 3	46.7320757	-117.1805297	713.30	2339.64	McVay 2007
Pullman 4	46.7356189	-117.1764921	714.80	2344.56	McVay 2007
Pullman 5	46.7134463	-117.1824449	745.77	2446.14	McVay 2007
Pullman 6	46.7475276	-117.1729806	738.79	2423.24	McVay 2007
Pullman 7	46.7358178	-117.1764898	715.02	2345.28	McVay 2007
Pullman 8	46.7226500	-117.1763740	767.99	2519.00	Pullman 2009
UI 3	46.7369638	-117.0209610	782.60	2566.94	McVay 2007
UI 4	46.7351199	-117.0249334	778.40	2553.15	McVay 2007
DOE	46.7305922	-117.0888225	760.54	2494.58	Marshall 2011
WSU 4	46.7301406	-117.1709891	720.28	2362.52	McVay 2007
WSU 5	46.7399097	-117.1277609	763.73	2505.04	McVay 2007
WSU 6	46.7342060	-117.1568036	772.78	2534.71	McVay 2007
WSU 7	46.7290802	-117.1697880	736.01	2414.12	McVay 2007
WSU 8	46.7319700	-117.1497400	788.72	2587.00	McVay 2007
WSU Test	46.7303546	-117.1709973	720.44	2363.04	McVay 2007
WSU Dairy	46.6917963	-117.2423699	783.11	2568.60	Google Earth®
Clay Street	46.8942632	-117.3571481	599.28	1965.65	McVay 2007
Fairview	46.8721423	-117.3689013	642.38	2107.00	McVay 2007
Glenwood 1	46.9295151	-117.2821430	637.20	2090.00	McVay 2007
Glenwood 2	46.9296049	-117.2794582	637.20	2090.00	McVay 2007
Garfield 3	47.0042601	-117.1397404	763.72	2505.00	Google Earth®
Garfield 4	47.0075677	-117.1429326	754.57	2475.00	Google Earth®
Albion 2	46.7859640	-117.2526940	730.79	2397.00	Google Earth®
Albion 3	46.8993333	-117.2513030	715.55	2347.00	Google Earth®

Table A02: Grande Ronde well location coordinates in Latitude/Longitude decimal degrees NAD 83 and top of casing elevation (modified from McVay 2007).

Observation Wells	Name	Albion 2	Glen 1	Glen 2	FV	ClaySt	WSU8	WSU7	WSU6	WSU4	UI4	UI3	Pul8	Pul7	Pul6	Pul5	Pal3	Pal1	Mos9	Mos 7 & 8	Mos6
	IDWR4	17.74	28.07	27.93	29.51	29.98	9.52	11.08	10.01	11.15	1.35	1.22	11.72	11.48	11.14	12.45	18.14	18.41	1.47	1.28	2.47
	Cornelius	13.47	28.51	28.44	26.49	27.85	4.51	4.67	4.86	4.82	10.11	10.48	4.34	5.57	6.64	3.94	24.21	24.81	9.59	11.18	2.48
	Pullman3	8.13	23.26	23.21	21.16	22.48	2.35	0.88	1.82	0.76	11.86	12.17	1.09	0.52	1.81	2.08	20.70	21.41	11.30	12.78	2.48
	Pullman4	8.06	23.00	22.94	21.09	22.36	2.08	0.89	1.51	0.74	11.55	11.85	1.44	0.02	1.35	2.51	20.22	20.93	10.99	12.45	12.41
	DOE	13.92	26.55	26.45	26.49	27.35	4.65	6.17	5.20	6.26	4.89	5.22	6.73	6.71	6.68	7.39	19.49	19.97	4.33	5.86	14.14
	WSU5	10.80	24.12	24.03	23.51	24.47	1.89	3.42	2.30	3.47	7.85	8.14	4.17	3.74	3.55	5.10	18.76	19.36	7.29	8.73	13.81
	WSU Test	8.77	23.69	23.63	21.80	23.08	1.63	0.17	1.16	0.02	11.14	11.46	0.95	0.74	1.91	2.07	20.63	21.32	10.58	12.08	7.21
	Motley (Premix)	19.51	29.81	29.67	31.33	31.80	11.01	12.55	11.53	12.64	1.54	1.19	13.14	13.02	12.78	13.77	19.41	19.61	2.10	0.58	10.08
	Clay Street	14.42	6.91	7.09	2.62	0.00	23.97	23.24	23.43	23.10	30.85	30.98	23.52	22.34	21.50	24.10	20.88	21.71	30.42	31.26	32.37

Table A03: PGB Well Distance Matrix in Kilometers.

#	Well Name	Geological Layer	Uncorrected Age (B.P.)	^{14}C, pmc
9	Pullman 3	Grande Ronde Basalt	12,993	20.77
10	Pullman 5	Grande Ronde Basalt	16,254	14.00
11	Pullman 6	Grande Ronde Basalt	17,125	12.60
12	Pullman 7	Grande Ronde Basalt	16,463	13.65
13	WSU 5	Grande Ronde Basalt	14,306	17.72
14	WSU 6	Grande Ronde Basalt	21,058	7.83
15	WSU 7	Grande Ronde Basalt	17,959	11.39
16	WSU 8	Grande Ronde Basalt	18,438	10.75
17	Glenwood	Grande Ronde Basalt	15,525	15.29
18	Fairview	Grande Ronde Basalt	15,129	16.04
19	Clay Street	Grande Ronde Basalt	14,003	18.38
20	Moscow 6A	Grande Ronde Basalt	23,741	5.66
21	Moscow 6	Grande Ronde Basalt	22,559	6.53
22	Moscow 8	Grande Ronde Basalt	21,111	7.78
23	Moscow 9	Grande Ronde Basalt	19,127	9.89
24	UI 4	Grande Ronde Basalt	19,716	9.21
25	UI 3	Grande Ronde Basalt	20,467	8.41
26	Palouse 1	Grande Ronde Basalt	21,925	7.05
27	Palouse 3	Grande Ronde Basalt	26,406	4.10
28	Paulson	Grande Ronde Basalt	15,477	15.38
29	Brawdy	Grande Ronde Basalt	4,420	58.59
30	McGreevy	Grande Ronde Basalt	6,636	44.81
31	Champion El.	Grande Ronde Basalt	11,832	23.90
	IDWR 4*	Grande Ronde Basalt	25,700	4.08
	Albion 3*	Grande Ronde Basalt	18,120	10.48
	WSU Dairy**	Grande Ronde Basalt	16,300	13.14

Table A04: Carbon 14 ages dates and percent modern carbon (pmc) from Douglas (2004), *= Carey (2011), and ** = Folnagy in May 2012.

APPENDIX B

Information on attached CD includes:

1) **Water Level Data**
2) **HOBO Data and Other Pumping Data**
3) **Calculated Drawdown Data for Observation wells**
4) **LC 2 AQTESOLV® File (DOE observation well)**
5) **LC 3 AQTESOLV® File (WSU Test observation well)**
6) **LC 4 AQTESOLV® File (Palouse 3 observation well)**

APPENDIX C

Aquifer Properties from Sparse Records of Groundwater Response to Seismic Waves

Attila J.B. Folnagy, Kenneth F. Sprenke, James L. Osiensky

Department of Geological Sciences, University of Idaho, Moscow, ID, 83844

Paper to be submitted for journal publication

May 1, 2012

ABSTRACT

Rayleigh waves from large earthquakes have periods ranging from ten to several hundred seconds and often produce at all epicentral distances, significant groundwater fluctuations for several hours. The direct comparison of seismic Rayleigh waves and associated groundwater fluctuations have previously been shown to provide useful techniques for evaluating aquifer properties. However, such methods require sampling of water levels on a scale of seconds rather than the more typical scale of minutes employed in most well recorders. A new approach is needed to deal with this sparse amount of hydraulic head data provided by the most data loggers relative to seismological data. In this study, we investigate the use of time domain water level records sampled five minutes apart during the passage of earthquakes waves for comparison with aquifer properties. We show that the Rayleigh wave displacement spectral density, if adjusted for wavelength, aquifer properties, and borehole effects, can be used to predict the mean-squared water level deflection during the passage of the wave. Thus by comparing relatively sparse time domain measurements of water level fluctuations to spectral measurements of the Rayleigh wave displacement (as measured by regional seismographs), assessments of aquifer properties such as transmissivity, storativity and thickness can be obtained. The precision of the method, strongly dependent on the number of water level measurements available during the passage of the Rayleigh wave, can be appraised by standard statistical methods.

INTRODUCTION

Earthquakes have long been known to produce oscillatory groundwater fluctuations even at large teleseismic distances (Blanchard and Byerly, 1935; Rexin et al., 1962; Cooper et al., 1965; and more recently Brodsky et al. 2003; Kitagawa et al. 2006; Shih, 2009 and many others). In the mid-1900s, when seismograph networks were uncommon, the U.S. Coast and Geodetic Survey kept a detailed catalog of water wells with analog recorders that were good hydroseismographs. Papers were written describing how to construct hydroseismographs and how to locate epicenters and estimate earthquake magnitudes from water well records (e.g. Vorhis, 1965). Ironically, the situation is reversed today. Networks of high quality broadband seismographs cover much of the world while most conventional water well recorders, though digital, sample several orders of magnitude too slowly for comprehensive comparison with seismic shaking. Nonetheless, we claim it is possible to extract a reasonable assessment of aquifer properties even from well records sampled on the order of minutes during the passage of the seismic Rayleigh wave.

Seismological theory predicts that while a seismic Rayleigh wave of wavelength λ_0 is passing, the relation between the vertical ground displacement and subsurface dilatation within a few hundred meters of the earth's surface is given by

$$\Delta_0 = - 1.836 \pi w_0 / \lambda_0 \qquad (1)$$

where Δ_0 is the amplitude of the dilatation, and w_0 is the amplitude of vertical displacement of the Rayleigh wave of wavelength $\lambda_0 >> z$ where z is the depth of the aquifer (Cooper et al., 1965; Shih, 2009).

For a confined aquifer, dilatation (the change in aquifer volume per unit volume) can be expressed in terms of specific storage Ss and water level change in an open borehole:

$$\Delta_0 = - S_s \, h_0 / R_0 \qquad (2)$$

where h_0 is the amplitude of the water level oscillation and R_0 is the borehole amplification factor (Cooper et al., 1965). This amplification factor mostly depends on the borehole radius, initial height of the water column, transmissivity of the aquifer, and,

to a minor extent, storativity (Bredehoeft, 1967). The borehole response can be estimated using the following formula (Cooper et al.,1965):

$$R_0 = [(1 - \{\pi r^2 / T \tau\} \text{ Kei } \alpha - 4 \pi^2 H_e / \tau^2 g)^2 + (\{\pi r^2 / T \tau \} \text{ Ker } \alpha)^2]^{-1/2} \quad (3)$$

where $\alpha = r (\omega S / T)^{1/2}$, r is the radius of the borehole, S is storativity, T is transmissivity, τ is wave period, ω is angular frequency of the wave, H_e is the effective height of the water column, and g is the gravitational acceleration. Ker and Kei are Kelvin functions of the second kind of order zero. These special functions can be looked up in tables or calculated (eg., http://www.keisan.casio.com/). The above equation assumes that the entire aquifer thickness is screened.

Combining equations (1) and (2), one obtains, in theory, a connection between the water level oscillation in the borehole and the Rayleigh wave displacement on the surface:

$$h_0 = (1 / Ss) (5.77 R_0 w_0 / \lambda_0) \quad (4)$$

However, in practice, the situation is not so simple. With the exception of Ss, all the variables in the above equation are functions of frequency. In practice, spectral methods need to be employed to transform the Rayleigh wave displacements and the water level fluctuations into their constituent frequency components to get useful results. Shih (2009), for example, used the cross spectral density of the two data sets to identify a narrow frequency band of highest coherence. Then, neglecting any borehole effects, the spectral densities and seismic wavelength at that narrow frequency band only were used to calculate the storage. The key to Shih's method was having complete spectra of both time series available so that the most coherent period can be identified.

However, accurate spectral methods require sampling of water levels on a scale similar to that of seismograph data (less than 1 sample per second). Such water head sampling is rarely performed (Brodsky et al., 2002; Woodcock and Roeloffs, 1996), making impractical the direct application of spectral methods in most water wells. However, large earthquakes produce high amplitude surface waves for an hour or more after the shock. From a statistical viewpoint, this results in a reasonable amount of data with which to

work. In this study, we propose a method to use water level records sampled on the scale of minutes during the passage of Rayleigh waves for the assessment of aquifer properties.

METHOD

The sparse amount of hydraulic head data provided by most well recorders relative to seismological data makes direct spectral comparisons impractical because the spectral density of the water deflections cannot be calculated. The following approach is suggested to deal with this problem.

For the problem at hand, the water fluctuations h(t) are represented as the discrete time sequence $h = \{h_0.....h_{n-1}\}$, and the Rayleigh wave displacements w(t) as the time sequence $w = \{w_{0}..w_{n-1}\}$. For now both are considered as discrete sequences of N samples taken simultaneously during the passage of the Rayleigh wave.

In terms of the discrete Fourier transform F , equation [4] can be written as follows, taking note that λ and R are dependent on frequency as indicated by the subscript k.

$$F\{ h\} = (1 / S_s)\ (5.77\ R_k / \lambda_k)\ F\{ w\} \qquad [5]$$

Now the complex conjugate of [5] is taken

$$F\{ h \}^* = (1 / S_s)\ \ (5.77\ R_k / \lambda_k)\ F\{w\}^* \qquad [6]$$

Multiplying [5] times [6}, and dividing by the number of samples N in the time sequences:

$$H_k\ = (1/ Ss^2)\ (33.3\ R_k^{\ 2}\ / \lambda_k^{\ 2})\ W_k \qquad [7]$$

where H_k is the spectral density of the predicted water level deflections, defined by

$$H_k = F\{ h \}\ F\{ h \}^* / N \qquad [8]$$

and W_k is simply the spectral density of w, defined by:

$$W_k = F\{w \}\ F\{w \}^* /\ N \qquad [9]$$

This adjustment ($33.3\ R_k^2 / \lambda_k^2$) for the wavelength and the borehole response is applied in the frequency domain and acts partly like a high-pass filter, reducing the influence of the longer wavelength (and typically higher amplitude) Rayleigh waves on the process and partly as a band-pass filter enhancing components near the resonant frequency of the borehole.

Dividing both sides of [7] by N, and using Parseval's theorem, one finds that the mean squared water deflection can be predicted from the mean value of the Rayleigh wave displacement spectral density after adjustment for wavelength and borehole effects. That is,

$$E\{ h^2 \} = E\{ (1/ S_s^2) (33.3\ R_k^2 / \lambda_k^2) W_k \} = E\{ H_k \} \qquad [10]$$

where the expected value operator *E* represents an average value over the sample interval.

The above equation can be used to compare a time domain measurements of the mean-squared water level fluctuations to an appropriately filtered spectral measurement of overall seismic Rayleigh wave displacement. Because the water level measurements are usually sparse compared to the seismological data, we do not have the full population of N observations of h^2 available. We use the number of samples available (m) to compute the mean-squared water deflection and employ the well-known formula for SEM, the standard error of the mean, to estimate the precision of the result:

$$SEM = s / m^{1/2} \qquad (11)$$

where s is the sample standard deviation of the squared water level deflections , and m is the number of water level observations available during the passage of the Rayleigh wave. Clearly, the more observations available, the more precise the estimate of $E\{h^2\}$ and any derived aquifer properties by this procedure.

POSSIBLE APPLICATIONS

The equation derived above to relate sparsely measured water level fluctuations to the seismic Rayleigh wave spectrum can be used to assess aquifer properties under several different scenarios. In the simplest case, if storativity and transmissivity of the aquifer have been estimated by previous well tests, these values can be appraised by the direct use of equation (10) to predict the mean-squared water level deflection for comparison to the mean-squared deflection actually observed. Any large discrepancy would suggest problems with the previous estimates of the aquifer properties.

Another possible application is for wells in which pump testing cannot be performed, such as near hazardous waste sites. In this case, if specific storage can be estimated (perhaps by earth tide analysis), an iterative procedure might be used to calculate R_k for trial values of transmissivity until a satisfactory match using equation (10) is found between the predicted and observed mean-squared water fluctuations.

Regardless of how the methodology is applied, one requires a complete time sequence of the Rayleigh wave displacements from which the discrete Fourier transform can be computed. Also necessary is knowledge of Rayleigh wave phase velocities so that wavelengths can be calculated at each frequency for the required adjustment. Also needed are sufficient measurements of the water level deflections during the passage of the Rayleigh wave to get a reasonable estimate of the mean-squared deflection. This last requirement will no doubt be the biggest source of error due to the sparseness of the data from most water level records. However, assuming aquifer properties are stable, results from many earthquake events can be combined to reduce the error to acceptable levels.

RESULTS

As an example of our method, we evaluated the response of an observation well (DOE) in the basalt-hosted Moscow-Pullman Aquifer of eastern Washington and northern Idaho to the passage of Rayleigh waves from the 2010 M8.8 Chile earthquake and the 2010 M9 **2**011 Tohoku Japan earthquake. Pertinent facts about the DOE well are tabulated in Table C01. The well is screened adjacent to basalt flow top immediately beneath a 30-m thick

sedimentary interbed. The well is cased except for the bottom one meter which penetrates the flow top.

The Pacific Northwest Seismograph Network (PNSN) University of Washington regional broadband stations in Enterprise, Oregon (BRAN) and Starbuck, Washington (TUCA) were the closest stations to the aquifer. The facilities of the IRIS Data Management Center were used for access to the waveforms for this event from regional broadband seismograph stations. Seismic data were downloaded from IRIS using the Java program JWEED. The vertical broadband velocity data initially recorded at 40 Hz were low pass filtered to remove frequencies above 0.5 Hz, decimated to a 1 second sampling interval, and then integrated to yield vertical displacement.

The USGS National Earthquake Information Center provides a very useful "Earthquake Travel Time Information and Calculator" on their website which was used to determine the following. Epicentral distance is commonly expressed in terms of great circle degrees. For the Chile quake, the epicentral distance is 91.42° at the Moscow-Pullman aquifer, compared to 90.83° at station BRAN and 91.6°at station TUCA. At these epicentral distances, amplitude corrections for geometric spreading between the stations are negligible. The Rayleigh wave (LR) arrives at BRAN 16 s earlier than at the aquifer and at TUCA 6 s later. The group velocity of LR is 3860 km/s. LR wave periods range from 10 s to several hundred seconds. The shortest wavelength is 38.6 km. The scale of the aquifer is of the order of 10 km. The initial trains of Rayleigh waves from the 2010 M8.8 Chile earthquake as recorded at BRAN and TUCA with time shifts appropriate for the Moscow-Pullman Aquifer area are shown in Figure CO1. The excellent agreement suggests that the regional stations can provide good estimates of Rayleigh wave displacements over the Moscow-Pullman aquifer.

The full record of vertical ground displacement above the aquifer due to the Chile earthquake is shown in Figure CO2. The Rayleigh wave, which is preceded by the P-wave and S-wave phases, arrives at the aquifer at 07:17:09 UTC. To compute the spectral density of the Rayleigh wave, we extracted the displacements from the arrival of

the Rayleigh wave at 07:17:09 out to 08:08:24 UTC, then filtered and decimated the data to use a sampling interval of 5 s, removing any noise above 0.1 Hz.

During this same time interval, the water level recorder in the observation well was collecting samples at 5 minute intervals (Figure C03). In order to eliminate effects of local and regional pumping from the water levels, we estimated the base line of the water levels using a 40 minute running average. The water level deflections from the base line were tabulated and squared. The observed mean-squared deflection, $E\{h^2\}$, was then calculated along with an estimate of the standard error using equation [11].

The spectral density H_k of the water level fluctuation was then predicted from the spectral density W_k of the Rayleigh wave using equation (7). Both spectral densities are shown in Figure C04 for a trial value of Ss. The mean value of Hk, also illustrated in Figure C04, was then repeatably compared to the observed mean-squared water fluctuation until a satisfactorory fit was obtained. The velocity dispersion curve for the western United States (Yang and Forsyth , 2006) was used to derive the wavelengths λ_k required. The borehole amplification factor (Figure C05) was computed from the borehole geometry and previously known values of S and T and the trial value of Ss. Because the well is screened for only 1 m, we reduced the transmissivity in equation (3) by multiplying it by a factor equal to the screened interval divided by aquifer thickness (S/Ss).

A trial Ss of 4.6×10^{-7} results in the best agreement between the predicted and observed mean-squared water fluctuations. However, as shown in Figure 6, fiducial limits (80%) on this result spread over nearly an order of magnitude. The above analysis was repeated for the Rayleigh wave associated with the 2011 M9 Japan earthquake. The observed water fluctuations for this event are shown in Figure C03. Although the Japan quake was closer than the Chile event, the ground displacement and water fluctuations were considerably smaller. As shown in Figure 6, an Ss of 3.12×10^{-6} was calculated for the Japan event. The 80% fudicial limits on this value extend even further than that the Chile event, a direct result of the extremely sparse 10 minute sampling for the Japan event. The geometric mean of the results for the two earthquakes results in an Ss of 1.15×10^{-6} m^{-1}.

This result can be validated to some extent by earth tides. Gravitational theory predicts that the lunar diurnal tide will result in harmonic subsurface dilatations within a few hundred meters of the earth's surface. At latitude θ, the resulting water level deflection in an open water well in a confined aquifer is given by

$$A_{O1} = - 1.56 \times 10^{-8} \sin(\theta) \cos(\theta) / S_s \quad (14)$$

where A_{O1} is the amplitude of the lunar diurnal fluctuation at a period of 1.0758 days (Bredehoeft, 1967; Merritt, 2004). Figure C07 shows the amplitude spectrum of the water level fluctuations for one year in the DOE well. We found A_{O1} in equation to be 0.0054 m, resulting in a specific storage of 1.44×10^{-6} m-1, a value in good agreement with our estimate of 1.15×10^{-6} m^{-1} from the two earthquakes.

Using our estimate of Ss based on the Rayleigh wave response and the previously determined value of S, an effective aquifer thickness of 65 m results. This suggests that the effective thickness of the Moscow-Pullman aquifer in this well is much less than that previously estimated. The predicted value of $E\{h^2\}$ based on the previously determined values of S, T, along with an aquifer thickness of 400 meters is orders of magnitude too high compared to the measured mean-squared water fluctuation from the Rayleigh wave analyses.

Given our better estimate of Ss and effective aquifer thickness from the Rayleigh wave analysis, we can also derive improved values of other aquifer properties (Table C01). Hydraulic conductivity k_h is T divided by aquifer thickness. We find k_h for the DOE well to be 0.0043 m/s, a value consistent with pervious highly fractured hard rock .(Bear, 1972). Porosity n can be derived from Ss and barometric efficiency using the following equation of Jacob (1940):

$$n = B_e \ Ss \ E_w / \gamma_w \quad (15)$$

where Be is barometric efficiency, E_w is the bulk modulus of water (2.2×10^9 Pa), and γ_w = 9.8×10^3 Pa/m. Our result for porosity is 24 %, reasonable value for a highly fractured basalt flow-top aquifer. These improved estimates of specific storage, effective aquifer

thickness, hydraulic conductivity, and porosity are important parameters for understanding and properly modeling this important sole-source aquifer.

CONCLUSION

Because high quality regional seismological data are now freely available in digital form for most areas of the world, the method proposed here could prove to be a valuable tool to complement and validate aquifer property estimates from more conventional methods. An advantage of the method is its logistical simplicity. Because of the statistical nature of the measurements involved, the well recorders do not have to be particularly sophisticated. As long as the timing is accurate to a few minutes and samples are recorded every five or ten minutes, a reasonable estimate of the mean-squared oscillatory fluctuation during the passage of the Rayleigh wave should be obtainable.

DISCUSSION

This method is applicable only for open water wells in confined aquifers which behave as predicted by seismological and hydrological theory. Some aquifers have poor well construction which inhibits flow into or out of the borehole (e.g., Cooper et al., 1965; Liu et al., 1989). In other aquifers, seismic shaking, even at teleseismic distances, is sufficient to alter permeability either permanently or cyclically perhaps by liquifaction, fracture blocking, air bubble growth (e.g. Elkhoury et al., 2006; Brodsky et al., 2003; Roeloffs, 1998; Linde et al., 1994). In these complex situations, water levels should be sampled on the order of seconds, not minutes, if meaningful synthesis with Rayleigh wave displacement is to be accomplished. In fact, considering how inexpensive computer memory is today, it would be a wonderful thing for the science of hydroseismology if hydrologists everywhere would increase the sampling rate on their well recorders to the order of seconds or better.

ACKNOWLEDGMENTS

We would like to extend our sincere appreciation to the Palouse Basin Aquifer Committee (PBAC) for funding this project and providing equipment and assistance. Since 1967, PBAC has performed a great service to the community as their work ensures

a long-term, quality water supply for the Palouse Basin region. Thanks also to the IRIS DMS, which is funded by the people of the United States of America through the Instrumentation and Facilities Program of the National Science Foundation.

REFERENCES

Bear, J. ,1972. Dynamics of Fluids in Porous Media. Dover Publications. ISBN 0-486-65675-6.

Blanchard F.B. and Byerly P., 1935. A study of a well gauge as a seismograph. Bulletin of the Seismological Society of America 25: 313–321.

Bredehoeft, J.D., 1967. Response of well-aquifer systems to earth tides: Journal of Geophysical Research v. 72, no. 12, p. 3,075-3,087.

Brodsky, E. E., E. A. Roeloffs, D. Woodcock, and I. Gall, 2003. A mechanism for sustained groundwater pressure changes induced by distance earthquakes, J. Geophys. Res., 108, 2390, doi:1029/2002JB002321.

Cooper, H. H., Jr., J. D. Bredehoeft, I. S. Papadopulos, and R. R. Bennett, 1965. The response of well-aquifer systems to seismic waves, J. Geophys. Res., 70, 3915–3926.

Elkhoury J.E., Brodsky E.E., and Agnew D.C., 2006. Seismic waves increase permeability. Nature 441: 1135–1138.

Fiedler, A., 2009. Well interference effects in the Grande Ronde aquifer system in the Moscow-Pullman area of Idaho and Washington. MS Thesis, University of Idaho: Moscow, ID.

Kitagawa Y., Koizumi N., Takahashi M., Matsumoto N., and Sato T., 2006. Changes in groundwater levels or pressures associated with the 2004 earthquake off the west coast of northern Sumatra (M9.0). Earth, Planets and Space 58: 173–179.

Linde A.T., Sacks I.S., Johnston M.J.S., Hill D.P., and Bilham R.G.,1994. Increased pressure from rising bubbles as a mechanism for remotely triggered seismicity. Nature 371: 408–410.

Liu L.B., Roeloffs E., and Zheng X.Y., 1989. Seismically induced water level oscillations in the Wali well, Beijing, China.

McVay, M., 2007. Grande Ronde aquifer characterization in the Palouse Basin. MS Hydrology Thesis, University of Idaho: Moscow, ID.

Merritt, M. L., 2004. Estimating Hydraulic Properties of the Floridan Aquifer System by Analysis of Earth-Tide, Ocean-Tide, and Barometric Effects, Collier and Hendry Counties, Florida U.S. Geological Survey Water-Resources Investigations Report 03–4267.

Moran, K, 2011. Interpretation of Long-Term Grande Ronde Aquifer Testing in the Palouse Basin. MS Thesis, University of Idaho: Moscow, ID.

Ralston, D.R. 2000. Report of construction and testing of a new well for the city of Palouse, Washington. Ralston Hydrologic Services.

Rexin, E. E., J. Oliver, and D. Prentiss, 1962.Seismically induced fluctuations of the water level in the Nunn-Bush well in Milwaukee, Bull. Seismol.Soc. Am., 52, No. 1, 17–25.

Shih Ching-Fang David, 2009. Storage in confined aquifer: Spectral analysis of groundwater responses to seismic Rayleigh waves. Journal of Hydrology 374 ,p 83-91.

Stein, S., Wysession, M., 2003. An Introduction to Seismology, Earthquakes, and Earth Structure. Blackwell Publishing.

Vorhis, R. C., 1965. Earthquake Magnitudes from Hydroseismic Data. Ground Water, 3: 12–20. doi: 10.1111/j.1745-6584.1965.tb01196.

Woodcock, D. and E. A. Roeloffs, 1996. Seismically induced water-level oscillation in a fractured-rock aquifer well near Grants Pass, Oregon, Oregon. Geology, 58, 27–33.

Yang, Y., and D. W. Forsyth, 2006. Rayleigh wave phase velocities, small-scale convection, and azimuthal anisotropy beneath southern California, *J. Geophys. Res., 111*, B07306, doi:10.1029/2005JB004180.

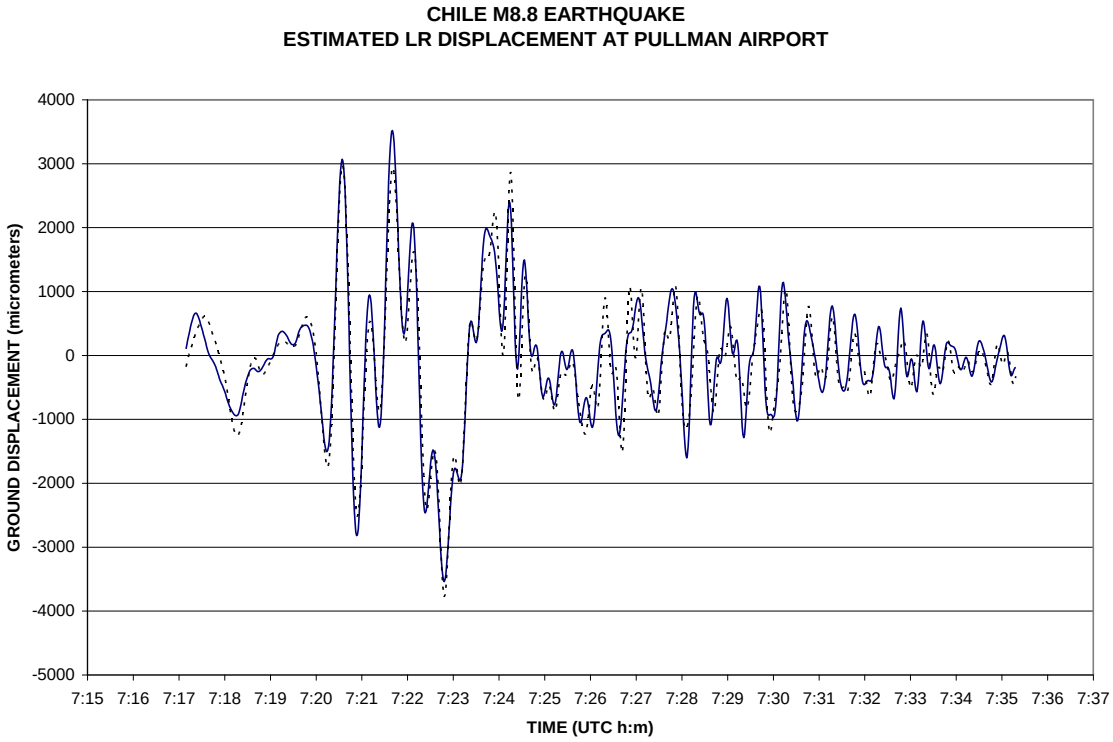

Figure C01: The initial train of Rayleigh waves arriving at the Moscow-Pullman aquifer from the 2010 M8.8 Chile earthquake as estimated from the two nearest broadband seismographs BRAN (solid line) and TUCA (dashed line). Faster traveling waves with periods of several minutes arrive first followed by slower shorter period waves. The wave train continued for about an additional hour with significant amplitude.

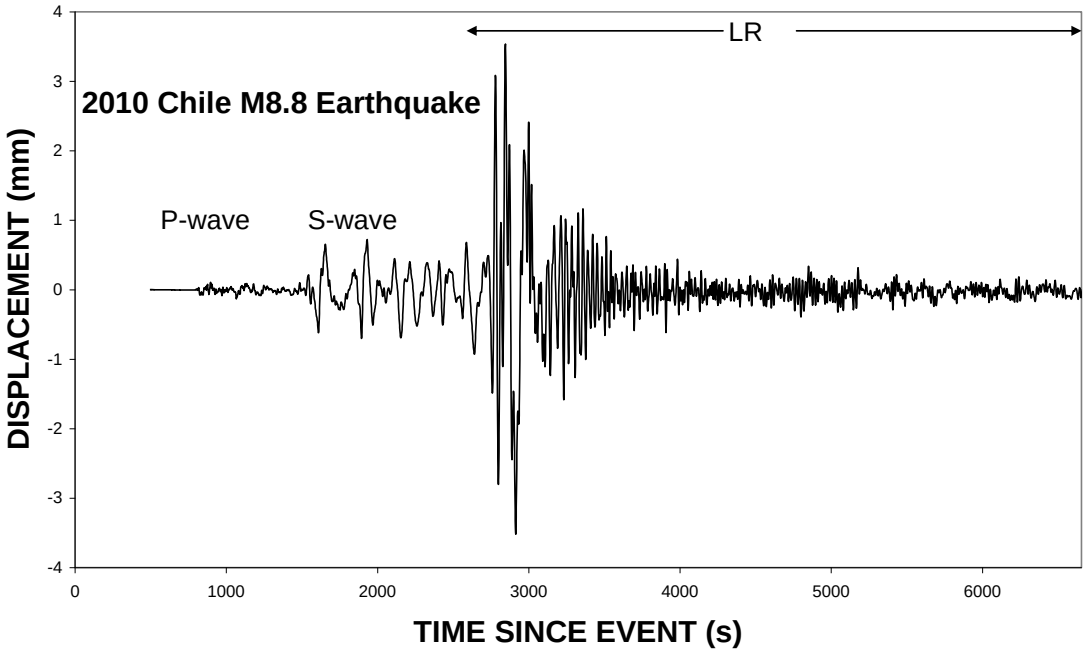

Figure C02: Vertical ground displacement at PUW based on station BRAN. The Rayleigh wave arrives 2575 s after the earthquake at 07:17:09 UTC. The Rayleigh wave analyzed in this study extends over 4095 seconds as illustrated by the arrows.

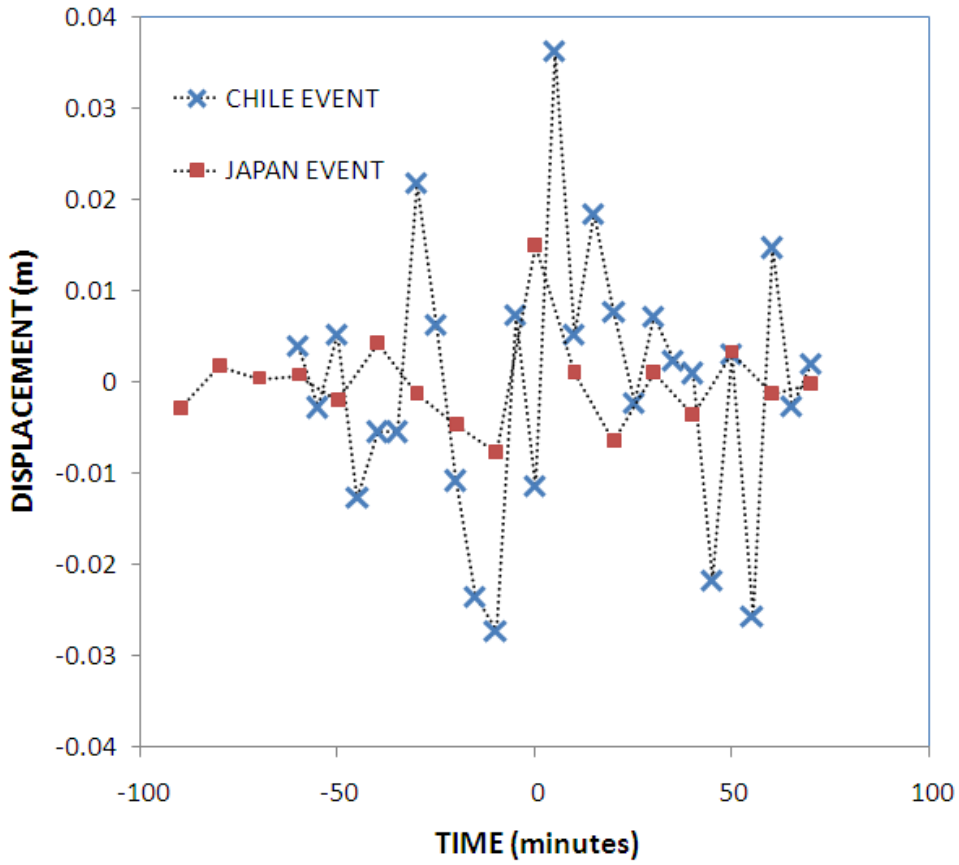

Figure C03: Water levels measured in observation well DOE in the Moscow-Pullman Aquifer during the passage of Rayleigh waves from the 2010 M8.8 Chile Earthquake and the 2011 Japan M9 Earthquake. The Rayleigh wave arrives at time 0 on the graph. The sample interval for the Chile event was 5 seconds, and for the Japan event 10 seconds.

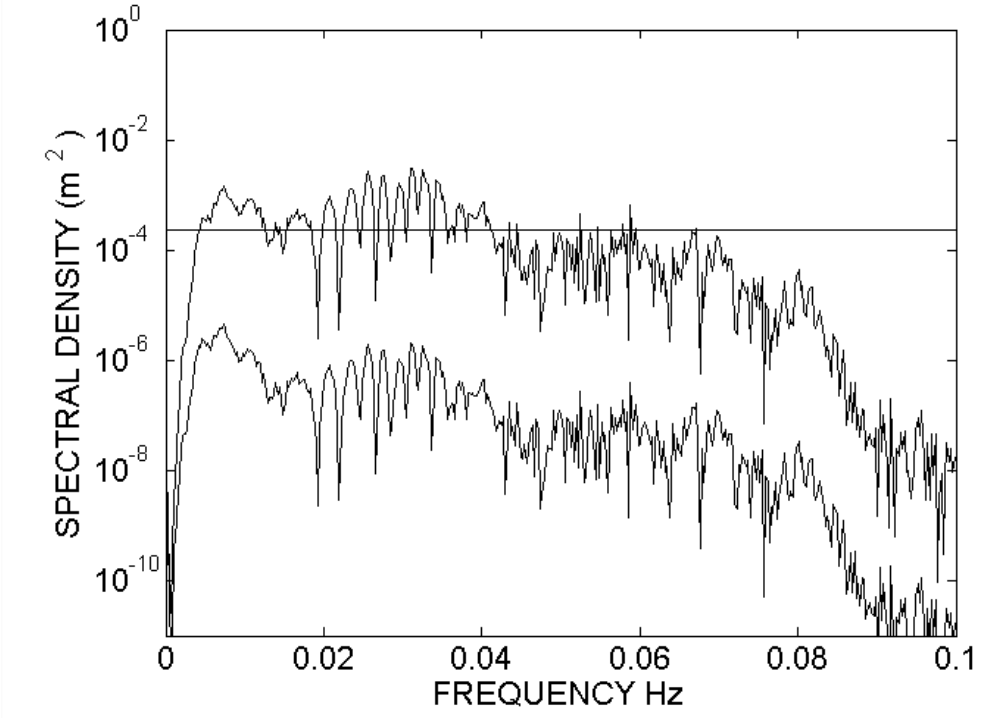

Figure C04: Spectral density W_k of the Rayleigh wave displacement for the Chile earthquake (lower curve) and spectral density H_k of the predicted water level fluctuation for a trial value of S_s (upper curve). The horizontal line is $E\{H_k\}$, the mean value of H_k used for comparison with time domain measurements of $E\{h^2\}$.

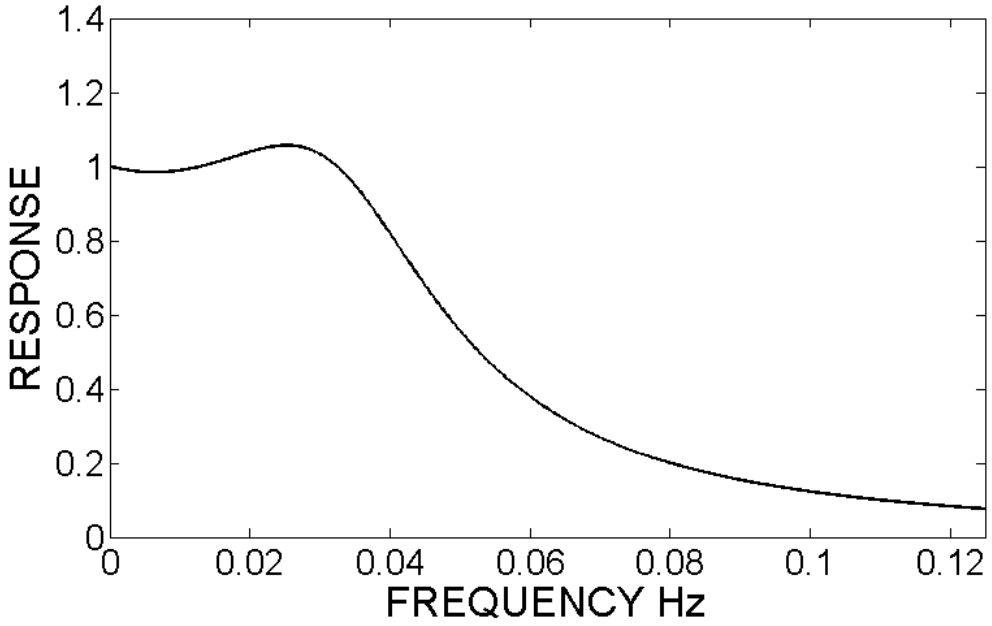

Figure CO5: Amplification factor for the DOE well.

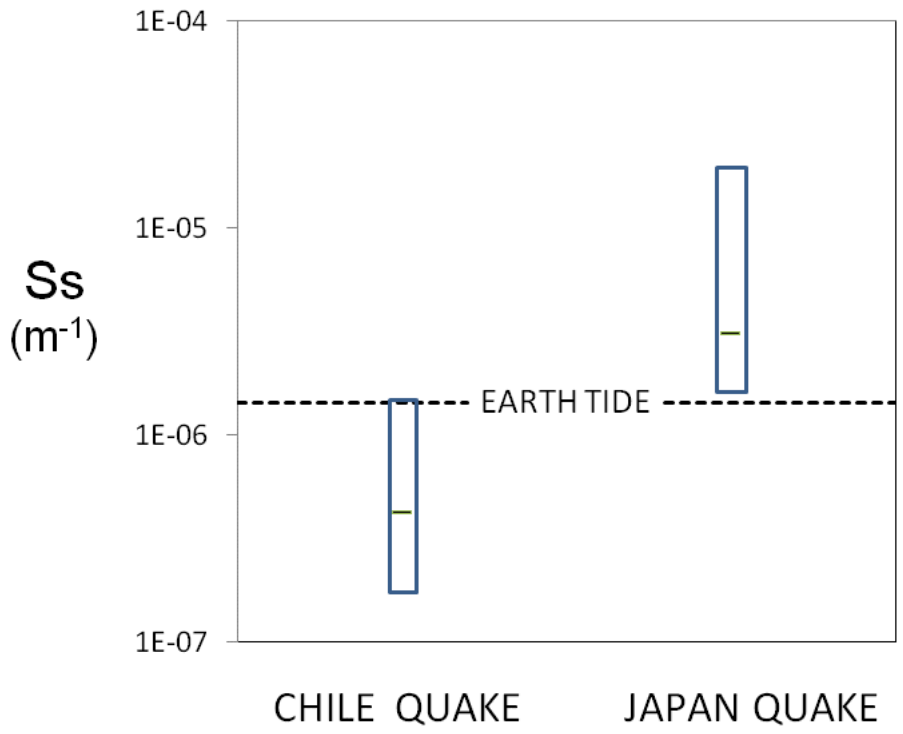

Figure C06: Specific storage results for the two earthquakes analyzed.. The bars show 80% fudicial limits on the results for each event. The specific storage of 1.44 x 10^{-6} m^{-1} found from the earth tide analysis which suits the overlap of the two distributions is also shown.

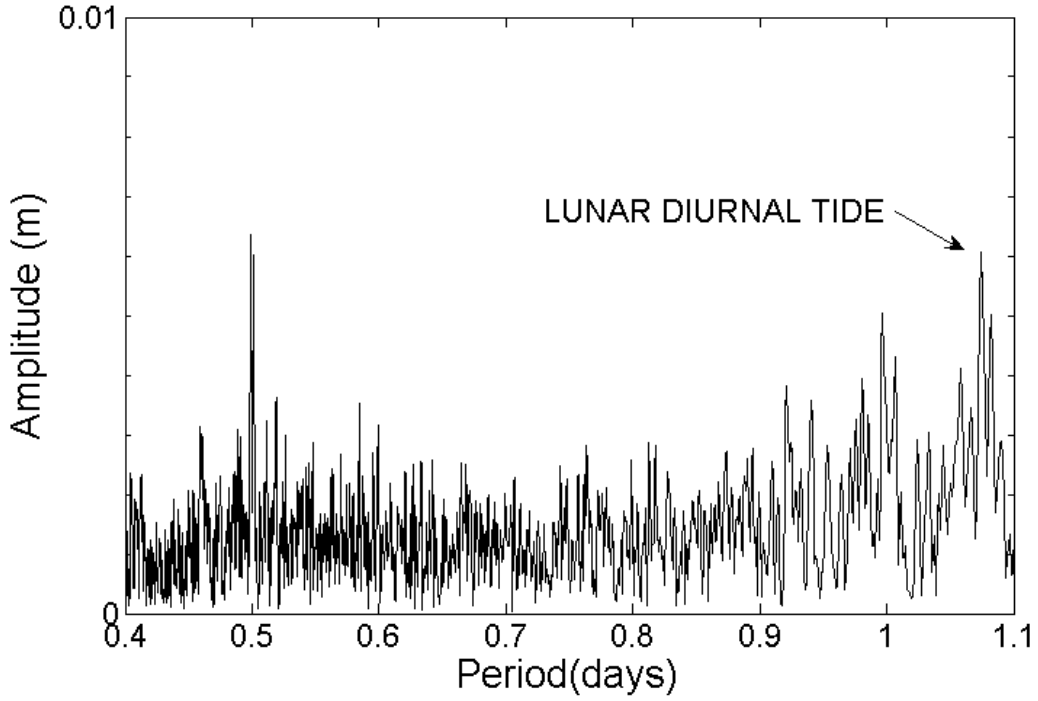

Figure C07: Amplitude spectrum of water fluctuations in the DOE well based on a year of well recorder data sampled at 5 minute intervals. The data are noisy due to nearby pumping; however, the lunar diurnal peak at 1.076 days is apparent with an amplitude of over 5 mm.

WELL NAME	DOE
RADIUS OF BOREHOLE	0.08 m
WATER LEVEL ABOVE SCREEN	226 m
SCREENED INTERVAL	1 m
TRANSMISSIVITY	20000 m^2/day
STORATIVITY	7.5×10^{-5}
AQUIFER THICKNESS (est.)	400 m
BAROMETRIC EFFICIENCY	0.94

EARTH TIDAL RESPONSE	
LUNAR DIURNAL (O1)	0.0054 m

EARTHQUAKE RESPONSE	CHILE QUAKE	JAPAN QUAKE
MEAN-SQUARED FLUCTUATION	2.35×10^{-4} m^2	0.366×10^{-4} m^2
STANDARD ERROR	0.99×10^{-4} m^2	0.271×10^{-4} m^2

Table C01: Pertinent facts about the observation well analyzed.

WELL NAME	DOE
SPECIFIC STORAGE	1.15×10^{-6} m^{-1}
EFFECTIVE AQUIFER THICKNESS	65 m
HYDRAULIC CONDUCTIVITY	308 m/day (0.43 cm/s)
POROSITY	0.24

Table C02: Aquifer properties derived from Rayleigh wave analysis of the DOE well.

APPENDIX D

The Potential for Artificial Storage and Recovery (ASR) in the Palouse Basin

D.1 Introduction

D.1.1 Problem

The main issue that will be addressed is that the Moscow-Pullman Basin is facing a declining aquifer water level. Other cities in the northwestern United States have mitigated this problem by implementing an ASR program. Moscow-Pullman Basin water managers and scientists do not understand the system well enough to affirm that the system has reached equilibrium or will ever reach equilibrium. Recharge is also limited. It is believed that of one inch of rain absorbed by the ground, only one centimeter will make it to the Grande Ronde for recharge, roughly 2,800 years after it fell to the ground (qtd. in Banner). This is troubling to people that rely on the aquifer for municipal and other uses.

D.1.2 Objective

The intentions are to investigate ASRs viability in the Moscow-Pullman Basin. This chapter is intended to indentify ASR's potential, as well as the uncertainties behind the method.

This section will stress the processes that go into ASR program development and design. The chapter describes:

- Constraints and uncertainties of ASR
- Benefits of ASR
- Successful case studies in the CRBG

D.1.3 Methods

The benefits and uncertainties of ASR will be explained by discussing the related scientific articles. The ASR Program development and design steps were published

suggested by the R. David G. Pyne, the author of Groundwater Recharge and Wells, A guide to A.S.R. He emphasizes three phases that an ASR project will have to progress through. They include:

Phase 1: Preliminary feasibility assessment and conceptual design,
Phase 2: Field investigations and test program, and
Phase 3: Recharge facilities expansion

This project will discuss these phases as they relate to the benefits and uncertainties of ASR. Also covered will be a review of articles highlighting the successful Yakima, Washington, Beaverton and Salem, Oregon ASR projects in the CRBG.

D.2 Constraints and Impacts of Aquifer Storage and Recovery (ASR)

D.2A Socio-economic constraints

The two categories of constraints faced by ASR developers are technical and socio-economic constraints. This report will primarily focus on the technical aspects, but will briefly discuss the socio-economic constraints because they will determine if a project has the momentum to get off the ground.

The socio-economic issues include satisfying the local government officials and the public by showing that ASR will provide benefits, incentives, and is economically viable for the community in a reasonable time scale. Overcoming the socio-economic constraints is necessary to advance a project from phase one and into phase two. The current situation in the Moscow-Pullman Basin is that Moscow is not interested in ASR currently, while Pullman has considered ASR as an option in the past, but has run into socio-economic road blocks. The main concern is about degrading the quality of the water of the Grande Ronde Aquifer.

D.2B Technical constraints

Recovery efficiency, well plugging and ground-surface water geochemistry issues are possible technical constraints that an ASR project could face in the Grande Ronde Aquifer. To a lesser extent, the Moscow Pullman Basin water managers would also have

to consider issues such as low permeable aquifer conditions and surface water/treatment water availability. Another issue is groundwater mounding which can reduce infiltration rates. The most reliable way to calculate groundwater mounding beneath a recharge basin may be to use calibrated groundwater models.

D.2B1 Recovery efficiency

Recovery efficiency is defined as the percentage of the water volume stored that is subsequently recovered while meeting a target water quality criterion in the recovered water. Hydrogeology plays a key role in identifying and determining potential ASR zones recovery efficiency. Therefore the ideal aquifer system would be one that is compartmentalized and vertically confined so you can inject water into a certain area and retrieve this water later without being concerned about it dispersing to an inaccessible area. This situation is important for a long term storage ASR program (water banking). It is vitally important to understand the extent of preferential flow paths in the area due to their influences on the extent of interaction between injected and resident water. Therefore larger flow gradients can move the injected water out of the recovery well pumping area, and lower the recovery efficiency. Recovery efficiency is also partially dependent upon density stratification effects due to density directly affecting the heads and flow within a system. The Grande Ronde aquifer is susceptible to density stratification, but the process isn't fully understood.Thus more evaluation must be conducted in the Grande Ronde Aquifer to understand the vertical effects of stratification on the groundwater flow system.

D.2B2 Well Plugging

Artificial recharge of groundwater usually results in increasing resistance to flow and consequently head buildup near the well. This is termed as plugging and ultimately determines the required frequency of redevelopment. An increased understanding of plugging mechanism will be useful in diagnosing the magnitude and origin of plugging during operations. One of the processes that accelerate plugging includes entraining air and gas binding that clogs the pores near the well. Also biological growth in and around the well screen can lower a wells efficiency. This biological growth is proportional to the

amount of carbon and nutrients present in the recharge water and soil. Geochemical reactions can also occur during recharge and adversely affect aquifer permeability or cause changes in the quality of the water. Plugging by deposition of total suspended solids from the recharge source water will take place unless proper filtration or settling methods were completed. Also particle arrangement adjacent to the well may reduce permeability with repeated cycles of recharge and recovery activities.

D.2B3 Geochemical Reactions

Geochemical reactions can be the biggest problem because they can affect recovery efficiency, water quality, and well efficiency. The geochemical reactions are a function of recharge water quality, native groundwater quality, aquifer mineralogy, and changes in temperature and pressure that occur during recharge and recovery. The reactions that are of the most concern to well efficiency and water quality are the precipitation of calcium carbonate, iron and manganese oxides, and the formation, dispersion and swelling of clay particles.

Due to the Grande Ronde Aquifer having high concentrations of manganese and iron oxides, geochemical reaction could be an issue when considering building an ASR program. Also the Moscow areas surface water flows over weathered granitics and basaltic alluvium as well as silt-loamy loess with clay lenses. The Moscow-Pullman water managers would have to consider geochemical issues through careful investigation to determine if such surface water solutes would react with the groundwater. One such investigation that should be run is an oxidation-reduction potential of the waters.

D.2B4 Water Quality

Water quality is a big factor that keeps many ASR program from getting started. Recharge water with high levels of suspended solids and other turbidity issues create problems for the recharge efforts. In some situations, arsenic and radon can also be a problem due to the rock types where the ASR systems capture zone is located. As discussed by Pyne in his book, scientists do not know why Disinfection Byproducts (DBP) levels drop in the recovered water after being injected into the well. Two

carcinogens, trihalomethanes and haloacetic acids were removed from the water while in storage for reasons that the scientists do not fully understand. High DBP level problems have occurred in ASR systems that are in unconfined systems with high dissolved oxygen. So it is believed that in anoxic environments, microbial growth consumes the DBPs. Having a similar pH between surface water and groundwater is also important. A pH above 8.0 limits the mobilization of manganese and lessens the chances of well plugging. To remedy the water quality issues the following practices can be implemented: wellhead filtration, pre and post treatment of water, and/or flow controls to reduce the velocity entering the well head.

D.3 Benefits of ASR

D.3.1 Applications of ASR

The Aquifer Storage and Recovery application that could be beneficial to the Moscow-Pullman Basin will be discussed in this section. Environmental and economical benefits will also be considered. The applications that the Moscow-Pullman water managers could consider using include: seasonal storage, long-term storage, restore groundwater levels, reduce subsidence, agriculture water supply, defer expansion of water facilities, and reclaimed water storage for reuse.

D.3.2 Seasonal and Long Term Storage

Seasonal storage is when water is injected during wet months and recovered during dry months. This is usually done in semi-arid areas such as central Washington, but this could be used by Pullman in the future with shifting climate regimes due to global warming. Long-term storage would be the most likely application for the Moscow-Pullman basin and this is when water is artificially recharged during wet months and is recovered when the capacity of existing facilities are inadequate to meet demand.

D.3.3 Declining Water Levels and Subsidence

As noted previously, the foremost issue that the Moscow-Pullman Basin is facing is a declining aquifer water level. It is declining at a rate of 1-1.5 feet per year, but this can

be reversed by incorporating an ASR system into the regional water management plan. Increased artificial recharge injection during spring flows would be an important factor in stabilizing declining water levels. Within the Moscow city limits the area has subsided in the geologic past. This is evident from the sediments of Bovill and the fluvial systems quaternary floodplain deposits being wider in the Moscow area. Artificial recharge would reduce the threat of subsidence in the Moscow-Pullman basin by restoring groundwater levels.

D.3.4 Water Treatment Facilities and ASR Storage

Moscow and Pullmans climate and precipitation regimes are ideal for an ASR program with 23 inches of rain fall and 48 inches of snowfall annually (Banner, 2009). These precipitation totals allow for the storage of surface water in the aquifer when high flows occur during the spring. The higher spring time flows require the storage of water in the form of snow. Therefore when an ASR program is dependent on injecting surface water, there needs to be a period of higher stream flows. These higher stream flows are needed so that the removal of water doesn't degrade the aquatic ecosystem. Implementing artificial recharge to the Grande Ronde Aquifer would need to occur during the spring before July when the stream flow rates are still adequate.

Water treatment facilities that have ASR storage capabilities are beneficial in that they reduce the diversion of limited summer stream flow and/or impounded surface water that aquatic ecosystems depend on. Instead they take advantage of the plentiful winter/spring stream flow or reclaimed water to store for later use. It is an effective source that is stored closer to the end water user reducing pumping and conveyance from a distant. This reduces the need for transmission lines to surface water body sources such as reservoirs. Reservoirs take up large areas of land space and render the area useless to terrestrial activities. Reservoirs are also very inefficient due to the great losses of surface water to evapotranspiration and seepage into the subsurface. Aquifer Storage and Recovery systems can store much larger volumes of water with little loss, but recovering and recharge can be slow. Aquifer Storage and Recovery facilitates can be built

incrementally compared to reservoirs and desalination plants which also gives them an edge when it comes to total costs and investments.

Aquifer Storage and Recovery is an environmentally acceptable water management alternative and are usually half the cost of other water supply options. When storage capacity is provided by nature and the only cost is implementing ASR, wells can be a successful investment for a community. Aquifer Storage and Recovery facilities require substantially less of a footprint on the land surface than a reservoir. Water transmission and treatment facility can be operated more efficiently and require less capacity. Pullman is considering expanding their waste water treatment facilities. Aquifer Storage and Recovery would be a good alternative and/or addition to the expansion plans with all the positive results of ASR programs in similar CRBG settings.

D.4 Successful Case Studies in the CRBG

D.4.1 Salem, Oregon ASR Program

The key to success for these programs was stepping through the phases of development and design. Taking advantage of initiating an ASR pilot program before final design and implementation of a full-scale facility was crucial for the city of Salem not to be in a situation for large financial losses. Most importantly they used a design/build concept and not the traditional and more likely to fail design/bid/construct method. The area of choice for artificial recharge has an underlying CRBG aquifer and has an extensive network of fractures and adequate storage capacity between approximate depths of 270-350 feet. This depth is similar to the depths that the Grande Ronde is pumped at. The aquifer also has 250 feet of protective sealing clays above the aquifer. Due to the fracture systems not prevalent throughout the entire study areas three wells were tapped for ASR. The other two wells did not have sufficient transmissibility. The type of pump to use for the recharge wells was a deep well turbine pump, and was chosen over the less expensive submersible pump. The choice was made based on recharge purposes and the needed back pressure at the surface to prevent cascading of water down the well. This would result in plugging of the well by air entrainment, iron/manganese oxidation, and aquifer air binding. The Grande Ronde artificial recharge would have to use a similar pump to

avoid plugging of its wells and would need to be determined during the design phase. Recharge can only be made with a pump locked against backspin rotation and with proper shaft thread direction to prevent unscrewing of the shaft. An ASR facility can be created out of existing wells or new wells.

D.4.2 Beaverton, Oregon ASR Program

Beaverton ASR program has been very successful as well with economic analysis determining ASR unit capital cost to be about $1.00 per gallon per day of capacity. They set a storage target of 450 million gallons per year using three injection wells with peak capacity at 6 million gallons a day. They have injected 2.5 billion gallons since 1999 and recovered 2.1 billion. The recovered water accounts for 12 % of Beaverton's drinking water annually. Higher than normal Radon levels were the only issue for water quality, but the levels have not exceeded EPA standards. A historic seep started flowing due to the natural rise of groundwater mounding and/or injection pressure response. Their monitoring data show that their CRBG aquifer is gaining in a historic critical groundwater area.

D.4.3 Yakima, Washington ASR Program

The goal of the Yakima ASR pilot project was to look for other alternatives to the proposed Black Rock dam. This project indicated that a full scale ASR program would be hydrogeologically and operationally feasible. They would recharge a well with a screened interval at 876 ad 1163 feet below ground surface in the Upper Ellensburg Formation (CRBG with interbedded sediments). The water quality was compliant with state drinking water standards. Disinfection byproducts concentration did increase temporarily during storage before decreasing. The DBP did remain below drinking water standards. The Yakima ASR recharge raised the water table a sustained six feet above previous levels and seventy percent of the water was recovered. The question that needs to be addressed is how ASR operation using chlorinated potable water containing disinfection byproducts will be addressed under water quality standards of drinking water.

D.5 Aquifer Storage and Recovery Conclusions

After conducting an investigation on the potential of ASR in the Palouse Basin, a description was conducted of the uncertainties, benefits, and successful case studies of ASR programs. Identifying and resolving the uncertainties that could affect the Moscow-Pullman water manager's decisions on ASR are crucial to the success of design and implementation. At the same time exemplifying the benefits of ASR will get the support from the public which will influence the city leadership to invest in pilot program and possible full implementation.

Explaining the successes of other northwestern cities' ASR programs and the processes that they took to design and develop is important in the future development of other ASR systems. At one time, the other three cities had been facing similar situations in their CRBG aquifer as the Palouse Basin. They have now found a way to use nature's ability to store water and recover it later in a safe and viable way. With increased pressures on the nation's aquifers, ASR programs should be considered in regional water management plans due to their proven performance with over 400 systems worldwide. Much more research will need to be done, but addressing the Palouse Basins issues of declining water levels now would be financially and scientifically responsible.

APPENDIX E

Earth tide Spectral Analysis and Rayleigh Wave Spectral Density Matlab® Software Code

E 1.0 Earth tide Spectral Analysis

```
This program computes the amplitude spectrum for
%  water level samples taken at 5 minute intervals
%  in order to measure AM1 and AO1 earth tides at periods of
%  0.5175 days and 1.076 days. The storativity of the well is then
%  calculated.
clear
%
% Change the following three lines to suit the well and data set being
% studied. The input file must contain a column of water elevations at
% 5 minute intevals without any gaps.

Well = 'Pal1 2010 '
FileName='C:\Documents and Settings\Attila\My
Documents\MATLAB\Earthtides_what_if\Pal12010.txt' % Be sure path is set
correctly
Latitude = 46.75  % Latitude in degrees

%
%
% Beware of any changes below (except maybe the axis for the plot)
Latitude=Latitude*pi/180;
d=dlmread(FileName);
length(d);
y=d(1:length(d),1)';
figure(1)
plot(y)
title([Well 'Raw Signal'])
xlabel('Sample Number')
ylabel('Water Elevation (m)')

% Remocve trend and taper data to zero at both ends
for i=1:length(d)
    y(i)= ( d(i)-d(1) )- (d(length(d))-d(1))*(i-1)/(length(d)-1);
end

% Set time scale to days
Fs = 288;                    % Sampling frequency (288 samples per day)
TT = 1/Fs;                     % Sample time
L = length(d);                     % Length of signal
t = (0:L-1)*TT;                % Time vector
% Sum of a 0.050 Hz sinusoid and a 0.120 Hz sinusoid
%x = .01*sin(2*pi*0.050*t) + .01*sin(2*pi*0.120*t);
%y = x + .01*randn(size(t));     % Sinusoids plus noise
figure(2)
plot(t(1:L),y(1:L))
title([Well ' Tapered Signal'])
xlabel('time (days)')
```

```
ylabel('Water Elevation (m)')
% Add zeros to improve resolution of spectrum
NFFT = 2^(nextpow2(L)+1); % Next power of 2 plus 1 from length of y
Y = fft(y,NFFT)/L;   % Fourier Transform
f = Fs/2*linspace(0,1,NFFT/2+1);  % Frequencies
f(1)=1E-9;  % To avois division by zero
period=1./f;  % Period equals one over frequency

% Plot single-sided amplitude spectrum.
figure(3)
plot(period,2*abs(Y(1:NFFT/2+1)))
axis ([0.4 1.2 0 .0002]); %change last number to adjust y scale
title([Well 'Earth Tide Spectrum'])
xlabel('Period(days)')
ylabel('Amplitude (m)')
% Find amplitudes for the two lunar tides
p5175= round((2*(NFFT/2+1))/((Fs*.5175)))+1;
AM2=2*abs(Y(p5175))
p1076= round((2*(NFFT/2+1))/((Fs*1.076)))+1;
AO1=2*abs(Y(p1076))
% Calculate storativity

Ss_M2 =  1.89E-8*cos(Latitude)*cos(Latitude)/AM2
Ss_O1 =  1.56E-8 *sin(Latitude)* cos(Latitude) / AO1

Ss= (Ss_M2+Ss_O1)/2

percent_error = abs(Ss_M2-Ss)/Ss*100
```

E 2.0 Earthquake Spectral Density Analysis

```
% This program predicts and analyzes the spectral density of water
level
% deflections due to the passage of a Rayleigh wave for wells in which
S
% and T are known. The input paramers below must be changed to match
the
% well and quake being analyzed. Charts are produced showing the
predicted
% and observed expected vaules of the squared deflections.
Discrepancies indicate
% problems with the predetermined values of S, T, or aquifer thickness.
%
% Try new values for S,T,Thickness to improve per cent error.
%
%The horizontal lines on Figure 4 illustrate the expected values of
%observed and predicted squared deflections. The closer the lines are,
the
%better. The lower graph on Figure 4 is the seismic wave spaectum. The
%upper graph is the predicted water level spectrum based on the well
and
%aquifer properties.
clear
%------------------------------------------------------------
% Data for IDWR4...Change as required for other wells
Well = 'DOE'
Quake= 'Japan Quake'
rw = 0.08 %radius of hole in meters
T = 20000/86400 % transmissivity in m2 per second (Divide m2/day by
86400.)
He = 226.4 % height of water column above screen + 3/8 screen length
S=0.000075 % storativity
Thickness =400 %Aquifer thickness in meters
Ss=S/Thickness    %Specific storage
Eh2_measured = 3.07E-4 % Measured expected value of squared water level
deflection
% Choose the correct infile below
Infile='C:\Documents and Settings\Attila\My
Documents\MATLAB\Amplification_what_if\Japan_Rayleigh_Wave'  % Be sure
to change path as necessary
%Infile='c:\bran\Haiti_Rayleigh_Wave';
%Infile='c:\bran\Sumatra_Rayleigh_Wave';
%Infile='c:\bran\Haiti_Rayleigh_Wave';

%------------------------------------------------------------------------
%------------------------------------------------------------------------
--
% Don't change anything from here down or suffer the consequences!!!
%-----------------------------------------------------------------
%-----------------------------------------------------------------
y=dlmread( Infile);

Fs = 0.25;                    % Sampling frequency
TT = 1/Fs;                     % Sample time
L = 1024;                     % Length of signal
```

```
t = (0:L-1)*TT;                % Time vector

NFFT=L;

f = Fs/2*linspace(0,1,NFFT/2+1); % Frequency counter 0 to 0.125 Hz

N=L; % Number of points in specral density
figure(1)
plot(Fs*t(1:L),y(1:L))
title('Signal')
xlabel('time (seconds)')
XK = fft(y,NFFT);   % Fast Fourier Transform

PHIK = XK.*conj(XK)/L;   % Spectral Density

figure(2)
%plot  spectral density
plot(f,PHIK(1:NFFT/2+1));
title ([ Well '  ' Quake '  Spectrum of Rayleigh Wave']);
xlabel('FREQUENCY Hz');
ylabel ('METERS SQUARED');


% The following is a table of Rayleigh wave disperion in western USA
% needed to filter the spectral density for wavelength

phase_vel= [2.,3.488;
    10.1533333447, 3.4885833332;
    20.1866666766, 3.60093333323;
    24.9700000093, 3.65588333325;
    28.7966666754, 3.71573333327;
    33.0900000081, 3.76473333328;
    39.7866666738, 3.79576666662;
    49.5866666724, 3.8196833333;
    66.80666667, 3.85433333331;
    82.6033333344, 3.91418333332;
    100.056666665, 3.98115000001;
    110.81333333, 4.03015000002;
    124.906666662, 4.08988333337;
    143.316666659, 4.15206666672;
    207.879999983, 4.38516666679;
    10000.,4.5 ];

phase_vel=flipud(phase_vel);
phase_vel(:,1)=1./phase_vel(:,1);
phase_vel(1,1)=0.;
phase_vel=1000*phase_vel';
xpv=phase_vel(1,:);
ypv=phase_vel(2,:);
yf=interp1(xpv, ypv, f );

filt1=((5.77./yf).*f).^2;    %Filter for wavelength and constant

% Calculate amplification factor R

R=zeros(1,513);
for k=2:length(f)
```

```
    period=(1/f(k));
    [A] = Cooper(period, rw, T, He, S) ;
    R(k) = A;
end
R(1)=1 ;

%Plot amplification
figure(3)
plot(f, R);
title([Well ' '  Quake ' BOREHOLE AMPLIFICATION FACTOR'])
xlabel('FREQUENCY Hz');
ylabel('RESPONSE');
% Apply filter for Ss and Amplification
filt = filt1.*R.*R./(Ss.*Ss);

%plot filtered  spectral density
F_PHIK(1:NFFT/2+1)=filt(1:NFFT/2+1).*PHIK(1:NFFT/2+1);



format long
%[f' PHIK(1:513)' F_PHIK'] %Display spectral density data for cut and
paste
format short
Predicted_Eh2=2*sum(F_PHIK)/NFFT  % This is the predicted value of
E(h2)
Predicted(1:513,1)=Predicted_Eh2;
Observed(1:513,1)=Eh2_measured;

figure(4)
semilogy(f,F_PHIK(1:513),f, Predicted,f,Observed, f, PHIK(1:513));
title([Well ' ' Quake '  PREDICTED SPECTRUM OF WATER FLUCTUATION'])
xlabel('FREQUENCY Hz');
ylabel('PREDICTED AND OBSERVED EXPECTED VALES (m2)');
axis([0 0.125 1E-12 1E3])

Percent_Error=(Predicted_Eh2-Eh2_measured)*100/Eh2_measured
```

APPENDIX F

AQTESOLV® Methods and Solution Description

The following description of the Neuman-Witherspood (1969) aquifer test solution and information on the procedure for automatic matching in AQTESOLV® are taken directly from the help files included within the software (HydroSOLVE, Inc. 2007. AQTESOLV® for Windows, v.4.5.).

Neuman-Witherspoon (1969) Solution for Confined Two-Aquifer Systems with Leakage

A mathematical solution by Neuman and Witherspoon (1969) is useful for determining the hydraulic properties of leaky confined aquifer systems (transmissivity and storage coefficient of the pumped aquifer; vertical hydraulic conductivity and storage coefficient of aquitard; and transmissivity and storage coefficient of the unpumped aquifer). Analysis involves matching the solution to drawdown data collected during a pumping test. Observation wells may be screened in the pumped aquifer, unpumped aquifer or aquitard.

Unlike the Hantush-Jacob (1955) and Hantush (1960) solutions for leaky confined aquifers, the Neuman and Witherspoon (1969) solution accounts for drawdown in the unpumped aquifer. Neuman and Witherspoon showed that the assumption of no drawdown in the unpumped aquifer (i.e., a constant head boundary condition) can lead to significant errors when estimating the hydraulic properties of the pumped aquifer.

AQTESOLV® provides visual and automatic methods for matching the Neuman and Witherspoon solution to pumping test and recovery test data. This easy-to-use and intuitive software promotes rapid and accurate determination of aquifer properties.

Illustration

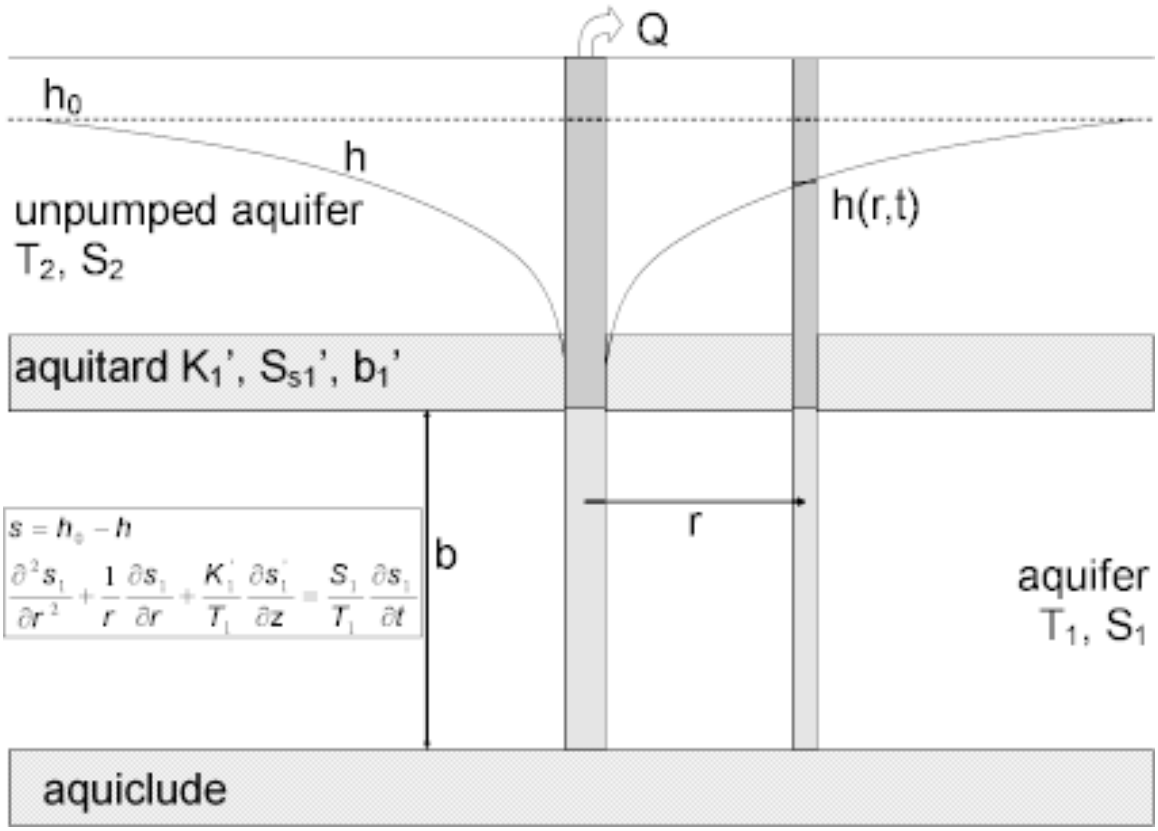

Equations

Neuman-Witherspoon (1969) derived an analytical model for a bounded, leaky, two-aquifer system composed of a confined pumped aquifer overlain by an unpumped aquifer that experiences drawdown. Eq. 1 describes groundwater flow in the pumped aquifer with vertical flow through the aquatard:

$$\frac{\partial^2 s_1}{\partial r^2} + \frac{1}{r}\frac{\partial s_1}{\partial r} + \overbrace{\frac{K_1'}{T_1}\frac{\partial s_1'}{\partial z}}^{\text{Vertical flow}} = \frac{1}{\alpha_1}\frac{\partial s_1}{\partial t}$$

Eq. 1

where

- s_1 is drawdown in the pumped aquifer [L]
- s'_1 is drawdown in the aquitard [L]
- T_1 is transmissivity in the pumped aquifer [L^2/T]
- r is radial distance [L]
- α_1 is hydraulic diffusivity in the pumped aquifer [L^2/ T]
- K_1' is horizontal hydraulic conductivity in aquifer [L/T]
- t is time [T]
- z is aquatard thickness

The boundary conditions for Eq. 1 include:

- at t equal to zero, a horizontal potentiometric surface exists
- at infinite distance the potentiometric surface is unchanged
- near or at the pumping well flow is defined by Darcys Law

Eq. 2 describes 1-D flow through the through the aquatard:

$$\frac{\partial^2 s_1'}{\partial z^2} = \frac{1}{\alpha_1'} \frac{\partial s_1'}{\partial t} \qquad \textbf{Eq. 2}$$

where

α'_1 is hydraulic diffusivity in the aquatard [L^2/ T]

The boundary conditions for Eq. 1 include:

- no drawdown at t equal to zero
- at interface with pumped aquifer, s'_1 is equal to s_1
- at interface with unpumped aquifer, s'_1 is equal to s_2

Eq. 3 describes groundwater flow in the unpumped aquifer with vertical flow through the aquatard:

$$\frac{\partial^2 s_2}{\partial r^2} + \frac{1}{r}\frac{\partial s_2}{\partial r} - \frac{K_1'}{T_2}\frac{\partial s_1'}{\partial z} = \frac{1}{\alpha_2}\frac{\partial s_2}{\partial t}$$

Eq. 3

where

- s_2 is drawdown in the unpumped aquifer [L]
- b_1' is thickness of aquitard [L]
- K_1' is vertical hydraulic conductivity in aquitard L/T]
- T_2 is transmissivity in the unpumped aquifer [L^2/T]
- α_2 is hydraulic diffusivity in the unpumped aquifer [L^2/ T]

The boundary conditions for Eq. 3 include:

- at t equal to zero, a horizontal potentiometric surface exists
- at infinite distance the potentiometric surface is unchanged
- near or at the pumping well flow is defined by Darcys Law

Assumptions

The following assumptions apply to the use of the Neuman and Witherspoon pumping test solution for a confined two-aquifer system with leakage:

- aquifer has infinite areal extent
- aquifer is homogeneous, isotropic and of uniform thickness
- aquifer potentiometric surface is initially horizontal
- control well is fully penetrating
- flow to control well is horizontal
- aquifer is leaky
- flow is unsteady
- water is released instantaneously from storage with decline of hydraulic head
- diameter of control well is very small so that storage in the well can be neglected
- aquitard has infinite areal extent, uniform vertical hydraulic conductivity and storage coefficient, and uniform thickness
- flow in the aquitard is vertical

Data Requirements

- pumping and observation well locations
- pumping rate(s)
- observation well measurements (time and displacement)
- saturated thickness (for partially penetrating wells)

Solution Options

- constant or variable pumping rate including recovery
- multiple pumping wells
- multiple observation wells
- boundaries

Estimated Parameters

- T (transmissivity)
- S (storativity)
- r/B (leakage parameter)
- β (leakage parameter)
- T2 (upper aquifer transmissivity)
- S2 (upper aquifer storativity)